SUDAAR 504

STANFORD UNIVERSITY

CENTER FOR SYSTEMS RESEARCH

UNSTEADY AERODYNAMIC MODELING
AND
ACTIVE AEROELASTIC CONTROL

by

John William Edwards

Guidance and Control Laboratory

Department of Aeronautics and Astronautics
Stanford, California 94305

OCT 1977
RECEIVED

February 1977

UNSTEADY AERODYNAMIC MODELING

AND

ACTIVE AEROELASTIC CONTROL

by

John William Edwards

Stanford University
Guidance and Control Laboratory
Department of Aeronautics and Astronautics
Stanford, California 94305

February 1977

ABSTRACT

Unsteady aerodynamic modeling techniques are developed and applied to the study of active control of elastic vehicles. The problem of active control of a super-critical flutter mode poses a definite design goal--stability, and is treated in detail in this thesis.

The transfer functions relating the arbitrary airfoil motions to the airloads are derived from the Laplace transforms of the linearized airload expressions for incompressible two-dimensional flow. The transfer function relating the motions to the circulatory part of these loads is recognized as the Theodorsen function extended to complex values of reduced frequency, and is termed the generalized Theodorsen function. A brief critique of previous attempts to generalize the Theodorsen function is given. Inversion of the Laplace transforms yields exact transient airloads and airfoil motions. Exact root loci of aeroelastic modes are calculated, providing quantitative information regarding subcritical and supercritical flutter conditions.

The technique of generalizing simple harmonic airload calculations to complex values of reduced frequency is extended to compressible flow regimes. It is conjectured that computer programs which calculate airloads for oscillatory motions can be generalized in a fairly straightforward manner to calculate airloads due to arbitrary motions. This is accomplished for the two-dimensional supersonic case.

The ability to calculate airloads for complex values of reduced frequency allows approximate techniques of calculating these loads to be evaluated. Matrix Padé approximants of airloads for two-dimensional airfoils are evaluated in this manner.

The exact airfoil motions contain portions associated with rational transforms and portions associated with nonrational transforms. The oscillatory response characteristic of a fluttering airfoil is associated

with the rational portion and a theorem is proved regarding the construction of a unique finite-dimensional, linear, constant-coefficient model of this portion of the system. This rational model does not require state augmentation to model unsteady aerodynamic effects and may be used to design active aeroelastic control systems.

The rational model and Padé model are used to design flutter suppression systems for airfoils in incompressible and supersonic flows using the optimal regulator design technique. Both techniques are shown to produce valid flutter mode control designs.

ACKNOWLEDGMENTS

TABLE OF CONTENTS

Chapter		Page

LIST OF FIGURES

-x-

LIST OF TABLES

LIST OF SYMBOLS

A	$N{\times}N$ performance index weighting
A_i	matrix of residues at s_i
$\mathcal{Q}_c$	aerodynamic operator (5.1)
$\mathcal{Q}(s)$	operator defined in (3.1)
a	speed of sound
B	$m{\times}m$ damping matrix
$\mathcal{B}(s)$	operator defined in (3.1)
b	semichord
C	feedback gain matrix
$C_1,\ C_2$	feedback gain matrices (5.11)
$C(\hat{s}) = F+iG$	generalized Theodorsen function
c	nondimensionalized distance from elastic axis to trailing-edge control surface hinge line
c_ℓ, c_m, c_h	lift, pitching moment, and trailing-edge flap hinge moment coefficients
c_p	pressure coefficient
D	submatrix defined in (4.8)
$D(s)$	characteristic equation
d	nondimensionalized distance from elastic axis to leading-edge control surface hinge line
E_1, E_2	submatrices defined in (4.8)
F	$N{\times}N$ state matrix
Γ_i	parameter defined in Table II-2
G	$n{\times}m$ control distribution matrix
G_1	$N{\times}m$ matrix defined in (4.30)

g	structural damping
g_i	parameter defined in Table II-2
$H_n^{(2)}(\bar{s})$	Hankel function of the second kind of order, n
h	nondimensionalized plunge coordinate (Fig. II-1)
h_i	parameter defined in Table II-2
I	expression defined in (2.48)
$I_n(\bar{s})$	modified Bessel function of the first kind of order, n
$I_\alpha, I_\beta, I_\gamma$	moments of inertia per unit length of total section, trailing-edge flap, and leading-edge flap about a,c, and d, respectively (Fig. II-1)
i	$\sqrt{-1}$
$\mathcal{J}$	inertial operator, (5.1)
J	performance index
$J_n(\bar{s})$	Bessel function of order n
K	n$\times$n stiffness matrix
$K_n(\bar{s})$	modified Bessel function of the third kind of order n
$k_1(t')$	Wagner's function
k_h	stiffness of wing in deflection
k_α	torsional stiffness of wing about a
k_β	torsional stiffness of trailing-edge flap about c
k_γ	torsional stiffness of leading-edge flap about d
$k = \omega b/U$	reduced frequency
L	n$\times$1 vector of aerodynamic loads
$\mathcal{L}[\cdot]$	Laplace transform of $[\cdot]$
M	Mach number
M^α	pitching moment about a, positive nose up

M^β	hinge moment of trailing-edge flap about c, positive tail down
M^γ	hinge moment of leading-edge flap about d, positive nose down
m	number of control surfaces
m_s	mass of wing per unit length
N	dimension of X
$N_j(s)$	adjoint matrix defined in (3.8)
n	number of degrees of freedom of wing
P	total force on wing positive downwards
$\tilde{P}$	aerodynamic energy expression (5.10)
P_0, P_1, P_2	n×n Padé approximant matrices
$p(x,y,t)$	pressure distribution on wing
p_i	parameter defined in Table II-2
Q	expression defined in (B.12)
$Q(\bar{s},M)=Q_1+iQ_2$	n×n matrix of aerodynamic load coefficients
q_i	parameter defined in Table II-2
q_i	generalized coordinate
q_{ij}	ijth element of $Q(\bar{s}, M)$
$\bar{q} = \nabla\phi$	perturbation velocity vector
R	n×1 vector defined in (B.31)
R_0	n×n Pade approximant matrix
$\text{Re}[\cdot], \text{Im}[\cdot]$	real and imaginary parts of $[\cdot]$
$\text{Res}(\cdot)\vert_{s_i}$	residue of $(\cdot)$ at s_i
$r_\alpha^2 = I_\alpha/m_s b^2$	radius of gyration of the wing divided by b
$r_\beta^2 = I_\beta/m_s b^2$	reduced radius of gyration of trailing-edge flap divided by b

$r_\gamma^2 \quad I_\gamma/m_s b^2$	reduced radius of gyration of trailing-edge flap divided by b
S_1, S_2	$1 \times n$ vector defined in (B.22)
S_z	static moment of wing per unit length about a_-
S_β, S_γ	static moments of leading- and trailing-edge flaps per unit length about c and d respectively
$\mathscr{S}$	structural operator (5.1)
s_i	parameter defined in Table II-2
$s = \sigma + i\omega = re^{i\vartheta}$	Laplace transform variable
$\bar{s} = \dfrac{sb}{U} = \bar{\sigma} + i\bar{\omega} = \bar{r}e^{i\vartheta}$	nondimensionalized Laplace transform variable
T	$N \times N$ matrix defined in (5.22)
$T - V$	Lagrangian (kinetic energy minus potential energy)
T_i	constants defined in App. C
t	time
t'	time nondimensionalized by U/b
t_i	parameter defined in Table II-2
U	freestream velocity
$U(s)$	$\mathscr{L}[u(t)]$
$U(x)$	unit step function
$u(t)$	$m \times 1$ input vector
u	perturbation velocity component along the x coordinate
V	potential energy
v w	perturbation velocity components along the y coordinate
$w(x,t)$	downwash boundary condition (2.2)
$X(s)$	$\mathscr{L}[X(t)]$
$x(s)$	$\mathscr{L}[\underline{x}(t)]$

$X(t)$	$N \times 1$ state vector
x	spatial coordinates nondimensionalized by b
$x_o^x = b+Ut$	downstream extremity of the wake
$\underline{x}(t)$	$n \times 1$ modal vector
x_α	nondimensionalized distance of center of gravity from a
$x_\beta,\ x_\gamma$	nondimensionalized distances of flap centers of gravity from c and d respectively
Y_i	constant defined in App. C
z	spatial coordinate nondimensionalized by b
$z(x,t)$	nondimensionalized wing surface location

Greek Symbols

α	angle of incidence of wing, positive nose up
β	trailing-edge flap coordinate, positive tail down
$\Gamma(s)$	gamma function
γ	leading-edge flap coordinate, positive nose down
γ_e	0.577215..., Euler's constant
$\gamma_w(x,t)$	wake vortex strength distribution
$\delta(t)$	impulse function
ϵ	infinitesimal quantity
$\zeta_\beta,\ \zeta_\gamma$	viscous damping ratios of leading- and trailing-edge flaps, respectively
η_i	constant defined in (2.21)
η_i'	constant defined in (3.5)
λ_i	eigenvalues associated with the aerodynamic energy matrix
$\mu = m/\pi\rho b^2$	mass ratio

ξ	nondimensionalized distance along wake
$\xi_k(t)$	normal mode coordinate
$\xi_R + i\xi_I$	complex vector associated with aerodynamic energy matrix
ρ	atmospheric density
σ	real part of s (rad/sec)
τ_p	hydraulic actuator time constant
$\Phi(x,z,s)$	$\mathcal{L}[\phi(x,z,t)]$
$\phi(x,z)$	velocity potential
$\phi_k(y)$	normal mode shape
X	location of bound vortex in X-Z plane
ω	imaginary part of s (rad/sec)
$\omega_h,\ \zeta_h$	hydraulic mode frequency and damping
ω_r	reference frequency in (5.12)
$\omega_h = \sqrt{k_h/m_s}$	plunge mode natural frequency
$\omega_\alpha = \sqrt{k_\alpha/I_\alpha}$	torsion mode natural frequency
$\omega_\beta = \sqrt{k_\beta/I_\beta}$	trailing-edge flap mode natural frequency
$\omega_\gamma = \sqrt{k_\gamma/I_\gamma}$	leading-edge flap mode natural frequency

Superscripts

T	matrix transpose
$\bullet$	time derivative
$-$	quantities defined in Fig. A-1
$\cdot$	dimensionalized space coordinates

a	aerodynamic
c	circulatory
D	divergence
f	flutter
L	lower wing surface
nc	noncirculatory
nr	nonrational
p	matrix Padé model
r	rational
s	structural
ss	steady state
U	upper wing surface
∞	freestream
$[\cdot]_{\cdot i}$	i^{th} column of $[\cdot]$
$[\cdot]_{i \cdot}$	i^{th} row of $[\cdot]$

Miscellaneous

∇	gradient operator
∇^2	Laplacian operator

Abbreviations

AS	augmented stability
CCV	control configured vehicle
DOF	degree of freedom

FR   fatigue reduction

GA   gust alleviation

FMC   flutter mode control

LAMS   load alleviation and mode stabilization

RC   ride control

PA   Padé approximant

PAs   Padé approximants

PM   Padé model

rms   root mean square

Chapter I

INTRODUCTION

During the past decade, an aircraft design philosophy has emerged which attempts to gain performance improvements by means of an interactive design process involving structural dynamics, aerodynamics, and control systems. This philosophy involves the use of active control systems to achieve aerodynamic and/or structural designs which have better performance, stability, or economy than can be achieved with conventional passive techniques. Many of these concepts have been implemented in the B-52 load alleviation and mode stabilization (LAMS) [Ref. 1], and control configured vehicle (CCV) [Ref. 2] programs. The concepts used in this control configured vehicle philosophy include: augmented rigid body stability, maneuver load control, ride control, fatigue reduction, gust alleviation, and flutter mode control. The first five items involve the static and dynamic performance of the flexible aircraft. The design goal of these items is typified by the C-5A active load distribution control system [3] which was designed to reduce the wing root bending moments experienced by the aircraft and thus increase its service life.

The last item, flutter mode control, is fundamentally different from the others in that the structural stability of the flexible vehicle is involved. While loss of the former items would result in degraded performance or a shorter vehicle life, loss of a flutter mode control system at a supercritical flutter condition would usually result in loss of the aircraft. Although the risk is high, the potential performance gains are correspondingly high and flutter mode control systems can be designed to reduce the structural weight of a vehicle or to increase the flight envelope of the vehicle by expanding flutter speed placards. Roger and Hodges [4] describe the flutter mode control system implemented for the B-52 CCV program and successfully flight tested, while Sandford et al. [5], document a system installed on a wind tunnel model.

-1-

The analysis techniques required are common to all of these CCV programs and involve the study of unsteady aerodynamics for arbitrary motions, structural dynamics due to unsteady loading, and aerodynamic loading caused by control surface motion. The design of flutter mode control systems places severe demands upon the analyst; the primary design goal is structural stability. Hence, this dissertation focuses attention upon techniques of analyzing flutter mode control systems. Of course, the techniques will also be applicable to the other CCV concepts.

A. SURVEY OF LITERATURE

The finite element method of structural dynamics is well developed [6] and will be assumed as the basis of the analysis of aircraft structures. The infinite dimensional spaces required to describe solutions are reduced to finite dimensional spaces by the familiar technique of truncated normal modes [7].

The study of unsteady aerodynamics has progressed along two directions:

(1) The calculation of the indicial loading due to impulsive motion;

(2) The calculation of the loads due to simple harmonic oscillations of the wing or section.

The former area was first investigated by Wagner [8] for two-dimensional incompressible flow. R. T. Jones [9] and Lomax et al. [10], continued this line of investigation. A method for calculating the loads due to simple harmonic oscillations of a wing section in incompressible flow was first given by Theodorsen [11]. The corresponding solution for subsonic flow was given by Timman and Van deVooren [12], and for supersonic flow by Garrick and Rubinow [13]. Methods for calculating the loads on three-dimensional wings due to oscillations of assumed or normal mode shapes have derived from Possio's integral equation [14]. Techniques of treating the singularities of the kernel function and obtaining solutions were given by Watkins et al. [15], and have been extended to wings with control surfaces by Rowe, et al., [16]. Another calculation process,

-2-

analogous to the finite-element method of structures, is the doublet-lattice technique of Albano and Rodden [17].

The prevalence of aerodynamic analysis techniques based upon the assumption of simple harmonic motions is undoubtedly due to the success of the theory in predicting flutter boundaries. Theodorsen and Garrick [18], and Smilg and Wasserman [19], are representative of the methods traditionally used in the calculation of flutter boundaries. The latter reference introduced the concept of artificial structural damping.

Attempts to extend Theodorsen's theory to deal with arbitrary motions (e.g., converging or diverging oscillations) were made by W.P. Jones [20], and by Luke and Dengler [21]. Jones concluded that Theodorsen's solution could be extended to diverging (unstable) oscillations but not to converging (stable) oscillations while Luke and Dengler's attempt to extend Theodorsen's solution to stable motions was rejected in a series of articles [22] - [26].

The inability of U-g flutter analysis and oscillatory aerodynamics to give quantitative information regarding stable, subcritical flutter conditions [Richardson, 27], [Hassig, 28], led to methods of approximating this behavior based upon convolution techniques. R.T. Jones [29] indicated the method of exponential approximation of Wagner's indicial loading function and used the convolution integral to obtain results for arbitrary motions. Jones' work was followed by Goland and Luke [30], Baird and Kelley [31], and Dugundji [32]. Recently, Vepa [33, 34] applied the technique of Padé approximation of oscillatory loads to derive expressions for loads due to arbitrary motion. Also, Morino [35, 36] has developed a new formulation based on the Green function solution of the governing partial differential equation which is valid for arbitrary motions.

Whereas the ability to calculate airloads for arbitrary motions is of interest to the aeroelastician for the insight gained concerning the approach to flutter, it is a necessity to the controls engineer who desires to design a flutter mode control system. The application of the design techniques of modern control theory requires that the plant to be controlled be described by a mathematical model, preferably by linear, constant-

-3-

coefficient, ordinary differential equations. Approximation techniques based upon exponential approximations to indicial response functions or Padé approximants lead naturally to such models in which the unsteady aerodynamic effects are simulated by augmented state variables. The B-52 CCV flutter mode control system was designed using this type of model [2] and utilized the frequency domain control synthesis method.

Optimal control theory is a well developed methodology for the synthesis of control laws to minimize a suitable performance index [Bryson and Ho, 37]. Designs of flutter mode control laws using augmented state methods to represent the unsteady aerodynamics and implementing the optimal regulator solution are described by Turner [38] and Dressler [39]. A program designed to study the active control of flexible aircraft which incorporates Morino's aerodynamic theory is described by Noll and Morino [40]. However, it has yet to be applied to a flutter mode control problem.

A different approach was taken by Nissim [41] who developed a flutter suppression scheme based upon the concept of aerodynamic energy. A wind tunnel program testing Nissim's design technique is described by Sandford, et al. [5].

Flutter mode control system designs are actually problems in distributed parameter system theory. Wang and Tung [42] surveyed the field and references [43] - [48] typify the results of the theory. Sung and Yü [49] present a formulation within which the flutter control problem can be treated, while Wang [50] presents a technique of stabilizing a system with a finite number of unstable modes which resembles the flutter problem.

B. THESIS OUTLINE

Chapter II presents the equations of motion of the typical section treated in this thesis and derives the generalized Theodorsen function for arbitrary airfoil motions. The Laplace inversion integral is used to derive loads due to transient motions and generalized unsteady aerodynamic loads are studied in compressible flow.

-4-

In Chapter III, the generalized loads developed in Chapter II are incorporated into the equations of motion, and the locus of roots of the aeroelastic system is determined. The Laplace inversion integral is used to calculate exact airfoil motions due to flap command inputs.

Chapter IV treats the problem of approximation of unsteady aerodynamic loads. R.T. Jones' approximation of the Theodorsen function, and Vepa's matrix Padé approximants of compressible loads, are compared to the exact solutions for aribtrary motions.

The active control of aeroelastic systems is treated in Chapter V. Controllability and observability of such systems are investigated and the aerodynamic energy design technique is studied. The "rational model" is presented and compared to the Padé model. The models are used to design optimal regulator solutions to the flutter mode control problem.

Chapter VI presents the conclusions of this thesis and recommendations for future research.

C. SUMMARY OF CONTRIBUTIONS

1. The problem of generalized aerodynamic loads due to arbitrary air-foil motions is investigated. The generalized Theodorsen function for in-compressible flow is derived using Laplace transform techniques. The same technique is applied to compressible unsteady airload calculations and results are presented for the case of two-dimensional supersonic flow. Exact root loci of aeroelastic modes are calculated and examples of exact transient responses due to stable motions are given.

2. The transient motions contain portions associated with rational transforms and portions associated with nonrational transforms. It is shown that the oscillatory motions typifying flutter phenomena are due entirely to the rational portion of the response.

3. The generalized aerodynamic loads are used to evaluate approximate techniques for calculating these loads. It is shown that exponential approximations of indicial loading functions and matrix Padé approximants of oscillatory airloads provide valid models of unsteady airloads for

-5-

values of complex reduced frequency near the imaginary axis.

4. The generalized Theodorsen function is used to study static divergence of typical sections. It is shown that static divergence corresponds to the emergence of a real positive pole of the system transfer function and occurs, in addition, to the original structural poles.

5. Flutter mode control systems are investigated. The controllability and observability of airfoils is studied. A theorem is given concerning the ability to construct a unique, linear model of the rational portion of the aeroelastic system which does not require state augmentation. The resulting rational model and the Padé model are used to design flutter mode control systems.

Chapter II

UNSTEADY AERODYNAMIC MODELING

A. TYPICAL SECTION EQUATIONS OF MOTION

The typical section which will be analyzed is shown in Fig. II-1. It has leading- and trailing-edge control surfaces which are aerodynamically unbalanced (hinge lines at leading/trailing edges), simplifying the description of the aerodynamics.[†] Linear and torsional springs (k_h and k_α) at the section elastic axis restrain motion in the plunge (h), and pitch (α) degrees of freedom, while torsional restraining springs (k_β and k_γ) restrain control surface deflections. All linear coordinates (x, z, h) have been nondimensionalized by the semi-chord, b. The equations of motion are derived in App. A following the conventions of Theodorsen [11], and Theodorsen and Garrick [51, 18] as

$$M_s \ddot{\underline{x}} = -K_s \underline{x} - B_s \dot{\underline{x}} + \frac{1}{m_s b^2} L + Gu \qquad (2.1)$$

where the subscript s indicates that the matrix operators are of structural origin, and

$$M_s = \begin{bmatrix} 1 & x_\alpha & x_\beta & x_\gamma \\ x_\alpha & r_\alpha^2 & [r_\beta^2 + x_\beta(c-a)] & [x_\gamma(d-a) - r_\gamma^2] \\ x_\beta & [r_\beta^2 + x_\beta(c-a)] & r_\beta^2 & 0 \\ x_\gamma & [x_\gamma(d-a) - r_\gamma^2] & 0 & r_\gamma^2 \end{bmatrix}.$$

The matrices M_s, K_s, B_s, and G are

[†] On an aerodynamically balanced control surface, the hinge line is some distance away from the leading/trailing edge such that the aerodynamic pressure distribution may be used to advantage in reducing the hinge moments developed by surface motion.
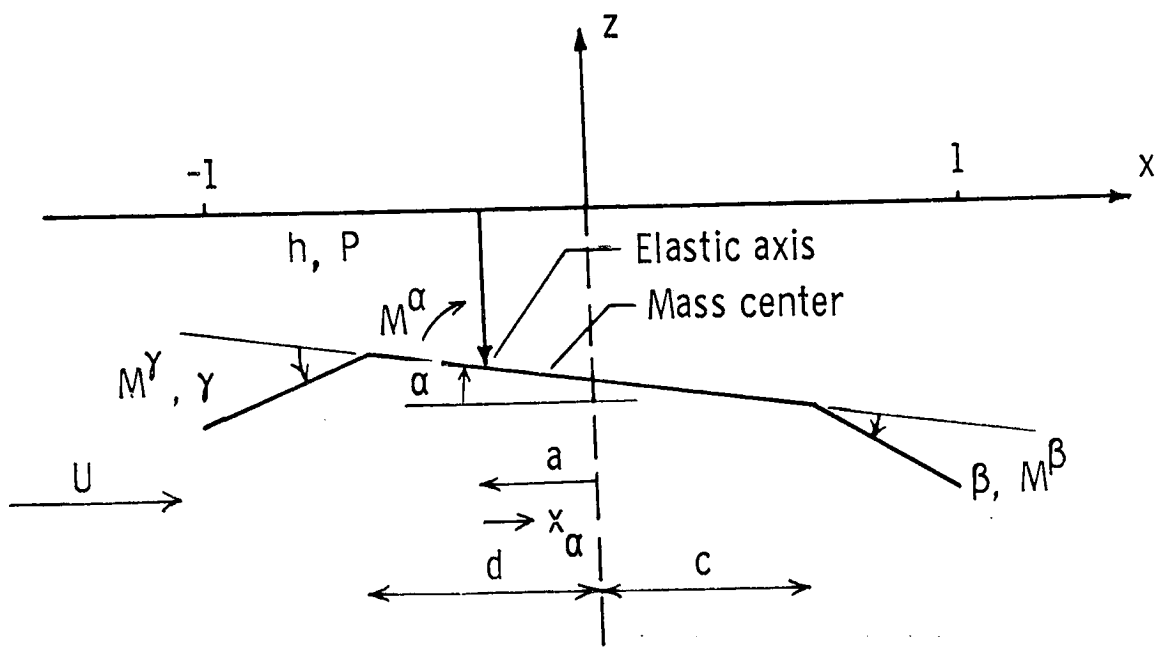
FIG. II-1   DIAGRAM OF A TYPICAL SECTION WITH AERODYNAMICALLY
UNBALANCED LEADING- AND TRAILING-EDGE CONTROL
SURFACES

$$K_s = \begin{bmatrix} \omega_h^2 & 0 & 0 & 0 \\ 0 & r_\alpha^2 \omega_\alpha^2 & 0 & 0 \\ 0 & 0 & r_\beta^2 \omega_\beta^2 & 0 \\ 0 & 0 & 0 & r_\gamma^2 \omega_\gamma^2 \end{bmatrix}$$

$$B_s = \begin{bmatrix} 0 & 0 & 0 & 0 \\ 0 & 0 & 0 & 0 \\ 0 & 0 & 2r_\beta^2 \omega_\beta \zeta_\beta & 0 & 0 \\ 0 & 0 & 0 & 2r_\gamma^2 \omega_\gamma \zeta_\gamma \end{bmatrix}$$

$$G = \begin{bmatrix} 0 & 0 \\ 0 & 0 \\ r_\beta^2 \omega_\beta^2 & 0 \\ 0 & r_\gamma^2 \omega_\gamma^2 \end{bmatrix} .$$

The use of control surface spring and damping constants to approximate irreversible position control systems is discussed in App. A. Equation (2.1) describes a four degree-of-freedom (DOF) model. Two and three DOF models may be obtained from (2.1) by deleting appropriate rows and columns of the matrices and vectors.

The specification of the aerodynamic load vector, L, completes the system description and is the subject of the remainder of this section.

B. UNSTEADY AERODYNAMICS

The development of the linearized, small disturbance partial differential equation for unsteady aerodynamic loads is presented in numerous textbooks and the presentation of Bisplinghoff, et al. [7], will be followed. The exact, nonlinear, unsteady flow partial differential equation satisfied by the velocity potential is

$$\nabla^2 \phi - \frac{1}{a^2}\left[\frac{\partial^2 \phi}{\partial t^2} + \frac{\partial q^2}{\partial t} + \bar{q} \cdot \text{grad}\left(\frac{q^2}{2}\right)\right] = 0 \qquad (2.2)$$

and the flow velocity is given by

$$\bar{q} = \nabla \phi \qquad (2.3)$$

where the ∇ and ∇^2 operators imply the use of dimensional coordinates

$$x^* = bx, \qquad y^* = by, \qquad z^* = bz . \qquad (2.4)$$

The flow velocity is related to the pressure through Kelvin's equation or the unsteady Bernoulli equation

$$\frac{\partial \bar{q}}{\partial t} + (\bar{q} \cdot \nabla)\bar{q} = -\frac{1}{\rho}\nabla p . \qquad (2.5)$$

Equations (2.1) through (2.3) are linearized by assuming that the fluid

-10-

velocity vector, $\bar{q}$, varies only slightly from the free-stream velocity, U. A disturbance velocity potential ϕ' is defined such that

$$\phi = \phi' + Ux^*$$

where the disturbance velocity components

$$u' = u - U = \frac{\partial\phi'}{\partial x^*}, \quad v = \frac{\partial\phi'}{\partial y^*}, \quad w = \frac{\partial\phi'}{\partial z^*}$$

are assumed to be small compared to U. Then the linearized partial differential equation for unsteady, compressible flow is

$$\nabla^2\phi' - \frac{1}{a_\infty^2}\frac{\partial^2\phi'}{\partial t^2} - \frac{2M}{a_\infty}\frac{\partial^2\phi'}{\partial x^*\partial t} - M^2\frac{\partial^2\phi'}{\partial x^{*2}} = 0 \qquad (2.6)$$

subject to the boundary conditions

$$w^* = \frac{\partial z_U^*}{\partial t} + U\frac{\partial z_U^*}{\partial x^*}, \qquad -b \leq x^* \leq b \qquad (2.7)$$

$$w^* = \frac{\partial z_L^*}{\partial t} + U\frac{\partial z_L^*}{\partial x^*}, \qquad -b \leq x^* \leq b \qquad (2.8)$$

where $z_U^*(x^*, t)$ and $z_L^*(x^*, t)$ describe the location of the upper and lower surfaces of the section as shown in Fig. II-2. The linearized version of (2.5) gives the pressure coefficient

$$c_p = \frac{p-p_\infty}{\frac{1}{2}\rho_\infty U^2} = -\frac{2}{U^2}\frac{\partial\phi'}{\partial t} - \frac{2}{U}\frac{\partial\phi'}{\partial x^*} \qquad (2.9)$$

yielding the pressures on the top and bottom surfaces of the airfoil as

-11-
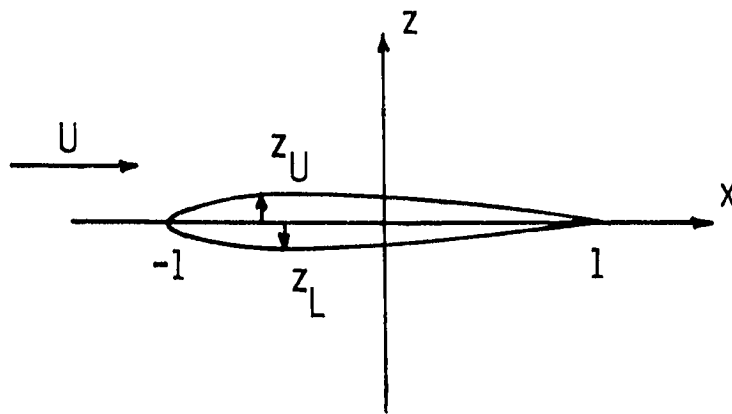
FIG. II-2   CROSS SECTION OF A THIN AIRFOIL

$$p_U - p_\infty = -\rho_\infty U \frac{\partial}{\partial x^*} \phi'(x^*, 0^+, t) - \rho_\infty \frac{\partial}{\partial t} \phi'(x^*, 0^-, t) \qquad (2.10)$$

$$p_L - p_\infty = -\rho_\infty U \frac{\partial}{\partial x^*} \phi'(x^*, 0^-, t) - \rho_\infty \frac{\partial}{\partial t} \phi'(x^*, 0^-, t) \ . \qquad (2.11)$$

Since the governing differential equation, (2.6) is linear, the solution may be constructed as a super-position of elementary solutions. The airfoil profile may be separated into a portion representing thickness, z_t^*, and a portion representing angle-of-attack and camber, z_a^*

$$z_U^* = z_a^* + z_t^* \qquad (2.12a)$$

$$z_L^* = z_a^* - z_t^* \ . \qquad (2.12b)$$

The thickness distribution, z_t^*, represents a symmetrical airfoil at zero incidence and, by symmetry, can provide no lift or pitching moment.

-12-

The distribution, z_a^*, represents a cambered, zero thickness, inclined mean line which produces the lift and pitching moments acting on the airfoil. This distribution may be further separated into a steady portion containing the airfoil camber and a nonsteady, mean-line portion nominally at zero angle-of-attack. It is the latter, 'flat-plate' airfoil which is the starting point for linearized, unsteady aerodynamic theory. Henceforth, $z_a^*(x^*, t)$ refers to this flat-plate airfoil and ϕ will be the velocity potential satisfying (2.6) subject to the boundary condition

$$ w_a^*(x^*, t) \equiv w^* = \frac{\partial z_a^*}{\partial t} + U \frac{\partial z_a^*}{\partial x^*} \quad . \tag{2.13} $$

The flow prescribed by this boundary condition is antisymmetrical with respect to the x-y plane, as described in Bisplinghoff [52], and the perturbation pressures at corresponding points on the top and bottom satisfy $p_U(x^*, 0^+, t) = -p_L(x^*, 0^-, t)$. Thus the pressure difference acting on the airfoil, positive for downward loading, is

$$ p(x^*, t) = p_U - p_L = -2\rho_\infty U \frac{\partial}{\partial x^*} \phi(x^*, 0^+, t) - 2\rho_\infty \frac{\partial}{\partial t} \phi(x^*, 0^-, t). \tag{2.14} $$

The aerodynamic loads acting on the airfoil are determined by integrating this pressure difference over appropriate portions of the airfoil.

$$ P = \int_{-b}^{b} p(x^*, t) dx^* \tag{2.15} $$

$$ M^\alpha = \int_{-b}^{b} (x^* - ab) p(x^*, t) dx^* \tag{2.16} $$

$$ M^\beta = \int_{cb}^{b} (x^* - cb) p(x^*, t) dx^* \tag{2.17} $$

$$ M^\gamma = \int_{-b}^{db} (db - x^*) p(x^*, t) dx^* \quad . \tag{2.18} $$

-13-

The method of solution of (2.6) depends upon the aerodynamic regime under investigation. In incompressible flow, $M = 0$, and the equation reduces to Laplace's equation

$$\nabla^2 \phi = 0 \qquad\qquad (2.19)$$

which is an elliptic partial differential equation. In subsonic and super-sonic flows, the equation becomes one of hyperbolic type. The solution of the partial differential equation has traditionally been simplified by assuming that the airfoil is undergoing simple harmonic oscillations in the various degrees of freedom, thus removing one of the independent variables, t. Further simplification of (2.6) results if two-dimensional flow is assumed, making the equations independent of the span-wise coordinate, y.

C. TWO-DIMENSIONAL, INCOMPRESSIBLE UNSTEADY AERODYNAMICS FOR SIMPLE HARMONIC MOTIONS

A solution of (2.6) was first obtained for the case of two-dimensional airfoils undergoing simple harmonic oscillations in incompressible flow. Theodorsen [11] was the first to publish the complete solution, although many other authors obtained similar results independently during the same period. Bisplinghoff et al. [52], and Garrick [53, 54] present summaries of the various authors and techniques. Appendix B contains a summary of Theodorsen's derivation as presented in Ref. 52. The solution consists of a superposition of flows due to a source-sink distribution, a bound vortex distribution along the chord, and a wake vortex sheet distribution convected downstream from the trailing-edge. The Kutta condition of smooth flow at the trailing-edge is enforced by Eq. (B.16),

$$Q = -\frac{1}{2\pi} \int_1^{1+\sigma} \sqrt{\frac{\xi+b}{\xi-b}} \, \gamma_w(\xi,\sigma) d\xi \; . \qquad (B.16)$$

Equation B.17, giving the circulatory lift, is representative of the integral equations involved in the unsteady loads

$$P_c = \rho b U \int_1^{1+\sigma} \sqrt{\frac{\xi}{\xi^2-1}} \; \Upsilon_w(\xi,\sigma) d\xi \quad . \qquad (B.17)$$

To proceed with the solution, Theodorsen assumed

(1) The airfoil motion, $w_a^*(x^*,t)$ consisted of simple harmonic oscillations (Eq. B.21), producing the wake vortex distribution given by (B.22);

(2) The motion had been sustained for an indefinitely long period, allowing the upper limits on the integrals in (B.16) through (B.18) to be replaced by ∞ .

It was then possible, using an integral representation of the modified Bessel function $K_\nu(s)$ (equivalent to Eq. B.28) to evaluate the ratios of integrals occurring in Eqs. B.24 and B.25 as

$$C(ik) = \frac{H_1^{(2)}(k)}{H_0^{(2)}(k) + iH_0^{(2)}(k)} = \frac{K_1(ik)}{K_0(ik) + K_1(ik)} \quad . \qquad (B.32)$$

The restriction on the use of the integral representation of $K_\nu(s)$, $\mathrm{Re}(s) > 0$, is not mentioned in the early references dealing with the subject. This restriction, in connection with the assumed airfoil motions (B.21 and B.22), implies the oscillatory divergent motion and wake vortex distribution shown in Fig. II-3a. The analysis so far presented would thus appear to be inapplicable to the convergent oscillations shown in Fig. II-3b. The fact that the theory agreed with experimental observations of flutter boundaries (e.g., Theodorsen and Garrick, Ref. 18) explains the acceptance of the theory for $\mathrm{Re}(s) = 0$ (purely simple harmonic oscillations), although the integrals upon which the theory is based are then divergent.

The simple harmonic loads acting on the airfoil are given by (B.35) and (B.36) as
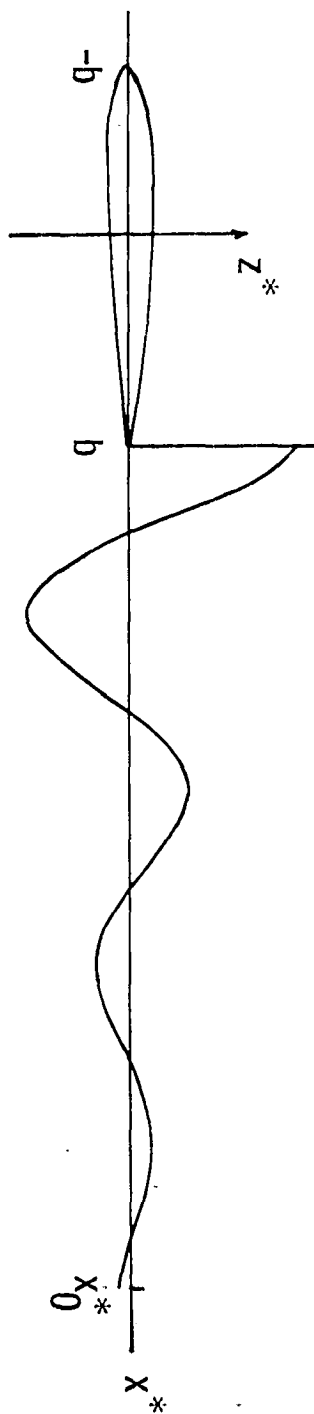
(a) DIVERGENT AIRFOIL OSCILLATIONS
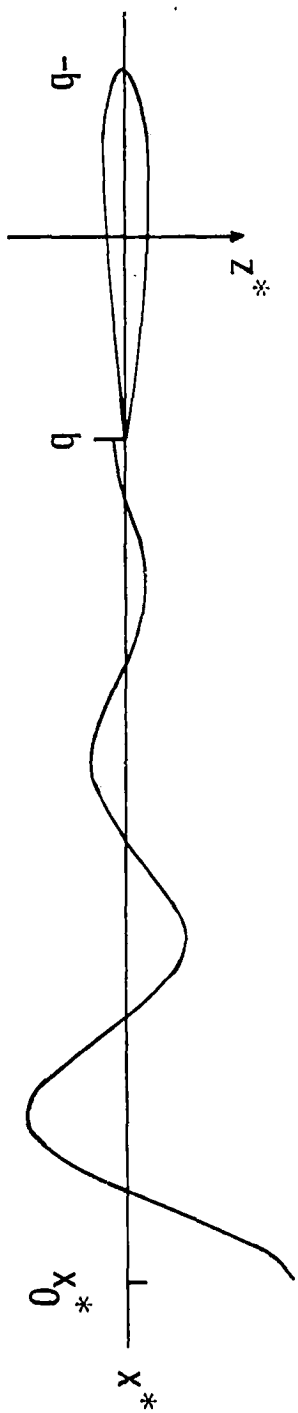
(b) CONVERGENT AIRFOIL OSCILLATIONS

FIG. II-3   WAKE VORTEX DISTRIBUTIONS CAUSED BY DIVERGENT AND CONVERGENT AIRFOIL OSCILLATIONS

$$L(ik) = \rho b^2 U^2 \left\{ -k^2 M_{nc} + ik(B_{nc} + C(ik)RS_2) + (K_{nc} + C(ik)RS_1) \right\} \underline{x}_o e^{ik\ell'} \tag{2.20}$$

where $\underline{x}(x,\ell') = \underline{x}_o e^{ik\ell'}$. Equation (2.1) specialized to simple harmonic oscillations and with $u = 0$ is then

$$\left\{ (M_s - \eta M_{nc}) + i\left[-\frac{1}{\omega} B_s + \frac{\eta}{k} (B_{nc} + C(ik)RS_2) \right] \right.$$
$$\left. + \left[-\frac{1}{\omega^2} K_s + \frac{\eta}{k^2}(K_{nc} + C(ik)RS_1) \right] \right\} \underline{x}_0 = 0 \tag{2.21}$$

where $\eta = 1/\pi\mu$.

For a section with n degrees of freedom, (2.21) is an nth order matrix equation which has a nontrivial solution only if the determinant of the matrix of coefficients is zero. For a given airfoil section, (2.21) is a function of μ, ω, and k, and the determinant of the coefficients yields a complex equation. A method of solving this equation is to assume values of μ and k (allowing the aerodynamic loads to be calculated) and factor the resulting real and imaginary equations, giving two sets of n values of ω. In general, a given value of ω will not be a factor of both equations, and the process is repeated for other values of k until a value is determined for which the real and imaginary parts of the determinant have a common factor, ω_f, the flutter frequency. The smallest value of U corresponding to a solution is called the flutter speed given by $U_f = \omega_f b / k_f$. This method of solution, termed Theodorsen's method, is described in Refs. 11 and 55.

An alternative method of solution which is more commonly used is the $U - g$ method described in Refs. 19 and 52. The artificial structural damping, g, is introduced by replacing the real quantity, $(1/\omega)^2$, with the complex factor

$$Z = \left(\frac{1}{\omega}\right)^2 (1 + ig) . \tag{2.22}$$

For a given choice of μ and k, (2.21) now represents a complex eigenvalue problem for the unknown, Z. With the eigenvalues, Z, determined,

the corresponding frequency, velocity, and structural damping are determined by

$$\omega_f^2 \; = \; \frac{1}{\text{Re}(Z)} \tag{2.23}$$

$$U_f \; = \; \frac{\omega_f b}{k} \tag{2.24}$$

$$g \; = \; \frac{\text{Im}(Z)}{\text{Re}(Z)} \; . \tag{2.25}$$

The critical flutter point is determined by the values of μ and k yielding a value of g equal to the assumed structural damping (usually zero).

The $U - g$ method is commonly used to perform flutter calculations for compressible flow in which case the Mach number is an additional independent variable. In this case, the calculated flutter speed U_f may not correspond to the density (altitude) and Mach number assumed in performing the claculations and the analysis must be repeated at several Mach numbers so that a "matched flutter point" may be determined by crossplotting the results.

It is obvious that a great deal of the calculation required to determine a flutter point is of limited further value since the conditions corresponding to the intermediate solutions are unphysical. Further, the resulting flutter boundaries give quantitative results only for the case of neutral stability (simple harmonic oscillations). The information concerning the subcritical and supercritical flutter conditions is qualitative at best. The cause of this situation is the assumption of simple harmonic motion in the calculation of the unsteady aerodynamic loads. Hence, an investigation of the possibility of calculating airloads for arbitrary motions is appropriate.

D. THE GENERALIZED THEODORSEN FUNCTION

Attempts to generalize the Theodorsen function by evaluating $C(ik)$ for complex values of k were made by W.P. Jones [20], and Luke and Dengler [21]. Jones concluded that $C(ik)$ could be generalized for

-18-

diverging airfoil motions (see Fig. II-3a), but not for damped converging motions (Fig. II-3b). Still, on the basis of numerical calculations and claiming that $C(ik)$ could be analytically continued into the left-half plane, Luke and Dengler published tables of $C(sb/U)$ for $s = \sigma + i\omega$, $\sigma < 0$. However, they did not offer a proof of this extension and in a series of replies [Van de Vooren, 22], [Laitone, 23], [W.P. Jones, 24], [Change, 26], their claim was rejected.

Earlier, Sears [56] had used the technique of Laplace transformation to obtain new derivations of indicial loading functions. Sears' presentation is essentially a derivation of the generalized Theodorsen function although this is not discussed in Ref. 56. No mention is made [56] of criteria for the existence of integrals nor of the evaluation of $C(ik)$ for complex values of k.

The generalized Theodorsen function will be derived in a form closely following Sears [56]. Assume that the airfoil was undisturbed prior to $t = 0$ $[w_a^*(x^*,t) = 0, \ t < 0]$ and that the airfoil motion has endured for $t = (x_0^* - b)/U$ sec, producing a wake that extends from $x^* = b$ to $x^* = x_0^*$ as shown in Fig. II-3. It is assumed that the airfoil motion $w_a^*(x^*,t)$ and the wake vortex distribution $\gamma_w(\xi^*,t)$ are Laplace transformable functions. Making the change of variables $\xi^* = x_0^* - Ut$ in (B.16) and (B.17) gives

$$Q = -\frac{U}{2\pi b} \int_0^\tau \sqrt{\frac{(\tau-t) + \frac{2b}{U}}{\tau-t}} \ \gamma_w(t)dt \tag{2.26}$$

$$P_c = \rho U^2 \int_0^\tau \sqrt{\frac{(\tau-t) + \frac{b}{U}}{(\tau-t)^2 + \frac{2b}{U}(\tau-t)}} \ \gamma_w(t)dt \tag{2.27}$$

where $\tau = (x_0^* - b)/U$. The change of variables has the effect of making the wake vortex distribution $\gamma_w^*(\xi^*,t)$, a function of a single variable $\gamma_w(t)$. Equations (2.26) and (2.27) are convolution integrals, and since the Laplace transform of the convolution of two functions equals the

product of the transforms of the two functions [57], Eqs. (2.26) and (2.27) become

$$\mathcal{L}[Q(t)] = -\frac{U}{2\pi b} \mathcal{L}\left[\sqrt{\frac{t + 2b/U}{t}}\right] \cdot \mathcal{L}[\gamma_w(t)] \quad ; \qquad (2.28)$$

$$\mathcal{L}[P_c(t)] = \rho U^2 \mathcal{L}\left[\sqrt{\frac{t + b/U}{t^2 + (2b/U)t}}\right] \cdot \mathcal{L}[\gamma_w(t)] \quad ; \qquad (2.29)$$

where

$$\mathcal{L}\left[\sqrt{\frac{t + 2b/U}{t}}\right] = \int_0^\infty \sqrt{\frac{t + 2b/U}{t}} \; e^{-st} \, dt$$

$$= \frac{b}{U} e^{s(b/U)} \int_1^\infty \sqrt{\frac{t + 1}{t - 1}} \; e^{-(sb/U)t} \, dt$$

$$= \frac{b}{U} e^{sb/U} \left[K_0\left(\frac{sb}{U}\right) + K_1\left(\frac{sb}{U}\right)\right], \; \text{Re}(s) > 0 \quad ; \qquad (2.30)$$

$$\mathcal{L}\left[\sqrt{\frac{t + b/U}{t^2 + (2b/U)t}}\right] = \int_0^\infty \sqrt{\frac{t + b/U}{t^2 + (2b/U)t}} \; e^{-st} \, dt$$

$$= \frac{b}{U} e^{sb/U} \int_1^\infty \sqrt{\frac{t}{t^2 - 1}} \; e^{-(sb/U)t} \, dt$$

$$= \frac{b}{U} e^{sb/U} K_1\left(\frac{sb}{U}\right), \quad \text{Re}(s) > 0 \; . \qquad (2.31)$$

In evaluating these expressions, the change of variables $t' = (Ut/b) + 1$ and (B.29) and (B.30) were employed. Eliminating $\mathcal{L}[\gamma_w]$ from (2.28) and (2.29)

$$\mathcal{L}[P_c(t)] = -2\pi\rho bUC(\tilde{s})\mathcal{L}[Q(t)] \tag{2.32}$$

where

$$C(\tilde{s}) = \frac{K_1(\frac{sb}{U})}{K_0(\frac{sb}{U}) + K_1(\frac{sb}{U})} \tag{2.33}$$

and

$$\tilde{s} = \frac{sb}{U} .$$

The Bessel functions in (2.33) are defined and analytic throughout the s-plane except for a branch point at the origin and a branch cut along the negative real axis [Sect. 9.6, p. 374, Ref. 58], and by analytic continuation [57], $C(\tilde{s})$ is the unique operator relating $Q(s)$ and $L_c(s)$ throughout the s-plane (except along the branch cut). The principal branch of the Bessel function will be taken as $-\pi < \arg s \leq \pi$ and with the restriction on the real part of s removed, (2.33) defines the generalized Theodorsen function. Setting $\tilde{s} = ik$ recovers the Theodorsen function, (B.31). The remaining unsteady loads $(M^\alpha, M^\beta, \text{and } M^\gamma)$ all involve the same ratio of integrals treated above, and the generalized Theodorsen function can be incorporated into the aerodynamic load expressions by replacing $C(ik)$ by $C(\tilde{s})$ in (B.33) and (B.36).

For small values of $|\tilde{s}|$, $K_0(\tilde{s})$ and $K_1(\tilde{s})$ are readily calculated by their ascending power series expansions which are given in App. D. With $\tilde{s} = \tilde{r}e^{i\vartheta}$ and $C(\tilde{s}) = F + iG$, the real and imaginary parts of $C(\tilde{s})$ are plotted in Fig. II-4 which extends the figure given by Luke and Dengler [21] to $\vartheta = +60°$ and $\vartheta = +180°$. The Theodorsen function is given by the curves for $\vartheta = 90°$ corresponding to the imaginary axis. As $\tilde{r} \to 0$, $C(\tilde{s}) \to 1$ and as $\tilde{r} \to \infty$, $C(\tilde{s}) \to 0.5$ independent of ϑ. The maximum value of C remains in the range $0.2 < \tilde{r} < 0.25$ independent of ϑ and increases monotonically as ϑ increases to $180°$.
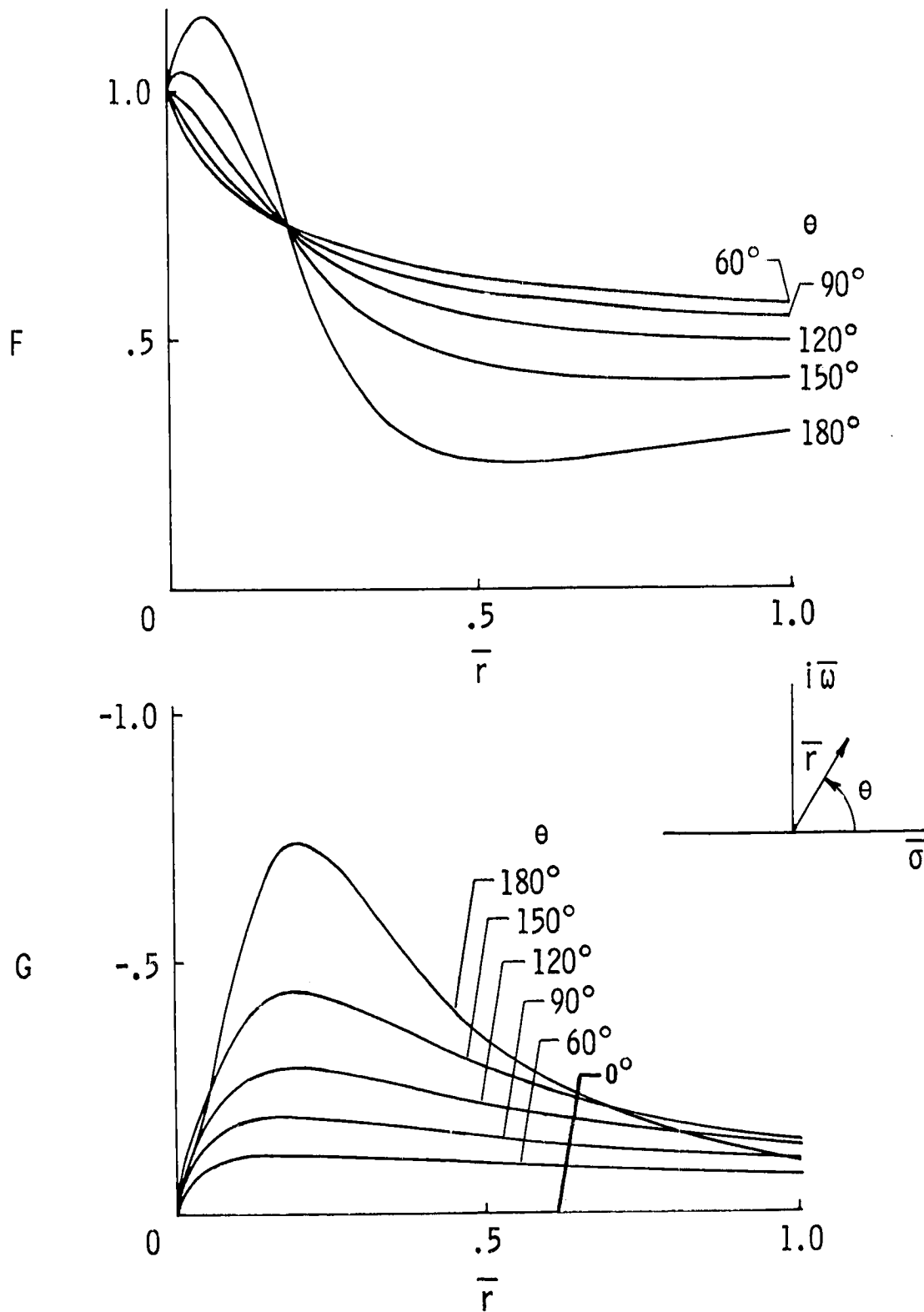
FIG. II-4   THE GENERALIZED THEODORSEN FUNCTION $C(\bar{s}) = F + iG$

Note $F(-\theta)$ $F(\theta)$, $G(-\theta)$ $-G(\theta)$.

Equation (2.32) indicates that $C(\bar{s})$ is to be regarded as a frequency domain operator or transfer function relating $Q(s)$ to $L_c(s)$. Equation (2.32) also proves that the Wagner function and $C(\bar{s})/\bar{s}$ form a Laplace transform pair as implied by R.T. Jones [29] and Goland [59], and proven by Sears [56]. For Wagner's problem, $Q(\bar{s}) = 1/\bar{s}$ and

$$\mathcal{L}[k_1(\sigma)] = -\frac{2\pi\rho bUC(\bar{s})}{\bar{s}} \quad .$$

It is interesting to note that Sears' development of this relation implicitly involved analytic continuation of $C(\bar{s})$ through the deformation of the inversion integral contour into the left half-plane, although Sears does not comment upon this point. Although Sears states that his method is applicable to arbitrary airfoil motions, it seems that his intent was to perform such calculations via the convolution integral, using exponential approximations to the indicial load functions as shown by R.T. Jones [29].

Equation (2.32) indicates that the transforms of the aerodynamic loads will be multiple-value functions due to the branch point of $C(\bar{s})$ at the origin. It is of interest to note that $Q(s)$ may contribute branch points also although this is not the case for typical airfoil motions.

Two additional derivations of the generalized Theodorsen function are available and are presented in App. D. The first derivation was given by W.P. Jones [20], while the second is based on the convolution integral.

An outline of the calculation of transient unsteady aerodynamics, and a discussion of the difficulties in earlier interpretations of $C(\bar{s})$, are offered in App. E.

The Laplace transforms of the unsteady aerodynamic loads and the airfoil equations of motion for arbitrary motions are given by (2.20) and (2.21) with ik replaced by $\bar{s}$

$$L(s) = \rho b^2 U^2 \left\{ M_{nc}\bar{s}^2 + [B_{nc} + C(\bar{s})RS_2]s + [K_{nc} + C(\bar{s})RS_1] \right\} \underline{X}(s) \quad , \qquad (2.34)$$

-23-

$$\left\{ (M_s - \eta M_{nc})s^2 + \left[B_s - \eta\left(\frac{U}{b}\right)(B_{nc} + C(\bar{s})RS_2) \right] s \right.$$

$$\left. + \left[K_s - \eta\left(\frac{U}{b}\right)^2 (K_{nc} + C(\bar{s})RS_1) \right] \right\} \underline{X}(s) = G\mathcal{U}(s) . \qquad (2.35)$$

Equations (2.34) and (2.35) are matrix polynomial functions of s whose coefficient matrices contain the nonrational function $C(\bar{s})$. (A rational functions of s is a function which can be expressed as a ratio of polynomials in s, [p. 60, Ref. 57].) In inverting these expressions, attention must be given to the branch cut of $C(\bar{s})$ along the negative real axis.

E. INVERSION INTEGRAL FOR UNSTEADY AERODYNAMIC LOADS

The time histories of the unsteady aerodynamic loads can be determined from (2.34) using the Laplace inversion integral [57]. To simplify the expressions, the unsteady lift, P(t), will be considered for two degree-of-freedom plunging and pitching motions. Equation (2.34) gives the transformed lift for this case as

$$P(s) = -\pi\rho b^3 \left[s^2 h(s) + \left(\frac{U}{b}\, s - as^2\right)\alpha(s) \right] - 2\pi\rho b U C(\bar{s})Q(s) \qquad (2.36)$$

where

$$Q(s) = sbh(s) + U\alpha(s) + b(\tfrac{1}{2}-a)s\alpha(s) . \qquad (2.37)$$

The inversion integral gives

$$P(t) = \frac{1}{2\pi i} \int_{\sigma_1 - i\infty}^{\sigma_1 + i\infty} P(s)e^{st}\, ds \qquad (2.38)$$

where σ_1 is to be chosen greater than all singularities of the integrand. The first expression in (2.36) is the noncirculatory lift, P_{nc}, and may

-24-

be inverted directly. The generalized Theodorsen function may be written in terms of the lift deficiency function $\phi(\bar{s})$ introduced by Von Karman and Sears [60] as

$$C(\bar{s}) = 1 - \phi(\bar{s}) \underline{\qquad} \tag{2.39}$$

$$\phi(\bar{s}) = \frac{K_o(\bar{s})}{K_o(\bar{s}) + K_1(\bar{s})} \cdot \tag{2.40}$$

Substituting in (2.38)

$$
\begin{aligned}
P(t) &= -\pi\rho b^3\left[\ddot{h} + \frac{U}{b}\dot{\alpha} - a\ddot{\alpha}\right] - 2\pi\rho bU\left[\dot{h}b + U\alpha + b(\tfrac{1}{2} - a)\dot{\alpha}\right] \\
&\quad - \rho bUi \int_{\sigma_1 - i\infty}^{\sigma_1 + i\infty} \phi(\bar{s})Q(s)e^{st}\,ds \quad.
\end{aligned}
\tag{2.41}
$$

The second term in (2.41) gives the "quasi-steady" lift P_{qs} which results from ignoring the effect of the wake while the third term gives the effect of the wake. The integral may be simplified by the deformation of the contour of integration [56] shown in Fig. II-5. The portions of the contour from a to b and from c to d lie above and below the branch cut of $\phi(\bar{s})$ along the negative real axis thus making the integrand single-valued within the contour. The damped complex conjugate poles shown in the figure are representative of the singularities which may be intro-duced by $Q(s)$. Sears treated the case of a step change in circulation $[Q(s) = 1/s]$, and proved that $C(s)/s$ has no singularities within the contour given by N, N_1, N_2, and the branch cut a-b, b-c, c-d. Thus the integrand is analytic at every point within the deformed contour and by Cauchy's integral theorem [57], the integral around the contour is zero. If $Q(s)$ is Laplace transformable, then the integrals along the semicircular arcs, N_1 and N_2 go to zero as the radius goes to infinity. The integrals along the cuts from N_1 and N_2 to the poles cancel since the integrand is continuous along these paths, while the circular paths of infinitesimal radius around the poles give $2\pi i$ times the residues of $[C(s)Q(s)e^{st}]$ at the poles. Therefore, the integral along the path
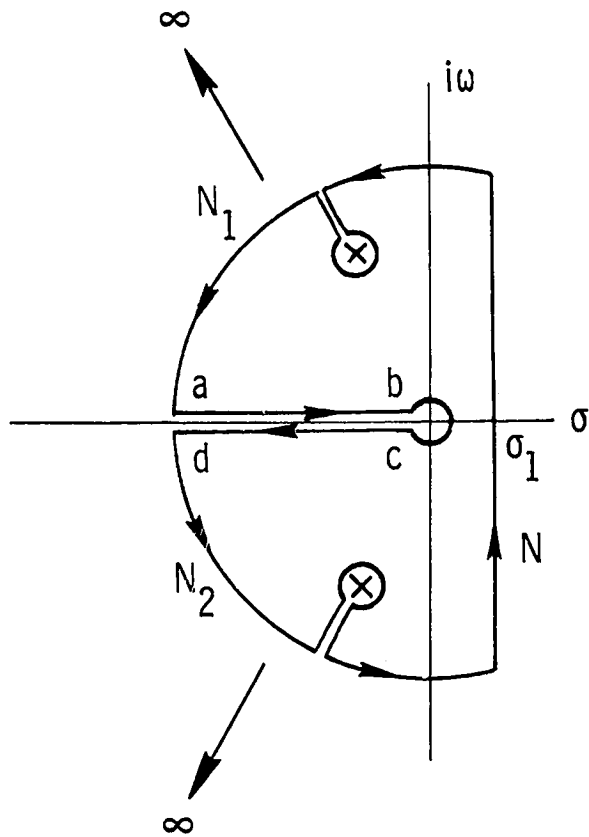
FIG. II-5   CONTOUR DEFORMATION USED TO EVALUATE
INVERSION INTEGRAL FOR INCOMPRESSIBLE
FLOW

N   is equal to

$$\int_N f(s)ds \;=\; \int_a^b f(s)ds \;-\; \int_c^d f(s)ds \;+\; \int_c^b f(s)ds$$

$$+\; 2\pi i \; \mathrm{Res}[f(s)]_{s=s_1} \;+\; 2\pi i \; \mathrm{Res}[f(s)]_{s=s_1^*} \tag{2.42}$$

where $f(s) = \phi(\bar{s})Q(s)e^{st}$.   Along   bc, $ds = \epsilon i e^{i\theta}d\theta$ and the third integral on the right-hand side is

$$\int_{-\pi}^{\pi} \phi\!\left(\frac{\epsilon b}{U}\, e^{i\theta}\right) Q\!\left(\epsilon e^{i\theta}\right) \epsilon i d\theta$$

which approaches zero as $\epsilon \to 0$ if $Q(s) \to \infty$ no faster than $1/s$ as $s \to 0$ which will be assumed henceforth. Along   ab, $s = re^{i\pi}$ while along   cd, $s = re^{-i\pi}$ and

$$\int_N \phi(\bar{s})Q(s)e^{st}ds \;=\; -\int_0^\infty \left[\phi\!\left(\frac{rb}{U}\, e^{i\pi}\right) - \phi\!\left(\frac{rb}{U}\, e^{-i\pi}\right)\right] Q(re^{i\pi})e^{-rt}dr$$

$$+\; 2\pi i\left\{ \mathrm{Res}\left[\phi(\bar{s})Q(s)e^{st}\right]_{s=s_1} + \mathrm{Res}\left[\phi(\bar{s})Q(s)e^{st}\right]_{s=s_1^*} \right\}. \tag{2.43}$$

Using the expressions

$$K_o(re^{\pm i\pi}) \;=\; K_o(r) \mp \pi i I_o(r)$$

$$K_1(re^{\pm i\pi}) \;=\; -K_1(r) \mp \pi i I_1(r)$$

$$K_o(r)I_1(r) + I_o(r)K_1(r) \;=\; 1/r \,.$$

Sears [56] showed that the integral in (2.43) was

$$-2\pi i \int_0^\infty \left[(K_{o}-K_1)^2 + \pi^2(I_o+I_1)^2\right]^{-1} \frac{Q(re^{i\pi})}{rb/U} e^{-rt}dr$$

-27-

where rb/U is implied as the argument of the Bessel functions. Finally, the unsteady lift is

$$P(t) = P_{nc} + P_r + P_{nr} \tag{2.44}$$

where

$$P_{nc} = -\pi\rho b^3\left[\ddot{h} + \frac{U}{b}\dot{\alpha} - a\ddot{\alpha}\right] \tag{2.45}$$

$$P_r = -2\pi\rho bU\left[\dot{h}b+U\alpha+b(\tfrac{1}{2}-a)\dot{\alpha} - \sum_{i=1}^{n} \text{Res}\left(\phi(\bar{s})Q(s)e^{st}\right)_{s=s_i}\right] \tag{2.46}$$

$$P_{nr} = -2\pi\rho bU \int_0^\infty \frac{Q(re^{i\pi})e^{-rt}}{\bar{r}\left[(K_o - K_1)^2 + \pi^2(I_o + I_1)^2\right]}dr \tag{2.47}$$

and $\bar{r} = rb/U$. P_r and P_{nr} symbolize the rational and nonrational portions of the circulatory lift. The rational portion P_r is comprised of the quasi-steady circulatory lift P_{qs}, and a portion due to the residues of ϕQe^{st} at the poles of $Q(s)$. The summation in P_r is over all poles of $Q(s)$. Typical airfoil motions result in rational functions for $Q(s)$ which may be expanded by partial fractions into a sum of elementary transforms. The residues at the poles of the elementary transforms may then be calculated and used in (2.44). Table II-1 lists several standard functions, $Q(t)$, their transforms $Q(s)$, and residue sums required in the evaluation of $P_r(t)$.

Table II-1

ELEMENTARY FUNCTIONS AND CORRESPONDING RESIDUES

$Q(t)$	$Q(s)$	$\sum_{i=1}^{n} \text{Res}(\phi(s)Q(s)e^{st})_{s=s_i}$
$\delta(t)$	1	0
1	$1/s$	0
$e^{-\sigma t}$	$1/s+\sigma$	$(1-F)e^{-\sigma t}$
$e^{-\sigma t}\sin \omega t$	$\omega/(s+\sigma)^2+\omega^2$	$e^{-\sigma t}[(1-F)\sin \omega t - G\cos \omega t]$
$e^{-\sigma t}\cos \omega t$	$s+\sigma/(s+\sigma)^2+\omega^2$	$e^{-\sigma t}[(1-F)\cos \omega t + G\sin \omega t]$

-28-

In evaluating the residue for $Q(s) = 1/(s+\sigma)$ the contour must be indented at $s = -\sigma$ giving semicircular arcs of infinitesimal radius.

The integral expression for P_{nr}, (2.47), cannot be evaluated analytically for typical airfoil motions but its integrand is a well behaved function and the integral may be evaluated numerically. Figure II-6 is a plot of the denominator of the integrand

$$I = \left\{ \bar{r} \left[\left(K_o(\bar{r}) - K_1(\bar{r}) \right)^2 + \pi^2 \left(I_o(\bar{r}) + I_1(\bar{r}) \right)^2 \right] \right\}^{-1}. \qquad (2.48)$$

As an example of the use of (2.44), $P(t)$ is calculated for the case of a single DOF plunge motion (α pinned) with

$$Q(t) = U e^{-\sigma t} \sin \omega t .$$

The plunge motion yielding this function is

$$h(t) = \frac{U}{b(\sigma^2 + \omega^2)} \left[\omega - e^{-\sigma t}(\sigma \sin \omega t + \omega \cos \omega t) \right] \qquad (2.49)$$

and (2.44) through (2.47) and Table II-1 give

$$c_\ell = \frac{P(t')}{(\tfrac{1}{2}\rho U^2)(2b)} = 2\pi \left\{ \tfrac{1}{2} e^{-\bar{\sigma} t'}(\bar{\sigma} \sin \bar{\omega} t' - \bar{\omega} \cos \bar{\omega} t') - e^{-\bar{\sigma} t'}(F \sin \bar{\omega} t' + G \cos \bar{\omega} t') \right.$$

$$\left. - \int_o^\infty \left[(K_o - K_1)^2 + \pi^2 (I_o + I_1)^2 \right]^{-1} \frac{\bar{\omega} e^{-\bar{r} t'}}{\bar{r}[(-\bar{r} + \bar{\sigma})^2 + \bar{\omega}^2]} \, d\bar{r} \right\}$$

$$(2.50)$$
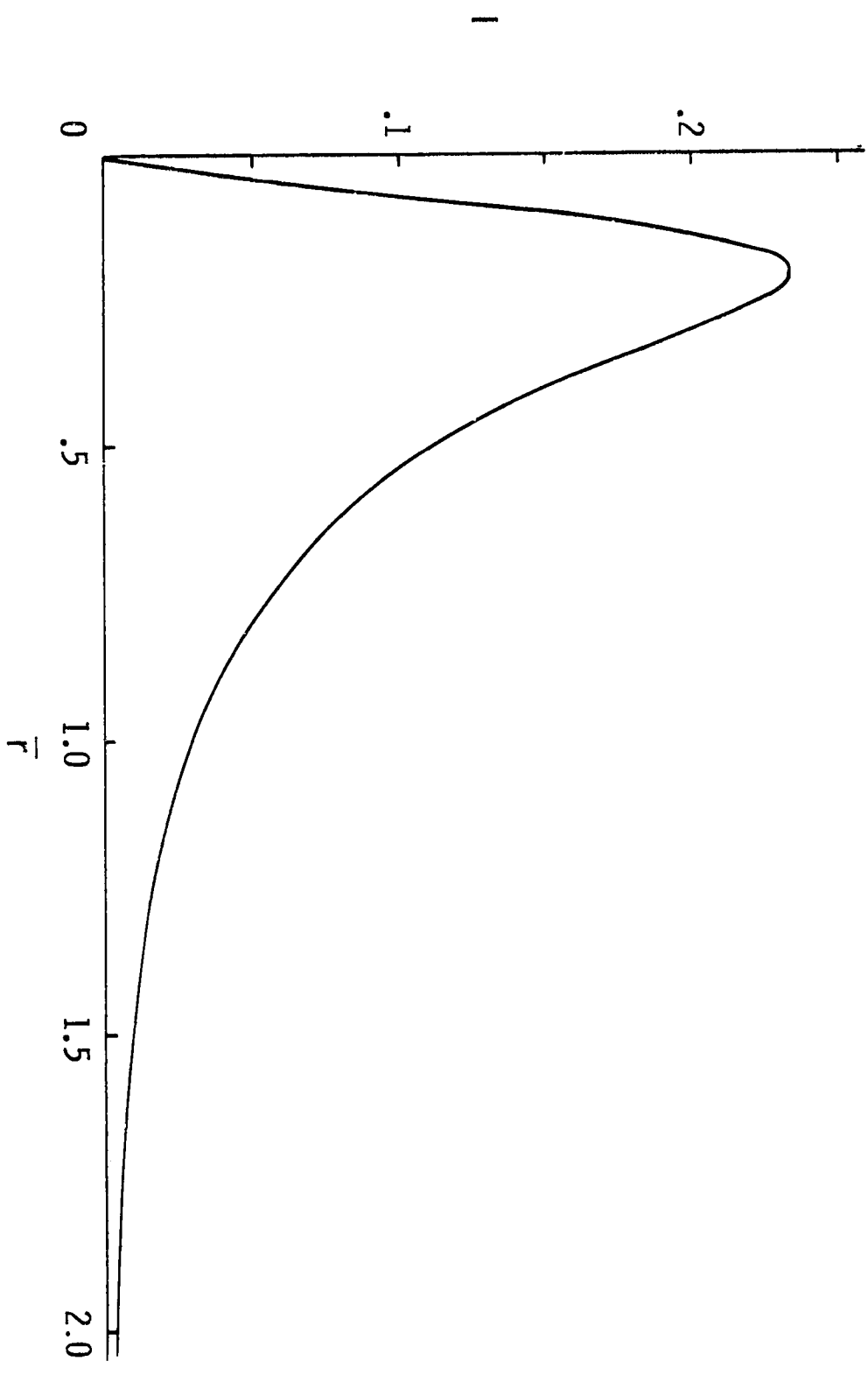
FIG. II-6   PLOT OF I VERSUS r̄

where $\bar{\sigma} = \sigma b/U$ and $\bar{\omega} = \omega b/U$. The three expressions on the right of (2.50) are $c_{\ell_{nc}}$, c_{ℓ_r}, and $c_{\ell_{nr}}$ respectively. Figure II-7 shows the total and component lift coefficients for $\bar{\sigma} = \bar{\omega} = 0.2/\sqrt{2}$ corresponding to a damped oscillation with 0.7 damping ratio, and 0.2 rad natural frequency. Since $Q(t)$ is continuous at $t = 0$, the circulatory lift must start at zero which requires that the rational and the nonrational portions of the lift cancel at $t = 0$. Figure II-7 shows this to be the case, with $c_\ell(0) = c_{\ell_{nc}}(0)$. The nonrational portion $c_{\ell_{nr}}$, decays quickly from its starting value for small t' but decays slowly to zero for large t' and is a monotonic function of t'.

A second example is a single DOF (degree of freedom) pitch-motion with

$$\alpha(t') \;=\; 1 - e^{\bar{\sigma}t'} \cos \bar{\omega}t' \;. \tag{2.51}$$

For this motion

$$Q(t') \;=\; U\left[1 - e^{-\bar{\sigma}t'}\cos\bar{\omega}t' + (\tfrac{1}{2}-a)e^{\bar{\sigma}t'}(\bar{\sigma}\cos\bar{\omega}t' + \bar{\omega}\sin\bar{\omega}t')\right]$$

and the resulting lift coefficient is

$$\begin{aligned}
c_\ell \;=\; 2\pi\Bigg\{ &-1 + e^{-\bar{\sigma}t'}\left(\left[F\left(1-\tfrac{\bar{\sigma}}{2}\right) - \tfrac{\bar{\omega}}{2}\,G\right]\cos\bar{\omega}t' + \left[G\left(\tfrac{\bar{\sigma}}{2} - 1\right) + \tfrac{\bar{\omega}}{2}\,F\right]\sin\bar{\omega}t'\right) \\
&+ \tfrac{1}{2}\,e^{-\bar{\sigma}t'}\left(\left[a(\bar{\omega}^2-\bar{\sigma}^2)-\bar{\sigma}\right]\cos\bar{\omega}t' - (2\bar{\sigma}\bar{\omega}a + \bar{\omega})\sin\bar{\omega}t'\right) \\
&+ \int_0^\infty \left[(K_0-K_1)^2 + \pi^2(I_0+I_1)^2\right]^{-1}\frac{1}{\bar{r}}\left[\frac{1}{\bar{r}} - \frac{(\tfrac{\bar{\sigma}}{2}-1)(-\bar{r}+\bar{\sigma})+\tfrac{\bar{\omega}^2}{2}}{(-\bar{r}+\bar{\sigma})^2+\bar{\omega}^2}\right]e^{-\bar{r}t'}\,d\bar{r}\Bigg\}\;.
\end{aligned}$$
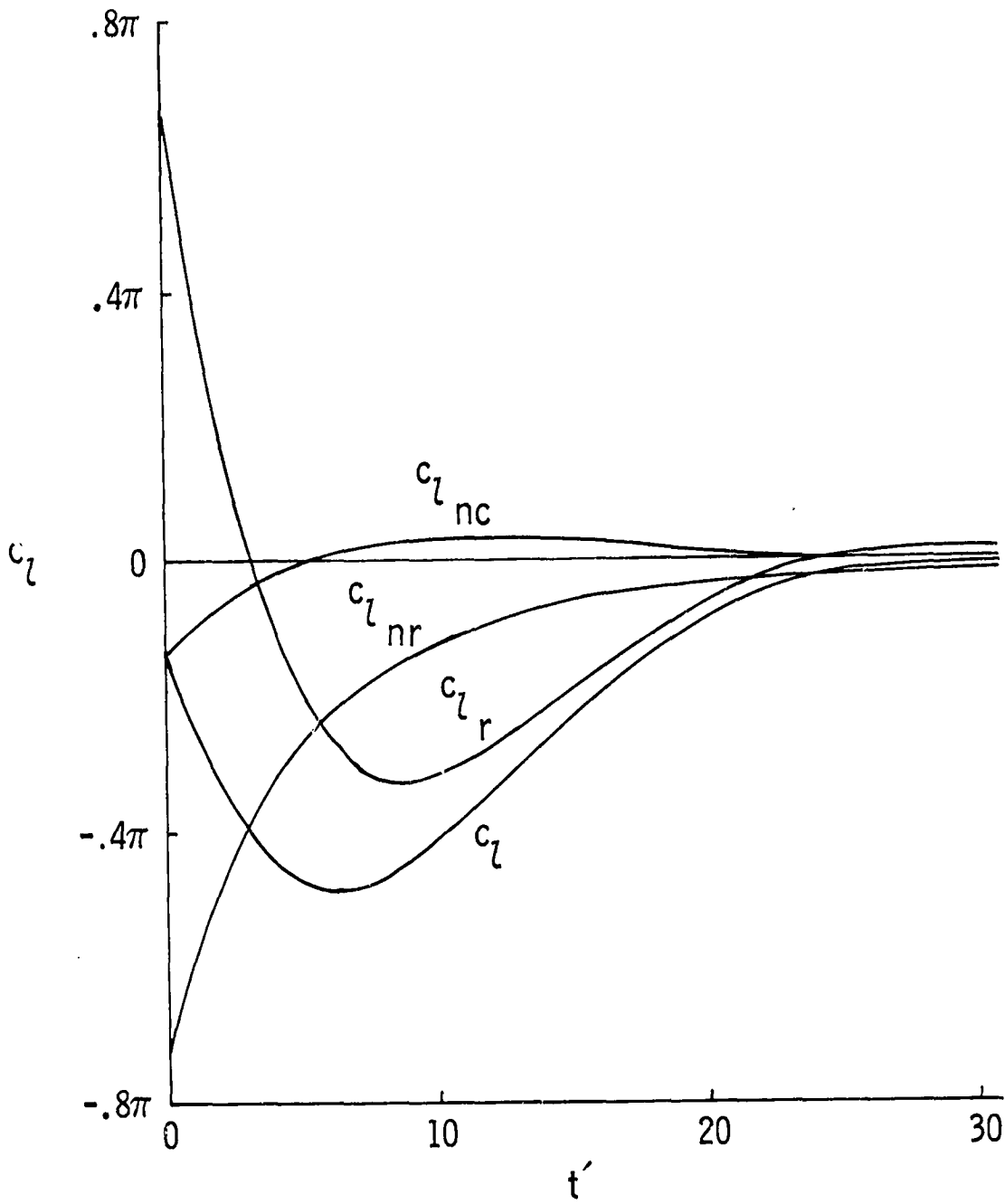
FIG. II-7   TOTAL AND COMPONENT LIFT COEFFICIENTS FOR THE
PLUNGE MOTION OF EQ. 2.49

Figure II-8 shows the total and component lift coefficients for $\bar{\sigma} = \omega =$ $0.2/\sqrt{2}$ and $a = 0$. For this case the value of $Q(t)$ at $t = 0$ is nonzero, indicating that the circulatory lift does not start at zero. This is evident in Fig. II-8 where it is seen that $c_{\ell_r}(0) \neq c_{\ell_{nr}}(0)$ and c_ℓ starts at a slightly larger value than $c_{\ell_{nc}}(0)$. Again, $c_{\ell_{nr}}$ decreases monotonically from its starting value and decays slowly to zero for large t'. At $t' = 30$, c_{ℓ_r} has settled to within 1% of its final value, while $c_{\ell_{nr}}$ has settled only to 16% of its final value and contributes 5% of the total lift.

From these two examples it is clear that the nonrational portion of the loads will dominate at large t' for stable airfoil motions. Thus the asymptotic behavior of the loads is of interest. Sears [56] studied the asymptotic behavior of the lift in Wagner's problem (step change in circulation) by using series expansions of the inversion integral integrand for small s since the behavior of $P(t)$ for large t is determined by the behavior of $P(s)$ for small s. The nonrational portion of the lift is given by the last term of (2.41)

$$P_{nr}(t) = \frac{2\pi\rho bU}{2\pi i} \int_{\sigma - i\infty}^{\sigma + i\infty} \phi(\bar{s})Q(s)e^{st}ds \ . \qquad (2.52)$$

Using the ascending power series for K_0 and K_1 given in App. F

$$\phi(s) = \frac{-\left[1 + \frac{\bar{s}^2}{4} + \cdots\right]\left(\log \frac{\bar{s}}{2} + \gamma_e\right) + \frac{\bar{s}^2}{4} + \cdots}{\frac{1}{\bar{s}}\left\{1 - \bar{s}\left(\log \frac{\bar{s}}{2} + \gamma_e\right) + \frac{\bar{s}^2}{2}\left(\log \frac{\bar{s}}{2} + \gamma_e - \frac{1}{2}\right) - \frac{\bar{s}^3}{4}\left(\log \frac{\bar{s}}{2} + \gamma_e - 1\right) + \cdots\right\}}$$

$$= -\bar{s}\left(\log \frac{\bar{s}}{2} + \gamma_e\right) - \bar{s}^2\left(\log \frac{\bar{s}}{2} + \gamma_e\right)^2 - \bar{s}^3\left\{\frac{1}{4}\left(\log \frac{\bar{s}}{2} + \gamma_e - 1\right)\right.$$

$$\left. - \frac{1}{2}\left(\log \frac{\bar{s}}{2} + \gamma_e - \frac{1}{2}\right)\left(\log \frac{\bar{s}}{2} + \gamma_e\right) + \left(\log \frac{\bar{s}}{2} + \gamma_e\right)^3\right\}$$

$$+ O\left(\bar{s}^4[\log \bar{s}]^4\right) \ . \qquad (2.53)$$

-33-
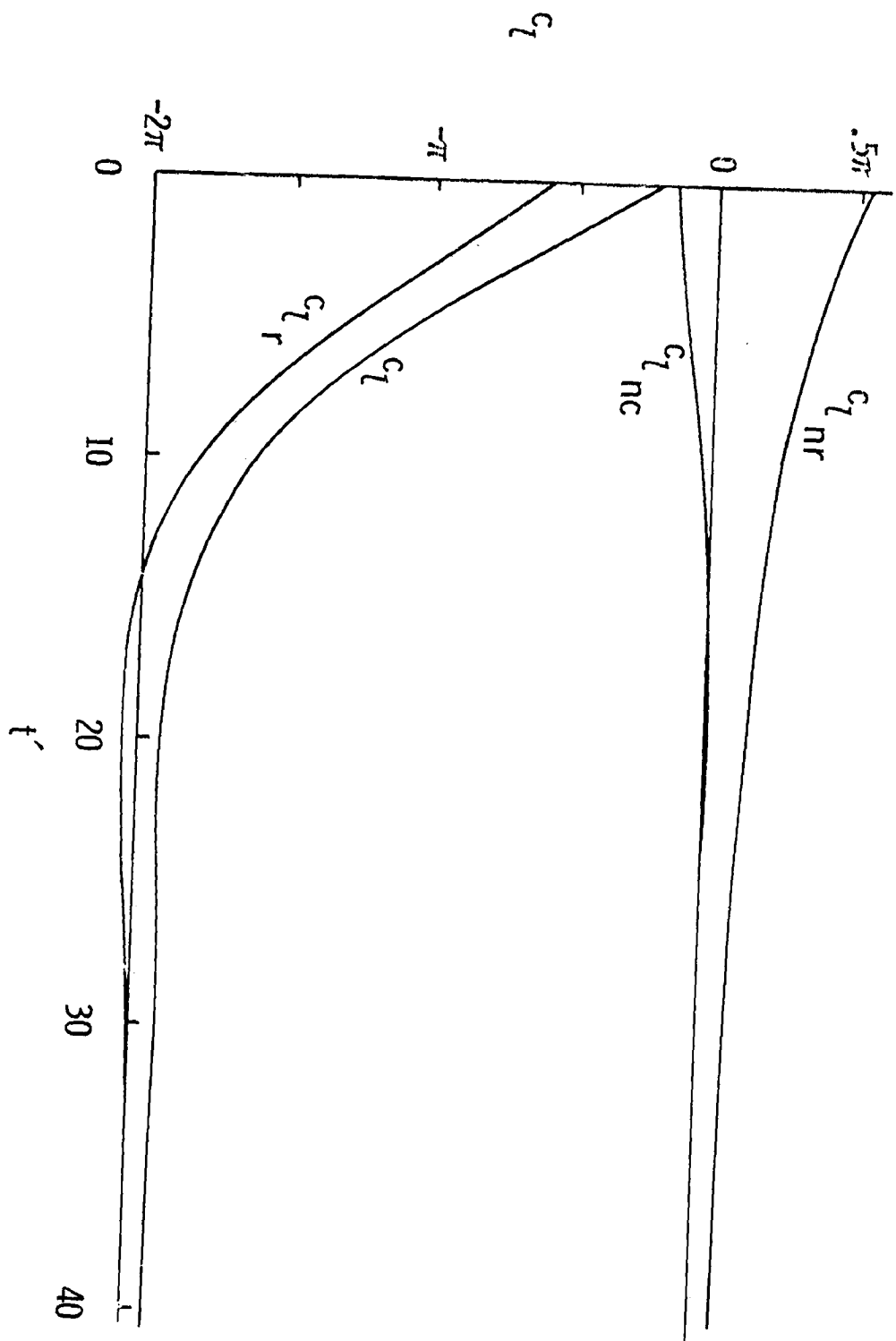
FIG. II-8   TOTAL AND COMPONENT LIFT COEFFICIENTS FOR THE TORSIONAL
MOTION OF EQ. 2.51

If $Q(s)$ is of the form

$$Q(s) = \frac{b_m \bar{s}^m + \cdots + b_1 \bar{s} + b_o}{a_n \bar{s}^n + a_{n-1} \bar{s}^{n-1} + \cdots + a_1 \bar{s} + 1} , \qquad m < n \qquad (2.54)$$

then for small s

$$Q(s) = (b_m \bar{s}^m + \cdots + b_1 \bar{s} + b_o)\left[1-(a_1 \bar{s} + \cdots + a_n \bar{s}^n) + (a_1 \bar{s} + \cdots + a_n \bar{s}^n)^2 - \cdots\right]$$

and the leading terms of $\phi(\bar{s})Q(s)$ are

$$\phi(\bar{s})Q(s) = -b_o \bar{s}(\log \frac{\bar{s}}{2} + \gamma_e) - (b_1 - b_o a_1)\bar{s}^2(\log \frac{\bar{s}}{2} + \gamma_e)$$

$$- b_o \bar{s}^2(\log \frac{\bar{s}}{2} + \gamma_e)^2 + \cdots . \qquad (2.55)$$

If $Q(s) = \bar{s}^n$ then the leading terms of $\phi(\bar{s})Q(s)$ are

$$\phi(\bar{s})Q(\bar{s}) = -\bar{s}^{n+1}(\log \frac{\bar{s}}{2} + \gamma_e) - \bar{s}^{n+2}(\log \frac{\bar{s}}{2} + \gamma_e)^2 + \cdots . \qquad (2.56)$$

Thus the asymptotic behavior of the loads is determined by operators of the form $\bar{s}^{n-1}[\log(\bar{s}/2) + \gamma_e]^m$. Sears evaluated (2.52) using this operator integrated along a deformed-contour. Sears' development involves the questionable step of utilizing expressions derived from the gamma function, $\Gamma(n)$, evaluated at negative integer values (where $\Gamma(n)$ is singular). Hence an alternative evaluation will be given which leads to the same results. Following Sears, the contour in (2.52) may be deformed as shown in Fig. II-5. The asymptotic lift for stable motions is given by the nonrational portion (the integral in (2.43) with $\phi(\bar{s})Q(s)$ given by (2.55) or (2.56). The expression which results from the operator $s^{n-1}[\log(\bar{s}/2) + \gamma_e]^m$ is

$$- \frac{1}{2\pi i} \int_{\infty}^{0} (\tilde{r} e^{-i\pi})^{n-1} \left[\log\left(\frac{\tilde{r} e^{-i\pi}}{2}\right) + \gamma_e \right]^m e^{-\tilde{r} t'} d\tilde{r}$$

$$- \frac{1}{2\pi i} \int_{0}^{\infty} (\tilde{r} e^{i\pi})^{n-1} \left[\log\left(\frac{\tilde{r} e^{i\pi}}{2}\right) + \gamma_e \right]^m e^{-\tilde{r} t'} d\tilde{r}$$

since the integral around the infinitesimal circle about the origin vanishes. For $m = 1$ this reduces to

$$- \frac{1}{2\pi i} \left\{ \int_{\infty}^{0} (-1)^{n-1} \tilde{r}^{n-1} \left(\log \frac{\tilde{r}}{2} - i\pi + \gamma_e \right) e^{-\tilde{r} t'} d\tilde{r} \right.$$

$$\left. + \int_{0}^{\infty} (-1)^{n-1} \tilde{r}^{n-1} \left(\log \frac{\tilde{r}}{2} + i\pi + \gamma_e \right) e^{-\tilde{r} t'} d\tilde{r} \right\}$$

$$= \frac{(-1)^n}{t'^n} \int_{0}^{\infty} \tilde{r}_1^{n-1} e^{-\tilde{r}_1} d\tilde{r}_1 = \frac{(-1)^n \Gamma(n)}{t'^n}$$

while for $m = 2$ the expression becomes

$$2(-1)^n \int_{0}^{\infty} \tilde{r}^{n-1} \log \frac{\tilde{r}}{2} e^{-\tilde{r} t'} d\tilde{r}$$

$$= \frac{2(-1)^n}{t'^n} \int_{0}^{\infty} \tilde{r}_1^{n-1} e^{-\tilde{r}_1} (\log \tilde{r}_1 - \log 2t') d\tilde{r}_1$$

$$= \frac{2(-1)^n}{t'^n} \left[\Gamma'(n) - \log(2t') \Gamma(n) \right]$$

since

$$\Gamma'(n) = \int_{0}^{\infty} \tilde{r}_1^{n-1} (\log \tilde{r}_1) e^{-\tilde{r}_1} d\tilde{r}_1 .$$

Thus, although $\bar{s}^{n-1}\left|\log(\bar{s}/2) + \gamma\right|^m$ does not possess a Laplace transform for $n \geq 1$, the inverse Laplace transform given by (2.52) can be evaluated asymptotically as $t' \to \infty$, and $\bar{s} \to 0$ in terms of this expression. The correspondence is

$$\bar{s}^{n-1}\left[\log \frac{\bar{s}}{2} + \gamma\right] \to \frac{(-1)^n \Gamma(n)}{t'^n} , \qquad\qquad n \geq 1; \qquad (2.57)$$

$$\bar{s}^{n-1}\left[\log \frac{\bar{s}}{2} + \gamma\right]^2 \to \frac{2(-1)^n}{t'^n}[\Gamma'(n) - \log(2t')\Gamma(n)], \quad n \geq 1 . \qquad (2.58)$$

Sears evaluated the asymptotic lift using the expression given in (2.56) with $n = 1$ (Wagner's problem) and obtained

$$c_{\ell_{nr}} \sim 2\pi\left(\frac{1}{t'} + \frac{2 \log (2t')}{t'^2} - \frac{2}{t'^2} + \cdots\right) .$$

Thus for step changes in $Q(t')$, the lift approaches its final value asymptotically as $1/t'$. For the airfoil motion given by (2.49), the asymptotic lift is found from (2.54) with $b_0 = \bar{\omega}/(\bar{\sigma}^2 + \bar{\omega}^2)$, $b_1 = 0$, and $a_1 = 2\bar{\sigma}/(\bar{\sigma}^2 + \bar{\omega}^2)$ giving

$$c_{\ell_{nr}} \sim \frac{-2\pi}{\bar{\sigma}^2 + \bar{\omega}^2}\left\{\frac{\bar{\omega}}{t'^2} + \frac{4\bar{\sigma}\bar{\omega}}{\bar{\sigma}^2 + \bar{\omega}^2}\frac{1}{t'^3} - \frac{2\bar{\omega}}{t'^3}\left(\Gamma'(3) - 2 \log(2t') + \cdots\right\} .$$

Thus stable airfoil motions for which $Q(s)$ is of the form of (2.54) approach final values asymptotically as $1/t'^2$. In Fig. II-7, $c_{\ell_{nr}} \sim (-\bar{\omega}/\bar{\sigma}^2 + \bar{\omega}^2)1/t'^2$, while in Fig. II-8, $c_{\ell_{nr}} \sim 1/t'$.

One further case of interest is that for which $Q(s) = \bar{s}^n$ with $n \leq -2$. An airfoil motion of this type is $\alpha = t'(n = -2)$. Then the leading term in (2.56) has an inverse Laplace transform given by

$$\mathcal{L}^{-1}\left[\frac{1}{-\bar{s}}\left(\log \frac{\bar{s}}{2} + \gamma_e\right)\right] = \log t'$$

and the asymptotic nonrational life coefficient is $c_{\ell_{nr}} \sim 2\pi \log t'$ while the rational lift coefficient is given exactly by $c_{\ell_r} = -2\pi t'$.

<div align="center">
F.   GENERALIZED COMPRESSIBLE AERODYNAMIC LOADS
</div>

F.1   General Formulation

When the flow is assumed to be compressible, the Mach number M becomes an additional independent variable and the governing partial differential equation, (2.6), is a hyperbolic equation. Solutions [15], [12] have been obtained by assuming simple harmonic motion and making the substitution $\phi(x, z, t) = \overline{\phi}(x,z)e^{i\omega t}$ which is equivalent to applying the Fourier integral transform [61] to the time variable of (2.6). In attempting to derive solutions for generalized motions, it is natural to apply the Laplace integral transformation. Defining

$$\Phi(x,z,s) = \int_0^\infty \phi(x\ z,t)e^{-st}\ dt \ .$$

(2.6) and (2.13) become

$$\Phi_{xx} + \Phi_{zz} - \frac{s^2}{a_\infty^2}\Phi - \frac{2Ms}{a_\infty}\Phi_x - M^2\Phi_{xx}$$

$$= -\frac{s}{a_\infty^2}\phi(x,z,0) - \frac{1}{a_\infty^2}\phi_t(x,z,0) - \frac{2M}{a_\infty}\phi_x(x,z,0) \ ;$$

(2.59)

$$\mathcal{L}[w_a(x,z,t)] = \Phi_z\Big|_{z=0} = s\mathcal{L}[z_a] - z_a(x,z,0) + U\frac{\partial}{\partial x}\mathcal{L}[z_a], \quad -b \le x \le b. \quad (2.60)$$

(The variables x and z are assumed to be dimensional throughout this section.) Let $\Phi = \Phi' + \Phi''$ with Φ'' a known function to be chosen such that

$$\Phi''_{xx} + \Phi''_{zz} - \frac{s^2}{a_\infty^2}\Phi'' - \frac{2Ms}{a_\infty}\Phi''_x - M^2\Phi''_{xx}$$

$$= -\frac{s}{a_\infty^2}\phi(x,z,0) - \frac{1}{a_\infty^2}\phi_t(x,z,0) - \frac{2M}{a_\infty}\phi_x(x,z,0) \ ,$$

(2.61)

<div align="center">
-38-
</div>

$$\left. \Phi''_z \right|_{z=0} \quad = \quad -z_a(x\ z,0) \ . \tag{2.62}$$

The equation for Φ' is then

$$\Phi'_{xx} + \Phi'_{zz} - \frac{s^2}{a_\infty^2}\Phi' - \frac{2Ms}{a_\infty}\Phi'_x - M^2\Phi'_{xx} \quad = \quad 0 \tag{2.63}$$

$$\left. \Phi'_z \right|_{z=0} \quad = \quad s\mathcal{L}[z_a] + U\frac{\partial}{\partial x}\mathcal{L}[z_a] \tag{2.64}$$

which is formally identical to the simple harmonic motion problem with the replacement of $i\omega$ by s.

Equation (2.63) is a homogeneous equation for Φ' whose boundary condition, (2.64), is linear with respect to $\mathcal{L}[z_a]$, while (2.61) is an inhomogeneous equation linear with respect to the initial condition $\phi(x,\ z,\ 0)$ and whose boundary condition (2.62) is linear with respect to the initial condition $z_a(x,\ z,\ 0)$. Hence the transformed loads $L(s)$ due to airfoil motions $\underline{X}(s)$ may be written as a matrix equation

$$L(s) \quad = \quad K'\underline{X}(s) + K''\underline{x}(0) \ . \tag{2.65}$$

It is interesting to note that for airfoil motions for which $z_a(x,\ z,\ 0) = z_{a_t}(x,\ z,\ 0) = 0$, Φ'' is identically zero and the entire solution is given by Φ'. Also, since stability of a linear system cannot be a function of initial conditions, the flutter problem is solely dependent upon Φ'.

The formal identity of the equations satisfied by $\bar{\phi}$ for simple harmonic motion and by Φ' for generalized motion implies that existing solutions of the simple harmonic motion problem may be applied directly to the determination of Φ' by the replacement of $i\omega$ by s. Thus the Mathieu function solution of Timman [12] can be generalized to provide solutions to (2.63) and (2.64).

It is anticipated that the decomposition indicated by (2.65) occurs in solutions based on the acceleration potential, ψ, since ψ and ϕ satisfy the same partial differential equation. Also, the generalization of the above Laplace transform method to finite wings in three-dimensional flow offers no difficulties. Thus programs based upon kernel function techniques [15], [17], [62], [16], may also be modified to calculate the Laplace transforms of generalized aerodynamic loads. It must be emphasized that the resulting transform is not the total solution, but corresponds to that portion of the solution which is linear in the transformed airfoil displacement modes.

F.2 Generalized Unsteady Supersonic Loads

In the case of two-dimensional supersonic flow, Garrick and Rubinow [13] obtained the solution for the simple harmonic loads using elementary solutions of (2.6) known as source pulses and gave the loads for the three degrees-of-freedom: plunge, pitch, and trailing-edge control surface. Hassig [63] extended Garrick's treatment to cover leading-edge control surfaces. The loads, due to arbitrary motion, which are linear in $\underline{X}(s)$ may be obtained from the expressions given by Garrick by the formal replacement of k by $-i\bar{s}$ as shown in the preceding section. (The resulting loads do not include those portions dependent upon the initial conditions of the motion.) The velocity potential of [13] on the upper surface of the airfoil becomes

$$\Phi(x,0^+,t) \;=\; \sqrt{\frac{b}{M^2-1}}\;\int_0^x w_a(\xi,s)\,e^{-(\bar{s}M/M^2-1)(x-\xi)}\,J_0\!\left[-i\frac{\bar{s}M}{M^2-1}(x-\xi)\right]d\xi \quad (2.66)$$

with the airfoil lying between $x = 0$ and $x = 1$.

Alternatively, (2.64) may be derived directly from (2.63) and (2.64) following the procedure of Stewartson [64] summarized in Ref. 7 [pp. 364-367]. Stewartson's procedure of Laplace transformation on x applied to (2.63) leads directly to (2.66) with the recognition of[†]

[†] $\mathcal{L}_x[\Phi(x,z,s)] \equiv \Phi(s_x, z, s)$

$$\mathcal{L}_x^{-1}\left[\sqrt{\dfrac{1}{s_x^2 - a_1^2}}\right] = I_0(a_1 x)$$

where $a_1 = \bar{s}M/a(M^2-1)$. Garrick's solution in terms of J_0 is recovered by use of the relations

$$I_0(s) = J_0(se^{\frac{1}{2}\pi i}) ; \qquad -\pi < \arg s \leq \tfrac{1}{2}\pi$$

$$I_0(s) = J_0(se^{-\frac{3}{2}\pi i}); \qquad \tfrac{1}{2}\pi < \arg s \leq \pi$$

and noting that the Bessel function J_0 is single valued. Thus the above inverse transform is

$$J\left(-i\,\frac{\bar{s}M}{(M^2-1)}\,x\right)$$

verifying (2.66) as the generalized velocity potential for supersonic two-dimensional flow.

Following the notation of Garrick [13], the axis of rotation is located at $x = x_0$ and the control surface leading edge is located at $x = x_1$. Generalizing the expressions for the loads given by Garrick produces

$$\begin{bmatrix} Pb(s) \\ M_\alpha(s) \\ M_\beta(s) \end{bmatrix} = \sqrt{\frac{8\rho b^2 U^2}{M^2 - 1}}\,\bar{s}^2\left[M_a(\bar{s})\bar{s}^2 + B_a(\bar{s})\bar{s} + K_a(\bar{s})\right] \begin{bmatrix} h(s) \\ \alpha(s) \\ \beta(s) \end{bmatrix}$$

where

$$M_a(\bar{s}) = \begin{bmatrix} r_2 & (r_3 - 2x_0 r_2) & t_3 \\ (q_2 - 2x_0 r_2) & \left(\frac{2}{3}q_3 - 2x_0(q_2 + r_3) + 4x_0^2 r_2\right) & \left(\frac{2}{3}s_3 + 2t_3(x_1 - x_0)\right) \\ p_2 & \left(\frac{2}{3}p_3 - 2x_0 p_2\right) & \frac{2}{3}s_3 \end{bmatrix}$$

$$B_a(\bar{s}) = \begin{bmatrix} \frac{1}{2}r_1 & (2r_2 - x_0 r_1) & 2t_s \\ (q_1 - x_0 r_1) & \left(2q_2 - 2x_0(q_1 + 2r_1) + 4x_0^2 r_1\right) & \left(2s_2 + 4t_2(x_1 - x_0)\right) \\ p_1 & 2(p_2 - x_0 p_1) & 2s_2 \end{bmatrix}$$

$$K_a(\bar{s}) = \begin{bmatrix} 0 & \frac{1}{2}r_1 & \frac{1}{2}t_1 \\ 0 & (q_1 - x_0 r_1) & \left(s_1 + t_1(x_1 - x_0)\right) \\ 0 & p_1 & s_1 \end{bmatrix} \cdot$$

The functional dependence of these matrices on $\bar{s}$ is meant to indicate that the parameters q_i, r_i, s_i, and t_i given in Table II-2 are functions of $\bar{s}$. All of these parameters may be derived from the 'Schwartz function',

$$f_0(M, \bar{\omega}) = \int_0^1 e^{-i\bar{\omega}u} J_0\left(\frac{\bar{\omega}}{M}u\right) du \tag{2.68}$$

[where $\bar{\omega} = -i(2\bar{s}M^2/M^2 - 1)$] by the recurrence relation

-42-

$$f_j(M, \bar{\omega}) = \frac{M^2}{\bar{\omega}(M^2-1)} \left\{ \left[1+(1-j) \frac{1}{\bar{\omega}} \right] e^{-i\bar{\omega}} J_o\left(\frac{\bar{\omega}}{M}\right) - \frac{1}{M} e^{-i\bar{\omega}} J_1\left(\frac{\bar{\omega}}{M}\right) \right.$$

$$\left. + i(1-2j)f_{j-1}(M, \bar{\omega}) + (1-j)^2 \frac{1}{\bar{\omega}} f_{j-2}(M, \bar{\omega}) \right\} , \qquad (2.69)$$

$$j = 1, 2, \ldots .$$

The g_λ and h_λ parameters are given by

$$g_\lambda = f_\lambda(M, \bar{\omega}x_1)$$

$$h_\lambda = f_\lambda[(M, \bar{\omega}(1-x_1)] .$$

Table II-2

SUPERSONIC AERODYNAMIC LOAD PARAMETERS

$r_1 = f_1$	$p_1 = q_1 - x_1 r_1 + x_1^2(g_o - g_1)$
$r_2 = f_o - f_1$	$p_2 = q_2 - 2x_1 r_2 + x_1^3(g_o - 2g_1 + g_2)$
$r_3 = f_o - 2f_1 + f_2$	$p_3 = q_3 - 3x_1 r_3 + x_1^4(g_o - 3g_1 + 3g_2 - g_3)$
$q_1 = f_1$	$t_1 = (1-x_1)h_o$
$q_2 = f_o - f_2$	$t_2 = (1-x_1)^2 (h_o - h_1)$
$q_3 = 2f_o - 3f_1 + f_3$	$t_3 = (1-x_1)^2(h_o - 2h_1 + h_2)$

$$s_1 = (1-x_1)^2 h_1$$

$$s_2 = (1-x_1)^3(h_o - h_2)$$

$$s_3 = (1-x_1)^4(2h_o - 3h_1 + h_3)$$

The Schwartz function (Eq. 2.68) is not expressible in terms of
elementary functions but it may be computed from the series

$$f_o(M, \bar{\omega}) \;=\; e^{-i\bar{\omega}} \sum_{n=o}^{\infty} \left(\frac{M^2-1}{M^2}\,\bar{\omega}\right)^n \frac{[\,J_n(\bar{\omega}) + iJ_{n+1}(\bar{\omega})\,]}{2^n n!(2n+1)}$$

given by von Borbely [65] where the Bessel functions of complex argument
are evaluated by their ascending power series given in App. F. Although
transient time responses of the loads for specific airfoil motions,
$X(s)$, could be computed from (2.67) via the Laplace inversion integral,
this has not been attempted. To perform this calculation would require
knowledge of the singularities of the transformed loads which are not
readily available. Note that the loads given by (2.67) do not involve
a single nonrational transform such as $C(\bar{s})$ for the $M = 0$ case.
Fortunately, the exact transient time responses for indicial motions have
been calculated by Chang [66] and Lomax, et al. [10]. The time responses
of the loads for indicial motions at supersonic velocities are typified
by discontinuous first derivatives and different functional dependence
for various time zones. These facts indicate that calculation of trans-
ient loads using inverse Laplace transformation would be laborious. Chang
used the indicial response functions to calculate the simple harmonic
loads from the convolution integral and noted [26] that arbitrary trans-
ient motions could be treated in the same manner. The primary use of
the transformed loads, (2.67), is for the investigation of airfoil
stability--the flutter problem.

Chapter III

SOLUTION OF THE AEROELASTIC EQUATIONS OF MOTION

The expressions for the loads, (2.34) or (2.67), may be substituted into the equations of motion, (2.1), giving

$$G(s)\underline{X}(s) = \mathfrak{B}(s) \tag{3.1}$$

with

$$G(s) = \left[M_s s^2 + B_s s + K_s - Q(\bar{s}) \right]$$

and

$$\mathfrak{B}(s) = G\mathfrak{U}(s) .$$

$Q(s)$ is derived from either (2.34) or (2.67). The primary goals of the analysis of (3.1) are the determination of the stability of the system and the calculation of transient motions.

Since the airfoil is a linear system, its stability is determined by the homogeneous version of (3.1)

$$G(s)\underline{X}(s) = 0 . \tag{3.2}$$

Table III-1

METHODS OF SOLUTION OF AEROELASTIC EQUATIONS

Method	Aeroelastic Equation	Solution	Stability Criterion
p	$\{M_s s^2 + K_s - Q(\bar{s})\}\underline{X}(s) = 0$	$\bar{s} = \gamma k + ik$	γ
k	$\{M_s - \frac{1}{\omega^2}K_s - \frac{1}{\omega^2}Q(ik)\}\underline{X}(ik) = 0$	$\frac{1}{\omega^2}(1+ig)$	g
p-k	$\{M_s s^2 + K_s - Q(ik)\}\underline{X}(s) = 0$	$\bar{s} = \gamma k + ik$	γ
augmented states	$\{M_s' s^2 + K_s' - Q'(\bar{s})\}\underline{X}'(s) = 0$	$s = \sigma + i\omega$	$\zeta = \cos^{-1}\frac{c}{\sigma^2 + \omega^2}$

-45-

Nontrivial solutions are given by the zeroes of the characteristic equation

$$\text{Det}\lfloor \mathcal{Q}(s) \rfloor = 0 \qquad (3.3)$$

which are the poles of the system. Table III-1 is drawn from Hassig [28] and summarizes the prevalent techniques of determining the zeroes of this equation. The structural damping matrix B_s has been eliminated for convenience. The matrix $\mathcal{Q}(s)$ involves structural, geometrical, and aerodynamic terms which influence the solution. The structural and geometrical terms are valid for arbitrary motions, while the motions for which the aerodynamic terms are valid depend upon the underlying theory. For instance, quasi-steady aerodynamics $(Q(s) = Q_1 s + Q_2)$ may be used to analyze arbitrary motions for low frequency effects, while calculations of flutter boundaries commonly utilize aerodynamics which are valid only for simple harmonic motions. The p-method is intended for use in the former case, in which $Q(\bar{s})$ is valid for arbitrary motions. If $Q(\bar{s})$ is a rational function of $\bar{s}$, (3.2) becomes a linear eigenvalue problem and solution by linear matrix techniques is possible. Otherwise, the roots of the equation must be determined by iteration. The advantage of the p-method is that the exact roots and the degree of stability of the system are determined, to the extent of the accuracy of $Q(\bar{s})$. The stability criterion is that the real parts of the roots of the equation, γk, must be negative.

The k-method is the traditional U-g method which is used to determine the flutter boundary utilizing simple harmonic loads. Complex roots are obtained by introducing the artificial structural damping factor g, and a root of the equation represents a point on the flutter boundary if the corresponding value of g equals the assumed value of g. Disadvantages of the k-method are: (1) many solutions are required to obtain "matched-point" flutter boundaries; (2) for a given airspeed, several solutions with different frequencies may occur, leading to problems of sorting the roots, and (3) information obtained regarding subcritical and supercritical flutter conditions is only qualitative. Regarding the last point, Richardson [27] and Goland and Luke [30] give calculations illustrating

-46-

the differences between rates of change of damping at the flutter speed calculated by the k-method and by more accurate methods.

The p-k method [67] attempts to improve upon the k-method for sub-critical and supercritical flutter conditions (i.e., non-simple harmonic motions) by allowing the reduced frequency to be complex instead of introducing the structural damping factor g. It assumes that if $Q(ik)$ is calculated for oscillatory loads at $\bar{s} = ik$, then the same loads will be good approximations to the true loads for $\bar{s} = \gamma k + ik$ if $\gamma \ll 1$. Results given by Hassig [28] confirm the usefulness of the method.

The augmented state method is fundamentally different from the first three methods of Table III-1 in that it attempts to model the unsteady aerodynamics with a rational transform. The primes on the matrices of the last row of Table III-1 imply that the matrices have been modified to include the augmented states. The advantage thus achieved is that the resulting system may be analyzed by linear eigenvalue techniques. Note that the p-method has been used in the past with quasi-steady aero-dynamics (thus ignoring the effect of the wake) to maintain the rational form of the equations, while the k- and p-k methods have sacrificed the rational form to include the wake effects in more accurate oscilla-tory aerodynamics. The augmented state method is based upon R.T. Jones technique [29], [6], of exponential approximations to indicial loading functions, and wake effects may be approximated at the expense of the extra states. Since this form is we: iited to the needs of active control, it has found application in aircraft stability augmentation studies and is studied in detail in the next chapter.

The differences in the stability criteria of the various methods may be delineated as follows: (1) the p and p-k methods determine a root at $\bar{s} = \gamma k + ik$; (2) the k-method determines a root at $\lambda_r + i\lambda_1 = (1/\omega^2)(1+ig)$; (3) the augmented states method finds a root at $s = \sigma + i\omega$. The stability criterion for the p and p-k methods is given by the signs of $\gamma = \tan \phi$ where ϕ is the angle between the ik axis and the root, while the stability criterion for the augmented state method is given by the sign of $\zeta = \dfrac{\sigma}{\sqrt{\sigma^2 + \omega^2}}$ corresponding to a characteristic

equation factor $(s^2 + 2\zeta\omega s + \omega^2) = [(s+\sigma)^2 + \omega^2]$. For roots close to the $i\omega$ axis, $\zeta \approx \gamma$. The stability criterion for the k-method is deduced from the characteristic equation (for a one DOF system) $m_s s^2 + k_s(1+ig) = 0$, or $s^2 + ig\omega^2 + \omega^2 = 0$. Thus the correspondence between g and ζ ; $2\zeta\omega s \approx ig\omega^2$ or $g \approx 2\zeta$. The nonphysical nature of solutions based on the k-method for nonzero values of g can be seen by factoring the characteristic equation:

$$ s = -\sqrt{\frac{k_s}{m_s}} (1 + ig)^{\frac{1}{2}} \approx \sqrt{\frac{k_s}{m_s}} \left[e^{i(\pi+\phi)} \right]^{\frac{1}{2}} $$

$$ s = \sqrt{\frac{k_s}{m_s}} \; e^{i(\pi/2+\phi/2)}, \quad \sqrt{\frac{k_s}{m_s}} e^{i(-\pi/2+\phi/2)} \quad . $$

The roots of the characteristic equation are not complex conjugate factors, emphasizing the unphysical nature of the solution.

The remainder of this chapter extends the p-method of solution by using the generalized aerodynamic loading functions derived in the last chapter to study arbitrary airfoil motions. In the next section, the stability problem is studied and the last section studies arbitrary transient motions of airfoils.

A. ROOT LOCI OF AEROELASTIC MODES

In Ch. II, analytic expressions for $Q(\bar{s})$ were given for two-dimensional incompressible and supersonic flow. The loads, Eqs. (2.34) and (2.67) are valid for arbitrary motions and give the exact airloads. They may be combined with the equations of motion as indicated in (3.1) and the stability of the aeroelastic systems studied via the p-method of Table III-1. Similar calculations are mentioned by Dengler, Goland, and Luke [25] in attempting to define their generalized Theodorsen function but have evidently never been published.

Since the loads are not rational functions of $\bar{s}$, a computer program was developed to numerically determine the roots of the characteristic equation. For the systems treated in this thesis, it was feasible to numerically expand the determinant in (3.1). A gradient search algorithm was employed to locate the zeroes of the determinant which are the poles of the aeroelastic system. The gradient was numerically determined by finite differences in the s-plane and the performance of the algorithm was quite satisfactory for the systems treated which included systems of four DOF (degrees of freedom), (eighth order).

Table III-2 shows the behavior of the algorithm in converging to a root. Convergence is shown for a three DOF section and a four DOF section. The nondimensional velocity was $U/b\omega_\alpha = 3.0$, near the flutter speed of both sections and the search was started at $s = 60$ rad/sec. For the three DOF section, the algorithm locates the root to four significant figures in three iterations. Five iterations are required to achieve the same accuracy for the four DOF section.

A-1 Incompressible Two-Dimensional Flow

Table III-3 lists the structural and geometrical parameters of the three DOF system used in the following calculations. The frequency ratio $\omega_h/\omega_\alpha = 0.5$ while the natural frequency of the flap mode is three times the torsion mode frequency.

The equations of motion, including the loads, were given by (2.35) and are repeated here:

$$\left\{ (M_s - \eta M_{nc})s^2 + \left[B_s - \eta(\frac{U}{b})(B_{nc} + C(\bar{s})RS_2) \right] s \right.$$
$$\left. + \left[K_s - \eta(\frac{U}{b})^2(K_{nc} + C(\bar{s})RS_1) \right] \right\} \underline{X}(s) = GU(s) . \tag{3.4}$$

The loads contain the generalized Theordorsen function $C(\bar{s})$ which is a function of s and U/b. Thus, with the nondimensional velocity specified, the roots of the equations of motion may be determined by iteration in the s-plane. Figure III-1 shows the exact locus of roots of the three DOF system of Table III-3 as a function of $U/b\omega_\alpha$. The inertia coupling

-49-

Table III-2

BEHAVIOR OF THE GRADIENT SEARCH ALGORITHM IN LOCATING A ROOT

THREE DEGREES-OF-FREEDOM SECTION

Iteration	s, rad/sec	Det[u(s)]
0	0.0 + i 60.0	—
1	-2.5363418 + i 68.550855	0.12961308D 9
2	-0.16576624 + i 70.790603	0.23088716D 8
3	-0.16618801 + i 70.313659	0.55576155D 6
4	-0.15470741 + i 70.313760	0.24297422D 5
5	-0.15479190 + i 70.314279	0.23286565D 4

FOUR DEGREES OF FREEDOM SECTION

Iteration	s, rad/sec	Det u(s)
0	0.0 + i 60.0	—
1	-4.9153988 + i 72.099953	0.11752462D 13
2	3.5790195 + i 77.749775	0.93748594D 12
3	3.9041393 + i 74.34059	0.15967193D 12
4	4.6414540 + i 73.766451	0.66348053D 10
5	4.6301405 + i 73.795187	0.10318925D 9
6	4.6305966 + i 73.795434	0.10057262D 8
7	4.6305615 + i 73.795414	0.61534265D 7
8	4.6305471 + i 73.795438	0.79781022D 6

Table III-3

THREE DEGREES-OF-FREEDOM SECTION PARAMETERS FOR INCOMPRESSIBLE FLOW

$\omega_\alpha = 100$ rad/sec $\qquad x_\alpha = 0.2 \qquad r_\beta^2 = 0.00625$

$\omega_h = 50$ rad/sec

$\omega_\beta = 300$ rad/sec $\qquad r_\alpha^2 = 0.25 \qquad \zeta_\beta = 0$

$\mu = 40$

$\qquad\qquad\qquad\qquad x_\beta = 0.0125$

$a = -0.4$

$c = 0.6$
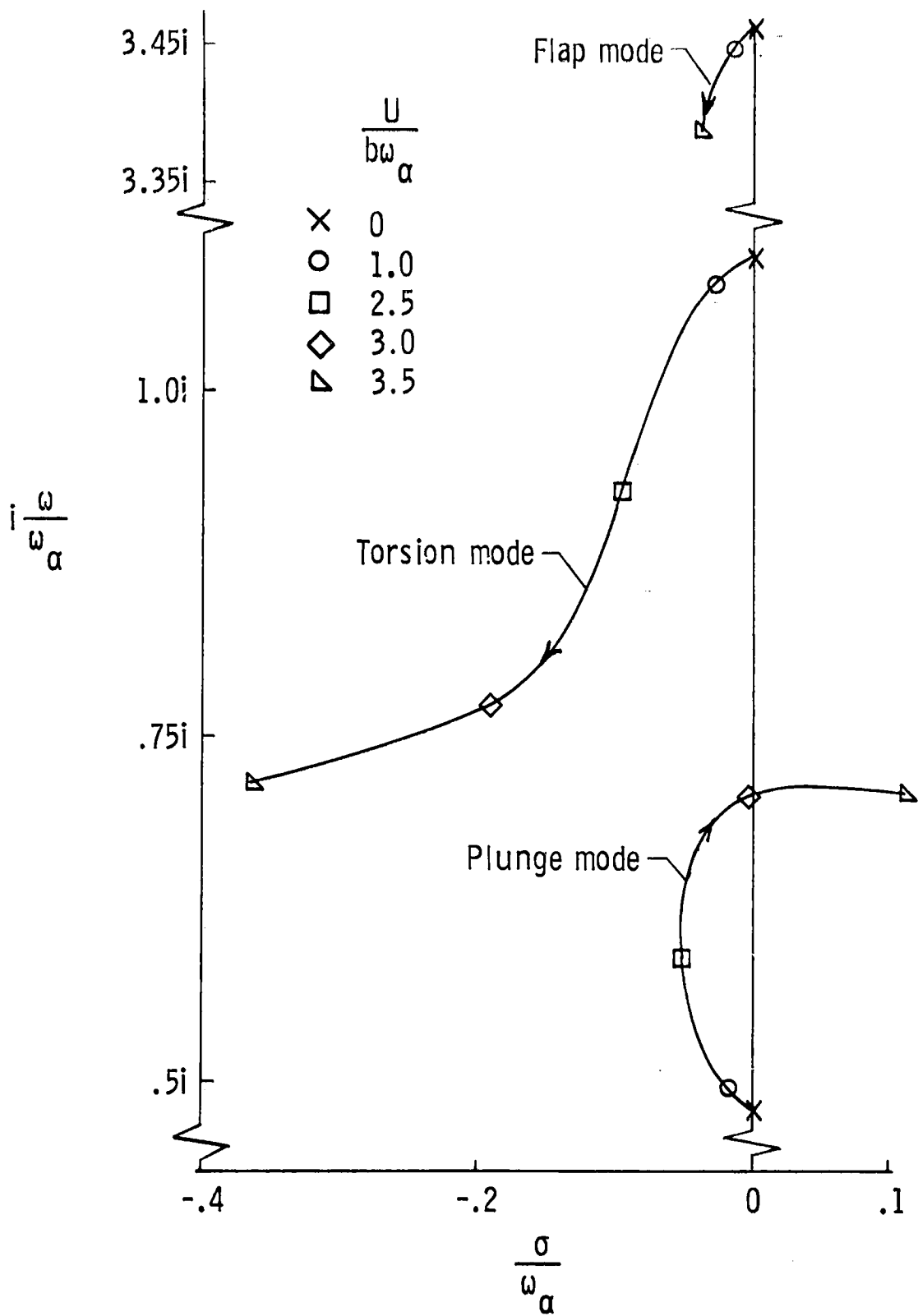
FIG. III-1   LOCUS OF ROOTS OF A THREE DEGREE-OF-FREEDOM SECTION
VERSUS U/bω_α IN INCOMPRESSIBLE FLOW

of the three modes causes the zero airspeed natural frequencies to be shifted from their uncoupled values. As the airspeed increases, the bending and torsion modes are seen to approach each other in the stable left-half plane with the bending branch becoming the flutter mode at $U/b\omega_\alpha \approx 3.0$. The flap mode remains stable throughout this speed range even though $\zeta_\beta = 0$.

Because the terms involved in the matrix of coefficients of (3.4) do not become infinite in the finite s-plane, the determinant has no poles and examination of the number of 360° phase changes of the determinant around a closed contour will directly indicate the number of zeroes within the contour [57, p. 61]. This was accomplished for the section of Table III-3 at $U/b\omega_\alpha = 3.0$ by evaluating the determinant along the branch cut on the negative real axis, and along circles of radius 0.0001 and 1000 rad/sec. Six 360° phase changes were obtained, accounting for the six known structural poles and it is concluded that these are the only isolated singularities of (3.4) at this airspeed.

The root locus format is used for the presentation of results rather than the conventional U-g, U-ω plots since the ability to calculate generalized aerodynamics makes this a more natural format. It avoids the numerical problems of root-sorting since the loci do not cross each other and it is required for active control design applications.

A-2   Supersonic Two-Dimensional Flow

Table III-4 lists the parameters of the three DOF section used to illustrate the aeroelastic root loci in supersonic flow. The loads, (2.67), are functions of the generalized supersonic reduced frequency parameter, $\bar{\omega} = -i2\bar{s}M^2/(M^2-1)$, and the algorithm described above may again be used for the determination of the system poles. The equations of motion, including the supersonic loads, are

$$\left\{ [M_s - \eta' M_a(\bar{s})]s^2 + \left[B_s - \eta'(\frac{U}{b}) B_a(\bar{s}) \right]s \right.$$
$$\left. + \left[K_s - \eta'(\frac{U}{b})^2 K_a(\bar{s}) \right] \right\} \underline{X}(s) = G\mathcal{U}(s) . \tag{3.5}$$

Table III-4

THREE DEGREES OF FREEDOM SECTION PARAMETERS FOR SUPERSONIC FLOW

$\omega_\alpha = 100$ rad/sec	$x_\alpha = 0.2$
$\omega_h = 50$ rad/sec	$r_\alpha^2 = 0.25$
$\omega_\beta = 317$ rad/sec	$x_\beta = 0.0125$
$\mu = 40$	$r_\beta^2 = 0.00625$
$a = 0$	$\zeta_\beta = 0$
$c = 0.6$	$b = 1.35$ m
	$a_\infty = 333$ m/sec

where $\eta' = 8\bar{\eta}^{-2}/\sqrt{M^2 - 1}$.

The locus of roots of this section are shown in Fig. III-2 as a function of Mach number. At $M = 1.25$, both the lowest frequency coupled-bending-torsion mode and the flap mode are unstable. It is suspected that the flap mode is primarily a single DOF flutter mode [68]. As the Mach number increases, both of these modes become stable at $M \cong 1.4$. Above $M \simeq 1.8$, the remaining coupled bending-torsion mode flutters. Hence, for the mass ratio $\mu = 40$, the range of stability for this section is $1.4 \leq M \leq 1.8$.

The aerodynamic matrices M_a, B_a, and K_a are derived from terms composed of finite integrals of exponentially weighted Bessel functions of integer order as shown by (2.68). Since these Bessel functions are single-valued analytic functions of s, there will be no branch points of (3.5) as in the incompressible case. However, a cursory review of supersonic indicial aerodynamics [e.g., Lomax et al., Ref. 10], leads to the conclusion that (3.5) must have more singularities than the six

-53-
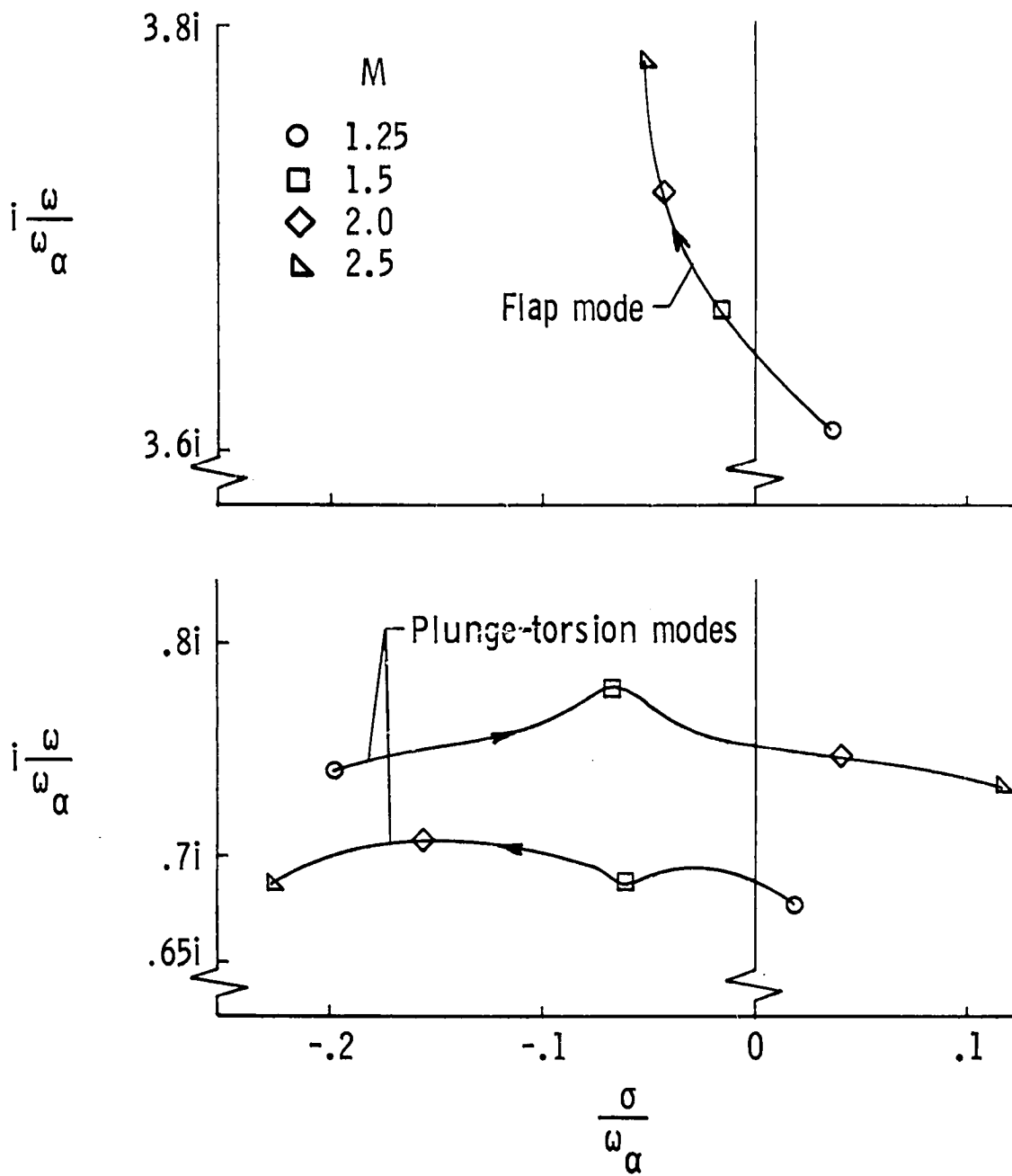
FIG . III-2   LOCUS OF ROOTS OF A THREE DEGREE-OF-FREEDOM SECTION
VERSUS M IN SUPERSONIC FLOW

structural poles, because these six poles cannot yield the complex indicial functions. Since the poles of the system are the zeroes of the determinant of the matrix of coefficients of (3.5), a search was made for additional zeroes of this function. A circular contour of radius 1000 rad/sec centered at the origin yielded six 360° phase changes of the determinant, accounting for only the six known structural poles. Further searching located the first additional zero as a complex conjugate pair at $s = -1315 \pm i\, 1501$, over ten times the frequency of the flutter mode. No other zeroes were located since the power series expansions used to evaluate the complex Bessel functions were numerically unstable at larger values of $|s|$. However, it is anticipated that an infinite sequence of additional zeroes of increasing modulus does exist, due to the oscillatory nature of the exponential weighting factor in the integrand of (2.68), and accurate transient response calculations would require the evaluation of a number of these zeroes of lowest modulus and their corresponding residues. Fortunately, the flutter problem can be studied by determining only the zeroes due to the structural poles, as indicated in Fig. III-2.

B. INVERSION INTEGRAL FOR ARBITRARY AIRFOIL MOTIONS

Returning to the case of incompressible flow, it is possible to calculate exact transient motions from (3.4) using the Laplace inversion integral. With the substitutions

$$
\mathcal{Q}(s) = \left\{ (M_s - \eta M_{nc})s^2 + \left[B_s - \eta (\frac{U}{b})(B_{nc} + C(\bar{s})RS_2) \right] s \right.
$$

$$
\left. + \left[K_s - \eta (\frac{U}{b})^2 (K_{nc} + C(\bar{s})RS_1) \right] \right\}
$$

$$
\mathcal{B}(s) = G\mathcal{U}(s) .
$$

-55-

Equation (3.4) becomes

$$\mathcal{C}(s)\underline{X}(s) = \mathcal{B}(s) \tag{3.6}$$

where $\mathcal{C}(s)$ and $\mathcal{B}(s)$ are $n \times n$ and $n \times m$ matrices whose elements are functions of s, and $\underline{X}(s)$ is an $n \times 1$ state vector. The number of degrees of freedom of the airfoil is n while the number of control inputs is m. If $\text{Det}[\mathcal{C}(s)] \neq 0$, $[\mathcal{C}(s)]^{-1}$ exists and the solution of (3.6) is

$$\underline{X}(s) = [\mathcal{C}(s)]^{-1}\mathcal{B}(s) . \tag{3.7}$$

Assuming $m = 1$ (extension of the following results to the multi-input case is straightforward), the transform of the jth state is

$$x_j(s) = \frac{N_j(s)}{D(s)} \mathcal{U}(s) \tag{3.8}$$

and

$$\underline{x}_j(t) = \frac{1}{2\pi i} \int_{\sigma - i\infty}^{\sigma + i\infty} \frac{N_j(s)}{D(s)} \mathcal{U}(s) e^{st} \, ds . \tag{3.9}$$

Cramer's rule is used to evaluate $\underline{x}_j(s)$, with $D(s) = \text{Det}[\mathcal{C}(s)]$ and $N_j(s) = \text{Det}[\mathcal{C}(s)]$ with the jth column of $\mathcal{C}(s)$ replaced by G. Due to the complexity of (3.7), it is no longer feasible to obtain analytic expressions for the integrand but it may be evaluated numerically. Since the elements of $\mathcal{C}(s)$ contain $C(\bar{s})$, $\underline{x}_j(s)$ will have a branch cut along the negative real axis and the contour of integration may be deformed as shown in Fig. II-6 giving

$$\underline{x}_j(t) = \sum_{\ell=1}^{N} \text{Res}_\ell e^{s_\ell t} - \frac{1}{2\pi i} \int_0^\infty \left[\underline{x}_j(re^{i\pi}) - \underline{x}_j(re^{-i\pi}) \right] e^{-rt} dr , \tag{3.10}$$

where s_ℓ, $\ell = 1, 2, \ldots, N$ are the poles of (3.8), and the residues are evaluated at the poles by

$$\text{Res}_\ell = \frac{N_j(s_\ell)}{D'(s_\ell)} \cong \frac{N_j(s_\ell)}{D(s)-D(s_\ell)} (s-s_\ell) \cong \frac{N_j(s_\ell)}{D(s)} \Delta s$$

with $\Delta s = s - s_\ell$. (Since the poles are determined numerically by iteration, $D(s_\ell) \cong 0$.) The poles due to the structural equations of motion may be assumed to be complex conjugates with $s_\ell = a_\ell + ib_\ell$, $s_{\ell+1} = a_\ell - ib_\ell$. Poles due to $U(s)$ may be real or complex but for the following development, it is assumed there are N complex poles within the contour. Since $\underline{x}_j(t)$ must be real, the integrand must be pure imaginary and therefore $\underline{x}_j(re^{i\pi})$ and $\underline{x}_j(re^{-i\pi})$ are complex conjugate ex-expressions. With $N_j(s_\ell) = N_{j\ell}^R + iN_{j\ell}^I$

$$\underline{x}_j(t) = \sum_{\ell=1}^{N/2} 2e^{a_\ell t}\left[N_{j\ell}^R \cos b_\ell t - N_{j\ell}^I \sin b_\ell t\right] - \frac{1}{\pi}\int_0^\infty \text{Im}\left[\underline{x}_j(re^{i\pi})\right]e^{-rt}dr,$$

$$(3.11)$$

or

$$\underline{x}_j(t) = \underline{x}_{j_r}(t) + \underline{x}_{j_{nr}}(t) .$$

The incompressible flow transient response of the three DOF section of Table III-3 will be calculated for a unit step input command to the flap $U(s) = \beta_c(s) = 1/s$, for $U/b = 290 \text{ sec}^{-1}$. Figure III-1 indicates that the bending mode has a subcritical damping ratio of $\zeta \cong 0.03$ at this airspeed. To study the effect of changes in airspeed on the non-rational portion of the response, $\text{Im}[x_j(re^{i\pi})]$, $j = 1, 2, 3$ is plotted in Fig. III-3 for $U/b = 200, 290$, and 350 sec^{-1}. At time t, $\underline{x}_{j_{nr}}(t)$ is given by the integral of the product of the function shown in the figure and e^{-rt}. The value of $\underline{x}_{j_{nr}}(0)$ is proportional to the area under the curves, and since all of the functions go to zero at $r = 0$, $\lim_{t\to\infty} \underline{x}_{j_{nr}}(t) = 0$. In other words, the nonrational portion of the response
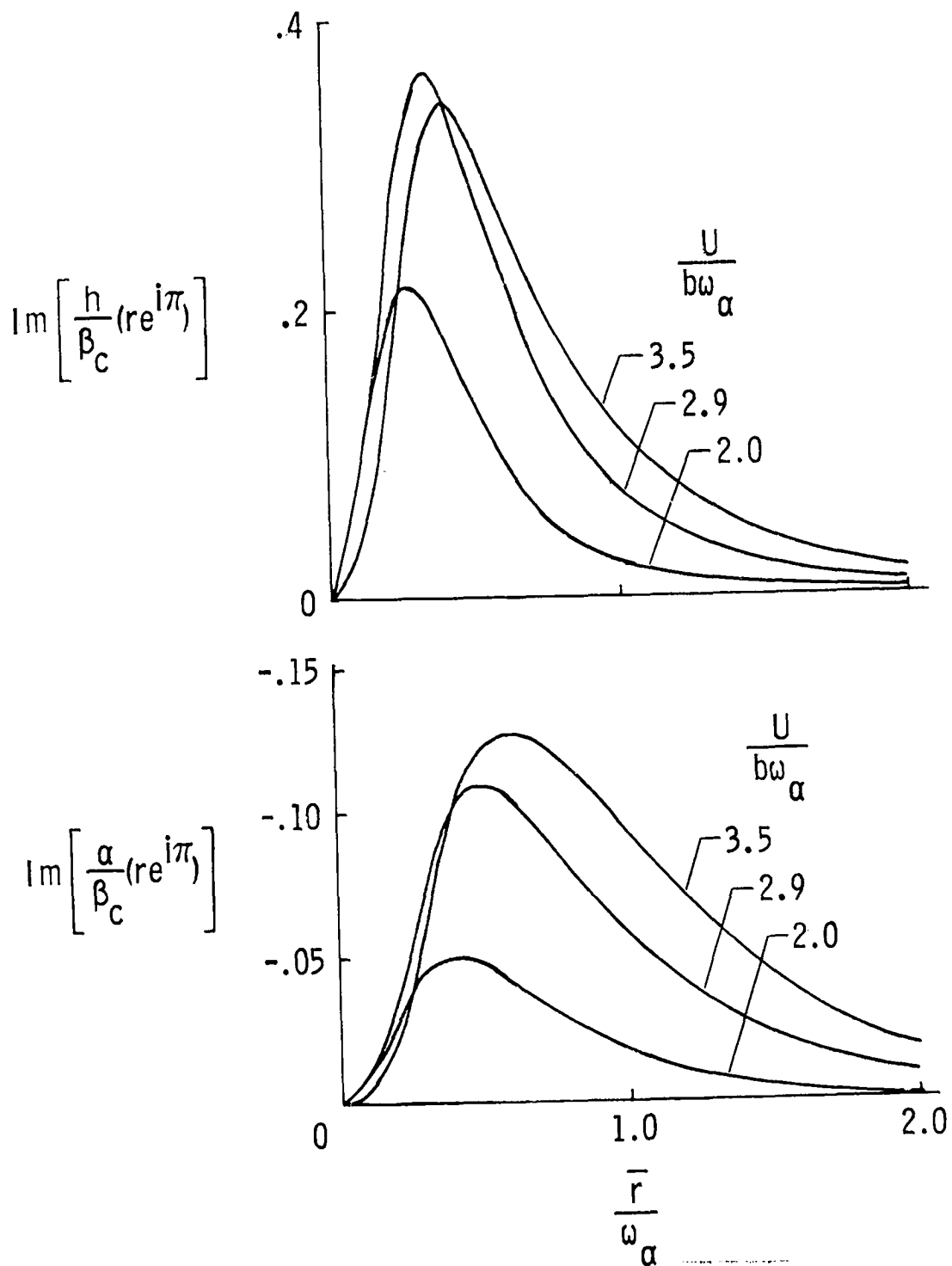
FIG. III-3   INTEGRANDS OF NONRATIONAL PORTION OF RESPONSE DUE TO STEP COMMAND TO THE FLAP. $M = 0$
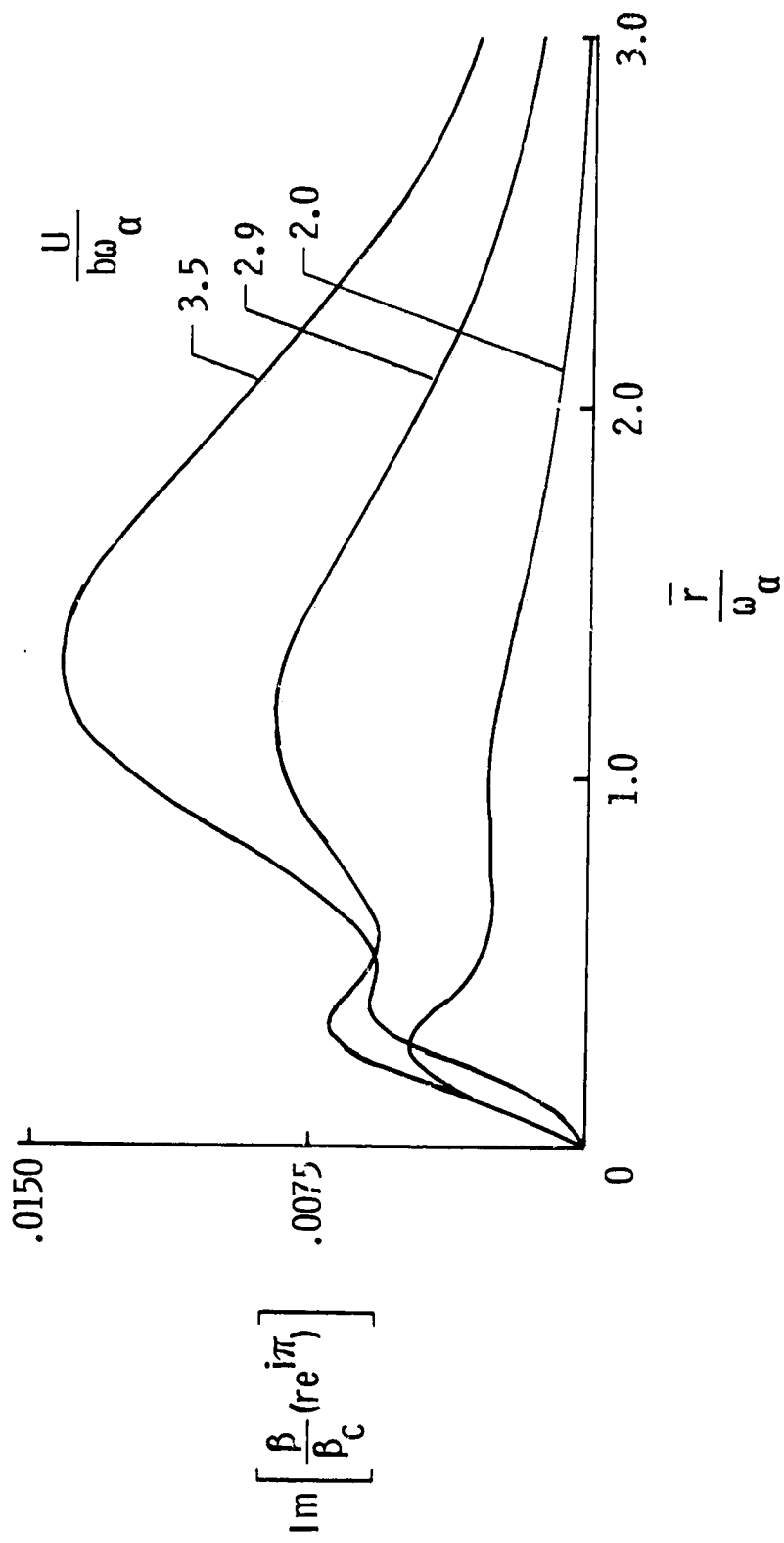
FIG. III-3   CONCLUDED

does not participate in the motion characteristic of an unstable fluttering airfoil. Note that all of the curves shown in Fig. III-3 are smoothly varying functions of U/b, even as the airfoil flutters at $U/b \simeq 300 \text{ sec}^{-1}$.

The poles and residues required to evalute (3.11) were calculated, and the integral was evaluated numerically. The component and total transient responses of the plunge and torsion modes are shown in Fig. III-4. In this case, the contour integral about the infinitesimal circle at the origin in Fig. II-6 will be nonzero, its value being the steady state value of $\underline{x}_j(t)$ due to the step change in β_c. These steady state values were determined from (3.6) by applying the final value theorem, $\lim\limits_{s \to 0} sX_j(s) = \lim\limits_{t \to \infty} \underline{x}_j(t)$ rather than by contour integration. The oscillatory harmonic mode superimposed on $\alpha_r(t)$ and to a smaller extent on $h_r(t)$ is due to the very lightly damped flap mode which is not shown. The nonrational portion of $h(t)$ is 75 percent of the rational portion of $h(t)$ at $t = 0$, while the corresponding percentage for $\alpha(t)$ is only 15 percent. As in the case of the transient loads, the nonrational portion of the response is characterized by a rapid initial decay followed by a slow asymptotic decay, the entire function being a monotonically decreasing function of t. Since the response of a mechanical system to a step input in torque must start at zero, the sum of the rational and nonrational portions should cancel the steady state value of $\underline{x}_j$. Hence, the small nonzero value of $\alpha(0)$ and the larger value of $h(0)$ are attributed to numerical inaccuracies in evaluating the residues.

The following comments are made with respect to Fig. III-4.

1. The oscillatory motions typifying flutter phenomena are due entirely to the rational portion of the response. If a method were available for modeling only this portion of the system, it would serve to describe the pertinent features of the flutter problem. This concept will be pursued in Ch. V.

2. The effect of the nonrational response on the oscillatory total response would tend to complicate the determination of the damping ratio of the rational portion. Techniques for determining damping ratios which do not address this fact may produce inconsistent damping estimates. This effect may be aggravated in cases with random structural excitations. If an estimate of the nonrational response were available, subtraction of this estimate from the total response may improve the damping estimates.
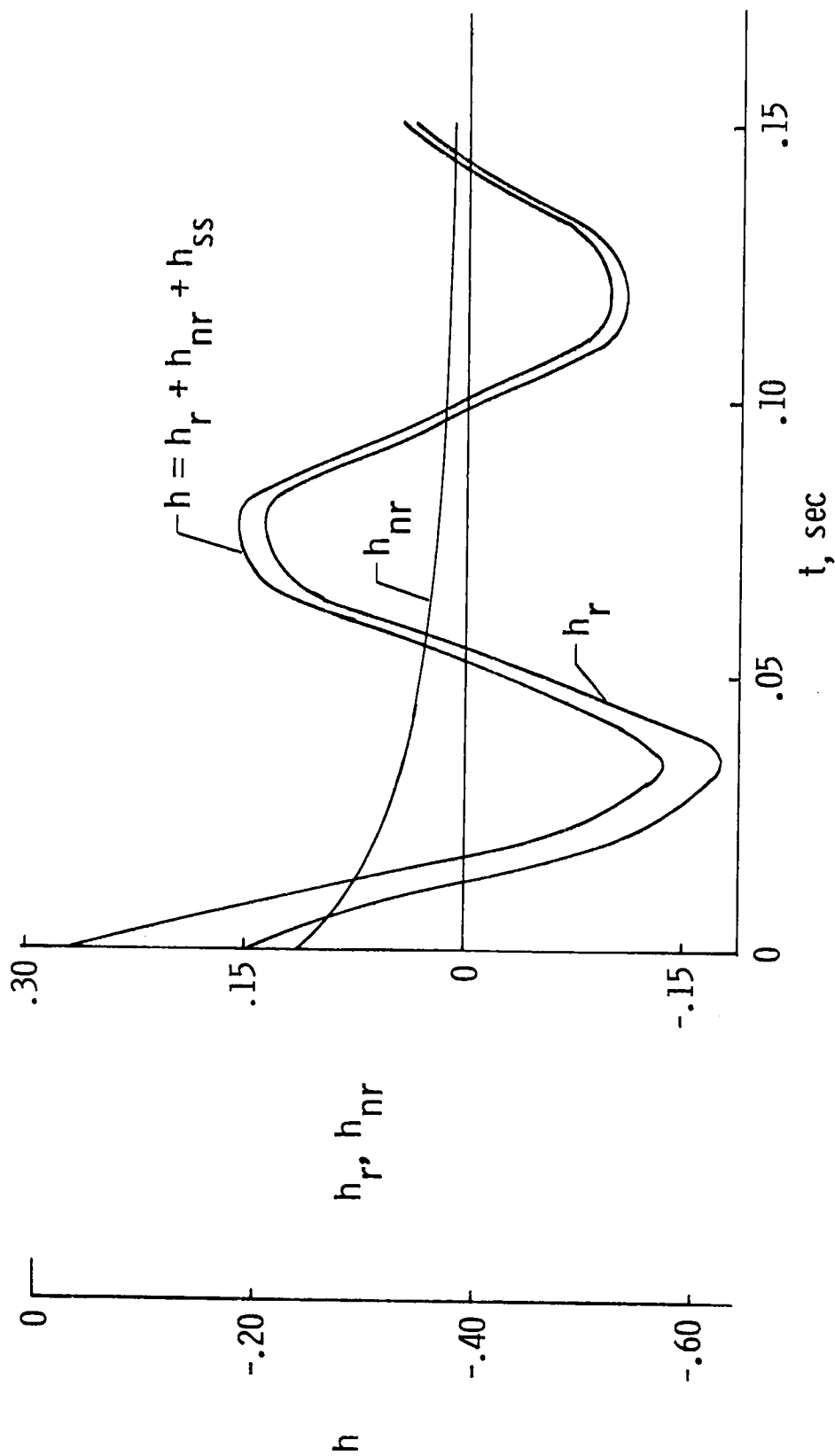
(a) PLUNGE RESPONSE ($h_{ss} = -0.39$)

FIG. III-4   RATIONAL, NONRATIONAL, AND TOTAL RESPONSES DUE TO A STEP COMMAND
TO THE FLAP, $M = 0$
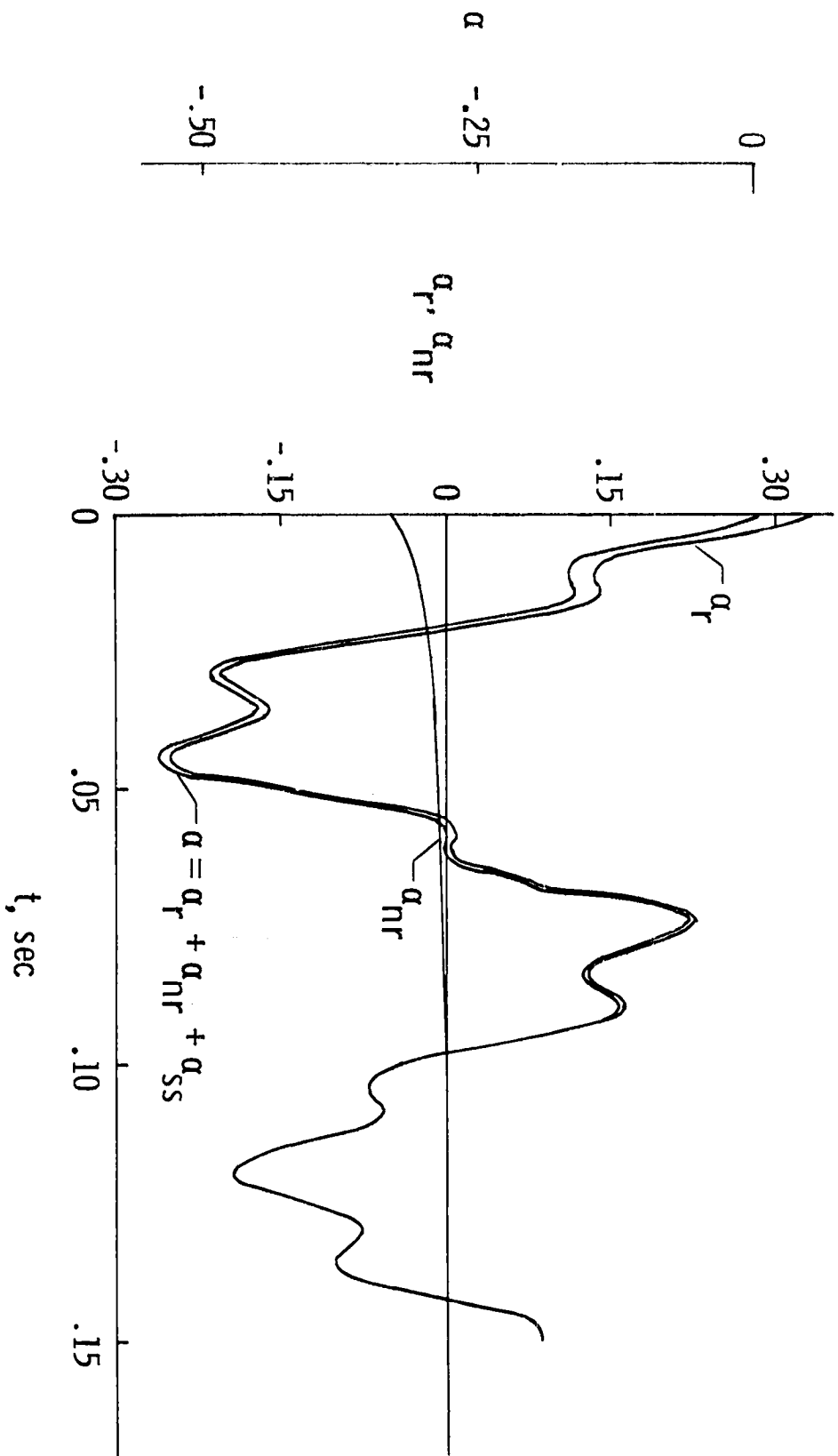
(b) PITCH RESPONSE ($\alpha_{ss} = -0.28$)

FIG. III-4 CONCLUDED

Chapter IV

PADÉ APPROXIMANTS AND AUGMENTED STATE METHODS

To obtain solutions of the aeroelastic equations of motion, Eq.
(2.1), it is necessary to specify the aerodynamic loads, L. In Chapter
II the exact analytic loads were given for two-dimensional incompressible
and supersonic flow, and a technique for obtaining similar loads for other
flow regimes was indicated. In Chapter III, these loads were incorporated
into the aeroelastic equations, and solutions were obtained by an iterative
search procedure. In the present chapter, the use of Padé approximants
of the loads to produce augmented state aeroelastic models will be studied.
The advantage to be gained is the ability to perform analysis with the
resulting constant coefficient, ordinary differential equations. The
penalty paid to achieve this advantage is that higher order models must
be manipulated. An implicit constraint of the technique is the minimiza-
tion of the required number of augmented states to adequately represent
the loads.

A. INCOMPRESSIBLE TWO-DIMENSIONAL FLOW

Augmented state methods for this flow regime derive from R.T. Jones'
[29], [9], exponential approximation of Wagner's indicial loading function.
Many investigators have used the method, including Goland and Luke [30],
Baird and Kelley [31], Dugundji [32], Richardson [27], and Lyons et
al., [69]. Jones' approximation is

$$k_1(t') \cong 1 - 0.165e^{-0.0455t'} - 0.335e^{-0.3t'} . \qquad (4.1)$$

Garrick [70] noted that the linearity of the governing equations allowed
the calculation of arbitrary transient lift functions by the convolution
integral

$$\frac{P(t)}{2\pi\rho bU} = Q(0)k_1(t) + \int_0^t k_1(t-\tau) \frac{dQ(\tau)}{d\tau}d\tau . \qquad (4.2)$$

or equivalently,

$$\frac{P(t)}{2\pi\rho bU} = k_1(0)Q(t) + \int_0^t k_1'(t-\tau)Q(\tau)d\tau. \tag{4.3}$$

Since $k_1(0) = \frac{1}{2}$, Laplace transformation of (4.3) yields

$$P(s) = 2\pi\rho bU\left\{0.5 + \mathcal{L}[k_1'(t)]\right\}Q(s). \tag{4.4}$$

Jones' approximation, (4.1), gives the transfer function relating Q to P as

$$\frac{P(s)}{Q(s)} = 2\pi\rho bU\left[\frac{0.5\bar{s}^2 + 0.2808\bar{s} + 0.01365}{\bar{s}^2 + 0.3455\bar{s} + 0.01365}\right]. \tag{4.5}$$

It is well known from linear system theory that the functional relation given by (4.5) may be described in the time domain by the constant co-efficient, linear, ordinary differential equations

$$\dot{x}_1 = x_2 \tag{4.6a}$$

$$\dot{x}_2 = -0.01365\left(\frac{U}{b}\right)^2 x_1 - 0.3455\left(\frac{U}{b}\right) x_2 + Q(t) \tag{4.6b}$$

$$P(t) = 2\pi\rho bU\left\{0.006825\left(\frac{U}{b}\right)^2 x_1 + 0.10805\left(\frac{U}{b}\right) x_2 + 0.5Q(t)\right\}.$$

Garrick proposed the approximation $k_1(t') \cong (t'+2)/(t'+4)$, but this function does not have a rational Laplace transform and the resulting approximation to $P(t)$ cannot be given by ordinary differential equations as in (4.6). Hence, in order to ensure the computational efficiency obtained by differential equations, it is customary to utilize approximations whose transforms are simple functions.

The rational transform in (4.5) may be evaluated at $\bar{s} = \bar{r}e^{i\theta}$ and the resulting real and imaginary portions compared to the generalized Theodorsen function shown in Fig. II-5. Figure IV-1 indicates that the approximation is a good representation of $C(\bar{s})$, especially in the right
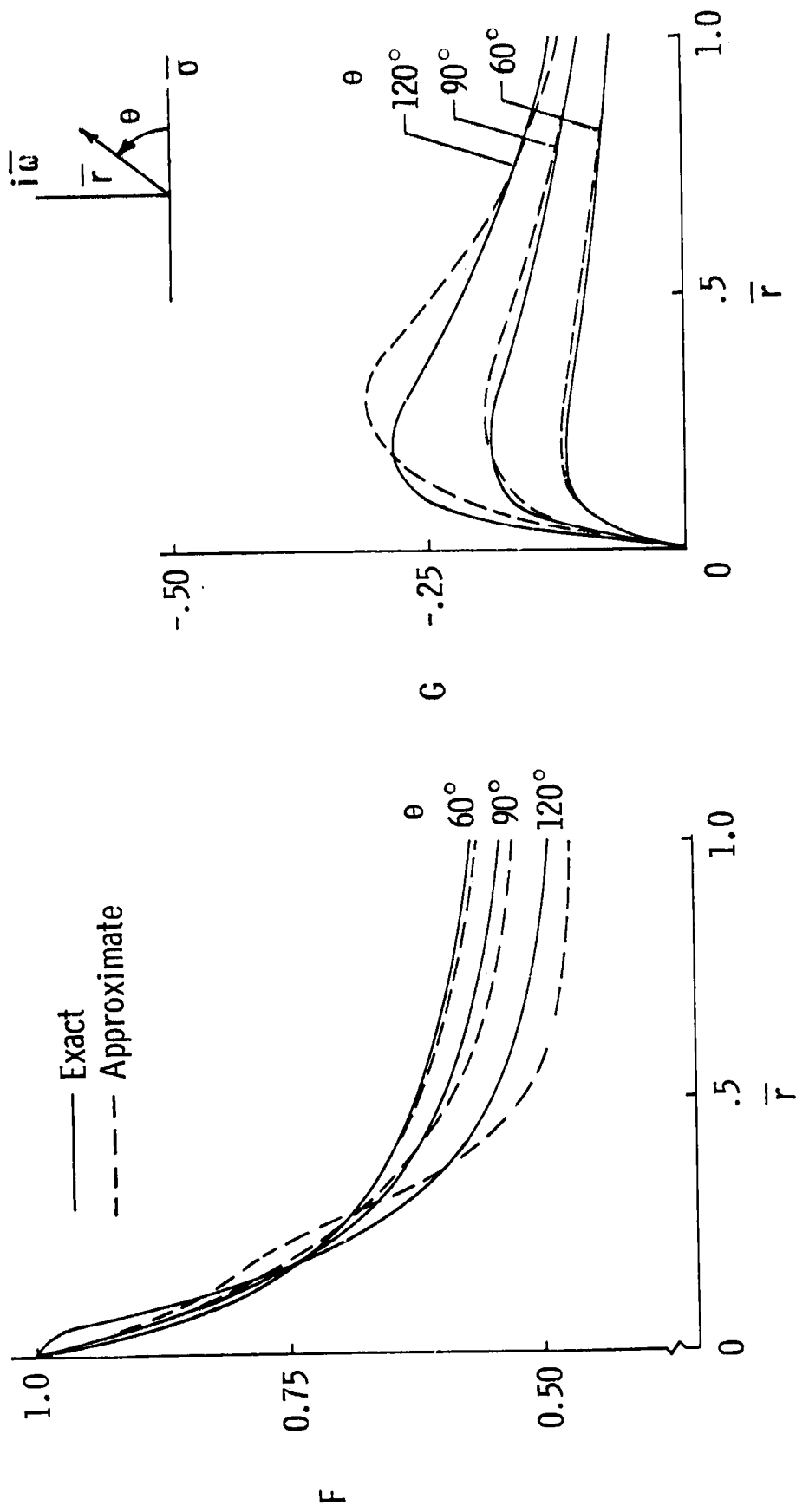
FIG. IV-1   COMPARISON OF THE GENERALIZED THEODORSEN FUNCTION AND R. T. JONES'
SECOND ORDER APPROXIMATION OF $C(\bar{s})$ AS A FUNCTION OF $\bar{r}$ AND θ

half-plane. The agreement deteriorates as $\bar{\sigma}$ increases beyond $90°$. This is primarily due to the proximity of the isolated poles at $\bar{s} = -0.0455$ and -0.3.

Figure IV-2 is a comparison between the exact nonrational lift coefficient shown in Fig. II-7, and the lift coefficient given by (4.5) for the motion given by (2.49). The exact coefficient is given by the last term of (2.50), while the approximate lift coefficient was obtained by partial fraction expansion with $Q(s) = \bar{\omega}/(\bar{s}+\bar{\sigma})^2+\bar{\omega}^2$ as

$$
c_{\ell_{nr}} \cong -2\pi \left\{ 0.5e^{-\bar{\sigma}t'} \sin\bar{\omega}t' \right.
$$

$$
+ \frac{a\bar{\omega}}{(0.0455-\bar{\sigma})^2+\bar{\omega}^2} \left[e^{-0.0455t'} - e^{-\bar{\sigma}t'} \left(\cos\bar{\omega}t' + \frac{\bar{\sigma}-0.455}{\bar{\omega}} \sin\bar{\omega}t' \right) \right]
$$

$$
\left. + \frac{b\bar{\omega}}{(0.3-\bar{\sigma})} \left[e^{-0.3t'} - e^{-\bar{\sigma}t'} \left(\cos\bar{\omega}t' + \frac{\bar{\sigma}-0.3}{\bar{\omega}} \sin\bar{\omega}t' \right) \right] \right\}
$$

$$
\tag{4.7}
$$

where $\bar{\sigma} = \bar{\omega} = 0.1414$, $a = 0.0074999$, and $b = 0.10055$. The approximate lift matches the exact lift very closely even for this heavily damped airfoil motion with $\zeta = 0.707$. This would indicate that equations (4.5) and (4.6) may be used to calculate accurate circulatory loads for incompressible flow.

A unique feature of the incompressible case is that all of the circulatory loads involve the single nonrational function $C(\bar{s})$, greatly simplifying the approximation problem. Equations (4.6) are in a form which is compatible with the structural equations, (2.1). The resulting model uses the augmented states

$$
\underline{x}_p = \begin{bmatrix} x_1 \\ x_2 \end{bmatrix}
$$

and is given by
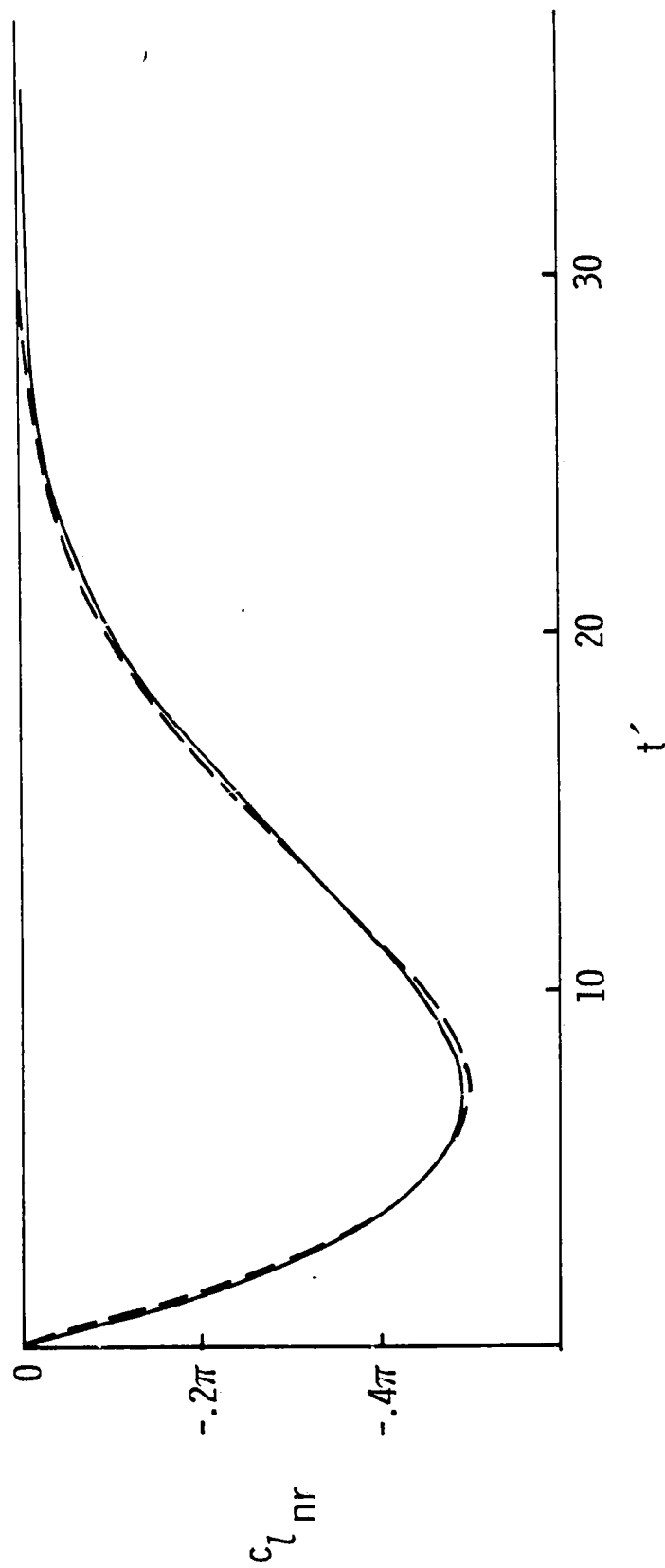
FIG. IV-2   COMPARISON OF NONRATIONAL LIFT COEFFICIENT AND LIFT COEFFICIENT
OBTAINED FROM R. T. JONES' APPROXIMATION

$$\begin{bmatrix} I & 0 & 0 \\ 0 & M' & 0 \\ 0 & 0 & I \end{bmatrix} \begin{bmatrix} \dot{x} \\ \ddot{x} \\ \dot{x}_p \end{bmatrix} = \begin{bmatrix} 0 & I & 0 \\ -K' & -B' & D \\ E_1 & E_2 & F_p \end{bmatrix} \begin{bmatrix} x \\ \dot{x} \\ x_p \end{bmatrix} + \begin{bmatrix} 0 \\ G \\ 0 \end{bmatrix} u \qquad (4.8)$$

where

$$M' = M_s - \eta M_{nc}$$

$$K' = K_s - \eta \left(\frac{U}{b}\right)^2 \left(K_{nc} + 0.5\ RS_1\right)$$

$$B' = B_s - \eta \left(\frac{U}{b}\right) \left(B_{nc} + 0.5\ RS_2\right)$$

$$D = \eta \left(\frac{U}{b}\right) R \left[0.006825 \left(\frac{U}{b}\right)^2, \quad 0.10805 \left(\frac{U}{b}\right)\right]$$

$$F_p = \begin{bmatrix} 0 & 1 \\ -0.01365 \left(\frac{U}{B}\right)^2 & -0.3455 \left(\frac{U}{b}\right) \end{bmatrix}$$

$$E_1 = \left(\frac{U}{b}\right) \begin{bmatrix} 0 \\ \hline S_1 \end{bmatrix}$$

$$E_2 = \begin{bmatrix} 0 \\ \hline S_2 \end{bmatrix} .$$

For an airfoil with n degrees-of-freedom, $\underline{x}$ is n-dimensional, while $\underline{x}_p$ is two dimensional. The submatrices in (4.8) are dimensioned conformably with these vectors and the total dimension of the model is $2n + 2$. Since the 'inertia matrix' of the left side of the equation is nonsingular, multiplication by its inverse gives the standard form used by control engineers

$$\dot{X} = FX + G_1 u \qquad (4.9)$$

with

$$X = \begin{bmatrix} \underline{x} \\ \dot{\underline{x}} \\ \underline{x}_p \end{bmatrix}, \qquad F = \begin{bmatrix} 0 & I & 0 \\ -(M')^{-1}K' & -(M')^{-1}B' & (M')^{-1}D \\ E_1 & E_2 & F_p \end{bmatrix}, \qquad G_1 = \begin{bmatrix} 0 \\ (M')^{-1}G \\ 0 \end{bmatrix}.$$

The elements of F are functions of (U/b) and the eigenvalues of F are approximate roots of the aeroelastic equations of motion. Figure IV-3 compares these eigenvalues to the exact roots of the section of Table III-3. From the close agreement between the exact roots and the approximate roots, it is concluded that the linear rational model of the incompressible two-dimensional section, (4.9), is interchangeable with the exact model, (3.4), for the purposes of engineering design.

It is also possible to compare the frequency responses of the exact and approximate models. The frequency response of $\underline{x}_1$ due to sinusoidal oscillation of u_j is obtained from (3.4) by tabulating $(\underline{x}_i/u_j)(i\omega) = N_j^i(i\omega)/D(i\omega)$. Similarly, the frequency response is calculated for the approximate model of (4.9) by tabulating the transfer function of $(X_i/u_j)(s)$ for $s = i\omega$. Figure IV-4 compares $(h/\beta_c)(i\omega)$ and $(\alpha/\beta_c)(i\omega)$ for the section of Table III-2. The good agreement between the frequency responses, especially in the range of flutter at $\omega \cong 70$ rad/sec, indicates that the poles and zeroes of the approximate model provide valid representations of the exact system. The dip in the amplitude seen on all of these frequency response plots in the range $70 < \omega < 80$ rad/sec indicates the presence of complex zeroes near the flutter poles. The location of these zeroes is critical to any active flutter control scheme and they will be studied in detail in the next chapter.

To apply the above technique to other aerodynamic regimes, indicial loading functions must be calculated so that the exponential approximations may be obtained. Although there is a significant literature concerning such functions [Lomax et. al, Ref. 10; Drischler, Ref. 71], their calculation is laborious [e.g., Rodden and Stahl, Ref. 72], and the technique has not been used widely.
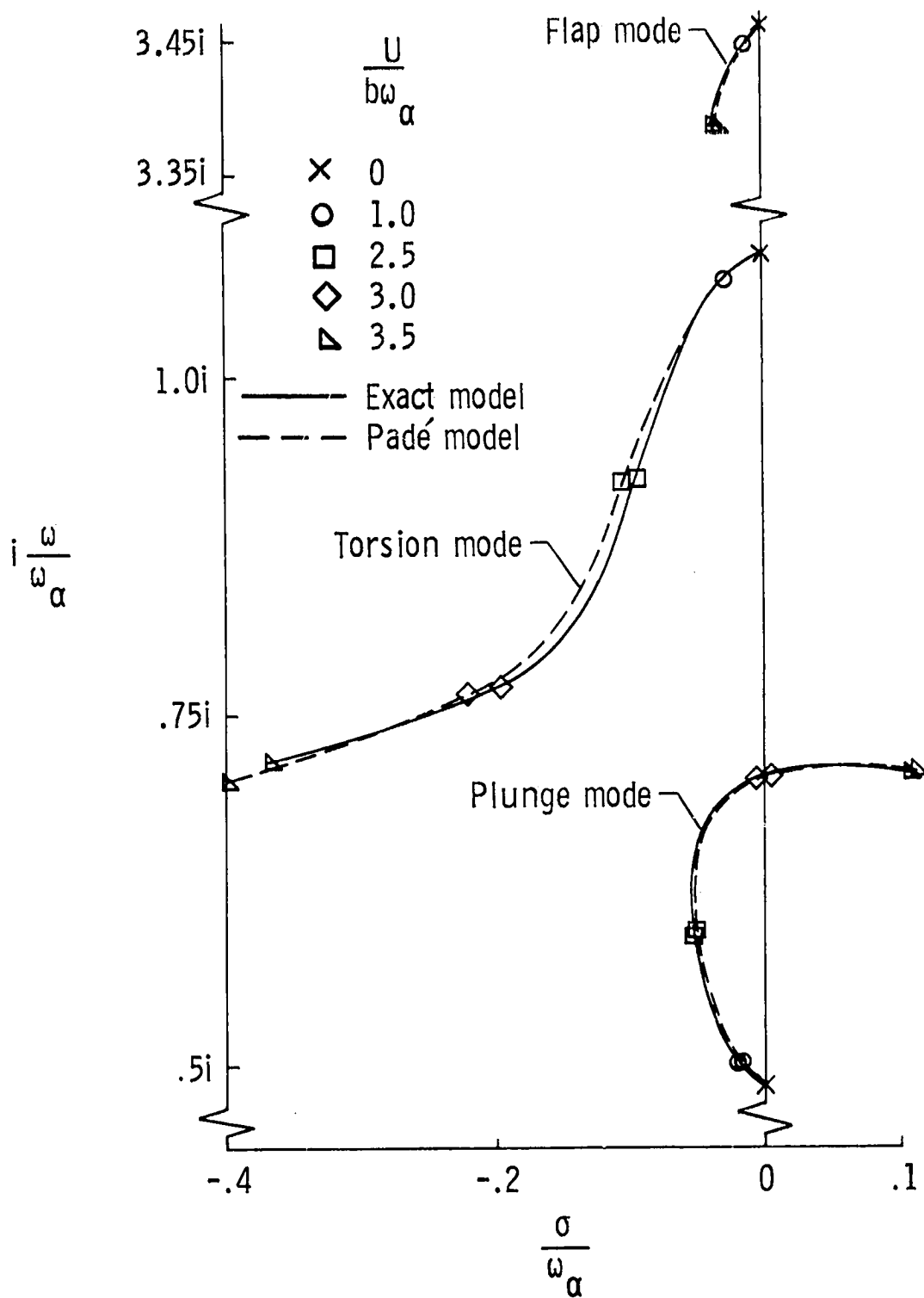
FIG. IV-3   COMPARISON OF ROOTS OBTAINED USING THE GENERALIZED
THEODORSEN FUNCTION AND R. T. JONES' APPROXIMATION
TO $C(\bar{s})$ AS A FUNCTION OF $U/b\omega_\alpha$
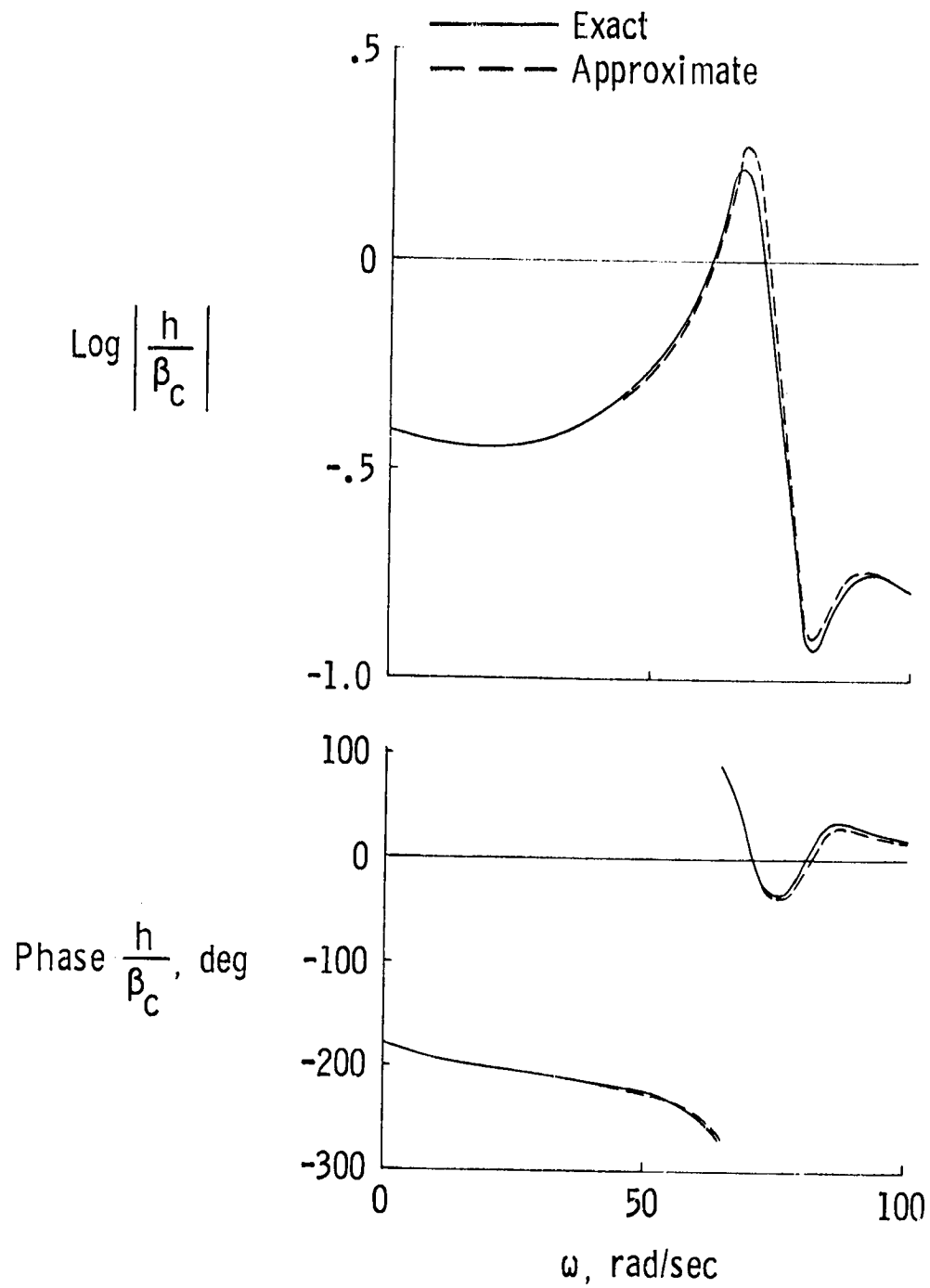
(a) PLUNGE

FIG. IV-4 COMPARISON OF FREQUENCY RESPONSES OF PLUNGE AND
TORSION DUE TO FLAP DEFLECTION OBTAINED FROM THE
EXACT MODEL AND R. T. JONES' APPROXIMATION FOR $C(\bar{s})$
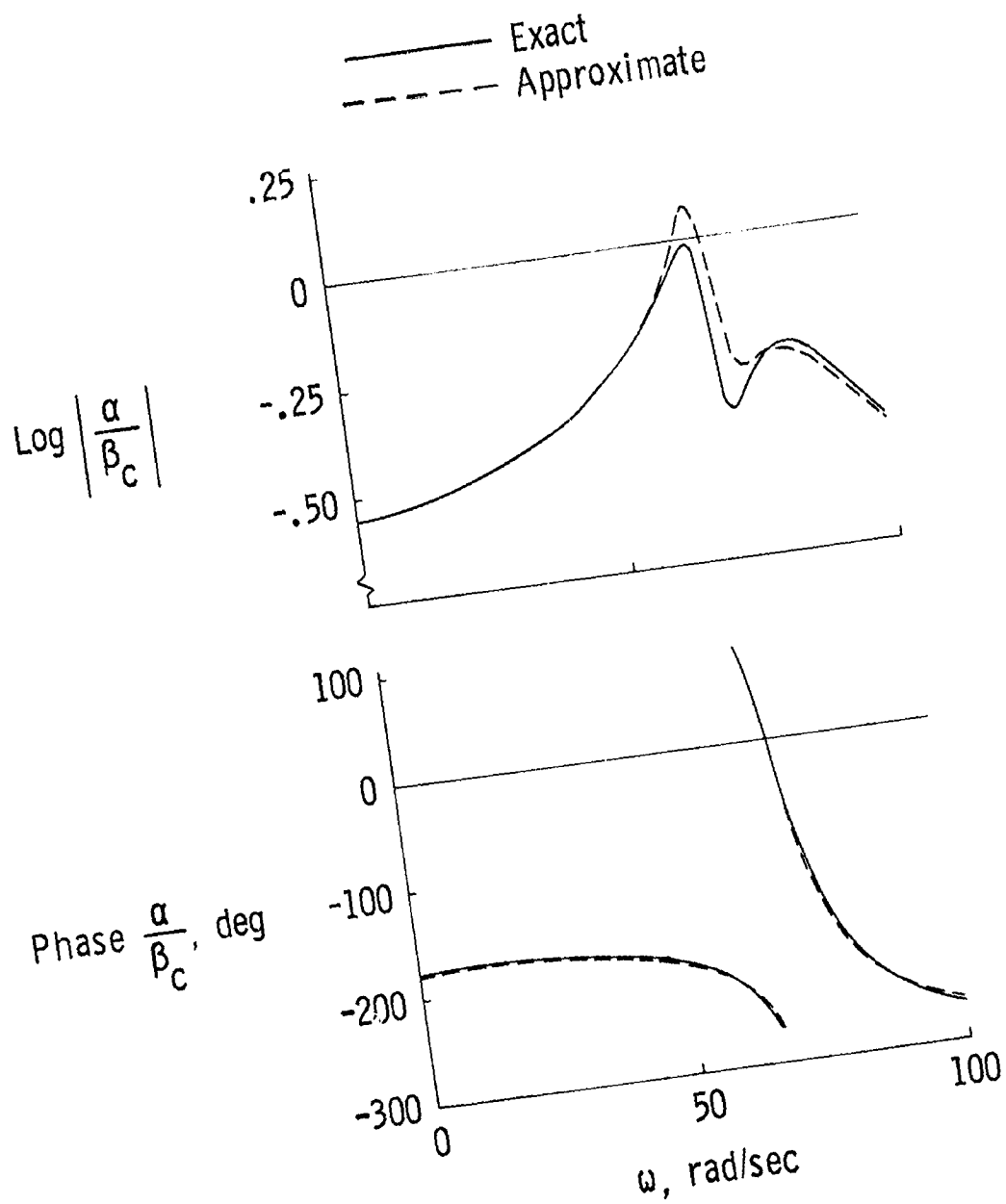
(b) TORSION

FIG. IV-4 CONCLUDED

B. VEPA'S PADÉ APPROXIMANT METHOD

The problems associated with the calculation of indicial loading functions led Vepa to an alternative method [69], [33], [34]. The availability of the aerodynamic loads for simple harmonic motions, from numerous well-developed techniques (e.g., kernel function or finite element methods), suggested the approximation of the loads by Padé approximants. A Padé approximant (PA) of a function is a ratio of two polynomials which approximates the function in some range of its argument. Baker [73] gives a thorough summary of the properties of Padé approximants for the case where a Taylor series expansion of the function is available. The usefulness of PAs is due to the ease of the analysis of the resulting analytic, rational functions as opposed to the original function. If the original function is known only in tabulated form, as for the aerodynamic loads, a PA may still be obtained by fitting the rational fraction $N(s)/D(s)$ to the tabulated values for $s = ik$ using (for example) a least square technique.

The intent of the application of such approximants to unsteady aerodynamic loads is to allow the aeroelastic equations to be solved for arbitrary motions, i.e., throughout the s-plane. This assumes the analyticity of the unsteady loads, a point of some confusion in the past due to the discussion of the generalized Theodorsen function. Nevertheless, such approximations have been utilized, a primary example being the design of the active flutter control system described by Roger and Hodges [4].

Vepa suggested that the PA of the generalized force, q_{ij}, in the ith mode due to deflection in the jth mode could best be represented by

$$q_{ij}(s,M) \;=\; \frac{a_o s^{N+1} + a_1 s + \cdots + a_N s + a_{N+1}}{M s^N + b_2 s^{N-1} + \cdots + b_{N+1}} . \qquad (4.10)$$

This is referred to as an [N,N+1] PA. The PA is constructed to yield the correct steady-state value q^o_{ij}, and may be modeled by N constant

-73-

coefficient, ordinary differential equations. The high frequency limit, $a_o s/M$, may be chosen to give the piston theory load, while in incompressible flow with $M = 0$, a_o yields the noncirculatory, 'virtual mass' load. Vepa [33] shows that the numerator coefficients, a_i, are determined by the denominator coefficients b_i, and by constraints (e.g., $a_{n+1} = b_{n+1} q^o_{ij}$). Thus the determination of the PA for q_{ij} involves the determination of the N constants, b_i, $i = 2, \ldots, N+1$. Hence, if $q_{ij}(ik,M)$ is tabulated for more than N values of k, the b_i may be determined by a linear least squares technique.

Vepa comments that in order to obtain accurate PAs, a large number of reduced frequency values are required in the high frequency and the low frequency range. In his Ref. 33, tables of [2, 3] PAs are given for plunge, rotation, and flap modes in two-dimensional flow for $M = 0.3$, 0.4, 0.5, 0.6, 0.7, 1.5, 1.75, and 2.0. The location of the roots of the denominator of (4.10) are of concern since the PAs of unsteady loads are approximations to stable dynamic systems and should themselves be stable. Also, in the incompressible case, the loads are multiple-valued functions with branch cuts and, since the PAs are single-valued, they cannot yield valid approximations along the cut. Baker gives examples indicating that the poles of the PAs cluster along the cut and conjectures that as the order of the PA tends to infinity, the poles tend to a 'pole-distribution' along the cut. Since the incompressible loads have a branch cut along the negative real axis, the poles of R.T. Jones' approximation would thus be expected to be found there and this is indeed the case, the stable poles being located at $\bar{s} = -0.0455$ and $\bar{s} = -0.3$.

This approximation technique would be an attractive method for the analysis of the aeroelastic system were it not for the high order of the resulting model. With each generalized load modeled by its own independent [N, N+1] PA, the dimension of the model is $2n + Nn^2$. For a three DOF section with [2, 3] PAs, the dimension is 24; 6 structural states and 18 PA states. On a realistic design problem, the dimension associated with the approximants may become ten times that of the original structural model. The design obtained in Ref. 4 used from 18 to 27 structural

-74-

modes, while the total dimension was as high as 200. It would obviously be desirable to obtain comparable accuracy with lower order approximations.

C. THE MATRIX PADÉ APPROXIMANT

Examination of the transient responses obtained by inverse Laplace transformation of the PAs led Vepa to attempt the approximation of the generalized load matrix, $Q(\bar{s}, M)$, by matrix PAs [73.]. The load matrix relates $\underline{X}(s)$ to L as

$$\frac{L}{\rho_b^2 U^2} = Q(\bar{s}, M) \, \underline{X}(s) \tag{4.11}$$

and the matrix PA is

$$Q(\bar{s}, M) = P(\bar{s}) R(\bar{s})^{-1} \tag{4.12}$$

where

$$P(\bar{s}) = \sum_{i=o}^{N+1} P_i \bar{s}^i, \qquad R(\bar{s}) = \sum_{i=o}^{N-1} R_i \bar{s}^i + I \bar{s}^N .$$

The minimum number of augmented states is given by $N = 1$,

$$Q(\bar{s}, M) = [P_o + P_1 \bar{s} + P_2 \bar{s}^2][I \bar{s} + R_o]^{-1} . \tag{4.13}$$

The properties of $Q(\bar{s}, M)$ are dependent upon the eigenvalues of the matrix R_o, and the philosophy underlying the use of the matrix PA is that the individual loads q_{ij} may be approximated by suitable linear combinations of 'shared' eigenvalues. As in the scalar case, the numerator matrices P_i are determined by R_o and independent constraints, while R_o is determined by a least squares procedure. The numerator matrices allow three constraints, one of which is the matching of the steady-state loads, $Q(0, M)$. This determines P_o as

$$P_o = Q_{ss}(0,M)R_o^{-1} . \tag{4.14}$$

The remaining two constraints may be used to enforce a match between the matrix PA and the tabulated simple harmonic loads at the anticipated reduced frequency of flutter, and with $Q(ik_f, M) = Q_1(k_f) + iQ_2(k_f)$

$$P_1 = \frac{Q_2(k_f)R_o}{k_f} + Q_1(k_f) \tag{4.15}$$

$$P_2 = \frac{Q_2(k_f)}{k_f} + \frac{Q_{ss}(0,M) - Q_1(k_f)}{k_f^2} R_o . \tag{4.16}$$

Although the piston theory limit is not enforced, the piston theory loads Q_{PT} are used with (4.16) to obtain a solution for R_o. The simple harmonic loads are given at m values of reduced frequency yielding

$$\frac{Q_1(k_\ell)-Q_{ss}(0,M)}{k_\ell^2} R_o = \frac{Q_2(k_\ell)}{k_\ell} - Q_{PT}; \qquad \ell = 1, \dots, m . \tag{4.17}$$

Equation (4.17) provides nm equations for the n^2 unknown elements of R_o and with $m > n$ a least squares solution is possible. The matrix PA of (4.13) requires only one augmented state for each degree-of-freedom of the structural model, and the resulting model has dimension $3n$ as opposed to $2n + Nn^2$ for the previous PA model.

The incorporation of the matrix PA of (4.13) into the structural equations is facilitated by transformation to the state space model—

$$\dot{x}_p = F_p x_p + G_p x \tag{4.18a}$$

$$\frac{L}{\rho b^2 U^2} = x_p + H_1 x + H_2 \dot{x} \tag{4.18b}$$

where

-76-

$$F_p = -[P_0 - P_1 R_0 + P_2 R_0^2] R_0 [P_0 - P_1 R_0 + P_2 R_0^2]^{-1}$$

$$G_p = P_0 - P_1 R_0 + P_2 R_0^2$$

$$H_1 = P_2$$

$$H_2 = \left(\frac{b}{U}\right)(P_1 - P_2 R_0) \ .$$

The matrix PA model is given by (2.1) and (4.18)

$$
\begin{bmatrix} I & 0 & 0 \\ 0 & M_s & 0 \\ 0 & 0 & 1 \end{bmatrix}
\begin{bmatrix} \dot{x} \\ \ddot{x} \\ \dot{x}_p \end{bmatrix}
=
\begin{bmatrix} 0 & I & 0 \\ -K_s + \eta\left(\frac{U}{b}\right)^2 H_1 & -B_s + \eta\left(\frac{U}{b}\right)^2 H_2 & \eta\left(\frac{U}{b}\right)^2 \\ G_p & 0 & F_p \end{bmatrix}
\begin{bmatrix} x \\ \dot{x} \\ x_p \end{bmatrix}
+
\begin{bmatrix} 0 \\ G \\ 0 \end{bmatrix} u. \quad (4.19)
$$

The accuracy of the matrix PA will be illustrated in the remainder of this section.

C.1 Supersonic Matrix Padé Approximants

Simple harmonic oscillatory supersonic loads (2.67) were calculated for a three DOF section with the elastic axis at midchord and a 20 percent chord aileron ($a = 0.0$, and $c = 0.6$). The load matrix, $Q(ik,M)$ was calculated for $k = 0.05$, 0.1, 0.2, 0.3, 1.0, 2.0, and 3.0 for the Mach numbers $M = 1.5$, 2.0, and 2.5. The steady-state loads were calculated from the Ackeret-formula

$$c_\ell = \frac{4}{\sqrt{M^2-1}} \frac{dz_a}{dx}$$

as

$$\frac{L}{\rho b^2 U^2} = \frac{1}{\sqrt{M^2-1}} \begin{bmatrix} 0 & 4 & -2(1-c) \\ 0 & 0 & (1-c^2) \\ 0 & (1-c)^2 & -(1-c)^2 \end{bmatrix} \begin{bmatrix} h \\ \gamma \\ \beta \end{bmatrix} . \quad (4.20)$$

-77-

The piston theory loads are derived from the starting pressure $\Delta p / \frac{1}{2}\rho U^2 =$
$= (4/M)(\partial z_a / \partial t)$

$$\frac{L}{\rho b^2 U^2} = \frac{1}{M}(\frac{b}{U}) \begin{bmatrix} -4.0 & 0.0 & -0.16 \\ 0 & -1.333 & 0.1386 \\ -0.16 & 0.1386 & -0.0486 \end{bmatrix} \begin{bmatrix} h \\ \alpha \\ \beta \end{bmatrix} . \qquad (4.21)$$

The matrix PAs were calculated for $M = 1.5$, 2.0, and 2.5 for the assumed flutter frequency $k_f = 0.2$, and the resulting approximants are tabulated in Table IV-1.

For this case, the exact loads may be calculated for general values of $\bar{s}$ and compared with the equivalent loads calculated from the PAs in Table IV-1. Figure IV-5 gives this comparison for the loads c_{ℓ_h}, $c_{m\alpha}$ and $c_{n\beta}$ at $M = 2.0$ for $\bar{s} = \bar{r}e^{i\theta}$ with $60° \le \theta \le 150°$. The two sets of loads are indistinguishable for $|k| = \bar{r} < 0.25$ and generally agree to within 5 percent for $\bar{r} < 0.5$.

The PAs of Table IV-1 were used to calculate the eigenvalues of (4.19) for the section of Table III-4. Figure IV-6 compares those eigenvalues to the exact roots of the aeroelastic equations from Fig. III-2. With $b = 1.35m$, and $a_\infty = 333$ m/sec, the reduced frequency is $0.11 < k < 0.23$. While the PA was constrained to yield the correct oscillatory loads at $k = 0.2$, good agreement between the exact and approximate roots is seen throughout this range of reduced frequencies.

From the discussion in Ch. III, Sect. A-2, it is known that the supersonic aerodynamics introduce an infinite sequence of poles of increasing modules to the aeroelastic system. Thus it may be anticipated that the eigenvalues of the PAs would provide estimates of these additional poles. The eigenvalues introduced by the PAs are given in Table IV-2. The first column of the table gives the eigenvalues of R_o (scaled by U/b). These poles are associated with the 'open-loop' aerodynamic medium as modeled by the PA. The second column of the table gives the eigenvalues of (4.19) introduced by the PAs, and may be interpreted as the 'closed-loop' poles resulting from the interaction of the structural

-78-

C-2

Table IV-1

SUPERSONIC MATRIX PADÉ APPROXIMANTS FOR A THREE-DEGREE-OF-FREEDOM SECTION

$(k_f = 0.2)$

	M = 1.5			M = 2.0			M = 2.5		
P_0	0.4626E1	0.6609E1	-0.1699E1	0.1464E2	0.1491E2	-0.1780E1	0.1657E2	0.1518E2	-0.1620E1
	-0.6151E1	-0.7645E1	0.1308E1	-0.1567E2	-0.1527E2	0.1403E1	-0.1680E2	-0.1483E2	0.1279E1
	0.1415E1	0.1793E1	-0.3296E0	0.3720E1	0.3651E1	-0.3518E0	0.4022E1	0.3574E1	-0.3207E0
P_1	-0.4528E1	-0.3060E1	-0.8441E0	-0.4346E1	-0.2458E1	-0.7223E0	-0.2719E1	-0.9679E0	-0.6308E0
	-0.6135E-1	-0.1365E0	0.6334E0	-0.1163E1	-0.1277E1	0.5780E0	-0.1752E1	-0.1696E1	0.5095E0
	-0.1333E0	-0.5630E-1	-0.1635E0	0.3037E0	0.3821E0	-0.1564E0	0.5376E0	0.5476E0	-0.1404E0
P_2	-0.2669E1	-0.1682E-1	-0.1060E0	-0.2010E1	-0.1675E-1	-0.8008E-1	-0.1613E1	-0.1661E-1	-0.6418E-1
	0.2161E-2	-0.9360E0	0.9377E-1	-0.1500E-1	-0.7049E0	0.6938E-1	-0.1874E-1	-0.5629E0	0.5557E-1
	-0.9598E-1	0.1200E0	-0.2847E-1	-0.6403E-1	0.8820E-1	-0.2149E-1	-0.5453E-1	0.6566E-1	-0.1714E-1
R_0	0.2033E1	0.2619E1	0.3200E-1	0.3726E1	0.3770E1	0.1534E-1	0.3985E1	0.3639E1	0.1540E-1
	-0.8560E0	-0.8239E0	-0.1785E-1	-0.2144E1	-0.1813E1	-0.1147E-1	-0.2533E1	-0.1924E1	-0.1232E-1
	-0.1075E2	-0.1336E2	0.2285E1	-0.4241E2	-0.4134E2	0.3797E1	-0.6013E2	-0.5311E2	0.4580E1

FIG. IV-5   COMPARISON OF GENERALIZED SUPERSONIC LOADS WITH LOADS OBTAINED FROM MATRIX PADÉ APPROXIMANTS AS FUNCTIONS OF $\bar{r}$ AND θ AT $M = 2.0$

(a) c_{ℓ_h}

(b) c_{m_α}

FIG. IV-5   CONTINUED

-81-

Re(c_{n_β})

Im(c_{n_β})

— Exact
-- Approximate

θ
60°
90°
120°
150°

(c) c_{n_β} CONCLUDED

FIG. IV-5   CONCLUDED

-82-
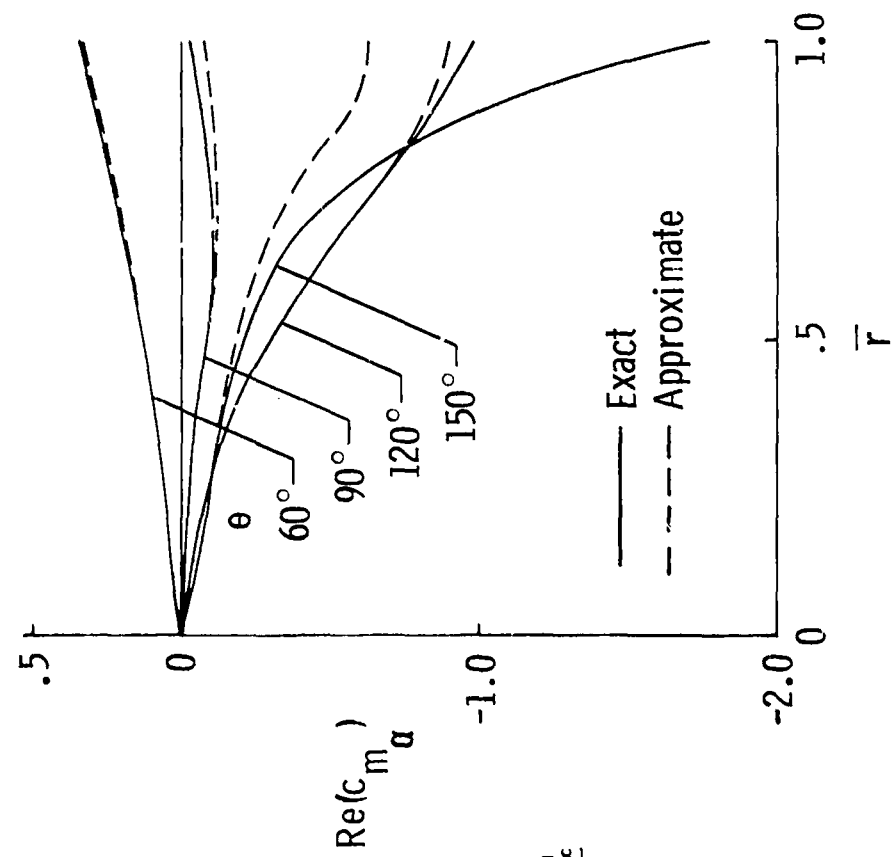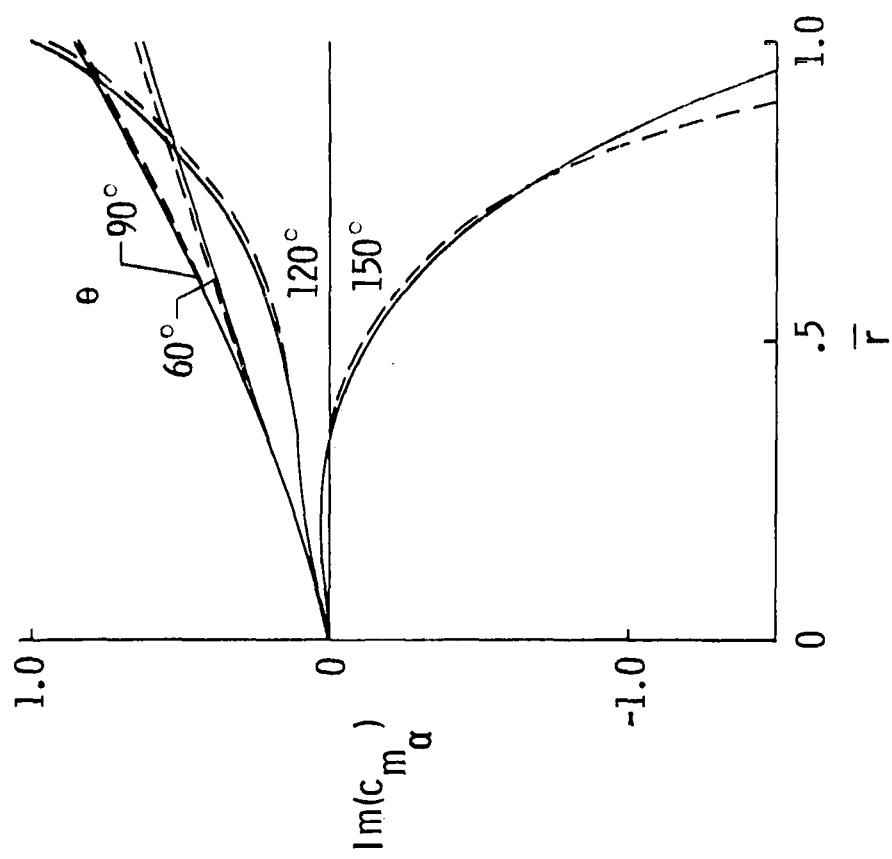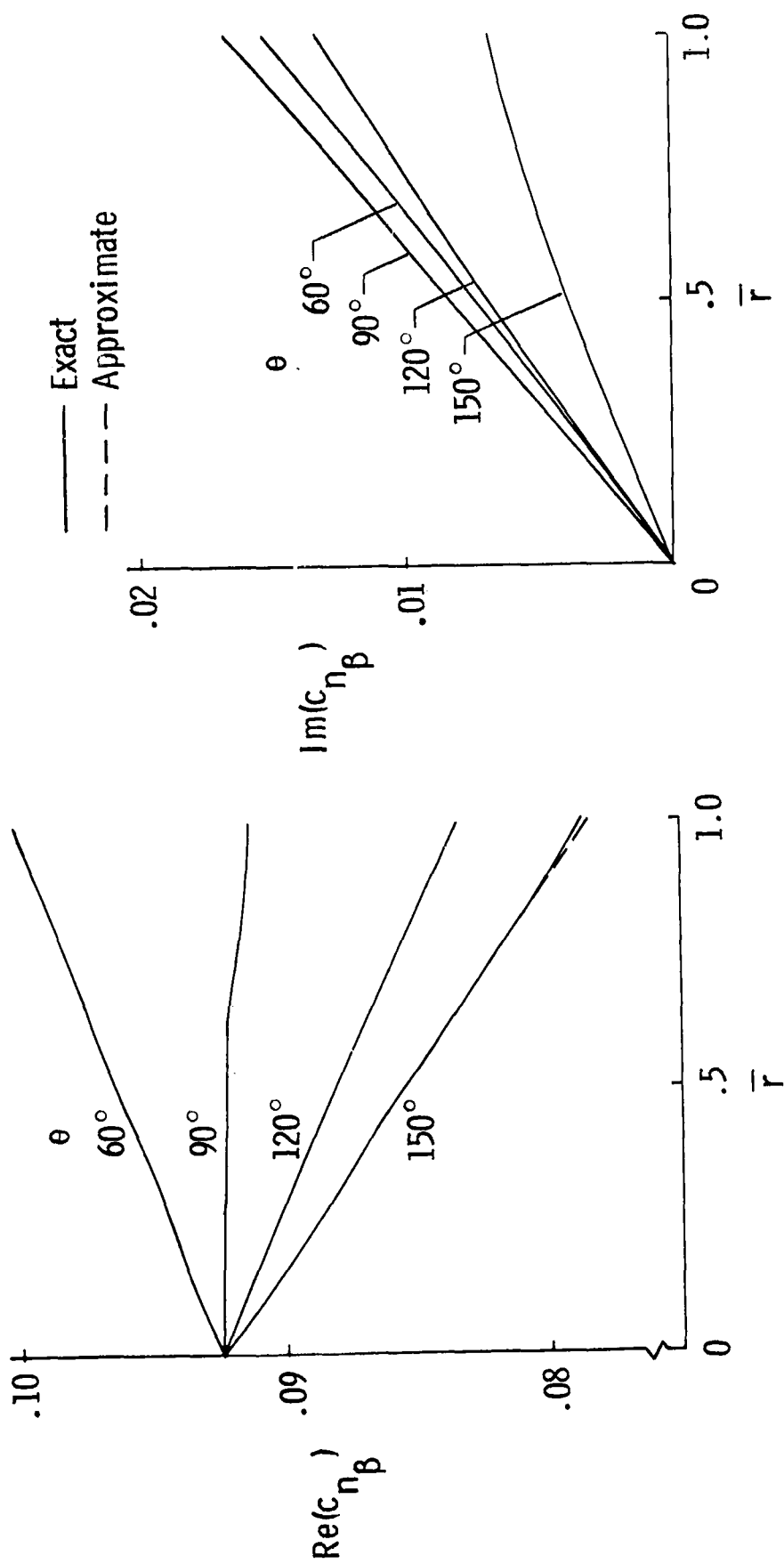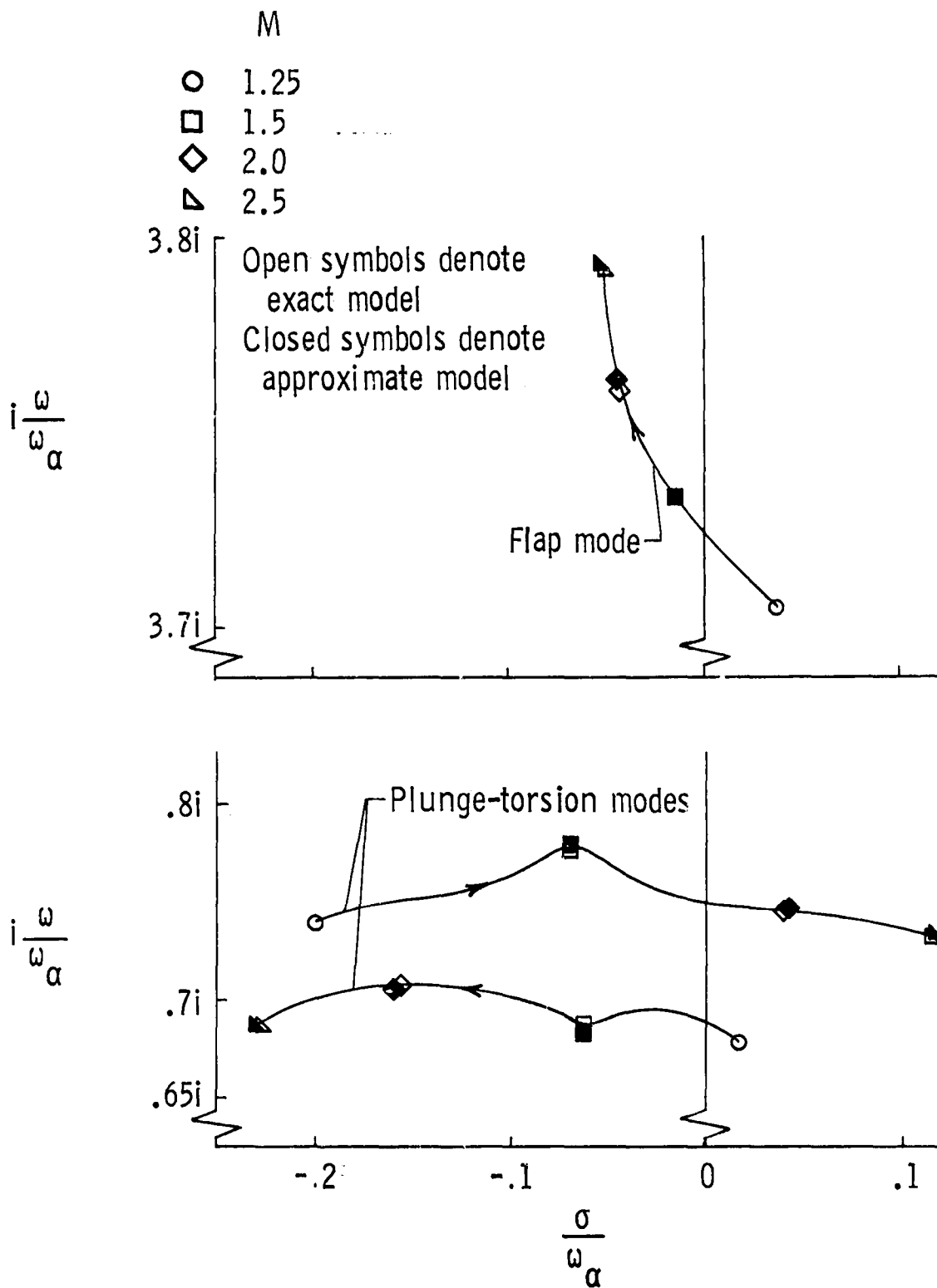
FIG. IV-6   COMPARISON OF ROOTS OBTAINED USING GENERALIZED
SUPERSONIC LOADS AND MATRIX PADÉ APPROXIMANTS
AS A FUNCTION OF M

dynamics with the aerodynamic medium.

Table IV-2
EIGENVALUES OF SUPERSONIC PADÉ APPROXIMANTS

M	Eigenvalues of $R_o(U\ b)$, rad sec		Eigenvalues of Eq. (4.19) (rad/sec)	
1.5	−690,	−193 ± i147	−844,	−243 ± i181
2.0	−1848,	−484 ± i331	−1855,	−480 ± i333
2.5	−2784,	−657 ± i448	−2785,	−655 ± i407

For this three DOF system, the eigenvalues of the PAs are characterized by a complex conjugate pair with slightly greater than critical damping and a real root of larger modulus. All of the eigenvalues are stable and increase in modulus with increasing Mach number. This correlates with well-known results of piston theory, in which no augmented states are required to model unsteady aerodynamics at hypersonic velocities. The eigenvalues are well above the bandwidth of the bending-torsion airfoil section $(\omega < 100$ rad/sec) and the slight difference between corresponding eigenvalues in the Table indicates that the modes of the PAs do not couple strongly with the structural modes. It is interesting to note that the complex pair at $M = 2.0$ do not correlate well with the exact eigenvalue of the aeroelastic system at $s = -1315 \pm i1501$ determined in Sect. III-A-2.

C-2   Subsonic Matrix Padé Approximants

Vepa has calculated matrix Padé approximants (PAs) for a three DOF section in subsonic flow and provided them to the author in a private communication [74]. Tables IV-3 and IV-4 present these PAs for $M = 0.3$, 0.4, 0.5, 0.6, and 0.7. Tabulated oscillatory aerodynamics at $k = 0$, 0.3, 0.4, 0.5, 0.6, and 5.0 were used to construct the approximants of Table IV-3 which assumed $k_f = 0.5$ while the approximants of Table IV-4 include the reduced frequency $k = 0.01$ and assume $k_f = 0.4$.

−84−

Table IV-3

SUBSONIC MATRIX PADE APPROXIMANTS FOR A THREE-DEGREE-OF-FREEDOM SECTION ($K_f = 0.4$)

	M = 0.3			M = 0.4			M = 0.5		
P_0	-0.5050E1	0.1197E1	-0.3825E0	-0.2390E1	0.9830E0	-0.2317E0	-0.1753E1	0.1353E1	-0.4838E-1
	-0.7954E1	0.8938E1	0.6498E0	-0.6570E0	0.6010E1	0.1018E0	-0.5862E0	0.5648E1	0.1382E1
	0.2522E0	-0.4337E0	-0.5253E-1	-0.5850E-1	-0.3046E0	-0.6760E-1	-0.3688E-1	-0.2690E0	-0.8100E-1
P_1	-0.2401E2	0.1778E2	-0.1398E1	-0.1029E2	0.1183E2	-0.2670E0	-0.7858E1	0.1043E2	0.6829E0
	-0.5749E1	0.2297E1	0.2044E0	-0.4534E1	0.1154E1	0.4874E0	-0.3423E1	0.1953E0	0.6213E0
	-0.3784E0	0.1790E0	-0.1080E0	-0.1773E0	0.1254E0	-0.9590E-1	-0.1290E0	0.1318E0	-0.8520E-1
P_2	-0.1241E2	0.1140E1	-0.8948E0	-0.9821E1	0.6305E0	-0.6222E0	-0.7869E1	0.6130E-1	-0.4935E0
	0.3262E0	-0.3340E1	0.6821E0	0.2630E-1	-0.2785E1	0.5569E0	0.8409E-1	-0.2629E1	0.4408E0
	-0.6440E0	0.3868E0	-0.1313E0	-0.4083E0	0.3080E0	-0.1089E0	-0.3335E0	0.3043E0	-0.9048E-1
R_0	0.3853E1	-0.5359E0	-0.9280E-2	0.2605E1	0.6820E-1	-0.1786E0	0.1927E1	0.3167E0	-0.2970E0
	-0.3194E1	0.3911E1	0.3181E0	-0.1174E0	0.2514E1	0.4534E0	-0.1237E0	0.2205E1	0.5641E0
	-0.3989E1	0.6124E1	0.6177E0	0.3802E0	0.3894E1	0.8001E0	0.1935E0	0.3314E1	0.9373E0

	M = 0.6			M = 0.7		
P_0	-0.1069E1	0.6490E0	0.4784E-1	-0.5380E0	0.1245E0	0.7260E-1
	0.4885E-1	0.2682E1	0.1373E1	0.3114E0	0.1047E1	0.1169E1
	-0.4579E-1	-0.1275E0	-0.7668E-1	-0.3965E-1	-0.5499E-1	-0.6399E-1
P_1	-0.5095E1	0.5260E1	0.9933E0	-0.3096E1	0.2110E1	0.9587E0
	-0.2702E1	-0.1564E0	0.6839E0	-0.2140E1	-0.3640E0	0.6730E0
	-0.7490E-1	0.6598E-1	-0.8460E-1	-0.2740E-1	0.1717E-1	-0.9430E-1
P_2	-0.6618E1	0.1810E-1	-0.4130E0	-0.5683E1	0.2013E-1	-0.3538E0
	0.6640E-1	-0.2201E1	0.3677E0	0.1032E0	-0.1878E1	0.3243E0
	-0.2628E0	0.2362E0	-0.8185E-1	-0.2052E0	0.1907E0	-0.8088E-1
R_0	0.1354E1	0.6853E0	-0.3673E0	0.8462E0	0.9774E0	-0.4008E0
	0.8270E-1	0.9667E0	0.5120E0	0.1332E0	0.3441E0	0.3873E0
	0.3595E0	0.1451E1	0.8308E0	0.3191E0	0.5420E0	0.6225E0

Table IV-4

SUBSONIC MATRIX PADÉ APPROXIMANTS FOR A THREE-DEGREE-OF-FREEDOM SECTION ($k_f = 0.4$)

	M = 0.3			M = 0.4			M = 0.5		
P_0	0.3200E0	0.5805E0	0.5514E-1	0.1565E0	0.3427F?	0.6050E-1	0.4140E-1	0.2176E0	0.5884E-1
	0.1259E2	0.6564E1	0.2320E1	0.8016E1	0.3830E1	0.2016E1	0.4400E1	0.2533E1	0.1684E1
	-0.7085E0	-0.3525E0	-0.1306E0	-0.4552E0	-0.2056E0	-0.1130E0	-0.1360E0		-0.9405E-1
P_1	0.6617E1	0.1089E1	0.2483E1	0.8552E1	0.1204E1	0.5338E1	-0.2646E0		0.1111E1
	0.1453E2	0.2502E1	-0.5063E1	0.1328E1	0.4518E0	-0.395?E1	0.5395E0		0.6205E0
	-0.5926E1	0.2089E0	-0.1378E0	-0.2620E2	0.7979E-1	-0.7637E-1	-0.1190E-1		-0.7996E-1
	0.1823E-1								
P_2	-0.1102E2	-0.8475E-1	-0.6862E0	-0.9525E1	-0.1109E-1	-0.5890E0	-0.6080E-1	-0.4942E0	
	-0.5264E0	-0.3859E1	0.6537E0	-0.3859E0	-0.2966E1	0.5064E0	-0.2677E0	0.4181E0	
	0.3298E0	-0.9494E-1	-0.7684E-1	-0.2060E0	0.2511E0	-0.8566E-1	-0.1849E0	-0.8161E-1	
						-0.1190E-1	0.4740E-1	-0.7996E-1	
R_0	0.2529E1	-0.4205E0	-0.1200E0	0.2064E1	0.2185E0	-0.2410E0	0.1511E1	0.6199E0	-0.3170E0
	0.5611E1	0.2894E1	0.1033E1	0.3452E1	0.1623E1	0.8623E0	0.1784E1	0.1014E1	0.6798E0
	0.9134E1	0.4607E1	0.1683E1	0.2583E1	0.2511E0	0.1401E1	0.2920E1	0.1616E1	0.1103E1

	M = 0.6			M = 0.7		
P_0	-0.8080E-2	0.1311E0	0.5484E-1	-0.1730E-1	0.7100E-1	0.4950E-1
	0.2328E1	0.1609E1	0.1398E1	0.1145E1	0.9860E0	0.1143E1
	-0.1336E0	-0.8680E-1	-0.7784E-1	-0.6630E-1	-0.5360E-1	-0.6380E-1
P_1	-0.1385E1	0.3194E0	0.9590E0	-0.1564E1	0.1772E1	0.7999E0
	-0.3080E1	0.4246E-1	0.7294E0	-0.2322E1	-0.3222E0	0.7857E0
	-0.1020E-1	0.2590E-1	-0.8720E-1	-0.4900E-3	0.1170E-1	-0.9953E-1
P_2	-0.6545E1	-0.2000E-2	-0.4176E0	-0.5661E1	0.5415E-1	-0.3535E0
	-0.1574E0	-0.2099E1	0.3662E0	-0.6545E-1	-0.1845E1	0.3214E0
	-0.1646E0	0.1875E0	-0.8130E-1	-0.1447E0	0.1822E0	-0.8320E-1
R_0	0.1062E1	0.8643E0	-0.3594E0	0.6645E0	0.1018E1	-0.3810E0
	0.8736E0	0.5957E0	0.5210E0	0.3844E0	0.3264E0	0.3801E0
	0.1436E1	0.9507E0	0.8441E0	0.6545E0	0.5227E0	0.6150E0

Vepa's sign conventions differ from those used herein in that: h, P are positive upwards, and β, M^{β} are positive for trailing-edge upwards rotation of the aileron. The pitching moment is calculated about midchord and a quarter-chord aileron is assumed. The oscillatory aerodynamics were calculated by Vepa using a kernel function program described in Ref. 33.

While no calculations are available to check the validity of these PAs for arbitrary complex values of s, they may be compared to known simple harmonic oscillatory loads. Figure IV-7 compares $c_{\ell h}$, $c_{m\alpha}$, and $c_{n\beta}$ for $\bar{s} = ik$ with the Tables [75], [76] based on Timman and Van deVooren's Mathieu function solution [12]. The PA of Table IV-3 gives an excellent match except for $Re(c_{n\beta})$ which is 10 percent low at k = 0.3. The approximants of Table IV-4, with the low frequency point k = 0.01 included, show a deterioration in agreement with the accepted values. The constraint imposed on the latter PA by requiring agreement at k = 0.4 is clearly seen, however. It is concluded that with appropriate checks, the matrix PA technique can provide a good augmented state model of oscillatory subsonic loads which are also valid approximations in the vicinity of the iω axis.

The eigenvalues of the R_o matrices of Tables IV-3 and IV-4 are given in Table IV-5. All of the eigenvalues are distributed along the negative real axis except for the PA of Table IV-4 at M = 0.3 and 0.4. Evidently, the inclusion of loads at k = 0.01 causes the approximant to develop complex conjugate roots with the resulting deterioration in agreement at higher values of k shown in Fig. IV-7. Henceforth, only the approximant of Table IV-3 will be used.
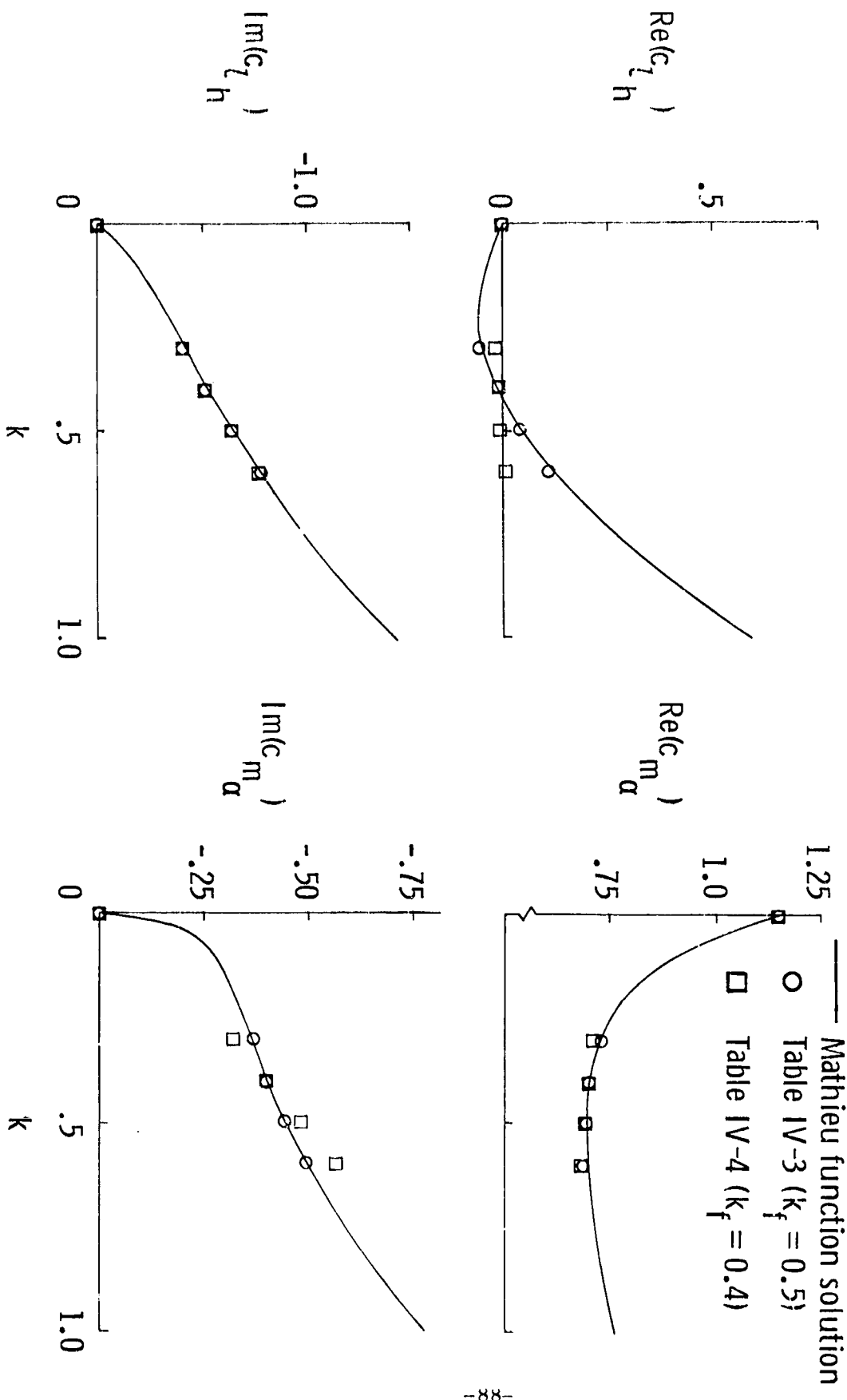
FIG. IV-7   COMPARISON OF SUBSONIC OSCILLATORY LOADS CALCULATED USING MATRIX PADÉ
APPROXIMANTS AND THE MATHIEU FUNCTION SOLUTION AT M = 0.5
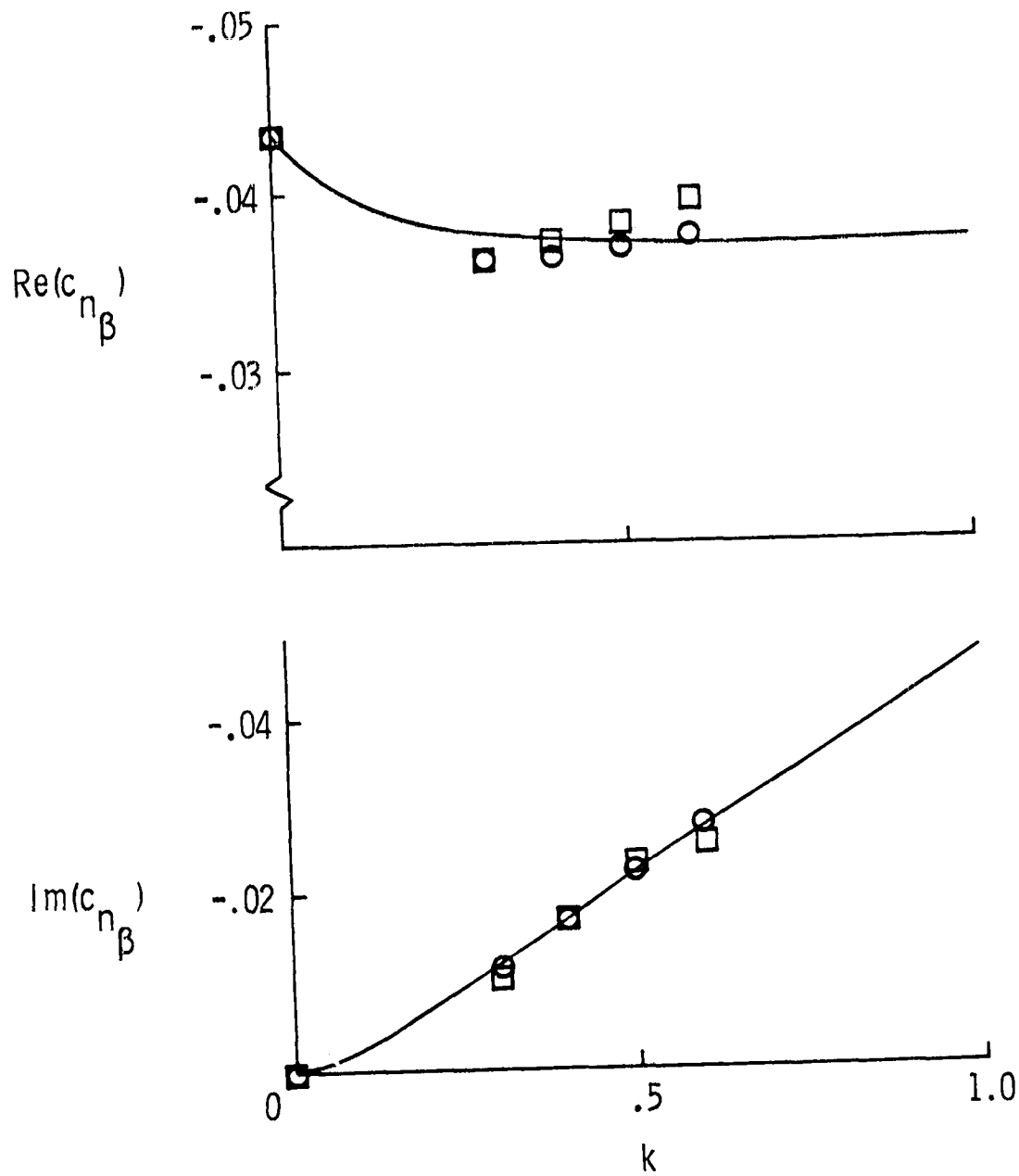
FIG. IV-7.   CONCLUDED

Table IV-5

EIGENVALUES OF R_0 FOR SUBSONIC MATRIX PADÉ APPROXIMANTS

	M	$\bar{s}_1$	$\bar{s}_2$	$\bar{s}_3$
	0.3	-0.09504	-2.807	-5.480
	0.4	-0.1095	-2.560	-3.250
Table IV-3	0.5	-0.1218	-1.863	-3.084
	0.6	-0.1091	-1.244	-1.798
	0.7	-0.08734	-0.5887	-1.137
	0.3	-0.02374	$-3.541 \pm i\ 1.560$	
	0.4	-0.02262	$-2.533 \pm i\ 0.6013$	
Table IV-4	0.5	-0.02212	-1.263	-2.343
	0.6	-0.02105	-0.6990	-1.782
	0.7	-0.04512	-0.3401	-1.221

D. STATIC DIVERGENCE

If the incremental moment generated by airfoil pitching is greater than the restoring moment of the torsional spring K_α, the airfoil is said to be statically divergent. The divergence velocity is given by [52, p. 193]

$$U_D = \frac{K_\alpha}{2b^2(\tfrac{1}{2} - a) \dfrac{\partial c_\ell}{\partial_\alpha}} \quad . \tag{4.22}$$

Static divergence in incompressible flow may be studied using the single DOF pitch equation

$$I_\ell s^2 \alpha(s) + K_\alpha \alpha(s) = 2\pi\rho b^2 U(\tfrac{1}{2}+a) C(\bar{s})[b(\tfrac{1}{2}-a)s + U]\alpha(s) \quad . \tag{4.23}$$

Substituting (4.22) and assuming $\partial c_\ell/\partial\alpha = 2\pi$

$$\left\{ s^2 - \omega_\alpha^2 \, C(\bar{s}) \, \frac{U}{U_D^2} \left[b(\tfrac{1}{2}+a)s + U \right] + \omega_\alpha^2 \right\} \alpha(s)$$

$$= \quad 0 \; . \tag{4.24}$$

Since static divergence is a low frequency phenomenon, the s^2 and s terms may be neglected, giving

$$\left[1 - C(\bar{s}) \left(\frac{U}{U_D} \right)^2 \right] \alpha(s) \; = 0 \; . \tag{4.25}$$

A pole of the aeroelastic system occurs at values of s for which the coefficient in (4.25) is zero. Since $C(\bar{s})$ is purely real only on the positive real axis, poles can only occur there. Also, along the positive real axis, $C(\bar{s})$ decreases monotonically from a value of 1.0 at $r = 0$ to 0.5 at $r = \infty$. Hence, a pole cannot occur for $U < U_D$ and for $U > U_D$, only one real pole can occur. This mode produces the motion of the diverging airfoil and occurs in addition to the $2n$ structural poles.

The occurrence of this divergence mode may be studied by locating the poles of the system in the s-plane. The exact system model of (3.4) or the Padé model of (4.9) may be used to locate these poles. The airfoil described by Table III-3 was modified to yield a divergence speed close to the flutter speed by setting $\mu = 5$ and $a = 0$. Table IV-6 compares the pertinent roots of the exact and Padé models as a function of airspeed. The plunge and torsion mode poles are given for both models and the augmented state pole with largest magnitude is given for the Padé model. The divergence speed of this three DOF section at $U/b\omega_\alpha = 1.13$ is indicated for the exact model by the emergence of an additional real pole on the positive real axis. Since the R.T. Jones approximation to $C(\bar{s})$ is accurate at low frequencies, the Padé model gives a valid approximation to

-91-

this mode. Static divergence of a finite wing was studied by Rodden and
Stahl [72] using strip theory and augmented states. They also found the
static divergence mode to be given by the augmented state with largest
magnitude.

Table IV-6

STATIC DIVERGENCE IN INCOMPRESSIBLE FLOW
(poles in rad/sec)

$\dfrac{U}{b\omega_\alpha}$	Exact Model	Padé Model
1.10	$7.407 \pm i\ 73.51$ $-36.10 \pm i\ 48.14$	$6.974 \pm i\ 73.29$ $-25.61 \pm i\ 31.79$ -0.6253
1.11	$7.825 \pm i\ 73.18$ $-37.02 \pm i\ 48.04$	$7.314 \pm i\ 72.96$ $-25.85 \pm i\ 31.80$ -0.347
1.12	$8.150 \pm i\ 72.86$ $-37.94 \pm i\ 47.95$	$7.650 \pm i\ 72.63$ $-26.09 \pm i\ 31.81$ -0.0652
1.13	$8.470 \pm i\ 72.55$ $-38.87 \pm i\ 47.85$ $+0.1885$	$7.982 \pm i\ 72.31$ $-26.33 \pm i\ 31.81$ $+0.2431$
1.14	$8.786 \pm i\ 72.23$ $-39.80 \pm i\ 47.75$ $+0.4853$	$8.309 \pm i\ 71.99$ $-26.58 \pm i\ 31.82$ $+0.5702$
1.15	$9.098 \pm i\ 71.92$ $-40.73 \pm i\ 47.60$ $+0.8172$	$8.632 \pm i\ 71.68$ $-26.82 \pm i\ 31.83$ $+0.9156$

Chapter V

ACTIVE CONTROL OF AEROELASTIC SYSTEMS

The advances made during the past decade in the reliability and acceptability of active control techniques as applied to the stability, control, and navigation functions of aircraft have induced similar advances in the aeroelastic design of aircraft. Garrick [77] provides a synopsis of this activity, while Table V-1 lists the categories commonly ascribed to this control configured vehicle (CCV) technique.

Table V-1

CONTROL CONFIGURED VEHICLES DESIGN CATEGORIES

augmented stability (AS)

maneuver load control (MLC)

ride control (RC)

fatigue reduction (FR)

gust alleviation (GA)

flutter mode control (FMC)

The different categories in the Table have traditionally been characterized as affecting either the low-frequency, rigid body response or the high frequency, elastic mode response. This 'bandwidth separation' in the CCV functions has become a moot subject as larger and/or more flexible aircraft are designed and the analysis of the interaction between the rigid body and elastic modes is becoming commonplace.

To control the aeroelastic system, it is necessary to apply a control force or torque. Although nonaerodynamic controls have been considered [78, Buchek], current designs use aerodynamic surfaces to produce the control loads. The B-52 Load Alleviation and Mode Stabilization program (LAMS) [1] utilized accelerometer measurements at the location of the control surface to produce augmented damping of subcritical structural response modes. In the subsequent B-52 CCV program [79], [2], all of the items of Table V-1 were incorporated. Roger and Hodges [4] document

the flutter mode control system flight tests of this program, which is the only flight tested FMC system in existence. This FMC design [2] utilized augmented state Padé approximants for the loads. Grosser et al. [3], outline the C-5A active lift distribution control system which incorporates MCL, FR, and GA systems. Wind tunnel studies of FMC systems are reported by Sandford et al. [5], and Haidl et al. [80]. The former test was designed using Nissim's aerodynamic energy technique [81] and encountered difficulty in stabilizing a leading edge control surface. The latter test studied wing-store flutter and incorporated a FMC system designed using oscillatory loads and a simple damping control law.

It is obvious that an analysis technique capable of treating FMC can also be applied to the less demanding tasks of AS, RC, FR, and GA. Also, the FMC problem provides a definite design goal-stability, whereas the other CCV categories have more subjective design criteria. Thus the FMC problem has been the subject of a number of analytical studies. Turner [38] used a modified p-k method with oscillatory loads to obtain a model amenable to modern control techniques while Dressler [39] used a series expansion in s for the loads to obtain an augmented state model and applied modern optima' control methods.

This brief review of the literature of FMC focuses attention on the key role played by the choice of the aerodynamic model. Most of the above studies were conducted by obtaining a model described by linear, constant-coefficient, ordinary differential equations. The complexity of the various aerodynamic modeling techniques ranges from no augmented states [38] to well over 100 augmented states [4]. It is significant that the only flight tested system, the B-52 CCV FMC system, used the most complex aerodynamic model. Garrick [77] compares the predicted flutter characteristics of the analytical model, the wind-tunnel model, and the flight test results of this program. The general trends of the damping of the flutter mode were predicted accurately, although the predicted flutter speed was off by 10 percent. Thus, there is room for improvement in the modeling of aeroelastic systems. Desirable characteristics of improved models include:

(1) improved accuracy in predicting arbitrary transient response,

(2) minimization or elimination of augmented states required to model the loads,

(3) maintaining the simplicity of ordinary differential equations for the model,

(4) applicability of modern control techniques to system synthesis,

(5) applicability to flight test results from the vehicle for which the active control system is to be designed.

The last item is stressed since it implies the possibility of tailoring a system to a vehicle during a flight test program. It might be hoped that future FMC systems will not require the degree of analytical study of the vehicle which was available to the B-52 CCV program. The design technique which will be developed in this chapter addresses itself to the above items.

A. CONTROL OF DISTRIBUTED PARAMETER SYSTEMS

The structural elements comprising an aircraft are three-dimensional elements (wings, fuselage, empannage, tail) whose dynamic behavior is described by partial differential equations with appropriate boundary conditions. Bisplinghoff and Ashley [52] formulate the aeroelastic equations in terms of operators as

$$(\mathcal{S} - \mathcal{C}_e - \mathcal{J})q = Q_D \tag{5.1}$$

where $\mathcal{S}$, $\mathcal{C}_e$, and $\mathcal{J}$ are structural, aerodynamic, and inertial operators, q is a generalized displacement, and Q_D is a known disturbance force. Depending on the formulation adopted, $\mathcal{S}$, $\mathcal{C}_e$, or $\mathcal{J}$ may be algebraic, differential, or integral operators. For instance, the structural operator for the bending displacement of a simple beam is $\mathcal{S} = \partial^2(EI\partial^2/\partial y^2)/\partial y^2$. Neglecting shear deformation and rotary inertia, the uniform slender-beam differential equation is

$$EI\frac{\partial^4 w}{\partial y^4} + \frac{\partial^2 w}{\partial t^2} - F_z(y,t) . \tag{5.2}$$

-95-

For cantilever boundary conditions and $q_c = 0$, the solution of (5.2) can be expressed as [7]

$$w(y,t) = \sum_{k=1}^{\infty} \phi_k(y)\xi_k(t) \tag{5.3}$$

with

$$\phi_k(y) = A_1\left(\sinh\sqrt{\frac{\omega_k}{a}}\,y - \sin\sqrt{\frac{\omega_k}{a}}\,y\right) + A_2\left(\cosh\sqrt{\frac{\omega_k}{a}}\,y - \cos\sqrt{\frac{\omega_k}{a}}\,y\right)$$

$$\xi_k(t) = B_k \sin \omega_k t + C_k \cos \omega_k t$$

$$a^2 = \frac{EI}{m}.$$

The natural frequencies ω_k are given by the solutions of the equation

$$1 + \cos\sqrt{\frac{\omega}{a}}\,\ell\,\cosh\sqrt{\frac{\omega}{a}}\,\ell = 0.$$

This example illustrates the key concepts embodied in the study of the control of distributed parameter systems. This field embraces the study of linear operators defined on a Hilbert space and seeks solutions to 'optimal control' problems specified by an appropriate performance index. The distinguishing feature of such problems is the infinite dimensionality of the solutions (or the elements of the space). This effect is clearly evident in (5.3) where the solution is described by an infinite sequence of normal modes. Much effort may be expended in establishing the existence of bounded inverses of the operators since, in this event, the solution may be uniformly approximated by a finite sum of 'normal modes'. (A given function is uniformly approximated by a sequence of functions if the approximation invariably becomes better as additional elements of the sequence are incorporated.) This is the basis of the well-known method of truncated normal modes in structural dynamics problems. Since the infinite sequence of orthogonal 'in vacuo'

modes of (5.3) span the solution space, the solution to the actual problem, with $Q_e \neq 0$, may be obtained by projecting the applied distributed force $F_z(y,t)$ onto these 'basis vectors'. The resulting generalized forces Q_i are given by

$$Q_i = \int_0^\ell F_z(y,t)\phi_i(y)\,dy \; .$$

In aeroelastic problems, the applied force is composed of forces due to motion of the structure and

$$Q_i = \sum_{j=1}^\infty q_{ij}\xi_j(t)$$

where q_{ij} is the generalized force in the ith mode due to deflection of the structure in the jth mode.

In the above example, the infinite dimensionality of the solution is explicitly indicated by the partial differential equation, (5.3), describing the structure. The examples treated in the previous chapters involve pitch and plunge of two-dimensional typical sections which may be regarded as representing the first bending and torsion modes of a three-dimensional flexible wing. The dynamics of such typical sections are described by ordinary differential equations. However, even these cases require infinite dimensional solution spaces since the applied loads are themselves solutions of partial differential equations (e.g., Eq. 2.6). In the former case (elastic structures) the spectrum of the structural operator contains an infinite sequence of discrete eigenvalues, ω_k, while in the latter case (typical section) the aerodynamic operator may have a continuous spectrum, as typified by the branch cut of $C(\bar{s})$, or it may be discrete, as in the case of two-dimensional supersonic loads. Note that the elastic structure problem involves the solution of two distributed parameter systems and the solution spectrum will be doubly infinite. Although the mathematical description of the structure and the aerodynamic medium thus appear to be on an equal footing, it is

-97-

the structure which is invariably viewed as the object to be controlled.

Wang and Tung [42] provided a framework for the study of distributed parameter control, and outlined the categories of (1) distributed input control, (2) boundary input control, and (3) total input control. They extended the concepts of controllability and observability, which were developed with regard to finite state space, to the infinite dimensional case and examined the problem of existence of solutions. Taking the view that an 'optimal control' should be defined with respect to the complete solution of the mathematical problem, they were led to performance indices defined on direct sums of Hilbert spaces. Problems posed in this vein have proven unwieldy with the examples considered usually having only one spatial dimension. References [43] through [46] illustrate the theory applied to the one-dimensional heat equations, while [47] and [48] study the one-dimensional hyperbolic equation and wave equation. It is of interest that several recent references [46], [50], and [49] address the more modest goal of 'stabilization' of distributed parameter systems rather than seeking an 'optimal control' in L^2.

In assessing the relevance of distributed parameter control theory to the aeroelastic problem, it must be noted that none of the three categories of control given in the last paragraph correctly describe the problem. The control force available in the aeroelastic problem is the pressure distribution caused by control surface deflection. It cannot be considered a distributed input since it is a one-dimensional function of the control deflection. Neither is it a boundary control for the structural partial differential equation since the boundary condition associated with the surface deflection relates to the aerodynamic equation. Hence a broader formulation is to address the problem properly.

Jian and Ching Yuan [49] have presented such a formulation. They model a distributed parameter system with an ordinary feedback controller as

-98-

$$m(y) \frac{\partial^2 w}{\partial t^2} + \frac{\partial}{\partial t} Cw + Bw + Aw = -Gx \qquad (5.4a)$$

$$\frac{dx}{dt} = Jx + S^1 w + S^2 \frac{\partial w}{\partial t} \qquad (5.4b)$$

where A, B, and C are matrix operators defined on a Hilbert space L^2, and G is a bounded operator mapping the n-dimensional vector space R^n into L^2. G is thus the operator relating control surface deflection, x, to a pressure distribution over the surface. The ordinary feedback control is derived from the n-dimensional vector x. S^1 and S^2 are 'observer-operators' mapping L^2 into R^n. In [49], the model of (5.4) is analyzed from a rigorous Hilbert space standpoint. The stability of the system with feedback control is studied and several perturbation theorems regarding the spectrum of eigenvalues are proven. Finally, the validity of truncated normal mode approximate solutions is verified. Unfortunately, no examples are given in [42].

The use of the truncated normal mode method lends insight to the concepts of controllability and observability of distributed parameter systems. In the context of aeroelastic wings whose motions are measured by 'point sensors' (e.g., rate gyroscopes, accelerometers, etc.), an aeroelastic mode will be unobservable to a sensor placed at a node of the mode (i.e., if the measurement distribution vector is orthogonal to the modal eigenvector). Similarly, an aeroelastic mode is uncontrollable by an aerodynamic control surface if the generalized aerodynamic force in the mode due to control deflection is balanced by the remaining elements of the aeroelastic equation, (5.1). In control theoretic terms this implies that the control distributor vector is orthogonal to the reciprocal eigenvector of the mode. The rigid two-dimensional sections analyzed herein are certainly observable if both displacement and angle sensors are employed. The controllability of such sections with respect to leading- and/or trailing-edge controls will be examined in the next section.

B. CONTROLLABILITY AND OBSERVABILITY OF AEROELASTIC MODES

Controllability of the linear, constant coefficient, finite dimensional system

$$\overset{\circ}{X} = FX + G_1 u \qquad (5.5a)$$

$$y = HX \qquad (5.5b)$$

was examined by Gilbert [82]. The dimensions are

- X = N-dimensional state vector
- u = m-dimensional input vector
- y = p-dimensional output vector
- F = N$\times$N matrix
- G_1 = N$\times$m matrix
- H = p$\times$N matrix.

If F has distinct eigenvalues, the transformation $X = Zz$ where the columns of Z are the eigenvectors of F, gives

$$\dot{z} = \Lambda z + (Z^{-1}G_1)u \qquad (5.6a)$$

$$y = (HZ)z . \qquad (5.6b)$$

The elements of the diagonal Λ matrix are the system eigenvalues, λ_i, $i = 1, \ldots, N$. Laplace transforming (5.6) gives

$$y(s) = \mathcal{H}(s)\mathcal{U}(s) \qquad (5.7)$$

with

$$\mathcal{H}(s) = (HZ)(sI - \Lambda)^{-1}(Z^{-1}G_1) = \sum_{i=1}^{N} \frac{A_i}{s-\lambda_i} \qquad (5.8)$$

where A_i is a p$\times$m matrix given by the vector outer product

$$A_i = (HZ)_{.i}(Z^{-1}G_1)_{i.} . \qquad (5.9)$$

-100-

$(HZ)_{.i}$ is the ith column of HZ and $(Z^{-1}G_1)_{i.}$ is the ith row of $Z^{-1}G_1$. The mode represented by λ_i will be uncontrollable if the ith row of $Z^{-1}G_1$ is zero and it will be unobservable if the ith column of HZ is zero. Equation (5.9) indicates that in either of these cases, $A_i = 0$, and the system transfer functions given by $H(s)$ will not contain the pole at λ_i. In other words, if λ_i is either uncontrollable or unobservable, then every transfer function in $H(s)$ will have a zero at λ_i and a pole–zero cancellation will occur. The fact that a pole–zero cancellation has occurred is not sufficient information to determine whether the system is uncontrollable or unobservable. This must be determined by examining the rows and columns of the input and output matrices. These observations regarding the relationship of pole–zero cancellations and controllability and observability are the basis of the design technique used for the B–52 CCV flutter mode control system [2]. Control surface positions and sensor locations were chosen to achieve the largest separation between the flutter mode and the nearest zero. In a realistic design situation, exact pole–zero cancellation may not occur but a near pole–zero cancellation may indicate that the required control power will be excessive. Also, near cancellation frequently leads to severe sensitivity problems.

C. CONTROLLABILITY OF A TWO–DIMENSIONAL TYPICAL SECTION

Since the aeroelastic mode shapes of flexible wings vary continuously as functions of velocity and dynamic pressure, it may be anticipated that observability and controllability problems will occur at discrete values of these parameters, if they occur at all. The typical sections analyzed in the previous chapters are observable if measurements of h, α, β, and γ are assumed. Thus, the controllability of the sections may be studied by examining the transfer functions of the Padé approximant augmented state models ('Padé models') given by (4.9) for the incompressible case or by (4.19) for the compressible case.

Table V–2 gives the parameters defining a nominal case for the four DOF section of Fig. II–1 in incompressible flow.

Table V-2

NOMINAL PARAMETERS FOR A FOUR-DEGREE-OF-FREEDOM
SECTION IN INCOMPRESSIBLE FLOW

$\omega_\alpha = 100$ rad/sec	$e = 0.6$
$\omega_h = 50$ rad/sec	$x_\alpha = 0.2$
$\omega_\beta = 500$ rad/sec	$r_\alpha^2 = 0.25$
$\omega_\gamma = 500$ rad/sec	$x_\beta = x_\gamma = 0.0125$
$\mu = 40$	$r_\beta^2 = r_\gamma^2 = 0.00625$
$a = -0.4$	$\zeta_\beta = \zeta_\gamma = 0.1$

The leading- and trailing-edge control surfaces span 20 percent of the
chord and have natural frequencies five times the torsion mode frequency.
A small viscous damping has been assumed to stabilize the flap modes.
The remaining parameters are identical to those of Table III-3.

It is well known [18] that the frequency ratio ω_h/ω_α has a strong
influence on flutter characteristics. Therefore calculations made with
the Padé model (4.9) for $\omega_h/\omega_\alpha = 0$, 0.25, 0.50, and 0.75 are pre-
sented in Fig. V-1. A subprogram was written which iterated to determine
the value of $U/b\omega_\alpha$ at which flutter occurred. The transfer functions
of $(h/\beta_c)(s)$, $(\alpha/\beta_c)(s)$, $(h/\gamma_c)(s)$, and $(\alpha/\gamma_c)(s)$ were determined at
this value of $U/b\omega_\alpha$ and at ± 25 percent of this value by the method
of [83]. Figure V-1 indicates the variation of the poles and zeroes
of these transfer functions as a function of ω_h/ω_α and $U/b\omega_\alpha$. As
ω_h/ω_α increases from 0 to 0.75, the value of $U/b\omega_\alpha$ at flutter decreases
from 3.41 to 2.13. The variation of the zeroes is of special interest
since they determine the controllability characteristics of the section.
It is evident that leading-edge flap control will not experience any
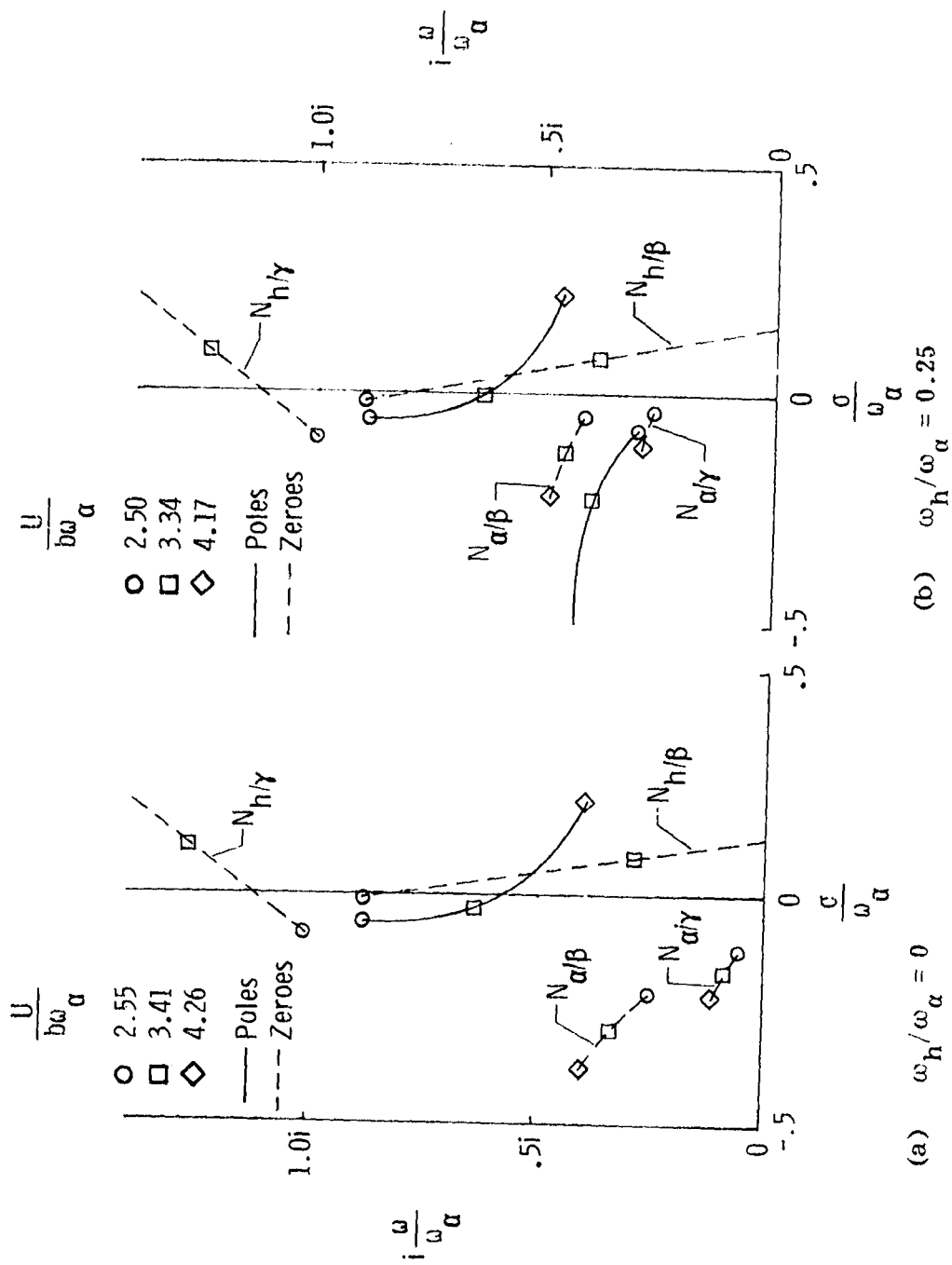controllability problems, since the locus of zeroes of both $(h/\gamma_c)(s)$

FIG. V-1 POLES AND ZEROES OF A FOUR DEGREE-OF-FREEDOM SECTION VERSUS $U/b\omega_\alpha$ AND ω_h/ω_α IN INCOMPRESSIBLE FLOW
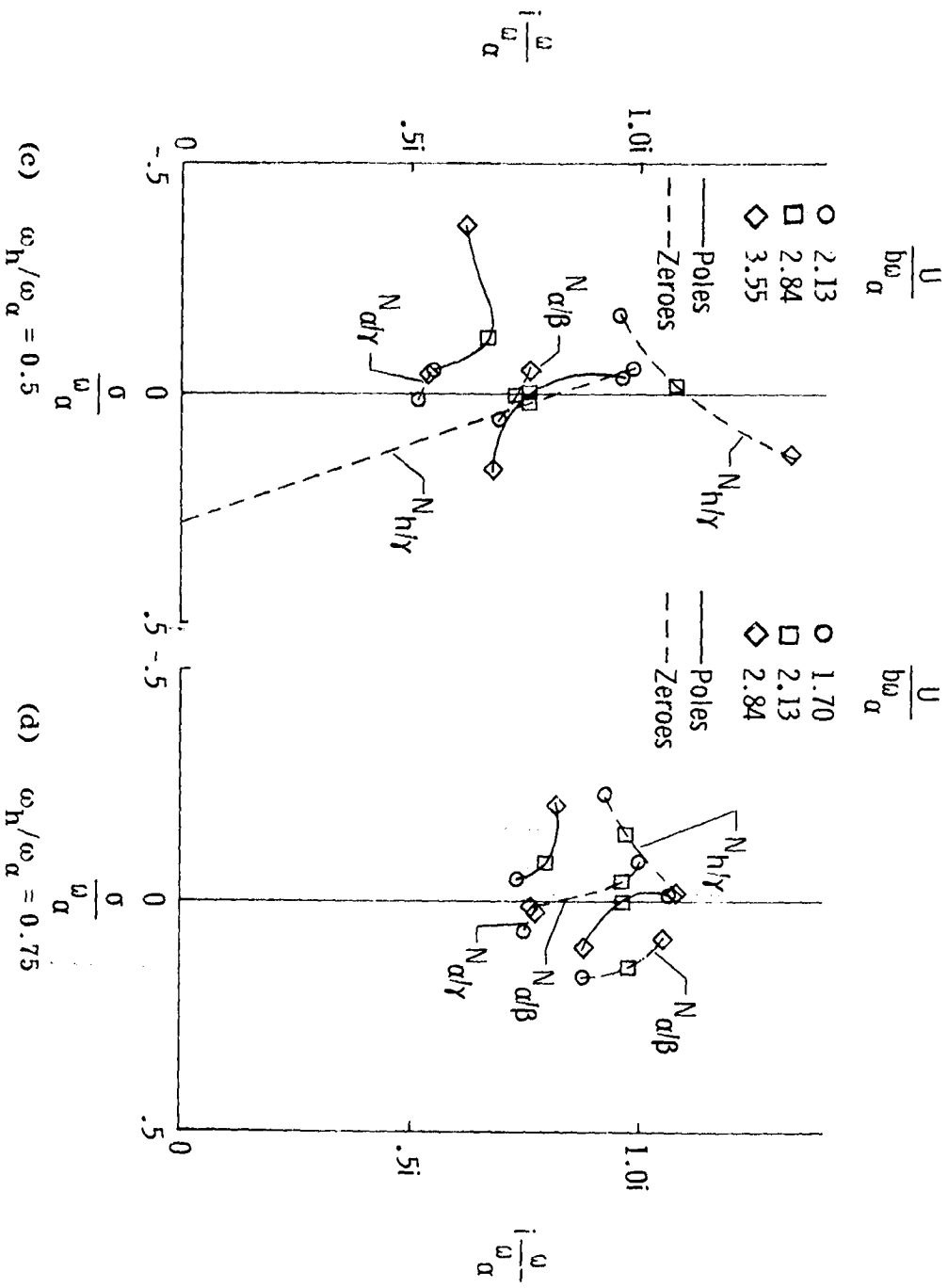
FIG. V-1   CONCLUDED

and $(\alpha/\gamma_c)(s)$ tend to fall outside the range $\omega_h < \omega < \omega_\alpha$. Since classical flutter of a typical section occurs with a merging of frequencies within this range, a pole-zero cancellation evidently will not occur for leading-edge control of a two-dimensional section.

The situation for the trailing-edge control surface is much different, with the locus of zeroes of $(h/\beta_c)(s)$ and $(\alpha/\beta_c)(s)$ tending to be in the range $\omega_h < \omega < \omega_\alpha$. In fact, at $\omega_h/\omega_\alpha = 0.5$, there is a near pole-zero cancellation in both degrees-of-freedom at $U/b\omega_\alpha = 2.84$. Hence the flutter mode is nearly uncontrollable at the flutter speed for this section. This explains the choice of $\omega_h = 50$ rad/sec for the nominal case in Table V-1. It represents a "worst-case" design problem and parameter variation studies about this configuration are of interest. The physical cause of the uncontrollable mode can be explained by noting that for this specific set of values of the parameters of Table V-1 and $U/b\omega_\alpha$, the structural and inertial forces and moments on the main section cancel the incremental lift and pitching moment due to flap motions when the section is oscillating in this 'uncontrollable' mode.

Figure V-2 gives the modal composition of the eigenvectors of the nominal section (Fig. V-1c) at $U/b\omega_\alpha = 2.13$, 2.84, and 3.55. The components of the eigenvectors are presented in complex phasor form and are referenced to the plunge mode, h, which is normalized to unity. The uncoupled flap modes ($\omega = 500$ rad/sec, $\zeta = 0.1$) at $s = -50 \pm i\ 497$ rad/sec have been modified by the coupling, giving a higher frequency mode at $\omega \simeq 590$ rad/sec and a lower frequency mode at $\omega \cong 265$ rad/sec The higher frequency mode is predominantly a trailing-edge flap mode while in the lower frequency mode the leading-edge flap predominates. Also, a significant reduction in the leading-edge flap mode damping has occurred which explains the necessity of the viscous damping ζ_γ. The remaining two modes are the (highly-coupled) bending-torsion modes, one of which becomes the flutter mode. Additional studies of two DOF bending-torsion sections (not shown) indicated a minimal influence of the flap dynamic coupling on the characteristics of the flutter mode.

-105-
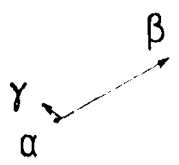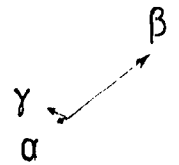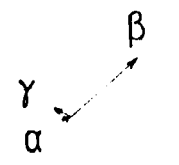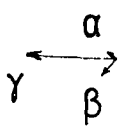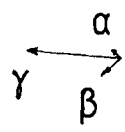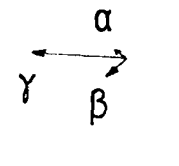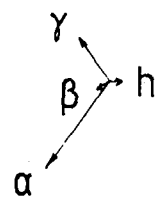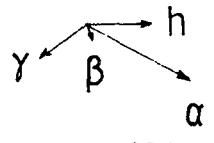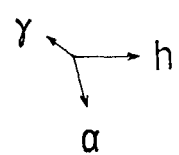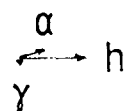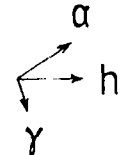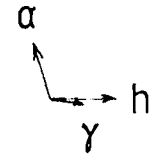
$U/b\omega_\alpha$ / Mode	2.13	2.84	3.55
Trailing-edge flap	$s = -46 \pm i584$	$s = -60 \pm i592$	$s = -74.6 \pm i603$
Leading-edge flap	$s = -6.8 \pm i272$	$s = -11.2 \pm i265$	$s = -17.8 \pm i254$
Torsion	$s = -3.7 \pm i96$	$s = -0.4 \pm i76.3$ (flutter)	$s = 16.9 \pm i67.9$
Plunge	$s = -4.7 \pm i54$	$s = -12.4 \pm i66.4$	$s = -36.2 \pm i61.8$

FIG. V-2   MODAL COMPOSITION OF THE EIGENVECTORS OF A
FOUR DEGREE-OF-FREEDOM SECTION VERSUS
$U/b\omega_\alpha$ IN INCOMPRESSIBLE FLOW

This is due to the very low inertias of the flaps relative to the main section.

Figure V-3 examines the controllability of the nominal section with respect to variations of the parameters: μ, a, r_α^2, $r_\beta(r_\gamma)$, $x_\beta(x_\gamma)$, $\zeta_\beta(\zeta_\gamma)$, and $\omega_\beta(\omega_\gamma)$. The mass ratio, μ, is the only quantity which is directly related to flight condition. The remaining parameters are related to structural and geometrical properties of the section. Variation of μ and the parameters related to the main section (x_α, r_α^2, a) have a strong influence on the controllability of the section. As might be expected, variation of the parameters related to the flaps have a small perturbing effect on the controllability. The behavior of the zeroes associated with the leading-edge flap remains unchanged for all of the variations of Fig. V-3. Figure V-4 shows the effect on the critical flutter mode at flutter due to variation of the trailing-edge flap chord, c. Variations in c 'detune' the uncontrollability condition.

Thus, from considerations of controllability, the leading-edge flap has advantages over the trailing-edge flap for active aeroelastic control purposes. This advantage is offset by (1) the large destabilizing hinge moments which the leading-edge flap must carry; (2) the associated power required to move the flap, and (3) the violation of the aerodynamic shape of the lifting surface in the critical leading-edge area. In addition, proper design of a trailing-edge controller may achieve the objectives without encountering a controllability problem. The successful flight test of the B-52 CCV FMC system indicates that this is possible.

It should be noted that the desirability of leading-edge control is not so obvious on finite wings which have a sequence of structural modes, ω_k. Figures V-1 and V-3 shows that the leading-edge control does not encounter controllability problems because the zeroes of the relevant transfer functions remain outside the range $\omega_h < \omega < \omega_\alpha$. This reasoning fails when applied to finite wings since then the zeroes may cause controllability problems with other modes.
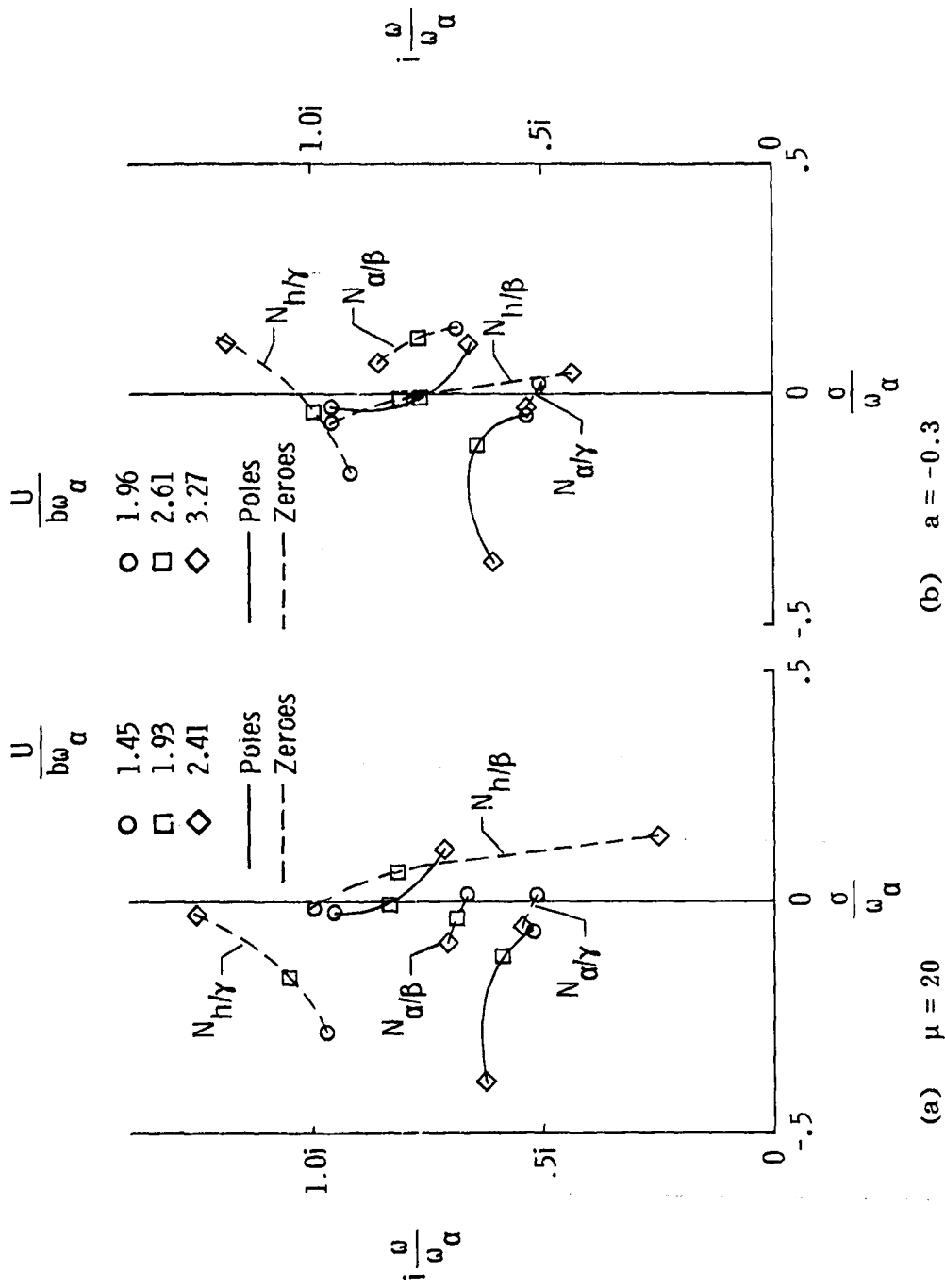
FIG. V-3   THE EFFECT OF PARAMETER VARIATIONS ON THE POLE AND ZERO LOCATIONS
IN INCOMPRESSIBLE FLOW

-108-

$\dfrac{U}{b\omega_\alpha}$

$\bigcirc$	2.48
$\square$	3.30
$\diamondsuit$	4.13

—— Poles
- - - - Zeroes

$N_{h/\gamma}$

$N_{h/\beta}$

$N_{\alpha/\beta}$

$N_{\alpha/\gamma}$

$\dfrac{\omega}{\omega_\alpha} i$

1.0i

.5i

0

$\dfrac{\sigma}{\omega_\alpha}$

.5

-.5

(d) $\quad r_\alpha^{\,2} = 0.5$

$\dfrac{U}{b\omega_\alpha}$

$\bigcirc$	2.37
$\square$	3.17
$\diamondsuit$	3.96

—— Poles
- - - - Zeroes

$N_{h/\gamma}$

$N_{h/\beta}$

$N_{\alpha/\beta}$

$N_{\alpha/\gamma}$

$\dfrac{\omega}{\omega_\alpha} i$

1.0i

.5i

0

$\dfrac{\sigma}{\omega_\alpha}$

.5

-.5

(c) $\quad x_\alpha = 0.1$

FIG. V-3   CONTINUED

(e) $x_\beta = x_\gamma = 0.00625$

(f) $r_\beta^2 = r_\gamma^2 = 0.0125$
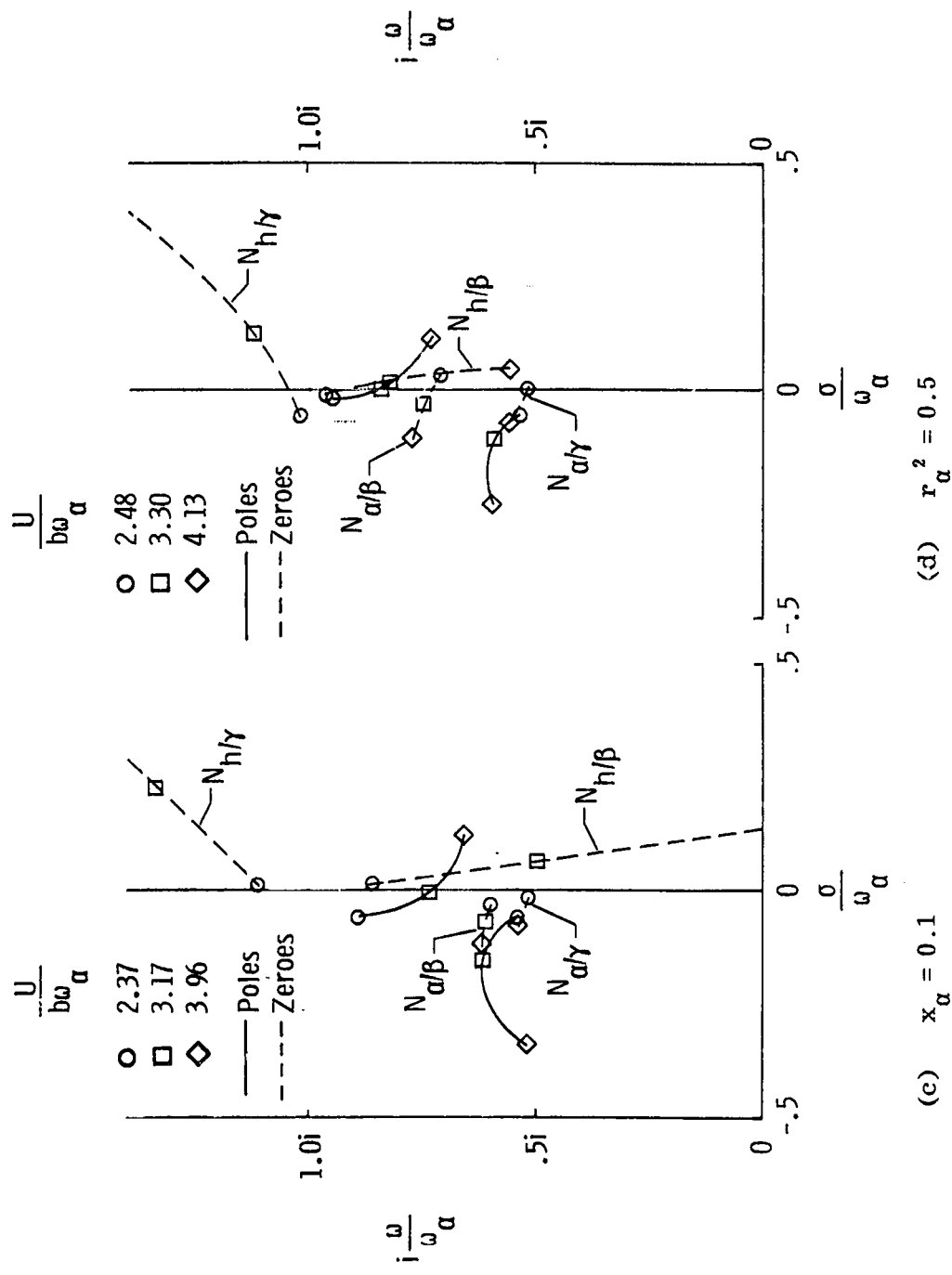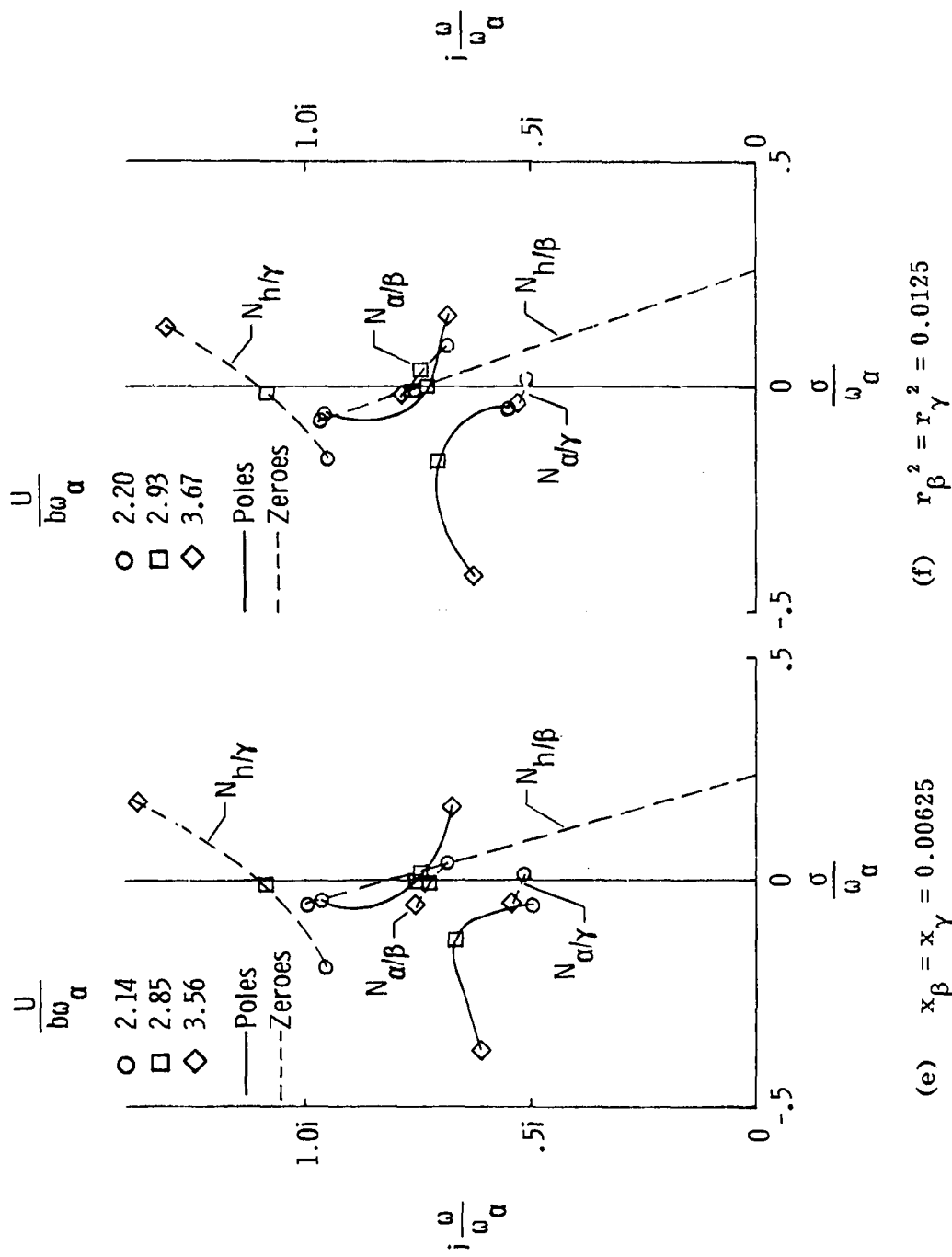
FIG. V-3   CONTINUED

FIG. V-3   CONCLUDED

(g) $\omega_\beta = \omega_\alpha = 1000$ RAD/SEC

(h) $\zeta_\beta = \zeta_\gamma = 0.05$
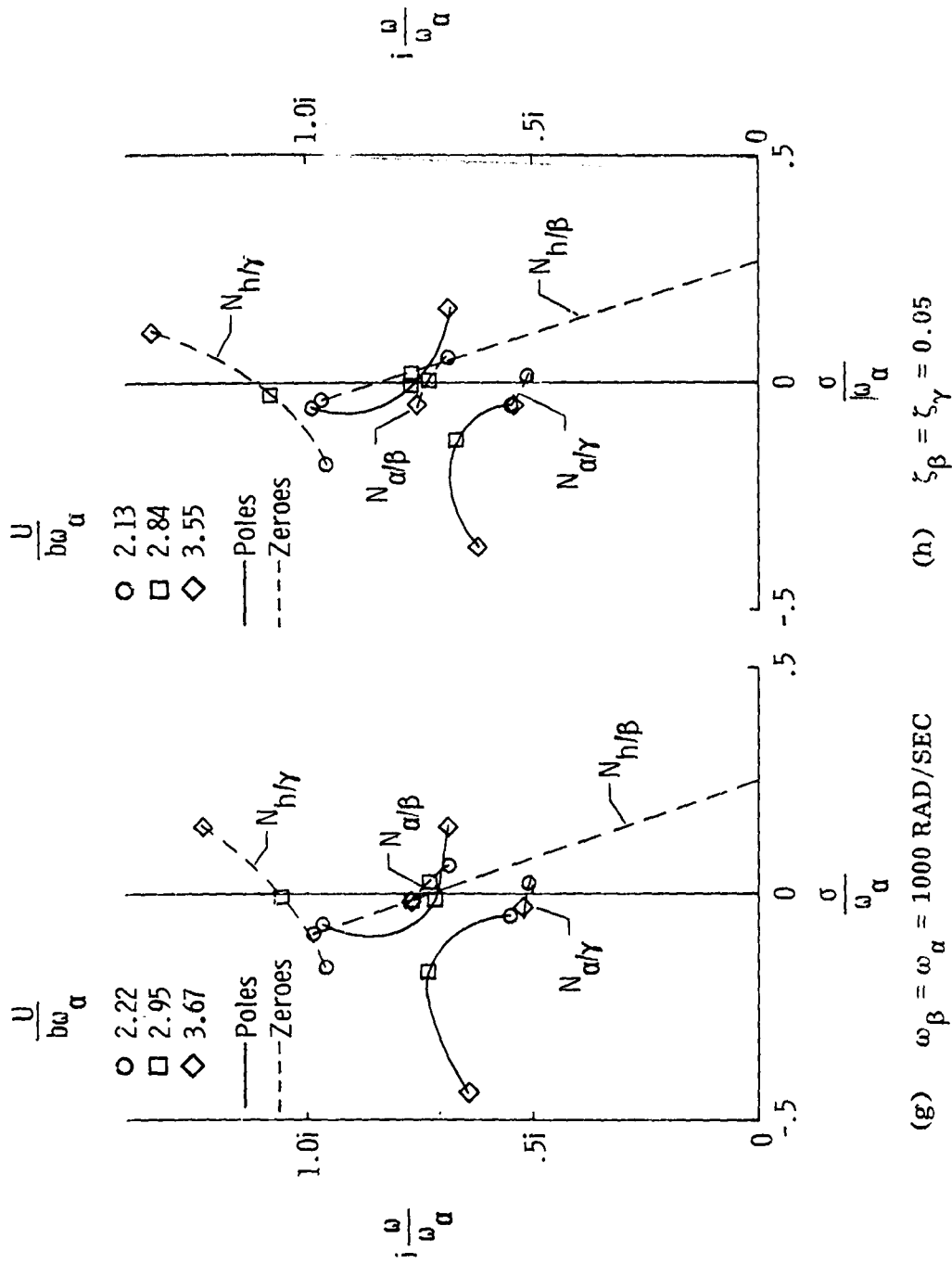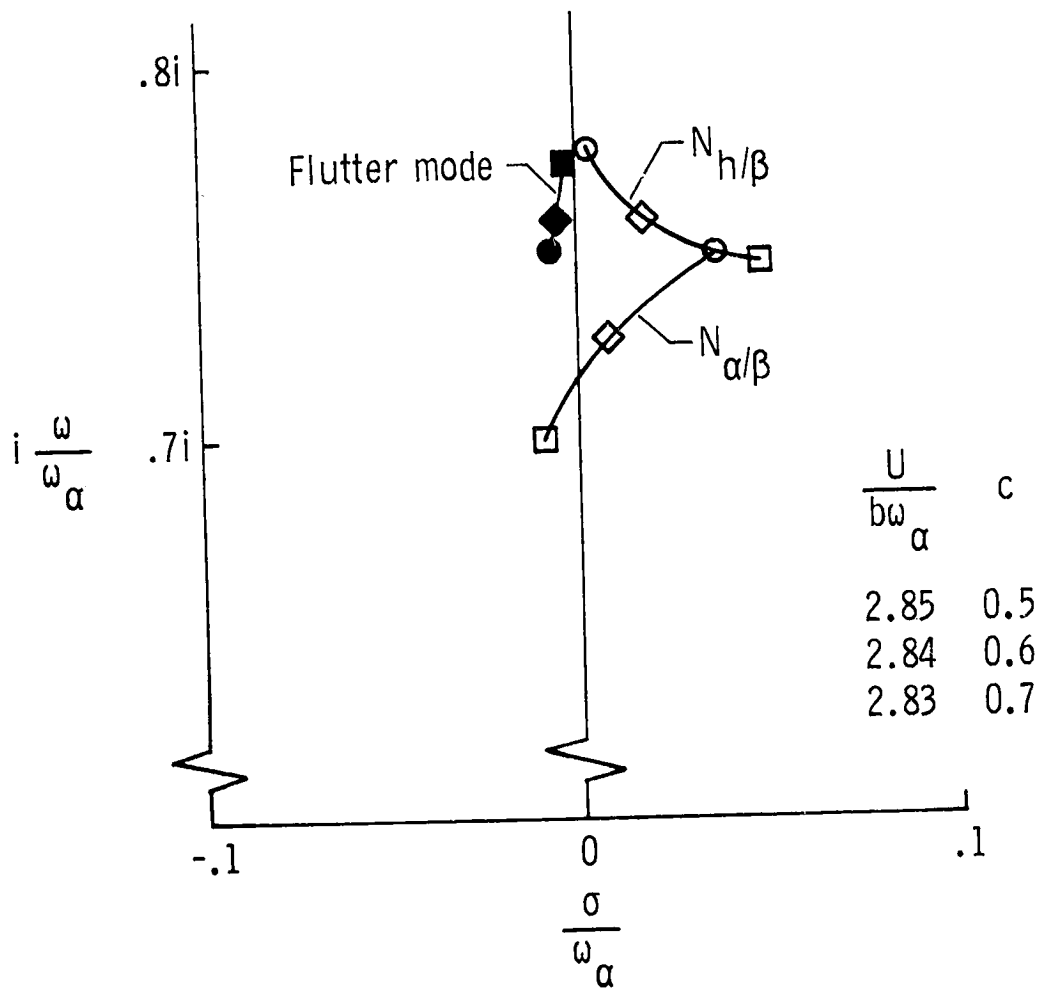
FIG. V-4   THE EFFECT OF THE TRAILING-EDGE FLAP CHORD, c, ON THE FLUTTER MODE AND ASSOCIATED ZEROES

Controllability of the three DOF section in compressible flow may be studied using the Padé model of (4.19). Figure V-5 indicates that the subsonic section of Table V-3 has much the same controllability problem as the incompressible section.

Table V-3

THREE DEGREE-OF-FREEDOM SECTION PARAMETERS FOR SUBSONIC FLOW

$\omega_\alpha = 50$ rad/sec	$x_\alpha = 0.2$
$\omega_\beta = 317$ rad/sec	$r_\alpha^2 = 0.25$
$b = 4$ ft	$x_\beta = 0.0125$
$a_\infty = 1000$ ft/sec	$r_\beta^2 = 0.00625$
$\mu = 40$	$\zeta_\beta = 0.0$
$c = 0.5$	
$a = -0.4$	

Figure V-6 shows the locus of zeroes of the $(\alpha/\beta_c)(s)$ transfer function of the three DOF section of Table III-4 in supersonic flow. The lack of sensitivity of these zeroes to Mach number, and the fact that the $(h/\beta_c)(s)$ transfer function has no complex zeroes near the flutter mode indicate that controllability of two-dimensional sections in supersonic flows is not a problem.

FIG. V-5   POLES AND ZEROES OF A THREE DEGREE-OF-FREEDOM SECTION IN SUBSONIC
FLOW CALCULATED USING MATRIX PADÉ APPROXIMANTS
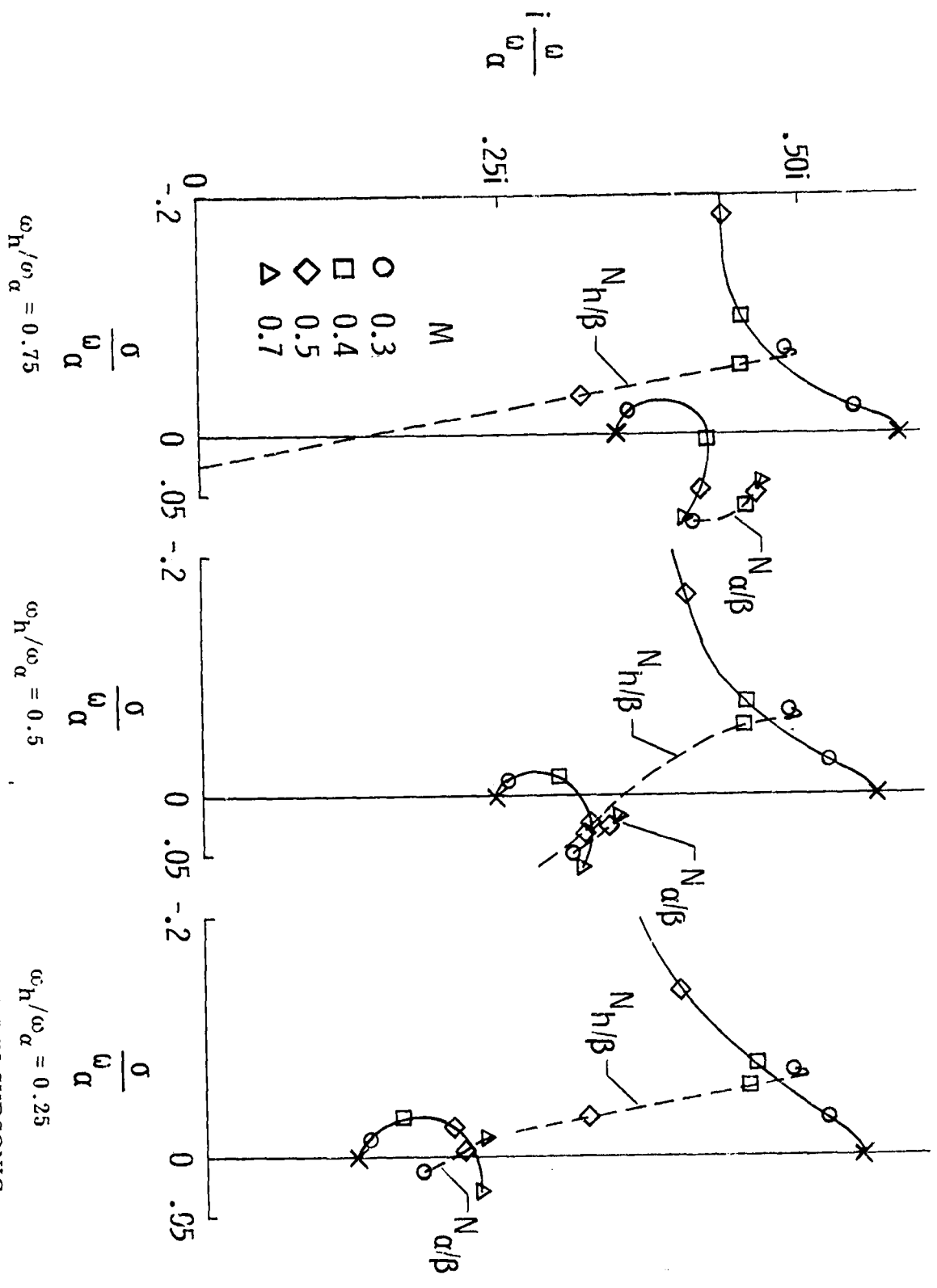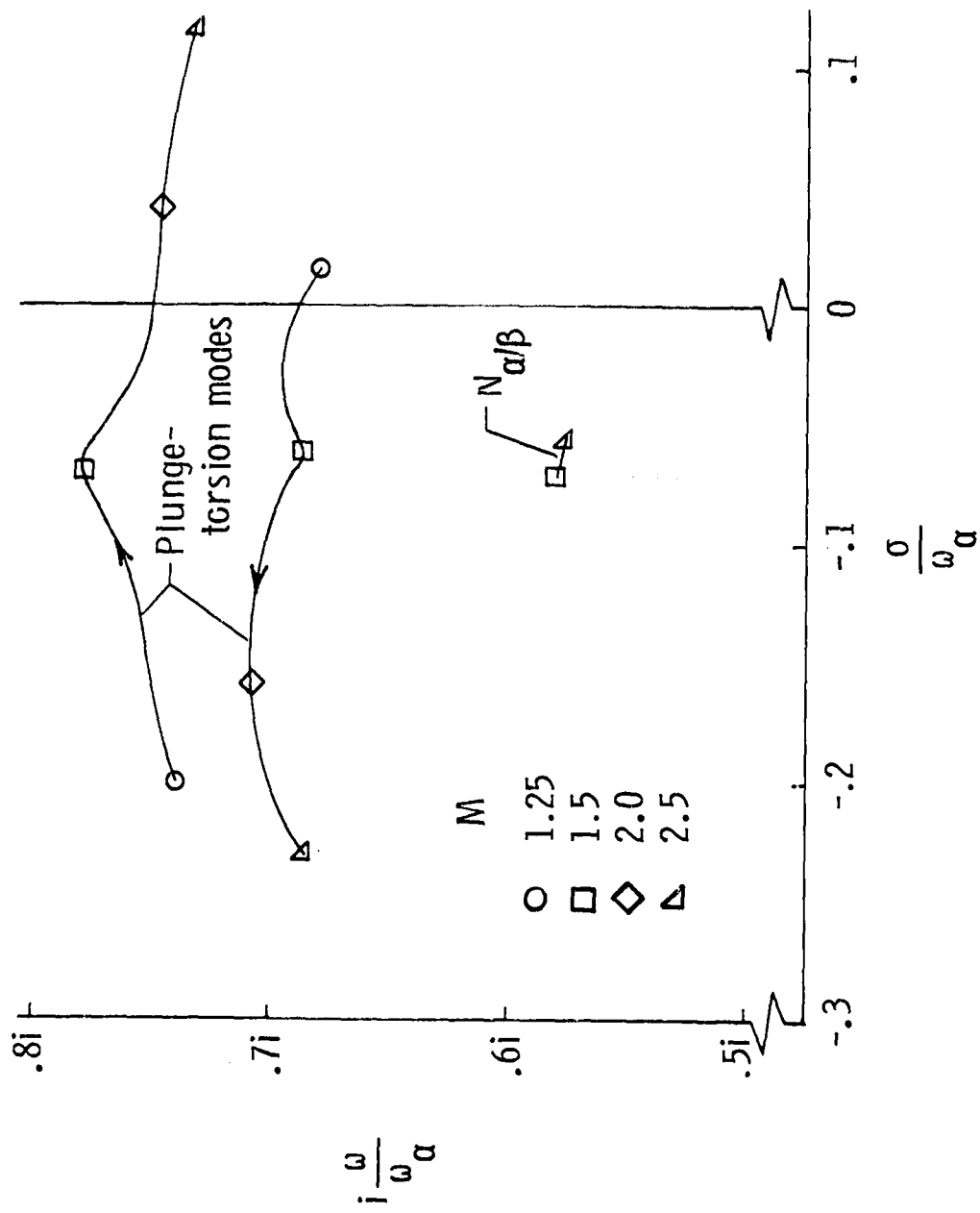
FIG. V-6   POLES AND ZEROES OF A THREE DEGREE-OF-FREEDOM SECTION IN
SUPERSONIC FLOW CALCULATED USING MATRIX PADÉ APPROXIMANTS

D. AEROELASTIC CONTROL BASED ON THE CONCEPT OF AERODYNAMIC ENERGY

Nissim [81] developed a technique of active flutter suppression which is based upon considerations of the energy required to sustain simple harmonic oscillations of a two DOF typical section. If the sign of this energy is positive, indicating energy must be supplied to the section to maintain the oscillation, the section is stable. A negative energy would indicate that the airstream was supplying energy to the section and it is assumed that the section would flutter if released. For forced simple harmonic oscillations of the section the aerodynamic energy is given by

$$\bar{P} = \frac{1}{2}\pi^2 \rho b^4 \omega \ell \left\{ \xi_R^T [\diagdown \Lambda \diagdown] \xi_R + \xi_I^T [\diagdown \Lambda \diagdown] \xi_I \right\}$$

$$= \frac{1}{2}\pi^2 \rho b^4 \omega \ell \left\{ \lambda_1 (\xi_{R_1}^2 + \xi_{I_1}^2) + \cdots + \lambda_n (\xi_{R_n}^2 + \xi_{I_n}^2) \right\}. \qquad (5.10)$$

The complex vectors $\xi_R + i\xi_I$ are generalized modal coordinates associated with the aerodynamic energy, and the elements λ_i of the diagonal matrix $[\diagdown \Lambda \diagdown]$ are the real eigenvalues of the Hermitian matrix

$$[-(Q_2 + Q_2^T) + i(Q_1 - Q_1^T)] .$$

The matrices Q_1 and Q_2 are the real and imaginary parts of the simple harmonic aerodynamic loads. $\bar{P}$, being a quadratic form, will be positive definite if $\lambda_1 > 0$, $i = 1, \ldots, n$ and thus the section will be stable. Nissim noted that this 'stability criterion' was dependent only upon the aerodynamic loads $Q_1 + iQ_2$ and did not involve the structural parameters of the section (μ, ω_α, x_α, etc.). Apparently the stability of the section could be determined without regard to the structural dynamics of the section. Nissim argued that this was a desirable formulation because of the wide variations in flight conditions which an aircraft may experience.

In order to achieve active control of a fluttering section, Nissim postulated the control law

$$
\begin{bmatrix} \beta \\ \gamma \end{bmatrix} = [C_1] \begin{bmatrix} h \\ \alpha \end{bmatrix} + i [C_2] \begin{bmatrix} h \\ \alpha \end{bmatrix} . \tag{5.11}
$$

With the flap deflections expressed as functions of h and α, the loads due to flap deflections could be calculated and added to Q_1 and Q_2. The stability of the section could then be determined by examining the sign of λ_1 and λ_2. This stability criterion had to be checked over a range of reduced frequencies, since the reduced frequency of flutter is not determined. Nissim determined the 'optimized' values of C_1 and C_2 for a section with leading- and trailing-edge controls as

$$
C_1 = \begin{bmatrix} -0.05 & -1.7 \\ 0.5 & 1.0 \end{bmatrix} , \qquad C_2 = \begin{bmatrix} 0.45 & 0.2 \\ -0.5 & 1.0 \end{bmatrix} .
$$

Nissim [81] also studied control with only a trailing-edge flap and found that it was barely possible to ensure the positive definiteness of $[\diagdown \Lambda \diagdown]$ over a range of k. Furthermore, the design was sensitive to variations in the feedback gain values and Nissim concluded that a practical flutter suppression system would require both leading- and trailing-edge controls.

The incompressible Padé model of (4.9) is capable of analyzing Nissim's design. The control law of (5.11) is implemented by noting that for an oscillating section $ih \cong \dot{h}/\omega$, giving the control law

$$
\begin{bmatrix} \beta \\ \gamma \end{bmatrix} = [C_1] \begin{bmatrix} h \\ \alpha \end{bmatrix} + \frac{1}{\omega_r} [C_2] \begin{bmatrix} \dot{h} \\ \dot{\alpha} \end{bmatrix} . \tag{5.12}
$$

The reference frequency ω_r is chosen to be in the vicinity of the flutter frequency. For the section of Table V-2, $\omega_r = 76$ rad/sec (Fig. V-1c), and Fig. V-7 shows the locus of roots as a function of $U/b\omega_\alpha$ for the uncontrolled and the controlled section. (The damping, $\zeta_\beta = \zeta_\gamma = 0.025$ in the figure.) The control law stabilizes the bending and torsion modes throughout the range of velocities $0 < U/b\omega_\alpha < 3.9$ but the leading-edge flap mode is unstable throughout this range. The closed loop bending mode

-117-

(a) BENDING AND TORSION MODES

(b) FLAP MODES
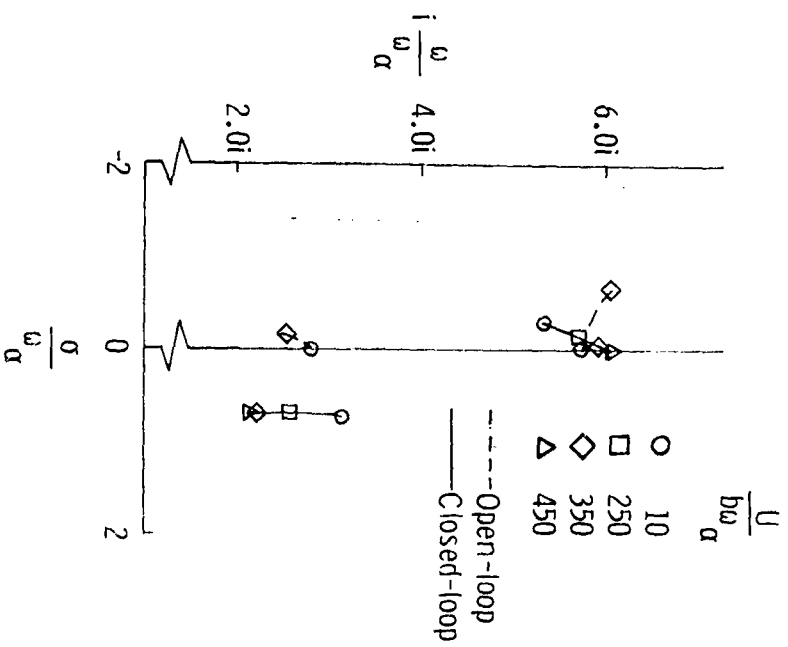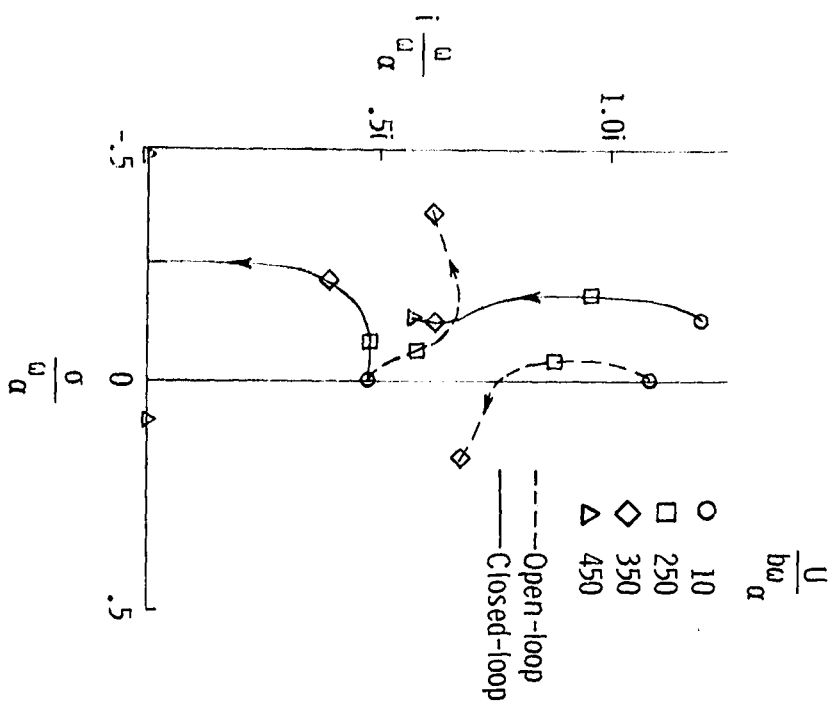
FIG. V-7   OPEN- AND CLOSED-LOOP ROOT LOCI OF A FOUR DEGREE-OF-FREEDOM
SECTION USING THE CONTROL LAW OF EQ. 5.12

approaches the real axis and leads to a statically divergent mode at $U \cdot b\omega_\alpha = 3.9$. A second case with $\omega_h = 25$ rad/sec was studied and a similar instability was observed in the flap mode. Hence, Nissim's design procedure is seriously deficient in neglecting the flap degrees-of-freedom.

Evaluating the aerodynamic energy design technique, the following comments are appropriate:

1. The technique is overly conservative in that it attempts to suppress flutter for all possible combinations of values of the structural and geometrical parameters defining the section.

2. The technique, which attempts to define a FMC system valid for all possible combinations of structural parameters, is incapable of producing a good design for a single trailing-edge control since at least one combination of parameters can be found for which the section is uncontrollable (viz., the section of Table V-1).

3. The technique addresses flutter suppression without regard to the structural properties of the section. To assess the flutter boundary of the final design, a standard U-g analysis must be performed using the final control law.

4. The aerodynamic energy eigenvalues would appear to have no direct relationship to the locus of roots in the s-plane. Thus they offer little guidance in design modifications.

It would appear possible to modify the aerodynamic energy design technique to handle the problem of leading-edge flap instability by including the flap modes in the design. The main problem in this extension would be the complexity of optimizing the control laws of a large order system over a large range of k.

The technique was extended to the design of a flutter suppression system for a delta-wing wind-tunnel model [5]. Nine flexible modes were included in the design but the leading- and trailing-edge control surface modes were not included. It is significant that for this large order system it was not possible to achieve a design having all of the eigenvalues

-119-

of $[\nwarrow\Lambda\nwarrow]$ positive over the desired range of k. Although the nonpositive
definiteness of $[\nwarrow\Lambda\nwarrow]$ would seem to imply that flutter suppression had
not been achieved, U-g analysis verified an increase in the flutter speed.

The resulting control laws were tested on the wind tunnel model at
$M = 0.6$, 0.7, 0.8, and 0.9. At the first three Mach numbers, the system
could not be evaluated due to a severe leading-edge control surface in-
stability. The instability was not encountered at $M = 0.9$ and the
flutter suppression system demonstrated a significant increase in the
flutter dynamic pressure. It is suspected that the leading-edge surface
instability is of a similar nature t· that analyzed in Fig. V-7.

E. FINITE STATE MODELS OF THE RATIONAL PORTION OF
AEROELASTIC SYSTEMS

The complexity of current design practices and the difficulties
experienced in implementing designs emphasize the need for simpler tech-
niques in active aeroelastic control. The ability to calculate unsteady
aerodynamic loads for arbitrary values of $\bar{s}$, coupled with the insight
gained in the study of the Laplace inversion integral for two-dimensional
flow point to a new technique of aeroelastic system modeling. This
technique is developed in this section and applied to the study of active
flutter control of a two-dimensional section.

The transformed equation describing the aeroelastic system is given
by (3.1)

$$G(s)X(s) = G\mathcal{U}(s) . \tag{5.13}$$

If rigid two-dimensional sections are being considered, $G(s)$ is an $n \times m$
matrix whose elements may contain nonrational transforms (e.g., $C(\bar{s})$ in
incompressible flow), while $\mathcal{U}(s)$ is an m-dimensional input. For flexible
wings, (5.13) may represent an infinite dimensional operator relation de-
fined on a Hilbert space. More commonly, the infinite discrete spectrum
of such a wing is truncated to the first n modes. Thus, both cases
may be treated by the finite dimensional version fo (5.13). The two-
dimensional section in incompressible flow will be used to illustrate the

-120-

developments of this section. The solution for the components of $\underline{X}(s)$ is

$$\underline{X}_i(s) \;=\; \frac{\sum\limits_{j=1}^{m} N_j^i(s) u_j(s)}{D(s)} \;; \qquad i = 1, 2, \ldots, n \qquad (5.14)$$

where $N_j^i(s)$ is the numerator transform obtained via Cramer's rule for the ith state due to the jth input. The inversion integral may be used to obtain

$$\underline{x}_j(t) \;=\; \sum_{k=1}^{m} \left\{ \sum_{i=1}^{n} \mathrm{Res}_{jk}^i \; e^{s_i t} \;-\; \frac{1}{\pi} \int_0^\infty \mathrm{Im}\!\left[\frac{X_{\sim j}}{u_k}(re^{i\pi})\right] e^{-rt} dr \right\} \cdot \qquad (5.15)$$

The summation inside the brackets has been termed the 'rational' portion of the response and is due to the isolated poles introduced by the structural degrees-of-freedom while the integral has been termed the 'nonrational' portion of the response.

The examples of the previous chapters have shown that the oscillatory transient response typifying flutter phenomena is due entirely to the rational portion. The response of the nonrational portion is nonoscillatory and decays monotonically to zero. Moreover, it is a small fraction of the total response. In addition, much of the analytical difficulty in studying the response of the system is caused by this nonrational portion. Therefore, a model of the rational portion of the system would be desirable, since it would apparently describe the principal characteristics of the oscillatory response.

The method to be described below is similar in spirit to that outlined by Wang [50], who showed that a class of linear distributed systems with purely discrete spectra and a finite number of unstable modes could be stabilized with a finite-dimensional linear feedback. However, Wang did not address the problem of the construction of a simpler approximate model describing the instability. The realization of the model of the

-121-

rational portion can be stated as a theorem.

THEOREM: The linear system represented by

$$\mathfrak{C}(s)\underline{X}(s) \;=\; G(s)\mathfrak{U}(s) \tag{5.16}$$

where $\underline{X}(s)$ is n-dimensional, $\mathfrak{U}(s)$ is m-dimensional, and $\mathfrak{C}(s)$ and $G(s)$ may contain nonrational functions of s, may be approximated by the linear, constant-coefficient system

$$\dot{X} \;=\; FX + G_1 u \tag{5.17}$$

with $X \in E^N$ and $u \in E^m$. The system matrices are given uniquely by

$$F \;=\; T\Lambda T^{-1}$$

$$\Lambda \;=\; \mathrm{diag}(s_1, \; s_2, \; \ldots, \; s_N)$$

$$T_{.i} \;=\; \left[A_i\right]_{.1}$$

$$G_1 \;=\; \sum_{i=1}^{N} A_i$$

where s_i, $i = 1, 2, \ldots, N$ are the isolated singularities of $\mathfrak{C}(s)$ and the elements of the $N \times m$ matrices A_i are $a_{jk}^{i} \equiv \mathrm{Res}_{jk}^{i}$ (read; the residue at the ith pole of the jth state due to the kth input).

Note that the finite-dimensional system of (5.17) represents the rational portion of the system of (5.16) which is due to the isolated poles at s_i, $i = 1, 2, \ldots, N$. The following proof assumes that $N = 2n$ where n equals the number of degrees-of-freedom of the system. It is possible that the nonrational functions contained in $\mathfrak{C}(s)$ may introduce singularities into the spectrum of $\mathfrak{C}$ over and above the singularities due to the dimension of $\underline{X}(s)$ (c.f., the two-dimensional supersonic case

-122-

of Sect. III-A-2). In this case, 2n of the system poles must be selected to construct the approximate system. A natural choice would be those poles associated with the n structural degrees-of-freedom.

The proof of the theorem will be constructive, giving an algorithm for the construction of F and G_1. The result of the following lemma will be needed.

LEMMA: The matrices of residues, A_i, $i = 1, 2, \ldots, N$ have rank 1.

PROOF: This may be seen by noting that (5.15) may be transformed and reorganized as

$$\underline{X}(s) = \sum_{i=1}^{N} \frac{A_i}{s-s_i} + R$$

(5.18)

with R representing the nonrational portion. The elements of the residue matrices, A_i, are given by $N_k^j(s_i)/D'(s_i)$.

Now consider the linear system obtained from (5.16) by evaluating the nonrational functions contained in $\mathfrak{a}(s)$ and $G(s)$ at the pole located at $s = s_i$. Denote the resulting matrices as $\tilde{\mathfrak{a}}(s,s_i)$ and $\tilde{G}(s,s_i)$. The solution of

$$\tilde{\mathfrak{a}}(s,s_i)\underline{X}(s) = G(s,s_i)\mathfrak{U}(s)$$

(5.19)

may be written as

$$\left[\frac{X}{\mathfrak{U}}(s)\right] = \frac{\tilde{A}_i}{s-s_i} + \cdots$$

(5.20)

where $\tilde{A}_i = \tilde{N}_k^j(s_i)/\tilde{D}'(s_i)$ are n×m residue matrices. Gilbert [82] proves that the $\tilde{A}_i$ matrices in (5.20) have rank 1 as is also evident from (5.9) At the pole, $s = s_i$, the systems of (5.16) and (5.19) satisfy the following relations

$$\tilde{D}(s_i) = D(s_i)$$

$$\tilde{N}_k^j(s_i) = N_k^j(s_i)$$

$$\tilde{D}'(s_i) \neq D'(s_i) \ .$$

Therefore

$$A_i = \frac{N_k^j(s_i)}{D'(s_i)} = \frac{\tilde{D}'(s_i)}{D'(s_i)} \tilde{A}_i$$

showing that A_i and $\tilde{A}_i$ differ only by a complex multiplier. Therefore the $N \times m$ matrices A_i in (5.18) also have rank 1.

To construct the matrices F and G_1 of (5.17) consider the diagonalizing transformation $X = Ty$. (The eigenvalues of F are assumed to be distinct.) Equation (5.17) is transformed to

$$\dot{y} = \Lambda y + gu \ . \tag{5.21}$$

In terms of X

$$\dot{X} = T\Lambda T^{-1} X + Tgu$$

showing that $F = T\Lambda T^{-1}$ and $G_1 = Tg$. The proof will be complete if unique matrices T and g can be found yielding these relations. Transforming (5.21) gives

$$y(s) = (sI-\Lambda)^{-1}gu = \begin{bmatrix} \frac{1}{s-s_1} & & & \\ & \cdot & & \\ & & \cdot & \\ & & & \frac{1}{s-s_{n'}} \end{bmatrix} gu \ .$$

Therefore

$$X(s) = Ty(s) = \left[T_{.1} \mid T_{.2} \mid \cdots \mid T_{.N}\right] \begin{bmatrix} \frac{1}{s-s_1} & & & \\ & \cdot & & \\ & & \cdot & \\ & & & \cdot \\ & & & \frac{1}{s-s_{n'}} \end{bmatrix} \begin{bmatrix} g_{1.} \\ \text{---} \\ g_{2.} \\ \text{---} \\ \vdots \\ \vdots \\ \text{---} \\ g_{N.} \end{bmatrix} \begin{bmatrix} u_1 \\ \vdots \\ u_m \end{bmatrix}$$

$$X(s) = \sum_{i=1}^{N} \frac{A_i}{s-s_i} \begin{bmatrix} u_1 \\ \vdots \\ \vdots \\ u_m \end{bmatrix}; \qquad A_i = T_{.i} g_{i.} \qquad (5.22)$$

This shows that it is possible to construct a unique realization (5.17) if and only if the matrices of residues A_i can be constructed as the outer produce of two vectors. In other words, Rank $(A_i) = 1$. But the above Lemma proves that this is the case for the system of (5.16). We are free to choose the form of $g_{i.}$ as

$$g_{i.} = \begin{bmatrix} 1 & a_2^i & \cdots & a_m^i \end{bmatrix}.$$

Then the columns of T are given by (5.22) as the first columns of the matrices, A_i. That is

$$T = \begin{bmatrix} T_{.1} \mid T_{.2} \mid \cdots \mid T_{.N} \end{bmatrix} \quad \text{where} \quad T_{.i} = \begin{bmatrix} A_i \end{bmatrix}_{.1}.$$

From the discussion following (5.21)

$$G_1 = Tg = \sum_{i=1}^{N} T_{.i} g_{i.} = \sum_{i=1}^{N} A_{i.}.$$

This completes the proof of the theorem.

It is interesting to note that the amount of information available about the rational portion of (5.16) is sufficient to uniquely determine the $N^2 + Nm$ unknown elements of F and G_1. There are N values of s_i,

N^2 independent elements of the matrices of residues A_i, and $N(m-1)$ constants a^i_j; $i = 1, 2, \ldots, N$; $j = 1, 2, \ldots, m$.

Reduced order approximate models of the system of (5.16) may be constructed by deleting selected poles since the theorem is usually true for the case in which the dimension of X is $N < 2n$. This follows since the proof of the theorem depends only upon the rank of the A_i matrices being unity. For the case $N < 2n$, these matrices will be submatrices of those considered in the theorem and will have rank less than or equal to one. Disregarding the very unlikely occurrence of a rank zero submatrix, the above statement follows.

The models constructed from the algorithm given by the Theorem will be termed 'rational models'. The matrices F and C_1 describing the rational model of the three DOF section of Table III-3 in incompressible flow are given in Table V-4 for $U/b\omega = 2.9$.

Table V-4

RATIONAL MODEL FOR A THREE-DEGREE-OF-FREEDOM SECTION

$(M = 0,\ U/b\omega_\alpha = 2.9,\ F \text{ and } G_1 \text{ in sec}^{-1})$

$$F = \begin{bmatrix} 0 & 0 & 0 & 1.0 & 0 & 0 \\ 0 & 0 & 0 & 0 & 1.0 & 0 \\ 0 & 0 & 0 & 0 & 0 & 1.0 \\ -3395 & -1243 & -1139 & -10.04 & -0.1475 & 0.3564 \\ 3127 & -9758 & 6593 & 13.33 & -29.22 & -6.567 \\ -2858 & 29344 & -113723 & -27.78 & 44.98 & -5.120 \end{bmatrix}$$

$$G_1 = \begin{bmatrix} 7.279 \\ -3.390 \\ 0.9792 \\ -95.52 \\ -8648 \\ 115638 \end{bmatrix}$$

The matrices of the Padé model are given in Table V-5 for the same case.

Table V-5

PADÉ MODEL FOR A THREE DEGREE-OF-FREEDOM SECTION

$(M = 0, U/b\omega_\alpha = 2.9, F$ and G_1 in $\sec^{-1})$

$$
F =
\begin{bmatrix}
0 & 0 & 0 & 1.0 & 0 & 0 & 0 & 0 \\
0 & 0 & 0 & 0 & 1.0 & 0 & 0 & 0 \\
0 & 0 & 0 & 0 & 0 & 1.0 & 0 & 0 \\
-2934 & -173.1 & -993.2 & -9.267 & -10.47 & -0.9598 & -10638 & -583.2 \\
2514 & -11178 & 6399 & 12.30 & -15.52 & -4.820 & 14122 & 774.2 \\
-1579 & 32302 & -113319 & -25.61 & 16.50 & -8.755 & -29396 & -1611 \\
0 & 0 & 0 & 0 & 0 & 0 & 0 & 1.0 \\
0 & 290 & 159.4 & 1.0 & 0.9 & 0.1487 & -1148 & -100.2
\end{bmatrix}
$$

$$
G_1 =
\begin{bmatrix}
0 \\
0 \\
0 \\
355.3 \\
-8939 \\
115712 \\
0 \\
0
\end{bmatrix}
$$

Table V-6 compares the transfer functions derived from the rational model with those of the Padé model. Since the F matrix of the rational model is constructed by performing a similarity transformation (5.21) on the matrix of the exact eigenvalues of (5.16), the rational model reproduces these exact poles while the Padé model gives a good approximation to these poles. In addition, the Padé model also contains the two augmented state poles. The nature in which the residues used to construct

-127-

Table V-6

COMPARISON OF TRANSFER FUNCTIONS OF RATIONAL AND PADÉ MODELS

$(M = 0, U/b\omega_\alpha = 2.9$, poles and zeroes in $\sec^{-1})$

1) POLES		Rational Model	Padé Model
bending		$-3.711 \pm i68.252$	$-2.659 \pm i69.149$
torsion		$-15.049 \pm i80.171$	$-17.485 \pm i79.122$
flap		$-3.431 \pm i340.38$	$-3.414 \pm i340.26$
			-12.523
			-74.099

2) ZEROES		
a) Rational Model	Gain	
x_1/β_c	7.2785	$(-4.09\pm i81.59)(-65.3+i364.68)(+107.43)$
x_4/β_c	-95.518	$(-3.47\pm i80.18)(+110.91\pm i1173.1)(-30.70)$
x_2/β_c	-3.3904	$(+2.82\pm i71.86)(-72.0\pm i151.21)(-2457)$
x_5/β_c	-8648.6	$(+3.3\pm i71.55)(-56.48\pm i152.21)(+10.44)$

b) Padé Model	Gain	
h/β_c	355.26	$(-3.25+i80.28)(+501.72)(-334.66)(-220.3)(-15.53)$
α/β_c	-8938.89	$(+3.84\pm i72.37)(-59.84\pm i162.29)(-56.09)(-12.01)$

F and G_1 were evaluated places constraints on the system realization given by the rational model which are seen in the structure of the submatrices of F in Table V-4. The equation for $\dot{X}_1$ is

$$\dot{X}_1 = X_4 + 7.279\,\beta_c \qquad (5.23)$$

indicating the expected relation between the states modeling h (X_1) and
ḣ (X_4). The small 'feedforward' term, $7.279\beta_c$, causes the relation
$\dot{X}_1 \neq X_4$ and is due to the unmodeled nonrational portion of (5.15). This
effect is also evident in the zeroes of Table V-6. The Padé model zeroes
satisfy the relation $(\dot{h}/\beta_c)(s) = s(h/\beta_c)(s)$ while $(X_4/\beta_c)(s) \neq$
$s(X_1/\beta_c)(s)$. The magnitude of the feedforward terms of the upper sub-
matrix of G_1 of Table V-4 is directly proportional to the relative
magnitude of the nonrational portion to the rational portion of the re-
sponse. It is interesting to note that the real zeroes of the rational
model indicate phase changes of approximately 90° between X_1 and X_4,
and X_2 and X_5 respectively.

The usefulness of the rational model must be evaluated by its ability
to predict the response of the system in the bandwidth of interest; that
is, at frequencies near the flutter frequency. Table V-4 shows that the
zeroes near the ω axis in the vicinity of the flutter frequency ($\omega \cong$
70 rad/sec) agree well between the rational model and the Padé model.
Frequency responses of the rational model are compared to the exact model
in Fig. V-8. The rational model agrees very well with the exact model
in the frequency range of flutter, with the agreement deteriorating with
increasing distance from the system poles. From this comparison and that
of Fig. IV-4, it is concluded that the rational model and the Padé model
are both capable of predicting system response at frequencies near the
flutter frequency.

In closing this section, it should be noted that the rational model
is not restricted to the two-dimensional incompressible flow case. It is
equally valid for compressible three-dimensional flow when used with
truncated normal mode structural representations and aerodynamic loads
calculated for arbitrary s. The advantage of the rational model is that
it does not require augmented states whereas the Padé model does. Also,
the rational model might be expected to give better performance than the
Padé model for points well removed from the ω axis.

Exact model
Rational model
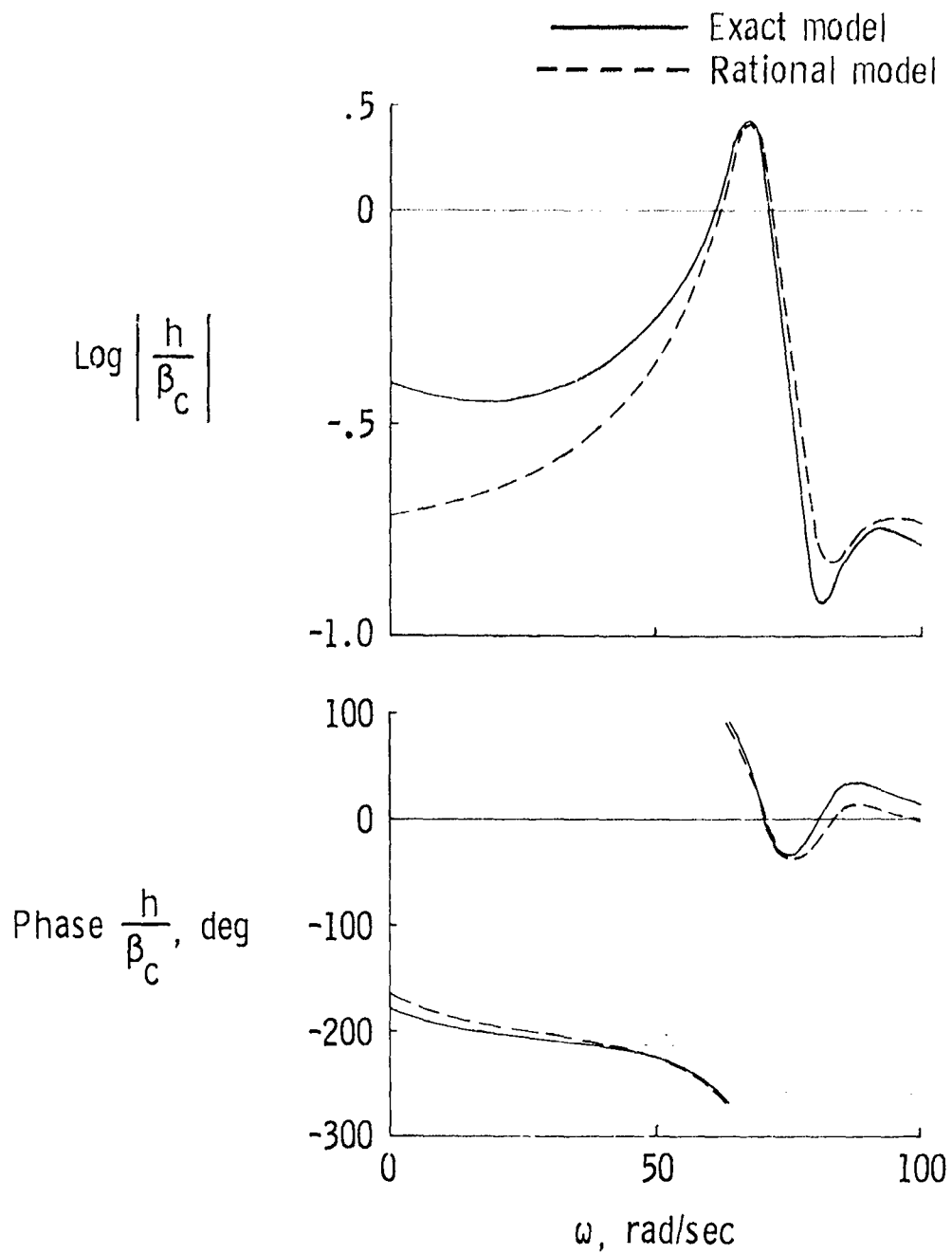
(a)   PLUNGE

FIG. V-8   COMPARISON OF FREQUENCY RESPONSES OF PLUNGE AND
TORSION DUE TO FLAP DEFLECTION OBTAINED FROM THE
EXACT MODEL AND FROM THE RATIONAL MODEL
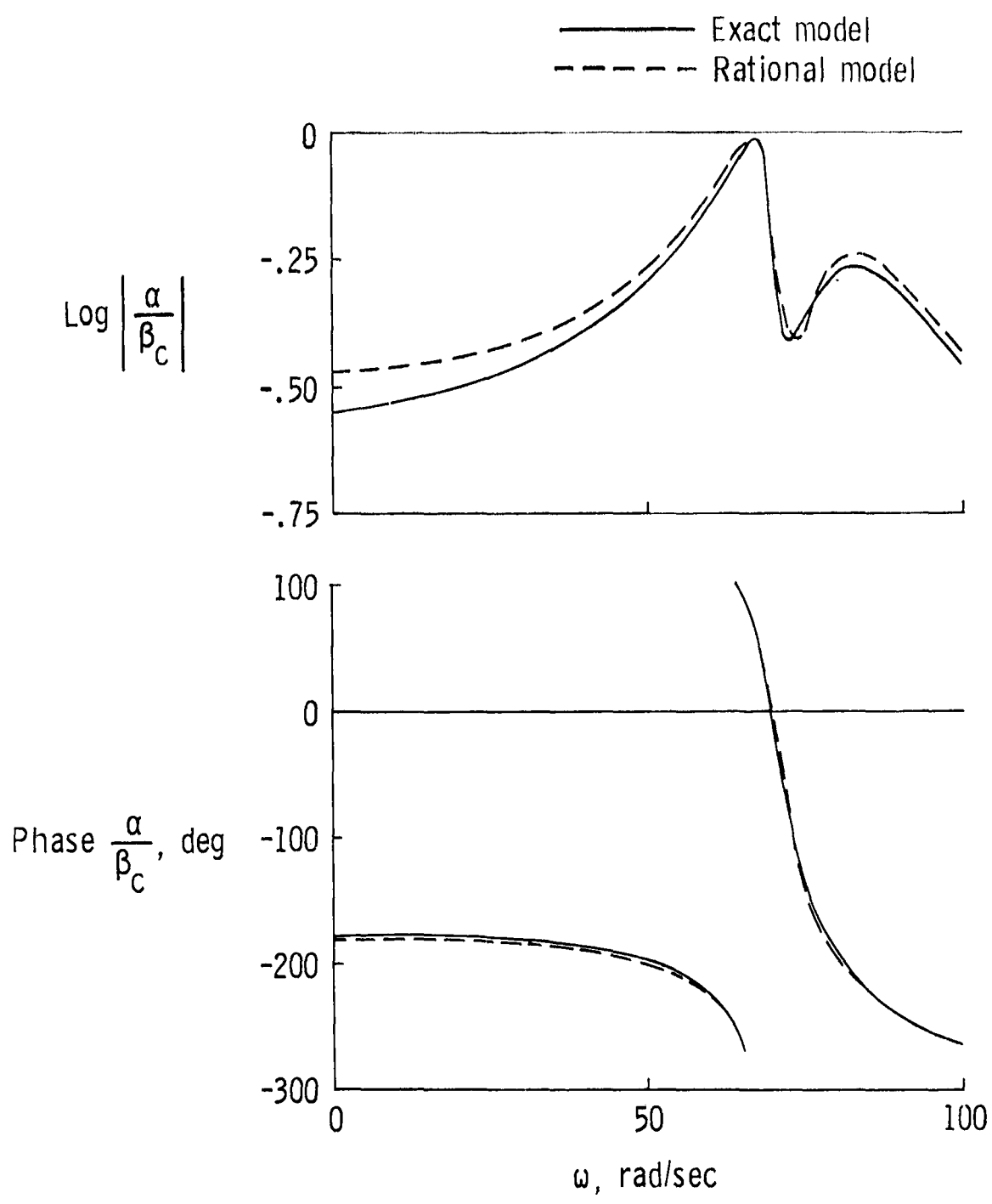
(b) TORSION

FIG. V-8   CONCLUDED

F. OPTIMAL CONTROL OF AEROELASTIC SYSTEMS

In this section active flutter design techniques will be studied using the rational model and the Padé model. Although the specific problem under consideration will be the control of a flutter mode, the same techniques are applicable to any of the control configured vehicle (CCV) concepts addressing dynamic structural or aircraft response.

Several of the most prominent examples of aeroelastic control have been designed using augmented state Padé models [2], [3], which resulted in quite large order systems. Attempts to apply modern optimal control techniques to these models have not had great success due to the requirement of feeding back all of the states of the model. The matrix Padé approximant method of Vepa promises to alleviate this problem somewhat by greatly reducing the number of augmented states. The rational model holds further promise in that augmented states are completely eliminated. The cost of this advantage is a certain ambiguity in the relationship of the states of the model to the physical measurements of the structure. This problem may be assessed by checking the performance predicted by the rational model with the corresponding performance obtained with the exact model using the same control law.

In the two-dimensional incompressible case, it is possible to compare the two models since exact unsteady airloads are available for arbitrary $\bar{s}$ (Sec. II-D) and the Padé model of Sect. IV-A involves only two augmented states. In both cases, the model is given as

$$\dot{X} = FX + G_1 u . \tag{5.24}$$

An appropriate performance index for the flutter problem is that of the optimal regulator [37]

$$J = \frac{1}{2} \int_0^\infty [X^T A X + u^T B u] dt . \tag{5.25}$$

Minimization of J satisfying the constraint of (5.24) is achieved via the steady-state solution of the matrix Riccati equation

-132-

$$\dot{S} = -SF - F^T S + SG_1 B^{-1} G_1 S - A \qquad (5.26)$$

where $S(0) = 0$. The linear feedback control law is given in terms of the steady-state Riccati matrix, S^0, as

$$u(t) = -B^{-1} G_1^T S^0 X(t) = CX(t) . \qquad (5.27)$$

The control weighting matrix B must be positive definite, while the state weighting matrix A must be positive semidefinite. Hall and Bryson [84] describe a digital computer program well suited to the solution of this problem. This program, OPTSYS, was utilized in the control law designs of this section.

The problem of choosing the weighting matrices A and B remains. A basic result of the theory is that if $A = 0$ (i.e., zero-state weighting), the action of the resulting control law upon the closed loop eigenvalues is to leave unchanged all stable eigenvalues, while open loop unstable eigenvalues located at $s = \mu + i\omega$ are reflected about the $i\omega$ axis to $s = -\mu + i\omega$. For structures with slightly supercritical flutter modes, this zero-state weighting technique is an attractive design method since the result is a modestly stable controlled mode. However, for larger values of the supercritical flutter speed, the technique leads to unreasonably high damping of the flutter mode. Also, the method cannot be used to improve the damping of subcritical flutter modes.

Anderson and Moore [85] describe a method which can be used in conjection with zero-state weighting to restrict the maximum value of the real part of all eigenvalues. Equation (5.24) is transformed and the change of variables $s' = s + \nu$ made giving

$$[s'I - (F+\nu I)]X(s') = G_1 U(s) . \qquad (5.28)$$

The result of the transformation is to shift all eigenvalues of F ν units in the direction of the positive real axis or, equivalently, to shift the origin ν units in the direction of the negative real axis. Equation

(5.28) indicates that this eigenvalue shift can be accomplished by adding ν to the diagonal elements of F. Hence, if F contains an unstable eigenvalue at $s = \mu + i\omega$ and it is desired to constrain all eigenvalues, λ, such that $Re(\lambda) < \eta$, this will be accomplished by the optimal regulator solution with zero-state weighting for the system

$$\dot{X} = (F + \nu I)X G_1 u \qquad (5.29)$$

with $\nu = -\frac{1}{2}(\mu - \eta)$. Eigenvalues, λ_i, with $Re(\lambda_i) < \eta$, are unaffected by the resulting control law.

The optimal regulator solution was obtained for the section of Table III-3 at $U/b\omega_\alpha = 3.25$ using the rational model and the Padé model. (The flap chord, $c = 0.5$, for this example.) Figure IV-3 compares the open loop roots of the two models and shows that the section damping is $\zeta \sim -0.09$. The weighting matrices were $A = 0$, $B = 1$. Table V-7 gives the feedback gains and the open and closed loop eigenvalue locations.

Table V-7

OPTIMAL REGULATOR GAINS AND EIGENVALUES FOR A THREE DOF SECTION
($M = 0$, $U/b\omega_\alpha = 3.25$, $A = 0$, $B = 1$, poles in rad/sec)

Case I: Rational Model

$C = \lceil 2.901 \quad -2.197 \quad -0.09393 \mid 0.04124 \quad 0.007558 \quad 0.0001064 \rceil$

Mode	Open Loop λ_i	Exact Closed Loop λ_i
bending (flutter)	$+6.420 \pm i71.03$	$-4.975 \pm i69.94$
torsion	$-28.68 \pm i73.56$	$-28.68 \pm i73.55$
flap	$-14.59 \pm i339.9$	$-14.59 \pm i339.9$

Case II: Padé Model

$C = [2.517 \quad -2.519 \quad -0.1076 \mid$

$\mid 0.0450 \quad 0.01168 \quad 0.0005183 \mid -5.778 \quad 0.1436]$

Mode	Open Loop λ_i	Exact Closed Loop λ_i
bending (flutter)	$+6.987 + i71.01$	$-5.790 + i71.48$
torsion	$-31.27 + i72.82$	$-32.89 \pm i69.45$
flap	$-14.53 + i339.6$	$-13.85 + i339.7$
	-13.78	--
	-79.93	--

-134-

The roots termed 'open loop' in the Table are the eigenvalues of the appropriate uncontrolled F matrix (viz., Eq. 5.17 for the rational model, and Eq. 4.9 for the Padé model). The roots termed 'exact closed loop' were obtained by implementing the feedback control laws in the exact system equations and locating the exact closed loop roots by iteration as described in Sec. III-A. For the rational model, (5.13) becomes

$$[G(s) - GC]X(s) = GU_c(s) \tag{5.30}$$

where $U(s) = U_c(s) + CX(s)$. To implement the Padé model control law, estimates of the two augmented states are required. This was accomplished by adding to (5.13) the known structure of the augmented states. In the notation of (4.8) this yeilds

$$\begin{bmatrix} G(s)-G(C_1+C_2 s) & \vdots & -GC_3 \\ \text{------------------} & + & \text{----} \\ E_1+E_2 s & \vdots & F_p \end{bmatrix} \begin{bmatrix} X(s) \\ \text{-----} \\ \underline{x}_p(s) \end{bmatrix} = \begin{bmatrix} G \\ \text{---} \\ 0 \end{bmatrix} U_c(s) \tag{5.31}$$

where C_1, C_2, and C_3 contain the gains associated with $\underline{x}$, $\underline{\dot{x}}$, and $\underline{x}_p$.

If the linear models represented by $\dot{X} = FX + G_1 u$ exactly described the dynamics of the section, then the closed loop roots would be identical with the open loop roots except for a sign change in the real part of the unstable roots. Deviations of the roots away from this condition indicate the presence of unmodeled (nonrational) effects.

Table V-7 shows that feedback gains from corresponding states of the two models are comparable and both designs stabilize the flutter mode. Except for the h feedback gain, the magnitudes of the gains of the rational model are less than those of the Padé model. The distance from the exact closed loop pole location to the predicted pole location is an indication of the ability of the models to deal with the unmodeled portion of the system. These distances for the flutter mode are: rational model, $\Delta s = 1.56$ rad/sec; Padé model, $\Delta s = 1.29$ rad/sec. The corresponding distances for the other two modes illustrate a basic difference between the models. The rational model is an exact model of the rational

-135-

portion of the system at a particular flight condition and the regulator design with zero-state weighting leaves the exact stable poles unchanged. The Padé model is an attempt to approximate the system throughout a given bandwidth (region of the s-plane). Thus the closed loop torsion and flap modes are displaced 3.74 rad/sec and 0.71 rad/sec respectively from their predicted locations. This effect of Padé models may be of concern in the design of flutter suppression systems for multi-mode structures in which there may be several marginally stable modes in addition to a flutter mode.

The characteristic of the rational model of matching the open loop rational portion of the system exactly emphasises the perturbation nature of control laws based upon this model. This implies that the deviation between the predicted and actual root locations will increase as the distance by which the flutter mode is moved increases. The deviation indicated in Table V-7 would seem to be acceptable. If the deviation were unacceptable, a second rational model could be constructed for the system resulting from the use of the first control law and a second regulator design performed, giving a second control law. If this attempt resulted in a satisfactory design, the final control law would be formed by the sum of the two control laws. Thus the rational model can be used in an iterative fashion, whereas a corresponding capability is not apparent in Padé models.

Figure V-9 indicates the effect on the open loop eigenvalues of the Padé model of incorporating the Padé gains of Table V-6 one at a time. It shows that the main contributors to the stabilization of the flutter mode are the h, α, and $\dot{h}$ gains. The $\dot{h}$ and $\dot{\beta}$ gains destabilize the flap mode, an effect which is counterbalanced by the α, β, and $\dot{\alpha}$ gains. Interestingly, the augmented state gains have little effect on the flutter mode, but they do influence the remaining modes.

Figure V-10 shows the effect on the exact closed loop pole locations for off-design airspeeds from $U/b\omega_\alpha = 0.5$ to 3.75. Both closed loop systems are unstable below the open loop flutter speed of $U/b\omega_\alpha = 3.0$, reflecting the near uncontrollability of this section by the trailing-edge control surface at this airspeed. Above this airspeed, both control
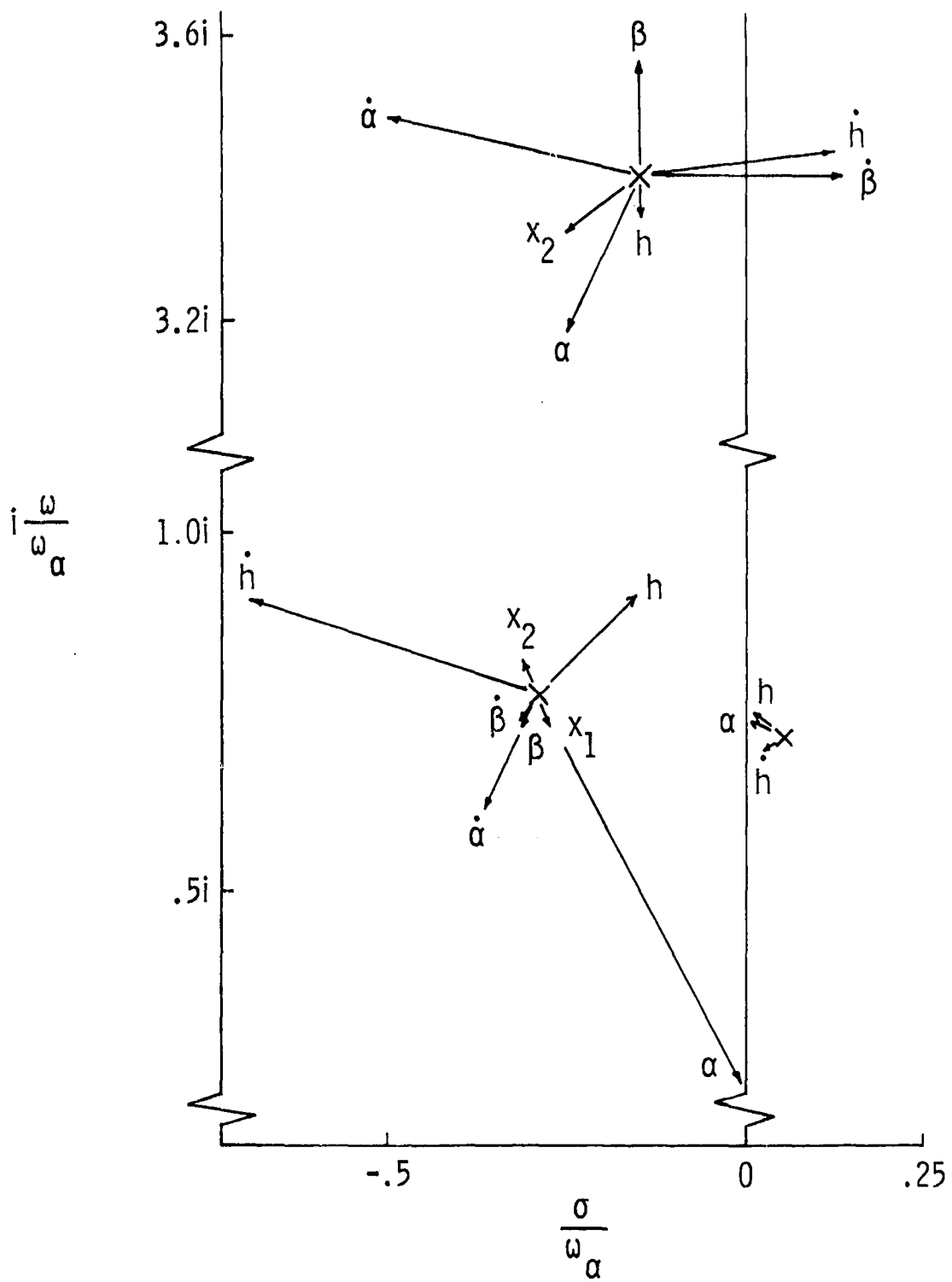
FIG. V-9 EFFECT OF SINGLE FEEDBACK CLOSURES ON SYSTEM POLES USING THE OPTIMAL REGULATOR GAINS OF TABLE 5.7II

$\dfrac{\omega}{\omega_\alpha} i$

1.3i

1.0i

.5i

$\dfrac{\sigma}{\omega_\alpha}$

-.5

0

.2

×

$\dfrac{U}{b\omega_\alpha}$	
	.5
	3.0
	3.25
	3.5
	3.75
	4.0

×   Open loop poles

———   Rational model design

– – –   Pade model design

(a)   PLUNGE AND TORSION MODES

$\dfrac{\omega}{\omega_\alpha} i$

3.5i

3.0i

$\dfrac{\sigma}{\omega_\alpha}$

-.5

0
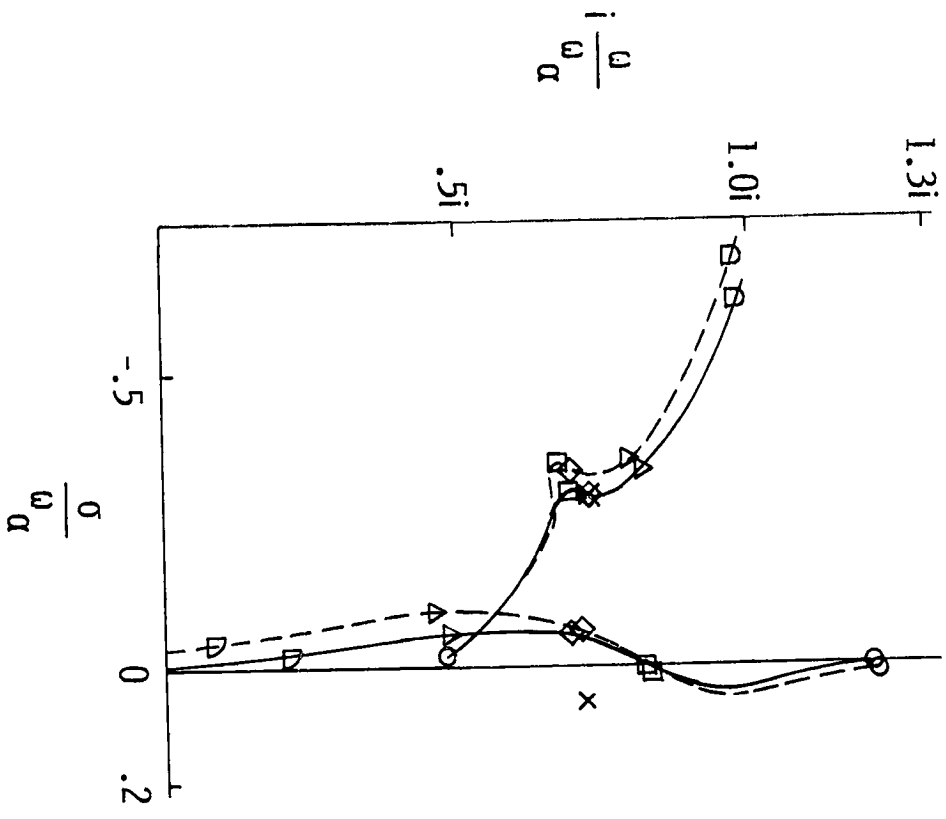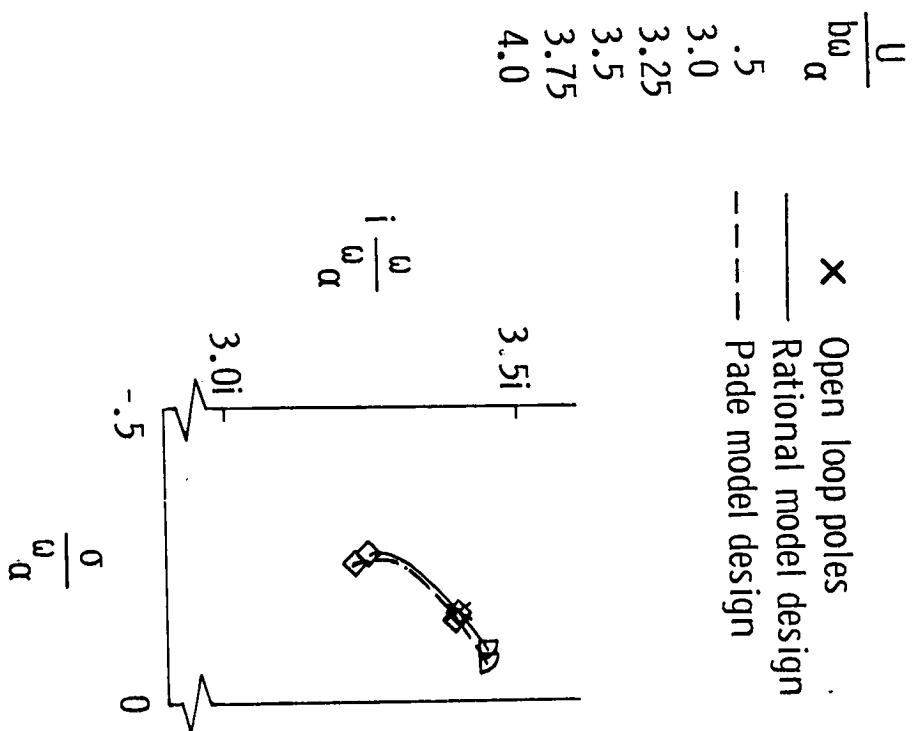
(b)   FLAP MODE

FIG. V-10   THE EFFECT OF OFF-NOMINAL VALUES OF $U/b\omega_\alpha$ ON THE CLOSED-LOOP POLES OF A THREE DEGREE-OF-FREEDOM SECTION IN INCOMPRESSIBLE FLOW USING THE OPTIMAL REGULATOR GAINS OF TABLE 5.7!

laws provide flutter mode control until a static divergence occurs at approximately $U/b\omega_\alpha = 3.80$. The Padé model maintains slightly better stability than the rational model throughout this airspeed region. This is due to the ability of the augmented model to approximate the nonrational effects over a wider bandwidth than the unaugmented model. However, this capability requires the complexity of augmented states, with the attendant problems of state estimation. It should also be noted that although the rational model control law was designed utilizing a 'nonphysical' model (viz., Eq. 5.17), the performance indicated by the 'exact closed loop' pole locations was obtained using measurements of real physical states $(h, \alpha, \beta, \dot{h}, \dot{\alpha}, \dot{\beta})$ and indicates the performance of the system under actual operating conditions.

The optimal control of the three DOF section was also investigated in supersonic flow. The section of Table III-4 was studied with the rational model and the matrix Padé model of (4.19). Table V-8 gives the optimal gains and eigenvalues for the two designs. The weighting matrices were $A = 0$, $B = 1$. Again, the corresponding gains of the two models are comparable with the rational model gains having smaller magnitude in all but two cases. For this compressible Padé model, three augmented states are required; one for each degree-of-freedom. The exact closed loop poles were not calculated for the Padé model. The agreement between the open and closed loop poles of the rational model indicates that the un-modeled effects are slight at this Mach number. Figure V-11 shows the effect of off-nominal values of M on the closed loop poles when the $M = 2$ feedback gains of the rational model are held constant. The figure indicates that the flutter Mach number has been increased from $M = 1.8$ to $M = 2.2$. Comparison with Fig. IV-6 indicates that the control law also stabilizes the flap mode at the lower Mach numbers.

As a final design case, the four DOF section of Table V-2 was analyzed using the rational model. Figure V-1c illustrates the nature of the flutter mode which was studied at $U/b\omega_\alpha = 3.55$. The flutter mode is unstable with a damping of $\zeta = -0.23$ and the airspeed is 25 percent above the flutter speed. Also, this section is nearly uncontrollable by the trailing-edge control surface at the flutter speed of $U/b\omega_\alpha = 2.84$.

Table V-8

OPTIMAL REGULATOR GAINS AND EIGENVALUES FOR A THREE-DEGREE-OF-

FREEDOM SECTION IN SUPERSONIC FLOW

($M = 2.0$, $A = 0$, $B = 1$, poles in rad/sec)

Case I: Rational Model

$C = [0.300 \quad 0.132 \quad 0.00401 \mid -0.00515 \quad 0.00932 . 0.000349]$

Mode	Open Loop λ_i	Exact Closed Loop λ_i
flutter	$-4.036 \pm i74.67$	$-4.078 \pm i74.24$
bending-torsion	$-15.69 \pm i70.67$	$-15.69 \pm i70.67$
flap	$-4.353 \pm i372.6$	$-4.346 \pm i372.6$

Case II: Padé Model

$C = [0.46 \quad -0.046 -0.078 \mid$

$\qquad \mid -0.004 \quad 0.010 \quad 0.0004 \mid 0.034 \quad 0.086 \quad -0.032]$

Mode	Open Loop λ_i	Exact Closed Loop λ_i
flutter	$-4.249 \pm i74.67$	--
bending-torsion	$-15.86 \pm i70.60$	--
flap	$-4.374 \pm i372.8$	--
	$-482.8 \pm i3323$	
	-1855	

Table V-8 gives three designs accomplished with zero-state weighting.
For Case I, $B = $ diag $(1,1)$, weighting the leading- and trailing-edge
control motions equally. The deviation of the closed loop flutter mode
from its anticipated location ($s = -16.66 \pm i68.08$ rad/sec) is accept-
able but the gains relating to the leading-edge control are significantly
higher than those associated with the trailing-edge control. The regulator
solution has designed a control law calling for more motion by the leading-

M
◇ 1.5
○ 2.0
□ 2.5
✕ Open loop poles

Design point

$i\dfrac{\omega}{\omega_\alpha}$

.8i

.7i

$\dfrac{\sigma}{\omega_\alpha}$

-.2   -.1   0

(a)   PLUNGE AND TORSION MODES

$i\dfrac{\omega}{\omega_\alpha}$

3.8i

3.6i

$\dfrac{\sigma}{\omega_\alpha}$
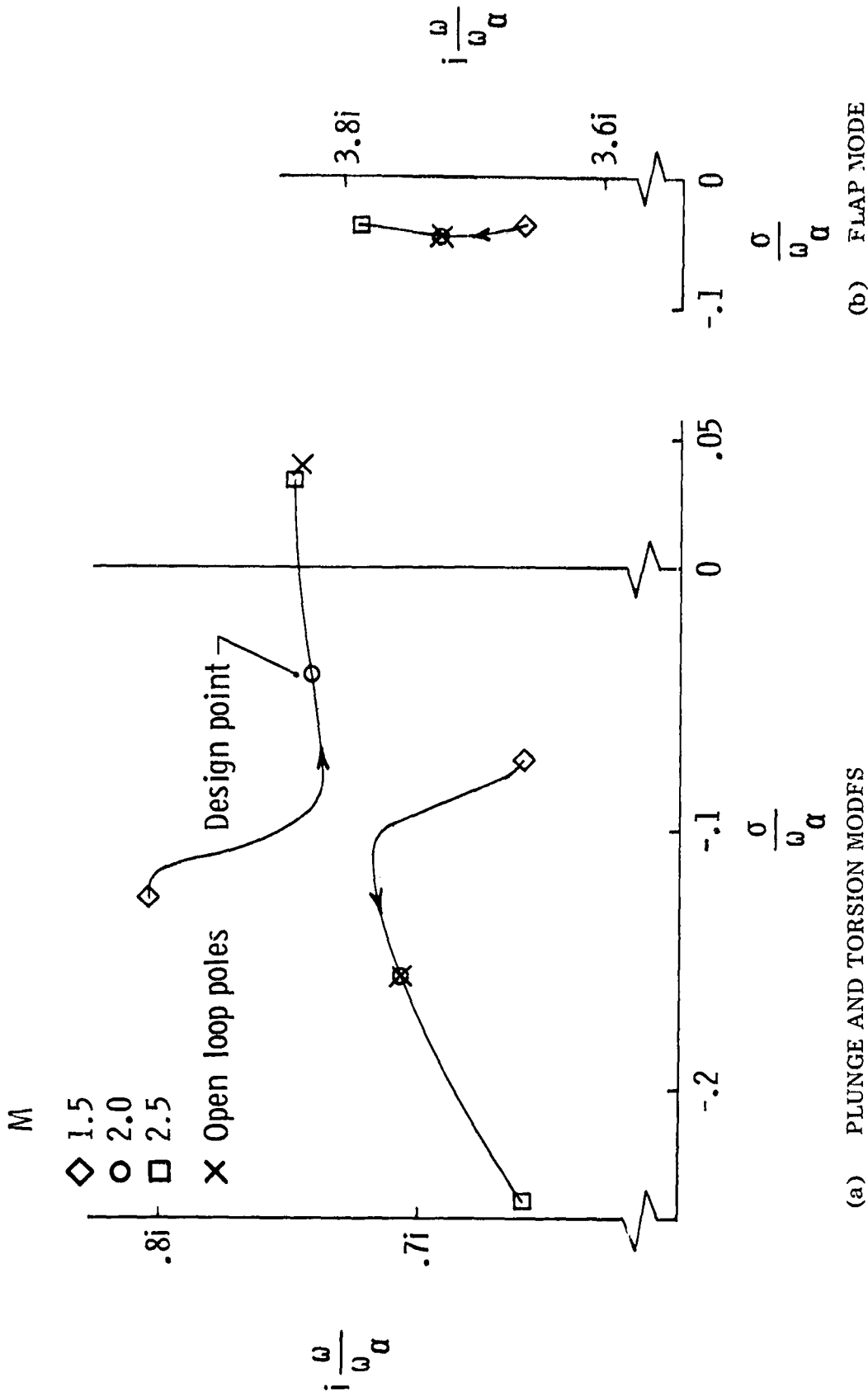
-.1   0

(b)   FLAP MODE

FIG. V-11   THE EFFECT OF OFF-NOMINAL VALUES OF M ON THE CLOSED LOOP POLES OF A THREE DEGREE-OF-FREEDOM SECTION IN SUPERSONIC FLOW USING THE OPTIMAL REGULATOR GAINS OF TABLE 5.8I

edge control since this surface produces greater loads for a given deflection than the trailing-edge control. This is undesirable since the leading-edge control is also subject to much greater hinge moments and would consume correspondingly greater power.

Thus the weighting on the leading-edge control motion was increased and Case II was designed with $B = $ diag $(1, 16)$. This change implies that that leading-edge control motion is 16 times more 'expensive' than trailing-edge control motion. Table V-9 shows that the deviation of the closed loop flutter pole from its expected value has almost doubled its value in Case I but is still acceptable. Also, the trailing-edge flap gains are roughly doubled from those of Case I while the leading-edge flap gains have been reduced by a factor of 5 to 10. The increased weighting on the leading-edge control has produced a design requiring more activity by the trailing-edge control. The increased deviation of the flutter mode from its expected location is probably due to the proximity of zeroes associated with the trailing-edge control.

The final case of Table V-9 illustrates the Anderson-Moore technique of axis shift in the s-plane to achieve a specified degree of stability. The desired damping sought by the regulator solution for Cases I and II is quite high ($\zeta = 0.23$) and a significantly smaller damping would be acceptable for high frequency structural modes. Using the Anderson-Moore technique with $\nu = -5$ rad/sec will result in a control law which attempts to place the flutter mode at $s = -6.66 + i68.08$ with a damping of $\zeta = 0.10$. Case III gives the resulting design for $B = $ diag $(1, 1)$. For this more modest design goal, the deviation of the exact closed loop pole from its anticipated location is only 1 rad/sec, les than half of the deviation of Case I.

Figure V-12 shows the migration of the bending and torsion modes for Cases II and III as a function of $U/b\omega_\alpha$. The feedback gains of Table V-9 were held constant and the exact closed loop eigenvalues located by iteration. The design of Case II is unstable at low values of $U/b\omega_\alpha$ and gain scheduling would be required to achieve acceptable performance. Evidently, ground checkout of this flutter suppression system would be

Table V-9

OPTIMAL REGULATOR GAINS AND EIGENVALUES FOR A FOUR-DEGREE-OF FREEDOM SECTION USING THE RATIONAL MODEL

(M 0, A = 0, $U/b\omega_\alpha = 3.55$, poles in rad/sec)

Mode	Open Loop λ_i
1. bending (flutter)	$+16.66 \pm 168.08$
2. torsion	-33.52 ± 163.63
3. L.E. flap	-14.71 ± 1254.38
4. T.E. flap	-62.75 ± 1605.10

Case I: B = diag (1,1)

$$C = \begin{bmatrix} 0.62 & 0.173 & 0.0105 & -0.0760 \\ 0.787 & 0.516 & 0.0369 & -0.139 \end{bmatrix}$$

$$\begin{bmatrix} 0.00333 & 0.00823 & 0.000511 & -0.000987 \\ 0.000586 & 0.0115 & 0.000739 & -0.00148 \end{bmatrix}$$

Mode	Exact Closed Loop λ_i
1. bending (flutter)	-15.29 ± 169.77
2. torsion	-33.52 ± 163.77
3. L.E. flap	-14.71 ± 1254.38
4. T.E. flap	-62.75 ± 1605.10

Case II: B = diag(1, 16.)

$$C = \begin{bmatrix} 1.479 & 0.451 & 0.0282 & -0.187 \\ 0.118 & 0.0745 & 0.00531 & -0.0204 \end{bmatrix}$$

$$\begin{bmatrix} 0.0075 & 0.0198 & 0.00124 & -0.00239 \\ 0.000121 & 0.00171 & 0.000109 & -0.00022 \end{bmatrix}$$

Mode	Exact Closed Loop λ_i
1. bending (flutter)	-12.92 ± 166.68
2. torsion	-33.52 ± 163.63
3. L.E. flap	-14.71 ± 1254.38
4. T.E. flap	-62.75 ± 1605.10

Case III: B = diag(1, 1.), $\nu = -5$ rad/sec

$$C = \begin{bmatrix} 0.439 & 0.0899 & 0.00485 & -0.0494 \\ 0.549 & 0.311 & 0.0219 & -0.0899 \end{bmatrix}$$

$$\begin{bmatrix} 0.00277 & 0.00574 & 0.000354 & -0.000677 \\ 0.00101 & 0.00785 & 0.00501 & -0.000997 \end{bmatrix}$$

Mode	Exact Closed Loop λ_i
1. bending (flutter)	-6.079 ± 168.91
2. torsion	-33.52 ± 163.63
3. L.E. flap	-14.71 ± 1254.38
4. T.E. flap	-62.75 ± 1605.10
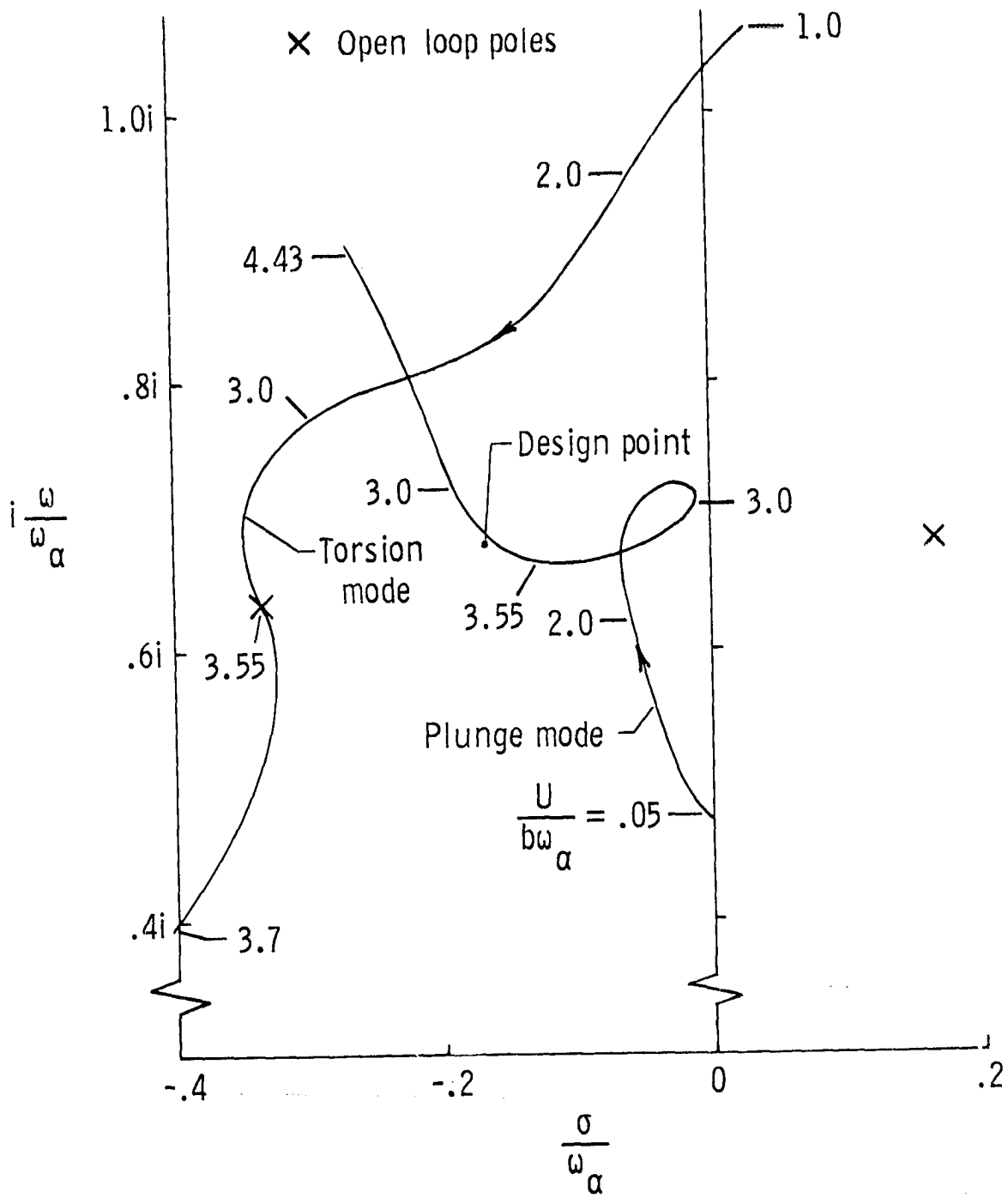
(a) $A = 0$, $B = \text{DIAG}(1, 16)$

FIG. V-12   THE EFFECT OF OFF-NOMINAL VALUES OF $U/b\omega_\alpha$ ON THE
CLOSED LOOP POLES OF A FOUR DEGREE-OF-FREEDOM
SECTION IN INCOMPRESSIBLE FLOW USING THE OPTIMAL
REGULATOR GAINS OF TABLE 5.9II, III
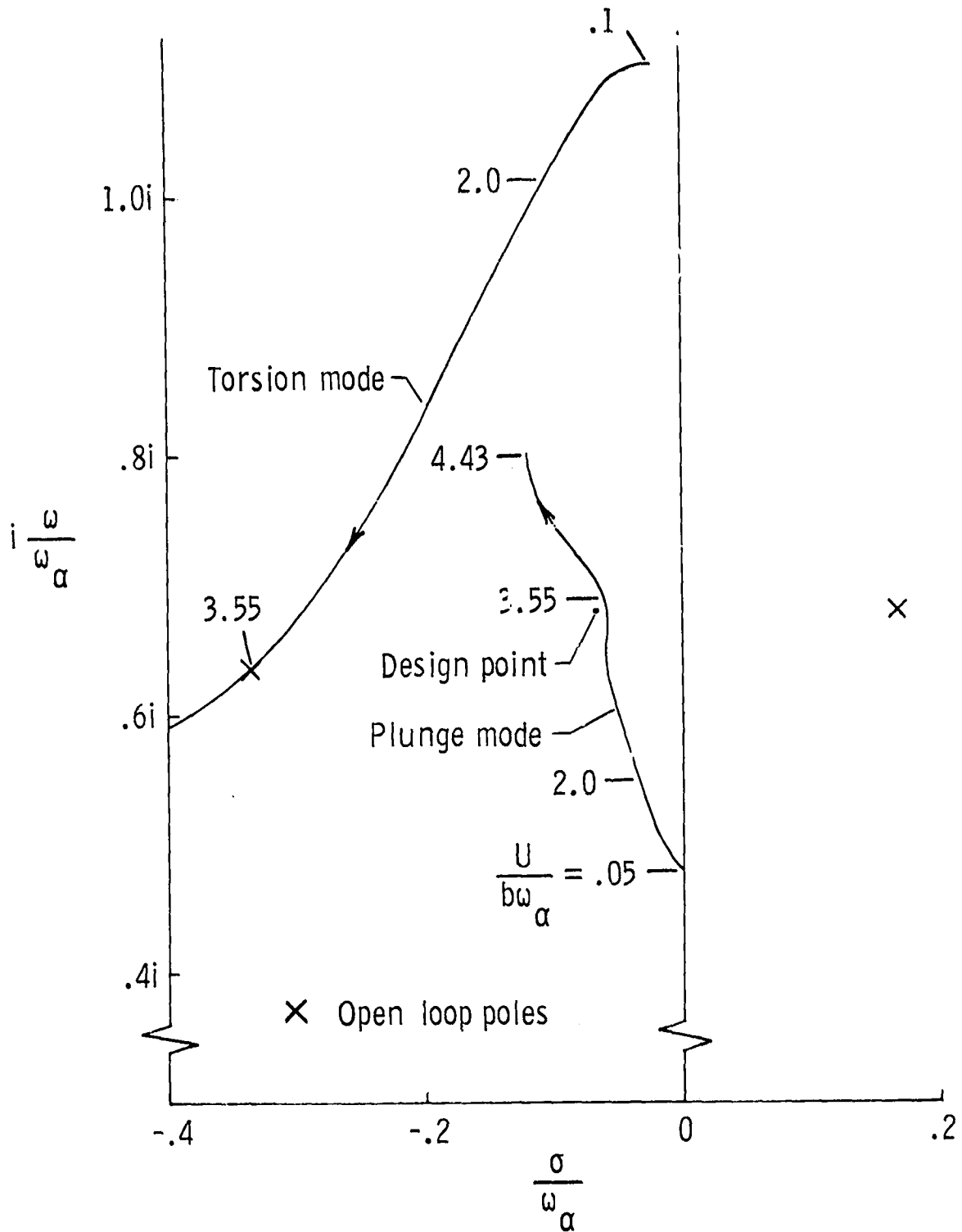
(b) $A = 0$, $B = \mathrm{DIAG}\,(1,\,1)$, $\nu = -5\ \mathrm{RAD/SEC}$

FIG. V 12   CONCLUDED

difficult due to the inertia coupling of the modes. Figure V-12a also shows the influence of the uncontrollable mode in the sensitivity of the locus near the open loop flutter velocity ($U/b\omega_\alpha$ 2.84). The performance of the control law of Case III at off-nominal values of $U/b\omega_\alpha$ (Fig. V-11b) indicates a smooth variation of the locus throughout the velocity range studied. This is due to the increased authority allowed the leading-edge flap by the reduction of the weighting on γ for Case III.

Both the torsion and the plunge modes of Cases II and III are stable for airspeeds well above $U/b\omega_\alpha = 4.0$. However, at $U/b\omega_\alpha = 3.98$ the section becomes statically divergent due to the emergence of a real positive root. As the airspeed increases beyond this divergence speed, this root becomes more positive. This static divergence of the actively controlled section is of the same nature as the static divergence of the uncontrolled section studied in Sect. IV-D. Whereas divergence of uncontrolled sections usually occurs at higher airspeeds than flutter, it is seen that active control of flutter may reverse this condition. Hence, the behavior of active flutter control techniques should always be investigated at the zero frequency condition where static divergence occurs.

The examples given in this chapter illustrate the application of modern optimal control theory to the design of flutter suppression systems. The matrix Padé model and the rational model are both capable of predicting closed loop performance. The disadvantage of the Padé model is in the estimation of the augmented states which would be required to implement the control law. The use of both leading- and trailing-edge control surfaces will obviously simplify the problem of stabilizing the flutter mode but the additional control surface introduces other problems of stability and power requirements. It should be noted that the nominal incompressible flow section investigated in this chapter represents a worst case design situation, in that it was nearly uncontrollable by the trailing-edge control surface at the flutter velocity. In a realistic design situation in which a flutter suppression system is to be designed for a particular flight condition or range conditions, it may well be possible to locate and size a single trailing-edge control surface to achieve the design goal.

SUMMARY AND RECOMMENDATIONS

A. SUMMARY

1. The transfer function relating airfoil motions to the airloads due to circulation in two-dimensional incompressible flow is derived and is identified as the generalized Theodorsen function, valid for arbitrary airfoil motions.

2. Examples of exact airloads due to transient, stable airfoil motions in two-dimensional incompressible flow are given.

3. It is shown that the solution of the unsteady aerodynamic partial differential equation for compressible flow contains a portion which is linear with respect to the transformed airfoil motions and a portion which is linear with respect to the initial conditions of these motions. The stability or flutter problem is solely dependent upon the first portion which is described by a partial differential equation formally identical to that of simple harmonic motion with the replacement of $i\omega$ by s. It is conjectured that computer programs which calculate simple harmonic airloads may be modified in a fairly straightforward manner to yield generalized airloads. The conjecture is shown to be true in two-dimensional supersonic flow and the derivation of generalized airloads for this case is given.

4. The generalized airloads are incorporated into the equations of motion and the exact locus of roots calculated, giving quantitative results regarding subcritical and supercritical flutter conditions.

5. Examples of exact airfoil responses due to command inputs are given. The responses are shown to be composed of portions due to rational and nonrational transforms. It is shown that the oscillatory motions typifying flutter phenomena are due entirely to the rational portion of the response.

6. The ability to calculate generalized aerodynamic loads allows the evaluation of approximate techniques of calculating these loads. The R.T. Jones' approximation for incompressible flow and the matrix Padé approximants of supersonic flow are shown to give accurate airloads for arbitrary motions well removed from the $i\omega$ axis.

7. It is shown that static divergence of typical sections in incompressible flow occurs due to the emergence of a real positive pole of the system transfer function. This pole occurs in addition to the original structural poles and is also predicted by Padé approximant methods if the low frequency behavior of the approximants is valid.

8. It is shown that the aerodynamic energy design technique for flutter suppression, which attempts to define flutter mode control laws valid for all possible combinations of structural parameters, has difficulty treating the typical section with a single trailing-edge control surface due to the possibility of the section being uncontrollable for some selection of parameters. Also, the technique must be extended to include control surface dynamics in order to circumvent a problem of leading-edge control surface instability.

9. A theorem is given stating the possibility of constructing a unique finite dimensional, linear model of the rational portion of the system response which does not require augmented states. The proof is constructive, giving an algorithm for the derivation of the 'rational model'.

10. Optimal regulator flutter mode control systems are designed using the rational model and the Padé model for incompressible and supersonic flow. Although the rational model represents only a portion of the total response, it is shown that perturbation feedback control based upon this model yields acceptable flutter mode control systems. It is also shown that active flutter control techniques may result in systems with divergence speeds below the actively controlled flutter speed. The behavior of such systems should always be investigated at the zero frequency condition where static divergence occurs.

B. RECOMMENDATIONS

1. Wind tunnel studies and flight tests should be performed to establish the validity of the transient responses presented herein, and to investigate the effects of the rational and nonrational portions of the response.

2. Existing computer programs which calculate simple harmonic airloads could be modified to calculate generalized airloads and the results compared with existing solutions, experimental wind tunnel, and flight data.

3. The possibility of obtaining approximating functions of generalized aerodynamic loads over a region of the s-plane should be studied. These approximations may be of the form

$$q_{ij}(s,M) = \sum_{\ell=1}^{m} f_\ell(\sigma,M)g_\ell(\omega,M)$$

and would be useful in calculating the locus of roots of the system. The merits of this exact root locus technique versus traditional U-g flutter analysis should be studied.

4. The relative merits of rational models and Padé models for the analysis and design of aeroelastic systems require continuing investigation.

5. The Laplace transform techniques used herein may be applied to the gust problem, leading to a unified theory of the control of aeroelastic systems excited by turbulence. The ability of the finite state, linear, 'rational model' of such systems to predict the main features of the total response may serve as a base for future applications such as gust alleviation and vehicle ride control.

6. The problem of estimation of the states of the rational model from measurements of the physical airfoil requires careful study since the states of the rational model do not correspond directly to physical measurements. To obtain complete correspondence, the nonrational portion

-149-

(or an estimate thereof) must be included. Hence, the operation of filters
or observers for state reconstruction based upon the rational model must
be carefully evaluated.

7. The concept of rational and nonrational portions of the airfoil
response may lead to improved estimates of flutter mode damping from
flight tests. If the nonrational portion of the response can be estimated,
subtraction of this estimate from the total response measurements would
provide estimates of the rational portion. Application of parameter
identification techniques to this portion may give improved damping
estimates.

Appendix A

EQUATIONS OF MOTION

The equations of motion of the section shown in Fig. II-1 are derived from Lagrange's equations

$$\frac{d}{dt} \frac{\partial}{\partial \dot{q}_i} (T-V) + \frac{\partial}{\partial q_i} (T-V) = Q_i \qquad (A.1)$$

where the kinetic energy is

$$T = \frac{b^3}{2} \int_{-1}^{1} z^2_\rho (x) dx .$$

The airfoil deflection for the Sect. of Fig. II-1 is

$$z_a = -h-(x-a)\alpha -(d-x)\gamma \mathcal{U}(d-x) - (x-c)\beta \mathcal{U}(x-c) . \qquad (A.2)$$

The potential energy V, is stored in springs attached at the control surface hinge lines (k_β, k_γ) and at the elastic axis (k_h, k_α).

$$V = \frac{1}{2}(k_h h^2 + k_\alpha \alpha^2 + k_\beta \beta^2 + k_\gamma \gamma^2) . \qquad (A.3)$$

Thus

$$T = \frac{1}{2}\left[mb^2\dot{h}^2 + I_\alpha \dot{\alpha}^2 + I_\beta \dot{\beta}^2 + I_\gamma \dot{\gamma}^2\right] + S_\alpha bh\ddot{\alpha}$$

$$+ S_\beta bh\ddot{\beta} + \dot{S}_\gamma bh\ddot{\gamma} + [I_\beta + S_\beta b(c-a)]\ddot{\alpha}\ddot{\beta}$$

$$+ [S_\gamma b(d-a) - I_\gamma]\ddot{\alpha}\ddot{\gamma} \qquad (A.4)$$

and the equations of motion for the section of Fig. II-1 are

$$m b \ddot{h} + S_\alpha \ddot{\alpha} + S_\beta \ddot{\beta} + S_\gamma \ddot{\gamma} + k_h h = P \tag{A.5}$$

$$S_\alpha b \ddot{h} + I_\alpha \ddot{\alpha} + [I_\beta + S_\beta b(c-a)]\ddot{\beta} + [S_\gamma b(d-a) - I_\gamma]\ddot{\gamma} + k_\alpha \alpha = M^\alpha \tag{A.6}$$

$$S_\beta b \ddot{h} + [I_\beta + S_\beta b(c-a)]\ddot{\alpha} + I_\beta \ddot{\beta} + k_\beta \beta = M^\beta \tag{A.7}$$

$$S_\gamma b \ddot{h} + [S_\gamma b(d-a) - I_\gamma]\ddot{\alpha} + I_\gamma \ddot{\gamma} + k_\gamma \ddot{\gamma} = M^\gamma . \tag{A.8}$$

In mechanizations of such typical sections in a wind tunnel or on a wing, the control surfaces are commonly controlled by electrohydraulic servos as described by Edwards [86] and Bergmann [87]. Then $k_\beta = k_\gamma = 0$ and additional terms giving the hydraulic pressure control torques would be added to (A.7) and (A.8). Edwards [86] derives the equations of such a hydraulic control system and gives the transfer function from control surface position command to control surface position as

$$\frac{\beta}{\beta_c}(s) = \frac{1}{(\tau_p s + 1)\left(\dfrac{s^2}{\omega_h^2} + \dfrac{2\zeta_h s}{\omega_h} + 1\right)} . \tag{A.9}$$

The hydraulic mode, described by ω_h and ζ_h, is typically a lightly damped mode well above the bandwidth of the servo (given by $1/\tau_p$ rad/sec).

To retain the control surface dynamics in the equations of motion without requiring attention to the servo loop dynamics, the artifice of control surface springs will be retained and viscous damping terms will be added to the control surface equations to provide stability. Also, to provide a mechanism for control surface positioning, the control surface spring constants will be multiplied by the difference between surface position and commanded surface position. Thus the terms $k_\beta \beta$ and $k_\gamma \gamma$ in (A.7) and (A.8) are replaced by $k_\beta(\beta-\beta_c) + 2I_\beta \omega_\beta \zeta_\beta \dot{\beta}$ and $k_\gamma(\gamma-\gamma_c) + 2I_\gamma \omega_\gamma \zeta_\gamma \dot{\gamma}$ respectively. The selection of $\omega_\beta = \sqrt{k_\beta / I_\beta}$, $\gamma = \sqrt{k_\gamma / I_\gamma}$, ζ_β, and ζ_γ alow the flap dynamics to approximate the hydraulic position servo loop dynamics of (A.9)

-152-

The aerodynamic loads acting on the section of Fig. II-1 may be derived from those given by Theodorsen [11] and Theodorsen and Garrick [51] for the section of Fig. A-1. This section has trailing-edge aileron and tab control surfaces which are aerodynamically unbalanced. Using a superscript bar notation to identify quantities related to the section of Fig. A-1, the coordinates of the two sections are related as

$$
\bar{\underline{x}} = \begin{bmatrix} \bar{h} \\ \bar{\alpha} \\ \bar{\beta} \\ \bar{\gamma} \end{bmatrix} = \begin{bmatrix} 1 & 0 & 0 & b(d-a) \\ 0 & 1 & 0 & -1 \\ 0 & 0 & 1 & 0 \\ 0 & 0 & 0 & 1 \end{bmatrix} \begin{bmatrix} h \\ \alpha \\ \beta \\ \gamma \end{bmatrix} = V\underline{x} \qquad (A.10)
$$

while the loads acting on the sections are related as

$$
L = \begin{bmatrix} P_b \\ M^{\alpha} \\ M^{\beta} \\ M^{\gamma} \end{bmatrix} = \begin{bmatrix} 1 & 0 & 0 & 0 \\ 0 & 1 & 0 & 0 \\ 0 & 0 & 1 & 0 \\ b(d-a) & -1 & 0 & 1 \end{bmatrix} \begin{bmatrix} \bar{P}b \\ \bar{M}^{\alpha} \\ \bar{M}^{\beta} \\ \bar{M}^{\gamma} \end{bmatrix} = V^T \bar{L} \ . \qquad (A.11)
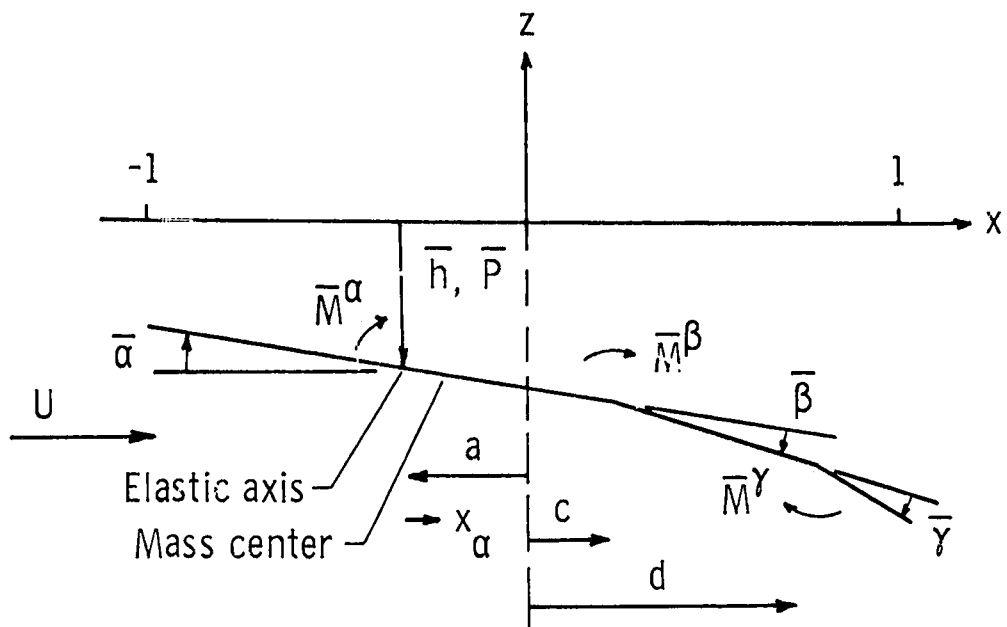$$

FIG. A-1   DIAGRAM OF A TYPICAL SECTION WITH
            AERODYNAMICALLY UNBALANCED
            AILERON AND TAB

Appendix B

UNSTEADY AERODYNAMIC LOADS FOR TWO-DIMENSIONAL

INCOMPRESSIBLE FLOW

This appendix summarizes Theodorsen's [11] derivation of the unsteady airloads as presented in Bisplinghoff [7].

The airfoil lying between $x^* = -b$ and $x^* = b$, as shown in Fig. B-1, is mapped onto the circle of radius $b/2$ by the Joukowski transformation,

$$x^* + iz^* = (X + iZ) + \frac{b^2}{4(X + iZ)} \quad . \tag{B.1}$$

The correspondence between points on the airfoil and points on the circle is $x^* = b \cos \varepsilon$, $z^* = 0$. Solution of (2.19) subject to the boundary condition, (2.13) (which is Laplace's equation in the plane) is achieved by superposition of elementary solutions of Laplace's equation. To satisfy the boundary condition, a distribution of sources is placed on the upper semicircle and a corresponding distribution of sinks is placed along the lower semicircle. The source strength distribution required is

$$H^+(x^*, t) = 2w_a^*(x^*, t) \quad . \tag{B.2}$$

This noncirculatory source-sink distribution gives the tangential velocity at the circle as

$$q_{nc_\theta}(\theta, t) = \frac{2}{\pi} \int_0^\pi \frac{w_a^* \sin^2 \phi \, d\phi}{\cos \phi - \cos \theta} \quad . \tag{B.3}$$

The noncirculatory velocity potential on the upper semicircle and the pressure difference on the airfoil are
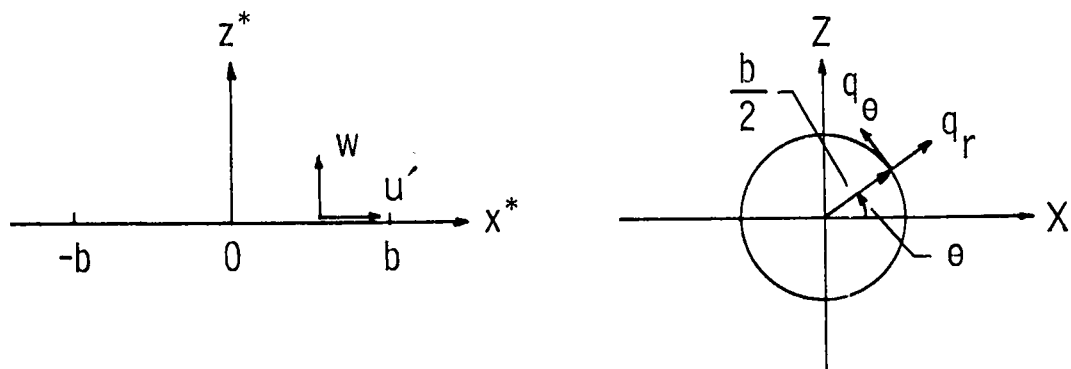
FIG. B-1   CONFORMAL TRANSFORMATION OF THE x*-z* PLANE TO THE X-Z PLANE

$$\phi_{nc}(\theta, t) \;\; = \;\; -\frac{b}{\pi} \int_0^\pi \int_0^\pi \frac{w_a^x \sin^2\phi \, d\phi \, d\theta}{\cos\phi - \cos\theta} \tag{B.4}$$

$$p_{nc}(\theta, t) \;\; = \;\; -2\rho_\infty \left[\frac{\partial\phi_{nc}}{\partial t} - \frac{U}{b \sin\theta} \frac{\partial\phi_{nc}}{\partial\theta} \right]. \tag{B.5}$$

The tangential velocity, (B.3), evaluated at the trailing-edge ($\theta = 0$) is nonzero for general airfoil motions and Kutta's condition of smooth flow off of the trailing-edge is violated.

To satisfy the Kutta condition, Theodorsen employed a bound vortex distribution over the airfoil chord, and a vortex distribution over the airfoil wake. Figure B-2 indicates the vortex flow for an isolated vortex pair in the X-Z plane. To maintain the circle as a streamline, a vortex of strength $+\Gamma_0$ at $X = b^2/4\chi$ is paired with a vortex of strength $-\Gamma_0$ at $X = \chi$.

Von Kármán and Sears [60] show that the corresponding situation in the $x^* - z^*$ plane consists of a vortex of strength $-\Gamma_0$ at $\xi = \chi + b^2/4\chi$ and a bound vortex sheet distributed over the airfoil chord of strength $\gamma(x^*, t)$.

The circulatory velocity potential on the upper semicircle due to the vortex pair Γ_0, $-\Gamma_0$ is

$$\phi_c(\theta, t) \;\; = \;\; \frac{\Gamma_0}{\pi} \tan^{-1} \sqrt{\frac{(\xi^*-b)(1+\cos\theta)}{(\xi^*+b)(1-\cos\theta)}} \tag{B.6}$$

and the corresponding pressure difference, from (B.5) is

$$p_c(\theta, t) \;\; = \;\; -\frac{\rho_\infty U \Gamma_0 [\xi^* + b \cos\theta]}{\pi b \sin\theta \sqrt{\xi^{*2} - b^2}}. \tag{B.7}$$
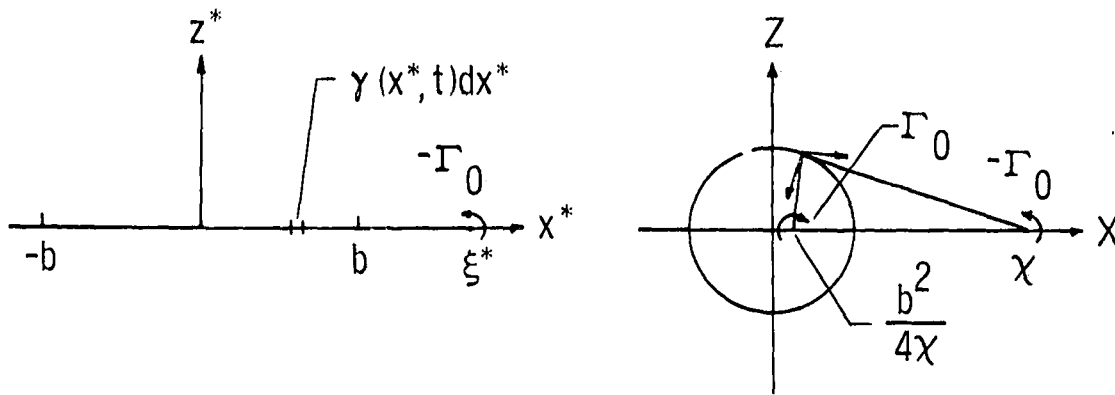
FIG. B-2   BOUND AND WAKE VORTICES IN THE x*-z* PLANE AND
THE X-Z PLANE

The tangential velocity at the circle induced by the vortex pair is

$$q_{c_\Omega}(0,t) \;=\; -\frac{\Gamma_o}{\pi b}\left[\frac{\chi^2 - \left(\frac{b}{2}\right)^2}{\chi^2 + \left(\frac{b}{2}\right)^2 - \chi b \cos 0}\right]. \qquad (B.8)$$

For arbitrary motions, there will be a distributed wake vortex sheet of strength $\gamma_w(\xi,t)$ and the effect of the shed wake is obtained by replacing Γ_o by $-\gamma_w(\xi,t)d\xi$ and integrating over the wake. For airfoil motion at uniform velocity starting at $t = 0$ the tangential velocity at the trailing-edge is

$$q_c(b,t) \;=\; \frac{1}{\pi b}\int_b^{b+Ut}\sqrt{\frac{\xi^*+b}{\xi^*-b}}\;\gamma_w(\xi^*,t)\,d\xi \qquad (B.9)$$

and the pressure difference on the airfoil is

$$p_c(\vartheta,t) \;=\; \frac{\rho U}{\pi b \sin 0}\int_b^{b+Ut}\left[\sqrt{\xi^2-b^2}\,(1-\cos\theta)+\sqrt{\frac{\xi^*+b}{\xi^*-b}}\cos 0\right]\gamma_w(\xi,t)\,d\xi^*. \qquad (B.10)$$

The velocity at the trailing-edge is given by $(B.3)$ and $(B.9)$ and the Kutta condition is enforced by requiring that this velocity be zero.

$$\frac{2}{\pi}\int_0^\pi \frac{w^*_a\sin^2\phi\,d\phi}{\cos\phi - 1} \;+\; \frac{1}{\pi b}\int_b^{b+Ut}\sqrt{\frac{\xi^*+b}{\xi^*-b}}\;\gamma_w(\xi^*,t)\,d\xi^* \;=\; 0. \qquad (B.11)$$

Equation $(B.11)$ relates the known downwash, w_a, to the unknown wake vortex strength $\gamma_w(\xi^*,t)$. The first integral in $(B.11)$ may be evaluated if w_a is specified. Theodorsen defined one-half this integral as

$$Q = \frac{1}{\pi}\int_0^\pi \frac{w_a^x \sin^2\phi\, d\phi}{\cos\phi - 1} \qquad (B.12)$$

giving

$$Q = U\bar{\alpha} + \dot{h}b + b(\tfrac{1}{2} - a)\dot{\bar{\alpha}}$$

$$+ \frac{U}{\pi} T_{10}\bar{\beta} + \frac{b}{2\pi} T_{11}\dot{\bar{\beta}} + \frac{U}{\pi} T_{10}(d)\bar{\gamma} + \frac{b}{2\pi} T_{11}(d)\dot{\bar{\gamma}} \qquad (B.13)$$

for the section of Fig. A-1, and

$$Q = U\alpha + \dot{h}b + b(\tfrac{1}{2}-a)\dot{\alpha}$$

$$+ \frac{U}{\pi} T_{10}\beta - \frac{b}{2\pi} T_{11}\dot{\beta} + \frac{U}{\pi}(T_{10}(d)-\pi)\gamma$$

$$+ \frac{b}{2\pi}(T_{11}(d) - \pi(1 - 2c))\dot{\gamma} \qquad (B.14)$$

for the section of Fig. II-1. The T-functions were evaluated by Theodorsen [11] and Theodorsen and Garrick [51] and are tabulated in App. C. Thus the Kutta condition, (B.11), may be written as

$$Q = -\frac{1}{2\pi b}\int_b^{x_o^*} \sqrt{\frac{\xi^*+b}{\xi^*-b}}\, \gamma_w(\xi^*,t)\,d\xi^* . \qquad (B.15)$$

Integrating the pressure difference (B.10) over the chord, the circulatory lift and pitching moment are

$$P_c = \rho U \int_b^{x_o^*} \frac{\xi^*}{\sqrt{\xi^{*2} - b^2}}\, \gamma_w(\xi^*,t)\,d\xi^* \qquad (B.16)$$

$$M_c^\alpha = \rho U b \int_b^{x_o^*}\left[\frac{1}{2}\sqrt{\frac{\xi^*+1}{\xi^*-1}} - (a+\tfrac{1}{2})\frac{\xi^*}{\sqrt{\xi^{*2}-b^2}}\right]\gamma_w(\xi^*,t)\,d\xi^* . \qquad (B.17)$$

Equations (B.15) and (B.17) show that the circulatory loads are related to the wake vortex strength by the two integral expressions

$$
I_1 = \int_b^{x^*_o} \sqrt{\frac{\xi^*+b}{\xi^*-b}}\ \gamma_w(\xi^*, t)\, d\xi^* \tag{B.18}
$$

and

$$
I_2 = \int_b^{x^*_o} \frac{\xi^*}{\sqrt{\xi^{*2}-b^2}}\ \gamma_w(\xi^*, t)\, d\xi^* . \tag{B.19}
$$

(The hinge moments M^β and M^γ may be expressed in terms of I_1 and I_2 also.) Theodorsen noted that if it were assumed that the airfoil had undergone simple harmonic oscillations for an indefinitely long period then

$$
w^*_a(x^*, t) = \bar{w}^*_a(x^*) e^{i\omega t} \tag{B.20}
$$

and

$$
\gamma_w(x^*, t) = \bar{\gamma}_w e^{i\omega(t-\xi^*/U)} = \bar{\gamma}_w e^{i(k\sigma-k\xi)} \tag{B.21}
$$

since the wake is assumed to drift downstream at the freestream velocity as shown in Fig. B-3. The reduced frequency, $k = \omega b/U$ introduced in (B.21) serves to indicate the relative 'unsteadiness' of the flow. The unknown wake vortex strength $\bar{\gamma}_w$ may now be factored out of the integrals and (B.15) to (B.17) become

$$
\bar{\gamma}_w = -\frac{2\pi Q}{e^{ik\sigma} \int_1^\infty \sqrt{\frac{\xi+1}{\xi-1}}\ e^{-ik\xi}\, d\xi} . \tag{B.22}
$$
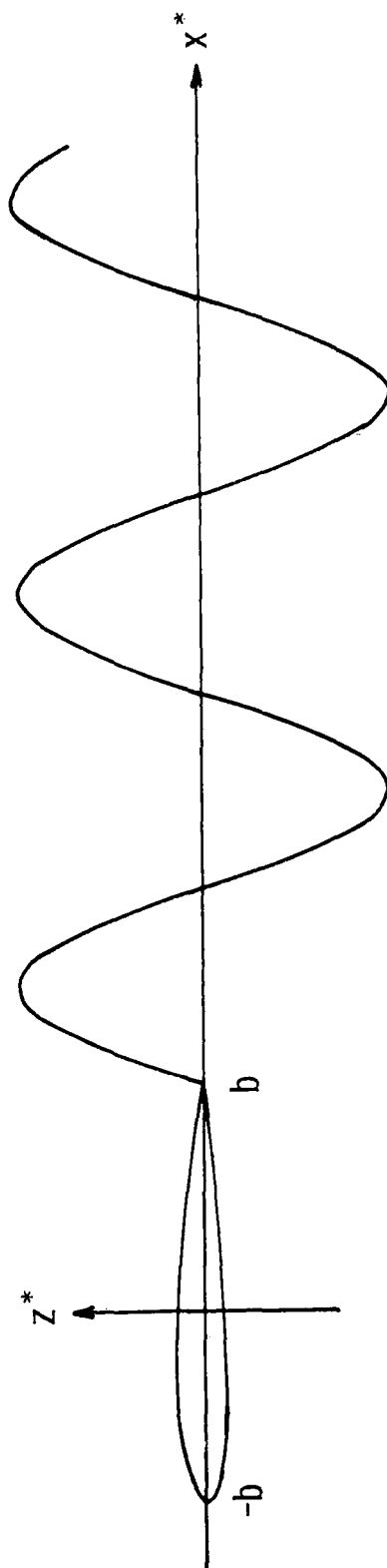
FIG. B-3   WAKE VORTEX STRENGTH FOR SIMPLE HARMONIC OSCILLATIONS OF
THE AIRFOIL

$$P_c = -2\pi \rho b U Q \frac{\displaystyle\int_1^\infty \frac{\xi \, e^{-ik\xi}}{\sqrt{\xi^2-1}} \, d\xi}{\displaystyle\int_1^\infty \sqrt{\frac{\xi+1}{\xi-1}} \, e^{-ik\xi} \, d\xi} \tag{B.23}$$

$$M_c^\alpha = -2\pi \rho b^2 U Q \left[\frac{1}{2} - (a+\tfrac{1}{2}) \frac{\displaystyle\int_1^\infty \sqrt{\frac{\xi}{\xi^2-1}} \, e^{-ik\xi} \, d\xi}{\displaystyle\int_1^\infty \sqrt{\frac{\xi+1}{\xi-1}} \, e^{-ik\xi} \, d\xi} \right] \tag{B.24}$$

where $\xi = \xi*/b$ and $\sigma = Ut/b$ are nondimensionalized distance and time, respectively.

The integrals may be identified as modified Bessel functions of the third kind, $K_\nu(s)$, [Ref. 57, p. 22] from the integral definition [Ref. 58, Eq. 9.6.23]

$$K_\nu(s) = \frac{\Gamma(\tfrac{1}{2})(\tfrac{s}{2})^\nu}{\Gamma(\nu+\tfrac{1}{2})} \int_1^\infty e^{-st}(t^2-1)^{\nu-\frac{1}{2}} dt; \qquad \begin{array}{l} \mathrm{Re}(\nu) > -\tfrac{1}{2}, \\ \mathrm{Re}(s) > 0, \end{array} \tag{B.25}$$

where $\Gamma(s)$ if the Gamma function [57]. For $\nu = 0$

$$K_0(s) = \int_1^\infty \frac{e^{-st}}{\sqrt{t^2-1}} \, dt \tag{B.26}$$

and since $K_1(s) = -K_0'(s)$

$$K_1(s) \;=\; \int_1^\infty \sqrt{\frac{t e^{-st}}{t^2-1}}\; dt \; . \qquad (B.27)$$

Therefore

$$K_0(s) + K_1(s) \;=\; \int_1^\infty \sqrt{\frac{t+1}{t-1}}\; e^{-st} dt \qquad (B.28)$$

and the ratio of integrals in (B.23) and (B.24), defined as the Theodorsen function $C(ik)$, is

$$C(ik) \;=\; \frac{K_1(ik)}{K_1(ik) + K_0(ik)} \;=\; \frac{H_1^{(2)}(k)}{H_1^{(2)}(k) + i H_0^{(2)}(k)} \; . \qquad (B.29)$$

The Hankel functions are given by $K_0(ik) = -\pi/2 \; i H_0^{(2)}(k)$ and $K_1(ik) = (-\pi/2)\, H_1^{(2)}(k)$ [Ref. 58, Eq. 9.6.4]. Theodorsen [11] did not mention the violation of the condition $Re(s)$ strictly greater than zero, in the application of (B.26) to (B.23) and (B.24).

The loads acting on the airfoil may be calculated from (B.5), (B.14), (B.23), (B.24), and (B.29) and from similar equations for the hinge moments. The integrals required were evaluated by Theodorsen [11] and Theodorsen and Garrick [51] and are tabulated in App. C. For the wing-aileron-tab section of Fig. A-1, the loads may be written as

$$\bar{L} \;=\; \bar{L}_c + \rho b^4 \bar{M}_{nc} \ddot{\bar{x}} + \rho b^3 U \bar{B}_{nc} \dot{\bar{x}} + \rho b^2 U^2 \bar{K}_{nc} \bar{x} \qquad (B.30)$$

where the matrices giving the 'noncirculatory' loads are

$$\bar{M}_{nc} = \begin{bmatrix} -\pi & \pi a & T_1 & T_1(d) \\ \pi a & -\pi(\frac{1}{8}+a^2) & -2T_{13} & -2T_{13}(d) \\ T_1 & -2T_{13} & \frac{1}{\pi}T_3 & \frac{1}{\pi}Y_6 \\ T_1(d) & -2T_{13}(d) & \frac{1}{\pi}Y_6 & \frac{1}{\pi}T_3(d) \end{bmatrix}$$

$$\bar{B}_{nc} = \begin{bmatrix} 0 & -\pi & -T_4 & T_4(d) \\ 0 & \pi(a-\frac{1}{2}) & -T_{16} & -T_{16}(d) \\ 0 & -T_{17} & -\frac{1}{\pi}T_{19} & -\frac{1}{\pi}Y_{18} \\ 0 & -T_{17}(d) & -\frac{1}{\pi}Y_{10} & -\frac{1}{\pi}T_{19}(d) \end{bmatrix}$$

$$\bar{K}_{nc} = \begin{bmatrix} 0 & 0 & 0 & 0 \\ 0 & 0 & -T_{15} & -T_{15}(d) \\ 0 & 0 & -\frac{1}{\pi}T_{18} & -\frac{1}{\pi}Y_{17} \\ 0 & 0 & -\frac{1}{\pi}Y_9 & -\frac{1}{\pi}T_{18}(d) \end{bmatrix}$$

and the 'circulatory' loads are given by

$$\bar{L}_c = \rho b^2 UC(ik)RQ \qquad (B.31)$$

where

$$R = \begin{bmatrix} -2\pi \\ 2\pi(a+\tfrac{1}{2}) \\ -T_{12} \\ -T_{12}(d) \end{bmatrix} .$$

The factor Q, (B.13), may be written

$$Q = US_1 \bar{\underline{x}} + bS_2 \dot{\underline{x}} \tag{B.32}$$

where

$$S_1 = \left[0, \quad 1, \quad \tfrac{1}{\pi} T_{10}, \quad \tfrac{1}{\pi} T_{10}(d) \right]$$

$$S_2 = \left[1, \quad (\tfrac{1}{2}-a), \quad \tfrac{1}{2\pi} T_{11}, \quad \tfrac{1}{2\pi} T_{11}(d) \right] .$$

The loads for the section with leading- and trailing-edge control surfaces (Fig. II-1) may be obtained from (B.30) and (B.31) using (A.17) and A.18). They are

$$L = L_c + \rho b^4 M_{nc} \ddot{\underline{x}} + \rho b^3 U B_{nc} \dot{\underline{x}} + \rho b^2 U^2 K_{nc} \underline{x} \tag{B.33}$$

where

$$M_{nc} = V^T \bar{M}_{nc} V$$

$$B_{nc} = V^T \bar{B}_{nc} V$$

$$K_{nc} = V^T \bar{K}_{nc} V$$

and

$$L_c = \rho b^2 UC(ik) V^T R [S_1 V x + S_2 V \dot{x}] . \tag{B.34}$$

It should be noted that not all factors comprising the circulatory loads are multiplied by $C(ik)$. This results in certain cancellations

of terms between the circulatory and noncirculatory loads and the subscripts in (B.30) and (B.33) are only descriptive.

Appendix C

UNSTEADY AERODYNAMIC LOADS IN TWO-DIMENSIONAL
INCOMPRESSIBLE FLOW

The aerodynamic loads acting on the section of Fig. A-1 were calculated by Theodorsen [11], and Theodorsen and Garrick [51] and involve the following expressions.

$$T_1 = \frac{1}{3}(2+c^2)\sqrt{1-c^2} + c\cos^{-1}c$$

$$T_3 = -\frac{1}{8}(1-c^2)(5c^2+4) + \frac{1}{4}c(7+2c^2)\sqrt{1-c^2}\cos^{-1}c$$

$$T_4 = c\sqrt{1-c^2} - \cos^{-1}c$$

$$T_7 = -\frac{1}{8}c(7+2c^2)\sqrt{1-c^2} - (\frac{1}{8}+c^2)\cos^{-1}c$$

$$T_8 = -\frac{1}{3}(1+2c^2)\sqrt{1-c^2} + c\cos^{-1}c$$

$$T_9 = \frac{1}{2}\left[\frac{1}{3}(1-c^2)^{3/2} + aT_4\right]$$

$$T_{10} = \sqrt{1-c^2} + \cos^{-1}c$$

$$T_{11} = (2-c)\sqrt{1-c^2} + (1-2c)\cos^{-1}c$$

$$T_{13} = -\frac{1}{2}(T_7 + (c-a)T_1)$$

$$T_{15} = T_4 + T_{10}$$

$$T_{16} = T_1 - T_8 - (c-a)T_4 + \frac{1}{2}T_{11}$$

$$T_{17} = -2T_9 - T_1 + (a - \frac{1}{2})T_4$$

$$T_{18} \qquad T_5 - T_4 T_{10}$$

$$T_{19} \qquad - \frac{1}{2} T_4 T_{11}$$

$$Y_1(c,d) \;=\; - \sqrt{1-c^2}\, \sqrt{1-d^2} - \cos^{-1}c\, \cos^{-1}d + d\sqrt{1-d^2}\, \cos^{-1}c$$
$$+ \sqrt{1-c^2}\, \cos^{-1}d - (d-c)^2 \log N(c,d)$$

$$Y_2(c,d) \;=\; 2\sqrt{1-d^2}\, \cos^{-1}c - 2(d-c)\log N(c,d)$$

$$Y_3(c,d) \;=\; \frac{1}{3}(c+2d)\sqrt{1-c^2}\, \sqrt{1-d^2} + d\,\cos^{-1}c\, \cos^{-1}d - \frac{1}{3}(2+d^2)\sqrt{1-d^2}\, \cos^{-1}c$$
$$- \frac{1}{3}(1+3cd-c^2)\sqrt{1-c^2}\, \cos^{-1}d + \frac{1}{3}(d-c)^3 \log N(c,d)$$

$$Y_4(c,d) \;=\; Y_3(d,c)$$

$$Y_6(c,d) \;=\; - \frac{1}{2}\sqrt{1-c^2}\, \sqrt{1-d^2}\left(1+\frac{1}{6}c^2+\frac{1}{6}d^2+\frac{11}{12}cd\right) - \left(\frac{1}{8}+cd\right)\cos^{-1}c\, \cos^{-1}d$$
$$+ \frac{1}{3}\left[\frac{d}{4}\left(\frac{5}{2} - d^2\right) + c(2+d^2)\right] \sqrt{1-d^2}\, \cos^{-1}c$$
$$+ \frac{1}{3}\left[\frac{c}{4}\left(\frac{5}{2} - c^2\right) + d(2+c^2)\right] \sqrt{1-c^2}\, \cos^{-1}d + \frac{(d-c)^4}{12} \log N(c,d)$$

$$Y_9(c,d) \;=\; Y_1 - T_4(c)T_{10}(d)$$

$$Y_{10}(c,d) \;=\; Y_3 - Y_4 - \frac{1}{2}T_4(c)T_{11}(d)$$

$$Y_{17}(c,d) \;=\; Y_1 - T_4(d)T_{10}(c)$$

$$Y_{18}(c,d) \;=\; Y_4 - Y_3 - \frac{1}{2}T_4(d)T_{11}(c)$$

$$Y_{19}(c,d) \;=\; Y_2 - 2\sqrt{1-d^2}\, T_{10}$$

$$N(c,d) \;=\; \left| \frac{1-cd - \sqrt{1-c^2}\,\sqrt{1-d^2}}{d-c} \right| .$$

ALTERNATIVE DERIVATIONS OF THE GENERALIZED
THEODORSEN FUNCTION

1. W.P. Jones [20], using the concepts of bound and free vorticity, was able to show that the functions involved in Theodorsen's problem satisfied the modified Bessel equation. He thus avoided the restriction, $Re(s) > 0$, involved in the integral representations of the Bessel functions and derived the generalized Theodorsen function

$$C(s) = \frac{K_1(\bar{s})}{K_0(\bar{s}) + K_1(\bar{s})} \,. \qquad (D.1)$$

In attempting to compare this form of $C(\bar{s})$ with that given by Theodorsen, Jones used the relation

$$K_\nu(s) = \frac{\pi}{2} i^{\nu+1} H_\nu^{(1)}(i\bar{s}) \qquad (D.2)$$

without regard to the restriction $-\pi < \arg \bar{s} \leq \frac{1}{2}\pi$. As a result, $C(s)$ was evaluated using different branches of the functions $H_0^{(2)}(s)$ and $H_0^{(2)}(\bar{s})$ in the first and second quadrants of the s-plane and Jones concluded, incorrectly, that $C(\bar{s})$ was discontinuous across the $i\omega$ axis.

2. The convolution integral may be used to verify that the generalized Theodorsen function is indeed the correct operator relating the downwash, $w(s)$, to the induced airloads for stable airfoil motions. The lift due to circulation is given by

$$P(s) = 2\pi\rho bUC(\bar{s})w(s) \qquad (D.3)$$

for some operator, $C(\bar{s})$. For the assumed form of (2.33),

$$C(s) \;=\; \frac{K_1(\bar{s})}{K_0(\bar{s}) + K_1(\bar{s})}$$

and the particular damped airfoil motion

$$w(t') \;=\; w_0 e^{-\bar{\sigma}t'} \cos \bar{\omega}t' \;=\; \mathrm{Re}\!\left[w_0 e^{(-\bar{\sigma}+i\bar{\omega})t'}\right]; \quad \sigma > 0 \quad (\mathrm{D}.4)$$

the inverse Laplace transform of $P(s)$ is

$$\frac{P(t')}{2\pi\rho b U} \;=\; \frac{1}{2\pi i} \int_{\sigma_1 - i\infty}^{\sigma_1 + i\infty} C(\bar{s})w(s)e^{\bar{s}t'}d\bar{s} \;. \qquad (\mathrm{D}.5)$$

The transform $w(s)$ is given by the real part of

$$w(s) \;=\; w_0 \left[\frac{(\bar{s}+\bar{\sigma}) + i\bar{\omega}}{(s+\sigma)^2 + \omega^2}\right] . \qquad (\mathrm{D}.6)$$

Since $\bar{\sigma} > 0$, σ_1 may be set equal to zero and with the substitution $\bar{s} = ik$

$$\frac{P(t')}{2\pi\rho b U} \;=\; \frac{w_0}{2\pi} \int_{-\infty}^{\infty} C(k)\, \frac{(ik+\bar{\sigma}) + i\bar{\omega}}{(ik+\bar{\sigma})^2 + \bar{\omega}^2}\, e^{ikt'}dk. \qquad (\mathrm{D}.7)$$

The symbol under the integral implies that the path of integration must pass below the branch point at the origin. Garrick [70] showed that the lift could be calculated for arbitrary motions using the convolution integral

$$\frac{P(t')}{2\pi\rho bU} = w(0)k_1(t') + \int_0^{t'} k_1(t_1') \frac{dw(t'-t_1')}{dt'} dt_1' . \qquad (D.8)$$

Also, $k_1(t')$ and $C(k)/k$ are related [70] by

$$k_1(t') = \frac{1}{2\pi i} \int_{-\infty}^{\infty} \frac{C(k)}{k} e^{ikt'} dt' \qquad (D.9)$$

where the fact that $k_1(t') = 0$ for $t' < 0$ has been used. Substituting the expressions given by (D.6) and (D.9) into (D.8) yields

$$\frac{P(t')}{2\pi\rho bU} = \frac{w_o}{2\pi i} \left\{ \int_{-\infty}^{\infty} \frac{C(k)}{k} e^{ikt'} dt' \right.$$

$$\qquad (D.10)$$

$$+ (-\bar{\sigma}+i\bar{\omega}) e^{(-\bar{\sigma}+i\bar{\omega})t'} \int_0^{t'}$$

$$\times \left. \left[\int_{-\infty}^{\infty} \frac{C(k)}{k} e^{ikt_1'} dk \right] e^{-(-\bar{\sigma}+i\bar{\omega})t_1'} dt_1' \right\} .$$

The expression in brackets inside the last integral represents $k_1(t')$ which is zero for $t' < 0$ and the integrals may be interchanged, giving

$$\int_{-\infty}^{\infty} \int_{-\infty}^{t'} \frac{C(k)}{k} e^{-(-\bar{\sigma}+i\bar{\omega}-ik)t_1'} dt_1' dk = - \int_{-\infty}^{\infty} \frac{C(k)}{k} \frac{e^{-(-\bar{\sigma}+i\bar{\omega}-ik)\sigma}}{(-\bar{\sigma}+i\bar{\omega}-ik)} dk .$$

Then (D.10) is

$$\frac{P(t')}{2\pi\rho bU} = \frac{w_o}{2\pi i} \int_{-\infty}^{\infty} \frac{C(k)}{k} e^{ikt'} \left[1 + \frac{-\bar{\sigma}+i\bar{\omega}}{(ik+\bar{\sigma})-i\bar{\omega}} \right] dk$$

$$(D.11)$$

$$= \frac{w_o}{2\pi} \int_{-\infty}^{\infty} C(k) e^{ikt'} \left[\frac{(ik+\bar{\sigma})+i\bar{\omega}}{(ik+\bar{\sigma})^2+\bar{\omega}^2} \right] dk \quad .$$

The expression for the lift given by $(D.7)$ and $(D.11)$ are identical, verifying the choice of (2.33) as the operator relating $w(s)$ to $P(s)$.

Appendix E

DISCUSSION OF THE GENERALIZED THEODORSEN FUNCTION AND
UNSTEADY AERODYNAMICS FOR ARBITRARY MOTIONS

The study of unsteady airloads due to transient motions was pioneered by Wagner [8] who calculated the lift on an airfoil started impulsively from rest. The resulting lift function $k_1(t')$ is known as Wagner's function and has not been successfully evaluated in terms of elementary functions. Due to the linearity of the governing partial differential equations, it was recognized that superposition of elementary solutions could be used to calculate unsteady airloads for arbitrary motions. Garrick [70] used the convolution integral to write the lift due to motion $w(t')$ as

$$\frac{P(t')}{2\pi\rho bU} = w(0)k_1(t') + \int_0^{t'} k_1(t'-t_1') \frac{dw(t_1')}{dt_1'} dt_1' . \qquad (E.1)$$

Garrick [70] also showed that $k_1(t')$ and $C(ik)/k$ were a Fourier transform pair,

$$C(ik) = ik \int_0^\infty k_1(t')e^{-ikt'} dt' \qquad (E.2)$$

$$k_1(t') = \frac{1}{2\pi i} \int_{-\infty}^\infty \frac{C(ik)}{k} e^{ikt'} dk . \qquad (E.3)$$

In (E.2) the fact that $k_1(t') = 0$ for $t' < 0$ has been used and the path of integration in (E.3) must pass below the singularity of the integrand at $k = 0$.

The application of Laplace transform techniques to unsteady aero-dynamic integral equations was suggested by R.T. Jones [29] and Sears [56] used the technique to obtain new solutions to Wagner's problem (indicial lift due to impulsive plunging), Kussner's problem (indicial lift, $k_2(t')$, due to penetration of a sharp-edged gust), and the oscillating airfoil problem. Sears' presentation is essentially a derivation of the generalized Theodorsen function although this aspect is not discussed in Ref. 56 and was apparently not pursued.

It is interesting to note that the early references in the field do not mention the restrictions on the existence of the integrals upon which the theory is based. Söhngen [88] was apparently the first to recognize the effect of the branch cut of $C(\bar{s})$ upon the loads. He noted that diverging airfoil motions led to airloads which behaved asymptotically as $e^{\bar{s}t'}$ while converging airfoil motions led to asymptotic loads proportional to $1/t'$. These correspond to the rational and nonrational portions identified in the text. This difference was bothersome and it appeared to correlate with the restriction upon the existence of the integrals in question (viz., $\mathrm{Re}(\bar{s}) > 0$), leading to the conclusion that $C(\bar{s})$ could not be extended into the left half-plane.

The first attempt to evaluate the Theodorsen function for complex values of k was by W.P. Jones [20] who concluded, incorrectly, that $C(\bar{s})$ was discontinuous across the imaginary axis. Thus, he concluded that C(ik) could be generalized for divergent oscillations (Fig. II-3a) but was invalid for convergent oscillations (Fig. II-3b). This reasoning was reinforced by the fact that Theodorsen had been forced to assume an explicit form for the airfoil motion and wake vortex distribution (B.20, B.21) in order to obtain a solution. This fact may be the source of the confusion wherein the Theodorsen function is interpreted as a time domain operator rather than a frequency domain operator (e.g., Ref. 22).

During this period, calculations were made of unsteady loads using the convolution integral (E.1) with the indicial function approximated by sums of exponential time factors as shown by R.T. Jones [29], [9]. The exponential approximations were capable of being evaluated for

C-3

arbitrary motion, and Goland and Luke [30] published root loci of aero-
elastic modes. The Laplace transform of the exponential approximation
to $k_1(t')$ can be interpreted as an ad hoc generalized Theodorsen function
and comparisons of numerical calculations [25] using such functions and
the exact tabulated $k_1(t')$ function led Luke and Dengler [21] to the
conclusion that $C(ik)$ could be extended to the entire s-plane. However,
their argument, based upon analytic continuation, did not seem convincing
in light of the above discussion and it was rejected in a series of
articles [22], [23], [24], [25], and [26]. At the heart of the discussion
was the requirement in Theodorsen's derivation of assuming an explicit
form of airfoil motion and wake vortex distribution (i.e., oscillatory
divergent and infinite extent) in order to evaluate the resulting inte-
grals. It seemed contrary to reason to claim that the resulting function
$C(ik)$ was valid for damped motions when the derivation of the function
required just the opposite assumption. Of course, the assumption of an
explicit motion is not required and the derivation of the generalized
Theodorsen function using Laplace transform techniques is given in the
text.

It would appear that the difficulties with the generalized Theodorsen
function influenced the subsequent development of compressible finite-wing
aerodynamic load calculations. These techniques [15], [17], [62] and [89]
invariably begin with the assumption of simple harmonic oscillations,
although the text shows that this assumption is not necessary. It must
be recognized that oscillatory loads are entirely adequate for the estab-
lishment of flutter boundaries and, until the advent of active aeroelastic
control schemes, there was little requirement for loads due to arbitrary
motions.

Morino [36] has derived a new formulation of the unsteady aerodynamic
loading problem based upon the Green function solution and claims that
this formulation is the only technique capable of analyzing loads due
to arbitrary motions. Presumably this claim is based upon the fact that
Morino's theory analyzes finite thickness wings and does not encounter
the singularities inherent in flat plate theories. However, the text
of this thesis shows that these singularities do not restrict consideration
to oscillatory motions and Morino's claim is false.

-177-

Appendix F

SERIES EXPANSIONS OF BESSEL FUNCTIONS

The following series expansions are given in Ch. 9 of Abramowitz and Stegun [58].

1. Ascending power series

$$J_n(s) = \left(\tfrac{1}{2}s\right)^n \sum_{k=0}^{\infty} \frac{\left(-\tfrac{1}{4}s^2\right)^k}{k!\,\Gamma(n+k+1)} \tag{F.1}$$

$$I_n(s) = \left(\tfrac{1}{2}s\right)^n \sum_{k=0}^{\infty} \frac{\left(\tfrac{1}{4}s^2\right)^k}{k!\,\Gamma(n+k+1)} \tag{F.2}$$

$$K_n(s) = \tfrac{1}{2}\left(\tfrac{1}{2}s\right)^{-n} \sum_{k=0}^{n-1} \frac{(n-k-1)!}{k!} \left(-\tfrac{1}{4}s^2\right)^k \tag{F.3}$$

$$+ (-1)^{n+1} \ln\left(\tfrac{1}{2}s\right) I_n(s)$$

$$+ (-1)^n \tfrac{1}{2}\left(\tfrac{1}{2}s\right)^n \sum_{k=0}^{\infty} \left\{\psi(k+1)+\psi(n+k+1)\right\} \frac{\left(\tfrac{1}{4}s^2\right)^k}{k!\,(n+k)!}$$

where

$$\Gamma(n+1) = n!$$

$$\psi(1) = -\gamma_e$$

$$\psi(n) = -\gamma_e + \sum_{k=1}^{n-1} k^{-1}, \qquad n \geq 2$$

$$\gamma_c = 0.5772156649 \ldots \quad .$$

-179-

2. Asymptotic expansions:

$$I_n(s) \sim \frac{e^s}{\sqrt{2\pi s}}\left\{1 - \frac{4n^2-1}{8s} + \frac{(4n^2-1)(4n^2-9)}{2!(8s)} - \frac{(4n^2-1)(4n^2-9)(4n^2-25)}{3!(8s)}\right.$$

$$\left. + \cdots \right\} , \qquad |\arg s| < \frac{\pi}{2} ; \qquad (F.4)$$

$$K_n(s) \sim \sqrt{\frac{\pi}{2s}}\, e^{-s}\left\{1 + \frac{4n^2-1}{8s} + \frac{(4n^2-9)(4n^2-1)}{2!(8s)} + \frac{(4n^2-1)(4n^2-9)(4n^2-25)}{3!(2s)}\right.$$

$$\left. + \cdots \right\} , \qquad |\arg s| < \frac{3}{2}\pi . \qquad (F.5)$$

REFERENCES

1. "Aircraft Load Alleviation and Mode Stabilization," AFFDL-TR-68-158, Air Force Flight Dynamics Lab., Wright-Paterson Air Force Base, Ohio, Dec. 1968.

2. "B-52 CCV Control System Synthesis," AFFDL-TR-74-92, Vol. II, Air Force Flight Dynamics Lab., Wright-Patterson Air Force Base, Ohio, Jan. 1975.

3. Grosser, W.F., W.W. Hollenbeck, and D.C. Eckholdt, "The C-5A Active Lift Distribution Control System," Impact of Active Control Technology on Airplane Design, AGARD-CP-157, June, 1975.

4. Roger, K.L., G.E. Hodges, and L. Felt, "Active Flutter Suppression-- A Flight Test Demonstration," J. of Aircraft, Jun. 1975, pp. 551-556.

5. Sandford, M.C., I. Abel, and D.L. Grey, "Development and Demonstration of a Flutter-Suppression System Using Active Controls," NASA TR R-450, Dec. 1975.

6. Przemieniecki, J.S., Theory of Matrix Structural Analysis, McGraw-Hill, 1968.

7. Bisplinghoff, R.L., H. Ashley, and R.L. Halfman, Aeroelasticity, Addison-Wesley, Mass., 1955.

8. Wagner, H., "Uber die Entshehung des Dynamischen Auftriebs von Tragflügeln," Z. Angew. Math. U. Mech., Bd. 5, Heft 1, Feb. 1925, pp. 17-35.

9. Jones, R.T., "The Unsteady Lift of a Wing of Finite Aspect Ratio," NACA Rept. 681, 1940.

10. Lomax, H., M.A. Heaslet, F.B. Fuller, and L. Sluder, "Two-and-Three-Dimensional Unsteady Lift Problems in High-Speed Flight," NACA Rept. 1077, 1952.

11. Theodorsen, T., "General Theory of Aerodynamic Instability and the Mechanism of Flutter," NACA Rept. No. 496, 1935.

12. Timman, R., and A.I. Van de Vooren, "Theory of the Oscillating Wing with Aerodynamically Balanced Control Surface in a Two-Dimensional, Subsonic, Compressible Flow," National Luchtvaartlaboratorium, Amsterdam, Rept. No. F. 54, 1949.

13. Garrick, I.E., and S.I. Rubinow, "Flutter and Oscillating Airforce Calculations for an Airfoil in Two-Dimensional Supersonic Flow," NACA Rept. No. 846, 1946.

14. Possio, C., "L'Azione aerodinamica sul profilo oscillante alle velocità ultrasonore," *Acta, Pont. Acad. Sci.*, Vol. I, No. 11, 1937, pp. 93-106.

15. Watkins, C.E., D.S. Woolston, and H.J. Cunningham, "A Systematic Kernel Function Procedure for Determining Aerodynamis Forces On Oscillating or Steady Finite Wings at Subsonic Speeds," NASA TR-48, 1959.

16. Rowe, W.S., B.A. Winther, and M.C. Redman, "Unsteady Subsonic Aerodynamic Loadings Caused by Control Surface Motions," *J. of Aircraft*, Jan. 1974, pp. 45-53.

17. Albano, E., and W.P. Rodden, "A Doublet-Lattice Method for Calculating Lift Distributions on Oscillating Surfaces in Subsonic Flows, *AIAA J.*, Vol. 7, No. 2, Feb. 1969, pp. 279-285.

18. Theodorsen, T., and I.E. Garrick, "Mechanism of Flutter, a Theoretical and Experimental Investigation of the Flutter Problem," NACA Rept. No. 685, 1940.

19. Smilg, B., and L.S. Wasserman, "Application of Three-Dimensional Flutter Theory to Aircraft Structures," Air Force Tech Rept. 4798, 1942.

20. Jones, W.P., "Aerodynamic Forces on Wings in Non-Uniform Motion," R. & M. No. 2117, *British A.R.C.*, Aug. 1945.

21. Luke, Y., and M.A. Dengler, "Tables of the Theodorsen Circulation Function for Generalized Motion," *J. Aero. Sci.*, Jul. 1951, pp. 478-483.

22. Van de Vooren, A.I., "Generalization of the Theodorsen Function to Stable Oscillations," *J. Aero. Sci.*, Mar. 1952, pp. 209-211.

23. Laitone, E.V., "Theodorsen's Circulation Function for Generalized Motion," *J. Aero. Sci.*, Mar. 1952, pp. 211-213.

24. Jones, W.P., "The Generalized Theodorsen Function," *J. Aero. Sci.*, Mar. 1952, p. 213.

25. Dengler, M.A., M. Goland, and Y.L. Luke, "Notes on the Calculation of the Response of Stable Aerodynamic Systems," *J. Aero. Sci.*, Mar. 1952, pp. 213-214.

26. Chang, C., "On Theodorsen Function in Incompressible Flow and C-Function in Supersonic Flow," *J. Aero. Sci.*, Oct. 1952, pp. 717-718.

27. Richardson, J.R., "A More Realistic Method for Routine Flutter Cal-
culations," Sym. on Structural Dynamics and Aeroelasticity, Boston,
Mass., Sept. 1965.

28. Hassig, H.J., "An Approximate True Damping Solution of the Flutter
Equation by Determinant Iteration," J. of Aircraft, Vol. 8, No. 11,
Nov. 1971, pp. 885-890.

29. Jones, R.T., "Operational Treatment of the Nonuniform Lift Theory
to Airplane Dynamics," NACA TN 667, 1938.

30. Goland, M., and Y.L. Luke, "A Study of the Bending-Torsion Aero-
elastic Modes for Aircraft Wings," J. Aero. Sci., Vol. 16, No. 7,
Jul. 1949, pp. 389-396.

31. Baird, E.F., and H.J. Kelley, "Formulation of the Flutter Problem
for Solution on an Electronic Analog Computer," J. of Aero Sci.,
Mar. 1950, pp. 189-190.

32. Dugundji, J., "A Nyquist Approach to Flutter," J. of Aero. Sci.,
Jun. 1952, pp. 422-423.

33. Vepa, R., "Finite State Modeling of Aeroelastic Systems," Ph.D.
Dissertation, Dept. of Applied Mechanics, Stanford University,
Stanford, Ca., 94305, Jun 1975.

34. Vepa, R., "On the Use of Padé Approximants to Represent Unsteady
Aerodynamic Loads for Arbitrarily Small Motions of Wings," AIAA
paper No. 76-17, 1976.

35. Morino, L., "A General Theory of Unsteady Compressible Potential
Aerodynamics," NASA CR-2464, 1974.

36. Tseng, K., and L. Morino, "Fully Unsteady Subsonic and Supersonic
Potential Aerodynamics of Complex Aircraft Configurations for
Flutter Applications," Proc. of AIAA Structures, Structural Dynamics,
and Materials Conf., King of Prussia, Penn., May 1976.

37. Bryson, A.E., Jr., and Yu-Chi Ho, Applied Optimal Control,
Blaisdell Press, Waltham, Mass., 1969.

38. Turner, M.R., "Active Flutter Suppression," Flutter Suppression
and Structural Load Alleviation, AGARD-CP-175, Jul. 1975.

39. Dressler, W., "Control of an Elastic Aircraft Using Optimal Control
Laws," Impact of Active Control Technology on Aircraft Design,
AGARD-CP-157, Jun. 1975.

40. Noll, R.B., and L. Morino, "Flutter and Gust Response Analysis of
Flexible Aircraft with Active Controls," Proc. of AIAA Structures,
Structural Dynamics, and Materials Conf., King of Prussia, Penn.,
May 1976.

41. Nissim, E., "Flutter Suppression Using Active Controls Based on the Concept of Aerodynamic Energy," NASA TN D-6199, 1971.

42. Wang, P.K.C., and F. Tung, "Optimum Control of Distributed-Parameter Systems," J. of Basic Eng., Mar. 1964, pp. 67-99.

43. Sakawa, Y., "Solution of an Optimal Control Problem in a Distributed-Parameter System," IEEE Trans. on Auto. Control, Oct. 1964, pp. 420-426.

44. Erzberger, H., and M. Kim, "Optimum Boundary Control of Distributed-Parameter Systems," Info. and Control, No. 9, 1966, pp. 265-278.

45. Wiberg, D.M., "Feedback Control of Linear Distributed Systems," J. of Basic Eng., Jun. 1967, pp. 379-384.

46. Sakawa, Y., and T. Matsushita, "Feedback Stabilization of a Class of Distributed Systems and Construction of a State Estimator," IEEE Trans. on Automatic Control, Vol. AC-20, No. 6, Dec. 1975, pp. 748-753.

47. Russell, D.L., "Optimal Regulation of Linear Symmetric Hyperbolic Systems with Finite Dimensional Controls," J. SIAM Control, Vol. 4, No. 2, 1966, pp. 277-294.

48. Malanowski, K., "On Optimal Control of the Vibrating String," J. SIAM Control, Vol. 7, No. 2, May 1969, pp. 260-271.

49. Sung Jian, and Yu Ching-Yuan, "On the Theory of Distributed Parameter Systems with Ordinary Feedback Control," Scientia Sinica, Vol. XVIII, No. 3, May-Jun. 1975, pp. 281-310.

50. Wang, P.K.C., "Modal Feedback Stabilization of a Linear Distributed System," IEEE Trans. on Auto. Cont., Aug. 1972, pp. 552-553.

51. Theodorsen, T., and I.E. Garrick, "Non-Stationary Flow About a Wing-Aileron-Tab Combination Including Aerodynamic Balance," NACA Rept. 736, 1942.

52. Bisplinghoff, R.L., and H. Ashley, Principles of Aeroelasticity, Wiley and Sons, Inc., 1962.

53. Garrick, I.E., "Nonsteady Wing Characteristics," Aerodynamic Components of Aircraft at High Speeds, Vol. VII, Sect. F, Princeton University Press, Princeton, N.J., 1957.

54. Garrick, I.E., "Unsteady Aerodynamics of Potential Flows," Applied Mechanics Surveys, (ed. by Abramson, N.H., et al.,) Spartan Books, Washington, D.C., 1966, pp. 965-970; reprinted in Aerodynamic Flutter, (ed. by Garrick, I.E.,) AIAA Selected Reprints, Mar. 1969.

-184-

55. Scanlan, R.H., and R. Rosenbaum, <u>Introduction to the Study of Aircraft Vibration and Flutter</u>, MacMillan Co., New York, 1951.

56. Sears, W.R., "Operational Methods in the Theory of Airfoils in Non-Uniform Motion," <u>J. of the Franklin Inst.</u>, Vol. 230, No. 1, Jul. 1940, pp. 95-111.

57. Carrier, G.F., M. Krook, and C.E. Pearson, <u>Functions of a Complex Variable</u>, McGraw-Hill Co., New York, 1966.

58. <u>Handbook of Mathematical Functions</u> (ed. by Abramowitz and Stegun), Dover, New York, 1965.

59. Goland, M., "The Quasi-Steady Air Forces for Use in Low Frequency Stability Calculations," <u>J. Aero. Sci.</u>, Vol. 17, No. 10, Oct. 1950, pp. 601-608, 672.

60. Von Kármán, T., and W.R. Sears, "Airfoil Theory for Non-Uniform Motion," <u>J. Aero. Sci.</u>, Aug. 1938, pp. 379-390.

61. Tranter, C.J., <u>Integral Transforms in Mathematical Physics</u>, Chapman and Hall Ltd., London, 1971.

62. Rowe, W.S., M.D. Redman, F.E. Ehlers, and J.D. Sebastian, "Prediction of Unsteady Aerodynamic Loadings Caused by Leading Edge and Trailing Edge Control Surface Motions in Subsonic Compressible Flow-Analysis and Results," NASA CR-2543, 1975.

63. Hassig, H.J., "Aerodynamic Flutter Coefficients for an Airfoil with Leading- and Trailing-Edge Flaps in Two-Dimensional Supersonic Flow," <u>J. Aero. Sci.</u>, Feb. 1954, pp. 131-132.

64. Stewartson, K., "On the Linearized Potential Theory of Unsteady Supersonic Motion," <u>Quarterly J. of Mechanics and App. Mechanics</u>, Vol. III, Part 2, Jun. 1950.

65. Von Borbely, S., "Aerodynamic Forces on a Harmonically Oscillating Wing at Supersonic Velocity (2-Dimensional Case)," R.T.P. Translation No. 2019, British Ministry of Aircraft Production. (From Z. Agnew. Math. Mech., Bd. 22, Heft 4, Aug. 1942)

66. Chang, C.C., "Transient Aerodynamic Behavior of an Airfoil Due to Different Arbitrary Modes of Nonstationary Motions in a Supersonic Flow," NACA TN 2333, 1951.

67. Irwin, C.A.K., and P.R. Guyett, "The Subcritical Response and Flutter of a Swept Wing Model," Tech. Rept. 65186, RAE, Farnborough, U.K., Aug. 1965.

68. Runyan, H.L., H.J. Cunningham, and C.E. Watkins, "Theoretical Investigation of Several Types of Single-Degree-of-Freedom Flutter," J. of Aero. Sci., Vol. 19, No. 2, Feb. 1952.

69. Lyons, M.G., R. Vepa, and S.C. McIntosh, "Control Law Synthesis and Sensor Design for Active Flutter Suppression," AIAA paper No. 73-832, 1973.

70. Garrick, I.E., "On Some Reciprocal Relations in the Theory of Non-stationary Flows," NACA Rept. 629, 1938.

71. Drischler, J.A., "Calculation and Compilation of the Unsteady Lift Function for a Rigid Wing Subjected to Sinusoidal Gusts and Sinusoidal Sinking Oscillations," NACA TN 3748, Oct. 1956.

72. Rodden, W.P., and B. Stahl, "A Strip Method for Prediction of Damping in Subsonic Wind Tunnel and Flight Flutter Tests," J. of Aircraft, Vol. 5, No. 1, Jan-Feb. 1969, pp. 9-17.

73. Baker, G.A., Jr., Essentials of Padé Approximants, Academic Press, New York, 1974.

74. Vepa, Ranjan, private communication, Apr. 1975.

75. "Tables of Aerodynamic Coefficients for an Oscillating Wing-Flap System in a Subsonic Compressible Flow," Nationaal Luchtvaartla-boratorium, Amsterdam, Rept. F.151, 1954.

76. de Jager, E.M., "Tables of the Aerodynamic Aileron-Coefficients for an Oscillating Wing-Aileron System in a Subsonic, Compressible Flow," Nationaal Luchtvaartlaboratorium, Amsterdam, Rept. F.155, 1954.

77. Garrick, I.E., "Aeroelasticity- Frontiers and Beyond," AIAA paper No. 76-219, 1976.

78. Buchek, P.M., M.G. Lyons, and S.C. McIntosh, "A Study of the Application of Modal Suppression to Flutter Control," Dept. Aeronautics and Astronautics, Stanford University, Stanford, Ca., 94305, SUDAAR No. 450, Jan. 1973.

79. Johannes, R.P., and G.O. Thompson, "B-52 Control Configured Vehicles Program," Advances in Control Systems, AGARD-CP-137, May 1974.

80. Haidl, G., A. Lotze, and O. Sensburg, "Active Flutter Suppression on Wings with External Stores," Active Control Systems for Load Alleviation, Flutter Suppression, and Ride Control, AGARD-AG-175, Mar. 1974.

81. Nissim, E., "Active Flutter Suppression Using Trailing-Edge and Tab Control Surfaces," AIAA J., Vol. 14, No. 6, Jun. 1976, pp. 757-762.

82. Gilbert, E.G., "Controllability and Observability in Multivariable Control systems," J. SIAM Control, Vol. 1, pp. 128-151.

83. Edwards, J.W., "A Fortran Program for the Analysis of Linear Continuous and Sampled-Data Systems," NASA TM X-56038, Jan. 1976.

84. Hall, W.E., Jr., and A.E. Bryson, Jr., "Optimal Control and Filter Synthesis by Eigenvector Decomposition," Dept. Aeronautics and Astronautics, Stanford University, SUDAAR No. 436, Nov. 1971.

85. Anderson, B.D.O., and J.B. Moore, Linear Optimal Control, Prentice Hall, Englewood Cliffs, N.J., 1971.

86. Edwards, J.W., "Analysis of an Electrohydraulic Aircraft Control-Surface Servo and Comparison with Test Results," NASA TN D-6928, 1972.

87. Bergmann, G.E., and F.D. Sevart, "Design and Evaluation of Miniature Control Surface Activation Systems for Aeroelastic Models," AIAA paper No. 73-323, Mar. 1973.

88. Söhngen, H., "Bestimmung der Auftriebsverteilung für Beliebige Instationare Bewegungen (Ebenes Problem)," Luftfahrtforschung, Bd. 17, Nr. 11 & 12, Dec. 1940.

89. Donato, V.W., and C.R. Huhn, Jr., "Supersonic Unsteady Aerodynamics for Wings with Trailing Edge Control Surfaces and Folded Tips," AFFDL-TR-68-30, Wright-Patterson Air Force Base, Ohio, 1968.